Evaluating radiological impacts due to uranium mining in the Erongo Region, Namibia

Vaino Indongo

orcid.org/0000-0001-9551-2401

Thesis accepted in fulfilment of the requirements for the degree Doctor of Philosophy in Science with Radiation Science at the North-West University

Promoter:	Prof. Manny Mathuthu
Co-promoter:	Dr. Zivayi Chiguvare

Graduation ceremony: October 2022

Student number: 31714358

Declaration

I, Vaino Indongo (student number: 31714358), solemnly declare that this thesis is my own work. It is being submitted for the fulfilment of the requirements for the degree Doctor of Philosophy (PhD) in Science with Radiation Science at Centre for Applied Radiation Science and Technology (CARST) under the Faculty of Natural and Agricultural Sciences of the North-West University, Mafikeng campus.

This thesis was never submitted in whole or in part anywhere else for any sort of award. In parts of this submission where other sources of information have been used, such sources have been cited in this work and acknowledged under references.

…27/09/2022…

Vaino Indongo — Date

(Student)

…… ……

Prof. Manny Mathuthu — Date

(Promoter)

…… 27/09/2022

Dr. Zivayi Chiguvare — Date

(Co-Promoter)

Acknowledgements

My heartfelt thanks go to my Creator, God, for his handful mercies of a lifetime and determination He granted me during this transitional process of studying towards this milestone. I would also like to sincerely express my profound gratitude to my supervisors, Prof. Manny Mathuthu and Dr. Zivayi Chiguvare for their dedicated and professional support, advises, guidance and invaluable inputs during this study. Your unwavering support in this study shall remain in memories forever.

Many thanks go to the whole Centre for Radiation Science and Technology (CARST) team, particularly Ms. Naomi D. Mokhine for her commitment and assistance on the analyses of samples for this study on inductively coupled plasma-mass spectroscopy (ICP-MS). I would also like to acknowledge everyone for their words of encouragement and motivation as well as the time spent with them in good and peaceful spirits.

Uncountable appreciation goes to the three institutions; that is International Atomic Energy Agency (IAEA), North-West University (NWU) and Namibia University of Science and Technology (NUST), who have made it possible in supporting this study financially, academically and granting of study leave, respectively. Finally, much would not have been achieved without the support from my wife Velonika and kids, my father and mother, David Indongo and Hilya Namushinga, as well as my siblings. Their words of inspirations, courage and motivation have made this dream a reality. May God bless!

ABSTRACT

The unambiguous and continuously increasing exposures of human beings to terrestrial radiations is highly attributed to naturally occurring radioactive materials in the environments. Background radiation had been increasing gradually due to mining and milling activities worldwide to acquire nuclear materials needed for a response to electrical demands globally. The most significant health effects associated with the continued exposure to NORMs are lung cancer and leukemia. The main aim of this study was to evaluate the radiological risks associated with naturally occurring radioactive materials from uranium mining activities to critical groups in Erongo Region, Namibia. The study analyzed the radiological emissions of gamma rays in soil samples using high-purity germanium detector and determined the elemental and radiological concentrations in dust and water using inductively coupled plasma-mass spectrometry Equipment. The target radionuclides were ^{238}U, ^{226}Ra, ^{232}Th and ^{40}K. The weighted mean values of activity concentrations with standard deviations measured for ^{238}U, ^{226}Ra, ^{232}Th and ^{40}K in soil samples using high-purity germanium detector ranged between 104.77±5.23 and 4610.29±50.57 $Bq.kg^{-1}$, 42.22±0.73 and 4909.40±18.13 $Bq.kg^{-1}$, 91.02±1.09 and 436.74±5.16 $Bq.kg^{-1}$, and 683.06±12.88 and 2225.00±52.65 $Bq.kg^{-1}$, respectively. All activity concentrations calculated were found to be significantly higher than the world averages levels of 35, 33, 45 and 420 $Bq.kg^{-1}$, respectively reported by United Nations Scientific Committee on the Effects of Atomic Radiation. Khan river was the only section of study with low radioactivity level. Mean values with standard deviation only for absorbed dose , radium equivalent, annual effective dose, internal and external hazard indices were ranging between 135.89±2.58 to 2290.70±23.53 $nGy.h^{-1}$, 253.45±2.03 to 5271.51±19.28 $Bq.kg^{-1}$ and 0.83± to 14.05± $mSv.y^{-1}$, 0.86±0.01 to 27.51±0.01 and 0.68±0.01 to 14.25±0.01, respectively. Gamma and alpha indices were calculated ranging from 0.93±0.01 to 17.69±0.07, and 0.21±0.01 to 24.55±0.09, respectively. The probability of cancer development in a biological body was estimated by a human health related hazard known as excess lifetime cancer risk. The calculated cancer risks were ranging from $2.92x10^{-3}$ to $4.99x10^{-2}$ for the soil samples, values which were significantly higher than both the world average ($0.29x10^{-3}$) and limit ($1.45x10^{-3}$) documented by United

Nations Scientific Committee on the Effects of Atomic Radiation and International Commission on Radiation Protection, respectively.

The elemental and activity concentrations for naturally occurring radioactive materials were also determined using inductively coupled plasma-mass spectrometry. The mean values in water from the tailings and boreholes were 17.18 and 3.17 $Bq.l^{-1}$ for ^{238}U, 1.72 and 0.024 $Bq.l^{-1}$ for ^{232}Th and 12.40 and 11.58 $Bq.l^{-1}$ for ^{40}K, respectively. These calculated radioactivity concentration values exceeded the drinking water quality guidelines levels recommended by World Health Organization for gross alpha screening and gross beta levels of 0.5 $mBq.l^{-1}$ and 1.0 $mBq.l^{-1}$, respectively.
The results show that both tailings and borehole water were unsuitable for human consumption and therefore, contact with edible food must be avoided by all means. For the dust from mine 2, the average activity concentrations were 80.94 $Bq.l^{-1}$ for ^{238}U, 673.12 $Bq.l^{-1}$ for ^{232}Th and 27.95 $Bq.l^{-1}$ for ^{40}K. The results had shown high transferrable probability of thorium radionuclide in the atmosphere than uranium and potassium nuclides. In dust, ^{232}Th was recorded with significant high value of radioactivity concentration at 673.12 $Bq.l^{-1}$, which was higher than the world average level of 45 $Bq.kg^{-1}$, documented by United Nations Scientific Committee on the Effects of Atomic Radiations.

On excess life cancer risks, the RESRAD-OFFSITE model 4.0 was used with ICRP 107 based radionuclide transformations transfer factors and ICRP 60 external, inhalation and ingestion dose conversion factors to perform the analysis. The cancer morbidity risks modelled for naturally occurring radioactive materials in both mines' samples had shown that ^{226}Ra was the highest contributor. The RESRAD modelling was performed on water, plants, soil and atmospheric exposure pathways by external gamma, inhalations and ingestions and had shown risk factors in descending order as $^{226}Ra > ^{232}Th > ^{40}K > ^{238}U$. In RESRAD-OFFSITE model code, the total cancer morbidity risks were recorded with about 3 persons per 1 000 populations (3×10^{-3}) by tailings soil (stockpiles) and surrounding soil samples of mine 1 less than 7 to 8 persons per 1 000 populations ($7 \times 10^{-3} – 8 \times 10^{-3}$) by tailings (stockpiles) soil samples in mine 2 less than 7 to 9 persons per 1 000 populations ($7 \times 10^{-3} – 9 \times 10^{-3}$) by uranium ore samples of mine 1 were at risks of

developing cancer. This could explicitly prove that the modelled cancer risks in the region were higher than the recommended level of 1×10^{-5} factor for a population and 1×10^{-3} for a subpopulation documented by the World Health Organization as well as the world average (0.29×10^{-3}) documented by the United Nations Scientific Committee on the Effects of Atomic Radiation.

Keywords: mining, milling, critical groups, elemental concentrations, radiological concentrations, HPGe detector, ICP-MS, RESRAD-OFFSITE model, cancer morbidity risks, population

Table of Contents

LIST OF TABLES

LIST OF FIGURES

LIST OF ABBREVIATIONS

AA	Atomic absorption
A_c	Activity concentration
AEB	Atomic energy board
AED	Annual effective dose
AED_{in}	Indoor annual effective dose
AED_{out}	Outdoor annual effective dose
AED_{tot}	Total annual effective dose
ALARA	As low as reasonably achievable
AMD	Acid mine drainage
AMS	Accelerator mass spectrometry
AR	Arandis
B_I	Branching ratio
Bq	Becquerel
$Bq.kg^{-1}$	Becquerel per kilogram
BW	Borehole water
CARST	Centre for Applied Radiation Science and Technology
CCRMP	Canadian certified reference materials programme
Ci	Curie
CNNC	China National Nuclear Corporation
CNSC	Canadian Nuclear Safety Commission
CNRS	total cancer risks
cps	counts per second
CRC	Collision/reaction cell
D	absorbed dose
DCF	Dose conversion factor
DNA	Deoxyribonucleic acid
DRC	Dynamic reaction cell
E/m	Energy per unit mass
EC	Electron capture

ELCR	Excess lifetime cancer risk
Equ.	Equation
ESV	Experience science values
EVC	Erongo volcanic complex
FAA	Flame atomic absorption
FAE	Flame atomic emission
FAO	Food and Agriculture Organization
Ge(Li)	Germanium crystal doped with lithium ions
GFAA	Graphite furnace atomic absorption
GSN	Geological survey of Namibia
HCL	Hydrochloric acid
HLD_A	average human's lifetime duration
HNBR	High natural background radiation
HNO_3	Nitric acid
HPGe	High purity germanium detector
IAEA	International Atomic Energy Agency
IAEA TRS	IAEA technical report series
IBSS	International basic safety standards
ICP-AES	Inductively coupled plasma-atomic emission spectroscopy
ICP-MS	Inductively coupled plasma-mass spectrometry
ICP-OES	Inductively coupled plasma-optical emission spectroscopy
ICRP	International Commission on Radiological Protection
ISL	In-situ leaching
ISO	International organization for standardization
GDMS	Glow discharge mass spectrometry
K_c	Counting correction factor
K_{cf}	Sample correction factor
KHN	Khan river
K_w	Nuclide decay correction factor
L_C	Critical level
L_D	Detection limit

LET	Linear energy transfer
LINAC	Linear accelerator
LQ	Linear quadratic
LSC	Liquid scintillation counter
LN_2	Liquid nitrogen
LCR	Lifetime cancer risk
M_A	Isotopic/unique molar mass
MDA	Minimum detectable activity
MDL	Minimum detectable limit
MeV	Megaelectron-volt
$mg.kg^{-1}$	Milligram per kilogram
$mg.L^{-1}$	Milligram per litre
MME	Ministry of Mines and Energy
MoHSS	Ministry of Health and Social Services
m_s	Mass of sample digested
NaI (Tl)	Sodium iodide thallium crystals
N_B	Total background counts
N_{CP}	Net peak counts
$nGy.h^{-1}$	NanoGray per hour
NORM	Naturally occurring radioactive materials
NORMALYSA	Naturally Occurring Radioactive Materials and LegacY Site Assessment
NPC	National Planning Commission
NRC	Norwegian Refugee Council
NRPA	National Radiation Protection Authority
N_S	Total number of counts per second
NUST	Namibia University of Science and Technology
NWU	North West University
OECD	Organization for Economic Co-operation and Development
PCR	Peak to Compton ratio
ppb	Parts-per-billion
ppm	Parts-per-million

ppt	Parts-per-trillion
REE	Rare-earth elements
RESRAD	RESidual RADioactivity
RIMS	Resonance ionization mass spectrometry
SEA	Strategic environmental assessment
SIMS	Secondary ion mass spectrometry
Sv	Sievert
QINT	Quantity of intake
TIMS	Thermal ionization mass spectrometry
TW	Tailings' water
UNSCEAR	United Nations Scientific Committee on the Effects of Atomic Radiation
USA	United States of America
U_3O_8	Uranium ore concentrate
vs	Version
WHO	World Health Organization
$\mu g.kg^{-1}$	Microgram per kilogram
$\varepsilon(E_\gamma)$	Absolute photo-peak efficiency
ε'	Coefficient of attenuation
σ	standard deviation

CHAPTER 1: BACKGROUND AND PROBLEM STATEMENT

1.1 Background of the study

The continuous human exposures to radiations from the environments are a serious concern worldwide. The word 'radiation' is scary as the word cancer. However, it is scientifically known for its power usage to keep warmth on the planet and influences volcanic eruptions, tsunamis, earthquakes (Nelson, 2014). Assessments of radioactive elements in the natural environments has become one of the crucial activities that need to be carried out, mostly in areas accessible to a human population (Khan *et al*., 2014; Onjefu *et al*., 2017). Natural radioactivity in the environment is found in sand, rocks, plants, water and air. Exposures of living organisms, including humans, to natural radioactivity at different levels depend on natural radionuclides present in each area (Alzubaidi *et al*., 2016; Isinkaye and Emelue, 2015). Human beings are continuously exposed to external body radiations from terrestrial and cosmic radiation.

Natural radionuclides such as potassium, uranium, and thorium with their decay products, such as radon and radium are ubiquitously and unevenly distributed in the earth's crust are chief sources of terrestrial radiations (UNSCEAR, 2000; UNSCEAR, 2017). Reported elemental concentration of uranium in the crust of the earth with a concentration of 1 – 10 ppm in granitic rocks and also sediments of granitic origin, and thorium ranges between 3 and 30 ppm of concentration for crustal minerals origin (Maxwell *et al*., 2013). In addition to these, the elemental concentration for potassium is found ranging from 0.1% to 5%, or even more, with an average of 2.5% in crustal rocks. The above reasons on the basis of studies being carried out in most parts of the world has prompted this research to investigate the levels of radioactivity in the environments in most parts of Namibia, especially mining and exploration zones. The aims were to investigate, assess and evaluate public and employees' exposures, radioactivity contaminations and possible leaks from underground, and to estimate changes in environmental radioactivity caused by nuclear accidents, industrial activities, and other human activities (Alzubaidi *et al*., 2016). There are also a number of reported cases of the health effects of the exposure of humans to chronic levels of these radionuclides (UNSCEAR, 2000). For instance, the

long-term exposure to radon through inhalation has several human health effects such as acute leucopoenia, chronic lung diseases, anaemia, and, to some extent, the necrosis of the mouth (Issa *et al*., 2013). Radium exposure causes bone, cranial, and nasal tumors. Thorium exposure can cause lung, pancreas, hepatic, bone, and kidney cancers and leukemia (Taskin *et al*., 2009).

Uranium mining contributes the largest number of human exposures to naturally occurring radioactive materials (NORM) in the world (Onjefu *et al*., 2021). Uranium mining in Namibia first started in 1976 when a uranium mine was commissioned in the Erongo region. This region was nicknamed as the "*Uranium Province of Namibia*", reportedly with high levels of background radiations in some areas (von Oertzen, 2017). A number of operation and exploration activities are ongoing in the region for possible mineral deposits. The estimated average background radiation in this region is high presumably associated with NORM containing uranium, radium, thorium and potassium radionuclides (MME, 2010). Groundwater is likely to have high level of uranium contaminations from primarily the deposits in bedrock, the saline aquatic environments of paleo-channels, calcrete in carnotite precipitates, sodium bicarbonates or acid treated uranium and leaching of other radionuclides from tailings.

Cosmological contribution to the background radiation in Namibia is about 0.3 $mSv.y^{-1}$ at the coastal areas, whilst about 0.7 $mSv.y^{-1}$ was observed in the central highlands of the country (MME, 2010). Majority of people living in the region are on the coastal towns of Swakopmund, Henties Bay and Walvis Bay, whilst a reasonably but still moderate number living in Arandis, Omaruru, Usakos, Uis, Gobabeb and Karibib towns. The population-weighted average of the region due to cosmic radiation is reportedly similar to the world's population-weighted average of 0.38 $mSv.y^{-1}$ (UNSCEAR, 1993). Terrestrial sources contribute to a maximum of about 7.3 $mSv.y^{-1}$ in the region, with an average of 0.7 mSv y^{-1} doubling the world average of 0.33 $mSv.y^{-1}$, which was assessed using radiometric surveys (Wackerle, 2009). The contribution to population-weighted average of terrestrial radiations in the region is lower than the average level of the region (0.7 $mSv.y^{-1}$). Natural terrestrial gamma radiation exposures, both indoor and outdoor, are comparable to the

world average of 0.48 $mSv.y^{-1}$, with typical values ranging from 0.3 – 1 $mSv.y^{-1}$ (UNSCEAR, 2017; WHO, 2011b).

Naturally, the average background radiations emitted from soil and rocks, cosmic sources, atmospheric radon (air), and radioactive elements in food, is about 2 – 3 mSv worldwide (UNSCEAR, 2000). UNSCEAR (2013) reported the global average annual effective dose exposure to all natural background radiation sources on individuals at 2.4 mSv (UNSCEAR, 2013). The annual effective dose reported on high natural background radiation (HNBR) areas by UNCSCEAR (2017) has been classified as low, intermediate, high and very high doses. The report has indicated low, intermediate, high and very high background areas receiving doses approximated at annual doses of 5 $mSv.y^{-1}$ or doses doubling the world average (2.4 $mSv.y^{-1}$), 5 – 20 $mSv.y^{-1}$, 20 – 50 $mSv.y^{-1}$ and > 50 $mSv.y^{-1}$, respectively (UNSCEAR, 2017). Research studies are crucial for comparisons to world averages and permissible levels of background radiations and various radiation exposures documented by different international standards. The maximum permissible annual dose to members of the public from all exposure pathways is 1 $mSv.y^{-1}$, excluding natural background radiations and medical doses (ICRP, 2007; UNSCEAR, 2000).

Uranium, thorium and potassium are considered as major hazardous radionuclides mainly discharged from mining and milling activities, hosted by NORM. These natural radionuclides are distributed unevenly in the soil and require serious attention in terms of radioactivity level for the benefit of the population's health to minimize radiation exposures. The most likely exposure pathways are inhalation (dust and radon), ingestion via ground water source and food crops, radioactive particles emitted from nuclear explosions known as fallouts and electromagnetic rays from extremely high-energy subatomic particles of cosmological origin (Arafat *et al*., 2017; Amrane and Oufni, 2017; Durusoy and Yildirim, 2017). Radionuclides can migrate through ground water aquifers, transported via the atmosphere, either as windblown dust (radioactive dust), or as radon, and eventually accumulate biologically in human bodies.

1.2 Problem statement

The existence and exposure of natural primordial radionuclides exposures to human society is a growing concern which can never be underestimated. Namibia, located on the south western part of the African continent, is richly blessed with abundance of variety of the world's most essential mineral resources and metals, such as diamonds, uranium, zinc, gold, copper, silver, lead, magnesium, semi-precious stones and industrial minerals (Salom and Kivinen, 2020). Employees and miners involved in the supply of raw materials required for nuclear weapons and electrical power have unknowingly fallen victims of natural radionuclide exposures mostly from human activities such as minerals explorations and mining activites. Chronic external and internal radiation exposures to human leads to diseases such as melanoma, leukaemia and lung cancers, a major concern on people who worked in the mining industry and those living in areas where nuclear weapons and reactor explosions took place in the past (UNSCEAR, 2017). Overally, a number of workers in the mining industry are likely to get exposed to radionuclides of high radioactivity which may result in development of cancer. These natural radionuclides are of relatively less importance from a dosimetry point of view (Joel *et al*., 2018). They originate from the earth's crust and can expose humans externally, by penetration of radiation into the skin, and internally through ingestion of food and water and inhalation of air.

Uranium mining and exploration in Namibia are basically performed in the ecologically sensitive central coastal area of the Namib desert, areas of the Dorob and Namib-Naukluft National Parks and promotes most of the country's economic growth (Schneider, 2018). The area is known for its high uranium enriched bedrock close to the earth's surface. Mining of uranium ores contributes to high radon emanation and high radon exposure hazards (Thabayneh, 2018). One of the processes in uranium mining is leaching, a process involving extraction of uranium from its raw ore by injecting either with concentrated acid or a base to dissolve the ore for extraction. In some instances, extraction is finalized by precipitation, after crushing, to extract uranium ore concentrate (U_3O_8), known as the yellow cake (Shindondola-Mote, 2009). These activities have the obvious potential to contribute to the increase of background radioactivity in the

environment as well as a possibility of soil, water and atmospheric pollution in the area and consequently affect the human population living in the vicinity.

Tailings remain radioactive, and chemicals used in the extraction process contributes to environmental exposures when dry. Radioactive dust arises from dry tailings as a result of wind blowing, increasing the level of environmental radioactivity and eventually the radius of exposure. Other problems have also been associated with uranium and her daughters' transportation in terrestrial and aquatic ecosystems, where radioactive elements are transferred from air, water and soils into plants, animals and eventually to man (Nielsen, 2013). Therefore, analyses on level of radiological hazard exposures from various mining and milling activities to the public and employees is necessary.

Studies on evaluation of ^{238}U, ^{232}Th and ^{40}K radioactivity concentrations in soils and radiological hazards associated with these primordial radionuclides in Namibia have been carried out by several authors using gamma and inductively coupled plasma-mass spectrometers (Njinga *et al*., 2016; Onjefu *et al*., 2017; Oyedele and Shimboyo, 2013). A study conducted and completed by Onjefu *et al*. (2016) discussed the occurrence and natural radioactivity concentration and heavy metals in the shore sediments of the coastal areas of Erongo Region (Onjefu *et al*., 2016). The study concluded with the modelled results of both indoor and outdoor occupancy factors, with higher outdoor factor and less indoor factors compared to UNSCEAR (2000) values. Their results lead to a conclusion that the region with annual effective dose rate, excess life cancer risk and internal hazards higher than the world recommended value of 0.07 $mSv.y^{-1}$, 0.29×10^{-3} and 1, respectively. All other radiological health hazards were below the recommended values. Munyaradzi *et al*. (2018) conducted a research on naturally occurring radionuclides from dust deposition and radon in in Karibib town of Erongo region in soil samples and radon monitors (CR-39) deployed in houses of the town (Munyaradzi *et al*., 2018). The study also concluded, that there is high radiological hazards in the town. However, this study did neither research on NORM in particulate matter of Swakop and Khan rivers' channels, nor on the radiological hazards to critical groups around the uranium mines in the Erongo region.

Further away from this study area, Amwaalanga *et al*. (2019) conducted a study of radioactivity concentrations in soils from the Zambezi River, Namibia. This study found significantly high values of radiological hazards, such as indoor and outdoor annual effective dose rates at 0.07 $mSv.y^{-1}$ and 0.45 $mSv.y^{-1}$, respectively (Amwaalanga *et al*., 2019). These radiological hazards were above the recommended values by United Nations Scientific Committee on Effects of Atomic Radiation (UNSCEAR). Also, Oyedele (2006) conducted a study in Windhoek and Midzi *et al*. (2019) conducted a study on radioactivity concentrations in soil samples from Karibib and Okahandja (Midzi *et al*., 2019; Oyedele, 2006). Their study findings showed that the radiological hazards were comparable to world's recommended values to the public (ICRP, 2007). In addition to estimation of radiological hazards, modelling tools are required to estimate the possible future cancer risks by radionuclides from NORM, especially in the mining area for radiological protection purposes to workers and the public in general.

A moratorium passed by the Ministry of Mines and Energy (MME) in 2007 on issuing prospecting licences for nuclear fuel in Erongo region has presumably also helped to control the exploration of minerals and mining activities (GSN, 2017). Of course uranium mines in Namibia were to conduct routine dose assessment and compile reports annually on radiation protection and safety in terms of Section 29 (2) documented in the Food and Agriculture Organization (FAO, 2005). Hence, a strategic environmental assessment (SEA) was recommended to the Namibian Government for the uranium province, which later gave birth to a Strategic Environmental Management Plan (SEMP), a useful long-term monitoring and decision-making tool, to address the impact of uranium mining in the country (GSN, 2017). However, the extent of the radiological risks possible radiological health risks from uranium mining to employees and members of the public, considering all exposure pathways, seems neither enough nor fully modelled. Independent scientific research studies would contribute to evidences appear in annual SEMP reports for future documentations on the correct overall exposures both from terrestrial radionuclides and radionuclides of cosmological origin. In this study, humans who are likely to get exposed to any source natural radionuclides fall in the category of critical group.

Persons considered to be critical groups are at risk of receiving exposures from mining activities where the representative level index and absorbed gamma dose rate exceed the maximum permissible limits (Arafat *et al*., 2017). As part of the environmental close observations and revitalization programs, assessments on radiological dose must be carried out to avoid a potentially unacceptable radiation exposures to the public (Krisanangkura *et al*., 2013). In view of the above, there is a need to thoroughly investigate if the general public and employees who have contact with soil, water, dust and food crops around the mines in the Erongo region, are being affected by radiations from uranium mines. Therefore, in this research, the determined radioactivity concentrations were used to assess (estimate and evaluate) human cancer risks primarily by individual radionuclides on members of the public and employees with the help of RESdual RADioactivity (RESRAD) modelling tool.

The research focused on NORM in soils and water from tailings, residential areas and the Khan river channel between two operating uranium mines in the region. The the radiological hazards to critical groups or within a considered radius around the two uranium mines in the Erongo region, who may be exposed will be assessed.. The safety of miners and that of the population is of paramount importance in environments predominantly prone to contaminations of NORM from mining and milling sites.

1.3 Aim and objectives

1.3.1 Aim

The aim of this study was to evaluate the radiological risks associated with NORM from uranium mining activities to critical groups.

1.3.2 Research objectives

The specific objectives were to:

- Determine the radioactivity concentrations of NORM (^{238}U, ^{226}Ra, ^{232}Th and ^{40}K) in soil from Arandis town and uranium mines' tailings using gamma spectrometry.
- Determine the elemental and radioactivity concentrations for U, Th and K in dust and water using ICP-MS.
- Evaluate the radiological hazard indices using mathematical models

- Estimate the radiological cancer risks to inhabitants of Arandis due to NORM using RESRAD modelling tool.
- Recommend or propose radiation protection measures for decision making and policy formulation for protection and safety of the inhabitants of the area based on the results of the study.

1.4. Limitations of the study

This study was initially planned for collections of samples from all possible areas that could increase exposure rate in the region. The first opportunity allowed for collections of water and soil samples from one mine and from the second mine, dust, water and soil samples were collected. The mining companies offered only the first opportunity for collections of soil and water samples used for this study. The collection of samples were restricted to two uranium mines and Arandis town because of the time limitation for completion of the study. The main focus was radiological impacts on critical groups – all representative groups/persons who may potentially be at risk of being exposed to radiations as a result of continuous human activities from the surrounding mines.

The next chapter discusses about literature review on industrial human activities on uranium and milling, NORM arising from human activities, the discovery of radioactivity and radioactive decay of radioisotopes, radioactive equilibria and decay chains of ^{238}U and ^{232}Th series. Chapter 2 has also covered biological effects and radiation protection in everyday lives. Two environmental survey meters were discussed as well as the analytical instruments used in detection of gamma dose and elemental concentrations in soils, dust and water.

In conclusion, the chapter discussed about the RESRAD modelling tool which was used to approximate the cancer risks in samples measured for the study. Considering exposure pathways exposure situations, the identifications of possible exposure levels was discussed for internal and external exposures to ionizing radiations.

CHAPTER 2: LITERATURE REVIEW

2.0 Introduction

Exploration, mining of nuclear materials and developments of nuclear power programme continue to be controversial topics in the world when it comes to safety and security to human population as well as nuclear waste disposal. Certain exposures and their associated risks reach the general population through environmental pathways. In order to understand the current state of human safety in any environmental settings requires assessments and evaluations of the levels of contaminants including natural radioactivity and exposures from human activities. Radioactive elements such as uranium (^{238}U), thorium (^{232}Th) and any of their decay products such as radium (^{226}Ra) and an inert gas radon (^{222}Rn)and potassium (^{40}K), , are examples of radionuclides found as naturally occurring radioactive materials (NORM). More importantly, the uranium radioactive decay products such as ^{210}Pb, ^{210}Po and ^{226}Ra require special attention (Nielsen, 2013), because they significantly expose humans to alpha radiations. The inert gas ^{222}Rn is a decay product of ^{226}Ra by alpha particle emission (Equation 2.1). These natural radioactive elements have been existing in the atmosphere and Earth's crust for many years and are well-known as terrestrial elements (UNSCEAR, 2010).

$$^{226}_{88}Ra \rightarrow {}^{4}_{2}He + {}^{222}_{86}Rn \qquad (2.1)$$

Uranium and its daughter products can be found in high concentrations in uranium ore bodies which are being mined in many countries throughout the world. Uranium, as a mineral, is used for production of cleaner electric power as a fuel (Kenny, 1977; Morrell and Jackson, 2013). As a result of increase in fuel demands, explorations of more resources cause an increase and boost production. As the demands escalates, and explorations and mining activities increases, the tendency for more contaminants to be released into our environments also increases. Cosmic radiations which are high-energetic particles emanating from the sun and outer space also contribute to the natural background radiation. They also contribute to human exposures as they interact with atoms in the earth’s atmosphere to produce secondary radiation of particles and gamma rays (Hassan, 2012). The secondary radiations are called cosmogenic radionuclides,

which do not have significant contribution to radiation absorbed dose (UNSCEAR, 2000). Therefore, attention is significantly paid to terrestrial isotopes which are radionuclides present in earth's crust.

2.1 Uranium mining and milling

Uranium is classified as a dense material preferably heavy as other dense elements like tungsten and gold. It is found in silver-grey color in the metallic form and dark grey to black when oxidized (Figure 2.1). Uranium can also be found this yellow color when in a compound form specifically known as yellowcake, like ammonium di-uranates (Gunhild von Oertzen, 2011).

Figure 2. 1: The colour of granitic rock with uranium ores (Geology.com, 2005).

The front end of the nuclear fuel cycle leads to electrical power production from uranium in nuclear reactors occurs through activities such as mining, milling, conversion, enrichment, fabrication of nuclear fuel and reprocessing (UNSCEAR, 2017). Industrialized nations, such as United States of America (USA), China and Russia, have increased uranium demands in 2003, termed as "*third uranium renaissance*", for nuclear activities and hence the renewed mining and explorations in Africa (Winde *et al*., 2017). Mining and milling activities, especially for uranium, contribute to the increase in

radioactivity levels, and hence the increase in background radiations in the world, in addition to other sources. Uranium mining industry in many countries is considered the significant source of hazardous nuclear products, both resulting in radiation doses and the number of people being affected (Nielsen, 2013). Metric tonnes of waste products, containing NORM, from a number of mining processes, such as uranium and phosphate mining, and contribute highly to background radiation (Alonso-Hernández *et al*., 2013). The amount of mine and mill residues present worldwide has increased and most are present hazardous zones due to high radioactive concentrations of long-lived toxic nuclides, like ^{226}Ra, ^{210}Pb, ^{210}Po and associated toxic stable metals (Carvalho, 2011). Human activities on earth often increase the exposures due to increase in concentrations of primordial radionuclides.

The extraction of uranium ores from the earth is a process involving its physical removal either through conventional surface, underground mining methods, or by chemically dissolving the uranium out of the rock ore by heap leaching and/or in-situ leaching (ISL) (UNSCEAR, 2017). There are different types of mining activities encountered in different parts of the world. Open pit, also known as strip mining is practiced on ore bodies that are close to the earth's surface and relatively cheap extraction methods for lower-grade ore. The other extraction methods applied on underground mines involves extractions through tunnel or some openings on the sides of mountains or hills and generally applied for higher-grades ores extractions (Aumalikova *et al*., 2020). All uranium mines in Namibia are open pits, and therefore, regarded as ore bodies of low-grade ores in terms of parts-per-million (ppm) range. In-situ leaching is applied for conditions where accessible and economical uranium can be recovered from shallow deposits on non-porous shale or mudstone (UNSCEAR, 2017).

Open-pit mining can slowly extend to the groundwater table, thus creating direct pathways for interaction of water with the radioactive materials Therefore, oxygen is introduced resulting in sulphide minerals oxidation in the ore host rock which then leads to acid mine drainage (AMD) in the mine. AMD is regarded as a common phenomenon and not specific only to uranium mining in particular. In turn, the direct access to underground water table creates pathways for introduction of the radionuclides and other contaminants into the

groundwater. The mining activities within themselves introduces many hazardous contaminants into the aqueous environments (Aumalikova *et al*., 2020; von Oertzen, 2017). Degradation products of explosive materials, oil machinery and transformer fluids are examples of these contaminants.

2.2 Naturally occurring radionuclide materials (NORM)

Natural occurring radionuclide materials are part of the environment we live in (Ojovan *et al*., 2019). Theoretically, radon and radium are major radionuclides, which originates from uranium and thorium decay series. NORM are existing globally in the environments. The source terms that contribute to NORM could be on-site such as storage tanks, pipes, stockpiles and equipment surfaces within mines (occupational external and internal exposures); and off-sites such as gamma ray emissions from tailings, runoff of cosmological origins and natural environments (public exposures).

Human beings are exposed to natural environmental radioactivity at different levels and the whole process depends on natural radioactive elements present in each area (Alzubaidi *et al*., 2016). The radioactivity levels (activity concentrations) can be used to assess public dose rates and radioactivity contamination and estimate possible changes in environmental radioactivity caused by accidents in nuclear environments, industrial activities, and other human activities (UNSCEAR, 2000).

Environmental background radioactivity in some places is also a result of increase in technically-enhanced natural occurring radioactive materials (TENORM) (Doyi *et al*., 2016). NORM that result from human activities, such as mining and burning of coal among others, which have increased the relative concentration of the radionuclides (Dudu *et al*., 2018). The enhancement of radionuclides is characterized by artificially enriching the activity concentrations, of SI unit $Bq.kg^{-1}$, for radionuclides of NORM related to dry mass (Nabhani *et al*., 2016). The principal radionuclides are isotopes of unstable atoms with a high atomic and mass number elements, the long-lived isotopes uranium-238 (Uranium series), uranium-235 (actinium series), and thorium-232 (thorium series) (Nabhani *et al*., 2016). There are three uranium elemental isotopes ^{238}U, ^{235}U and ^{234}U with natural abundances of 99.27%, 0.72% and 0.0055%, respectively (Ovaskainen, 1999). In

addition, there are other three artificial isotopes, such uranium-236 (^{236}U), uranium-233 (^{233}U) and uranium-232 (^{232}U), which are formed from nuclear fuel reactors.

Namibia is no exemption to natural occurring radionuclides mostly released from mining and milling activities, because it is blessed with natural mineral resources. The mining activities for minerals are carried out in most regions like Oshikoto around Tsumeb town, Otjozondjupa, Khomas, Karas and Erongo. Different areas of the landscape were studied in the past to analyse the activity concentrations of ^{238}U, ^{232}Th and ^{40}K in the soil samples such as the south (Oyedele and Shimboyo, 2013), North Dune beach in Henties Bay and granite materials in Erongo (Onjefu *et al*., 2017; Onjefu *et al*., 2021) and Karibib town (Munyaradzi *et al*., 2018).

2.3 Discovery of radioactivity

The world we live in, with everything either visible or invisible, is made up of fundamental particles of matter known as atoms (Murray and Holbert, 2014; Nelson, 2014). All solids, liquids or gases are composites of atoms. Atoms are the smallest particles of matter which contain sub-particles known as neutrons, protons and electrons. A unique atom, except hydrogen, has a nucleus at the centre consisting of protons and neutrons and a shell consisting of a cloud of electrons. Hydrogen atom, shown in Figure 2.2, has only one proton and an electron found in the nucleus and on the shell, respectively. This is the Bohr model of the hydrogen atom, with a Bohr radius of 0.53×10^{-10} m and a diameter of 1.06×10^{-10} m (Murray and Holbert, 2014). All nuclear radii range between 1 – 10 fm (1×10^{-15} – 10×10^{-15} m). The sub-particles of the nucleus are known as nucleons, they provide most of the atomic mass. All atoms of the same element, with the same number of protons and different number neutrons in the nucleus are called isotopes. For a hydrogen atom we have isotopes such as protium (^{1}H), deuterium (^{2}H) and tritium (^{3}H) (Webmaster, 2000). Some atoms may not be stable and, therefore, have to undergo transmutation to become stable. Tritium is a rare element of hydrogen produced from cosmic rays interacting with in the atmosphere (CNSC, 2014).

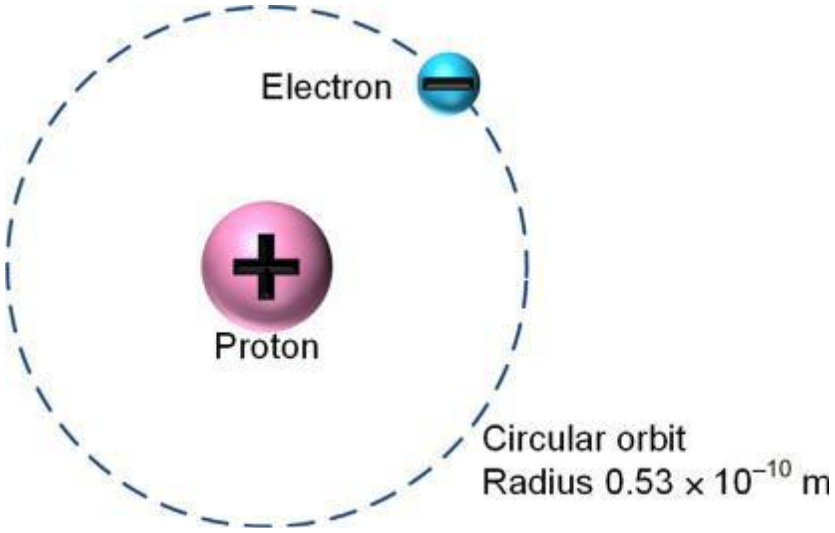

Figure 2. 2: Hydrogen Atom (Murray and Holbert, 2014).

X-radiations, all known as photon radiations were discovered in the late 1800s. The discovery of X-rays by Wilhelm Roentgen (1895) and radioactivity by Henri Becquerel (1896) has led to more researches towards this field by a number of scientists (Turner, 2008). It was thereafter, that the initially discovered radiation was investigated by French couple scientists, Marie Curie and Pierre Curie, who eventually concluded that radioactivity is an atomic property of substances (Martin, 2013). The Curies experimented by extracting uranium from an ore. In 1898 Marie Curie again discovered that not only uranium gave off the mysterious rays discovered by Becquerel, but thorium did as well (L'Annunziata, 2012). The conclusion was that pure uranium had less activity concentration compared to the remaining ore. The Curie couple, were able to also isolate the radioactive materials from the parent rocks. These two elements were given their names for a reason, polonium for Marie's homeland Poland, and the other one called radium which means a thing that radiates (Nelson, 2014). The findings by Becquerel and the Curies led them to win a joint Nobel Prize in Physics in 1903 (Habashi, 2001).

X-radiations, also known as photon radiations were discovered in the late 1800s. The discovery of X-rays by Wilhelm Roentgen (1895) and radioactivity by Henri Becquerel (1896) has led to more research in this field by a number of scientists (Turner, 2008). It was thereafter, that the initially discovered radiation was investigated by French couple scientists, Marie Curie and Pierre Curie, who eventually concluded that radioactivity is an

atomic property of substances (Martin, 2013). The Curies experimented by extracting uranium from an ore. In 1898 Marie Curie again discovered that not only uranium gave off the mysterious rays discovered by Becquerel, but thorium did as well (L'Annunziata, 2012). The conclusion was that pure uranium had less activity concentration compared to the remaining ore. The Curies couple, were able to also isolate the radioactive materials from the parent rocks. These two elements were given their names for a reason, polonium for Marie's homeland Poland, and the other one called radium which means a thing that radiates (Nelson, 2014). The findings by Becquerel and Curies led them to win a joint Nobel Prize in Physics in 1903 (Habashi, 2001).

Another scientist Paul Villard, in 1900, in France discovered a highly penetrating ionization radiation through an external magnetic field, which is gamma radiation, at Ecole Normal in Paris (L'Annunziata, 2012; Gerward, 1999). Figure 2.2 illustrates the design and findings of his experiment.

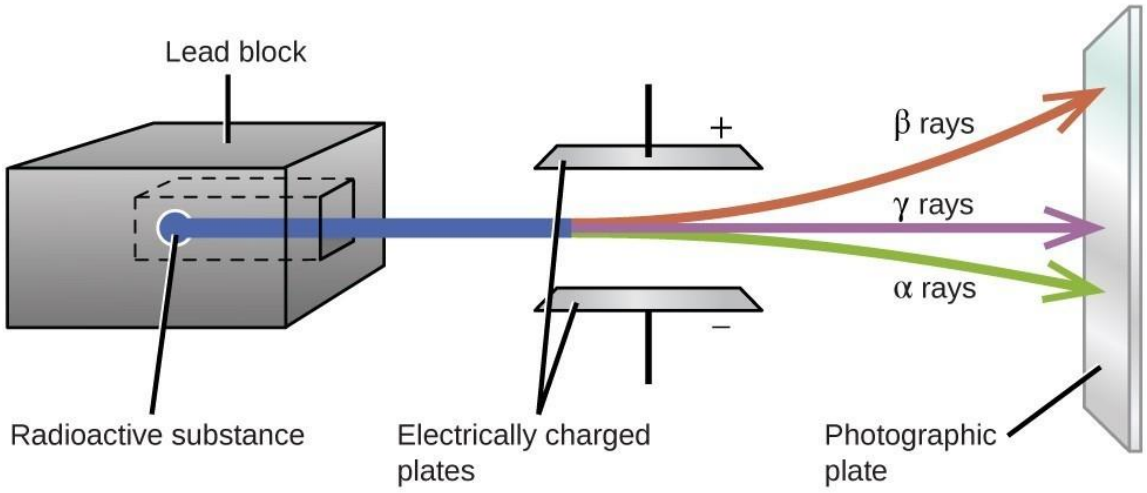

Figure 2. 3: Paul Villard's experimental sketch diagram (Nichols, 2020).

During this experiment, a radiation source was placed within a lead shield is an alpha, a beta and gamma rays emitter. These radiations were targeted onto photographic plates with emulsion sides A and B. The emulsions were set on 1 cm thick glass supports with a separation of 0.3 mm thick lead plate wrapped within an envelope of light-tight paper (L'Annunziata, 2012). The electrically charged plates deflected alpha and beta particles towards the negative and positive terminals, respectively.

Radiation is a form of radioactive energy released by atoms that travels through space. It is harmful at high levels, non-harmful at low levels. Energy at high level is called ionizating radiation, and it is known to be a particle (alpha, beta or neutron) or electromagnetic wave (gamma or X-ray) that is able to remove electrons from the atom after interaction, causing an atom to be charged or ionized. Non-ionizing radiation is energy at low level, considered as particle or electromagnetic wave unable to remove electrons from an atom. Many human beings have their lives and health depending on artificially produced ionizing radiation such as medical imaging and dental X-rays.

Concerns about non-ionizing radiation are minimal regarding human health. However, ionizing radiation has advantages and disadvantages. One good use is that ionizing radiation is that it can be used for diagnostic imaging purposes and treatment of diseases, like cancer. For instances, medical and dental X-rays are used for imaging and gamma (γ-) rays from cobalt-60 (^{60}Co) and linear accelerator (LINAC) X-rays are used for treatment of diseases. Figure 2.4 shows emission of a photon (gamma ray) and particle from the parent radionuclide. Gamma rays originate from radioactive decay of unstable radionuclide materials, natural or artificial. X-rays are emitted from man-made devices, i.e., vacuum tube is one that uses high voltage to accelerate electrons emitted from hot cathode at high velocity and interact with an anode. Since this work will focus more on NORM, X-rays and neutrons will not be discussed further. Therefore, more concentration will be on gamma rays, beta and alpha particles. Figure 2.5 shows the types of ionizing radiation and their penetration trajectories in various materials.

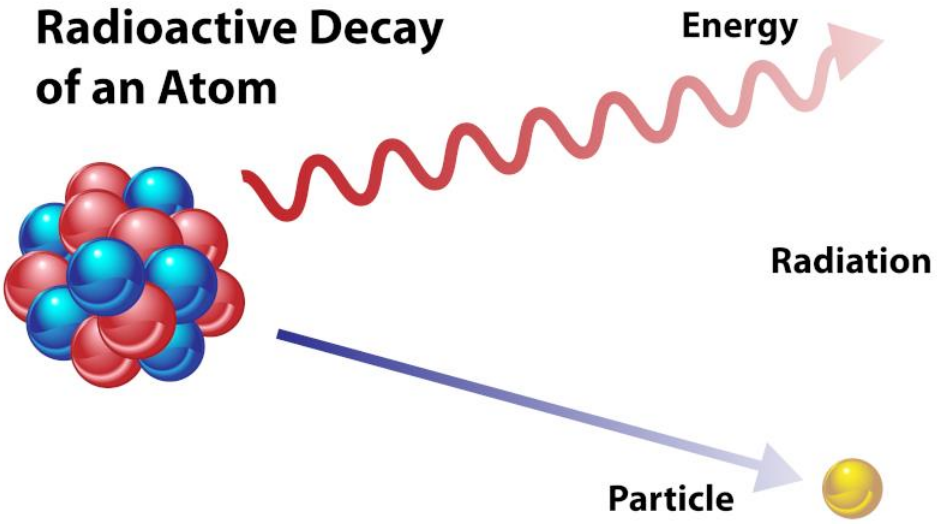

Figure 2. 4: Emission of electromagnetic wave and particle from a radioactive atom (NIETO, 2020).

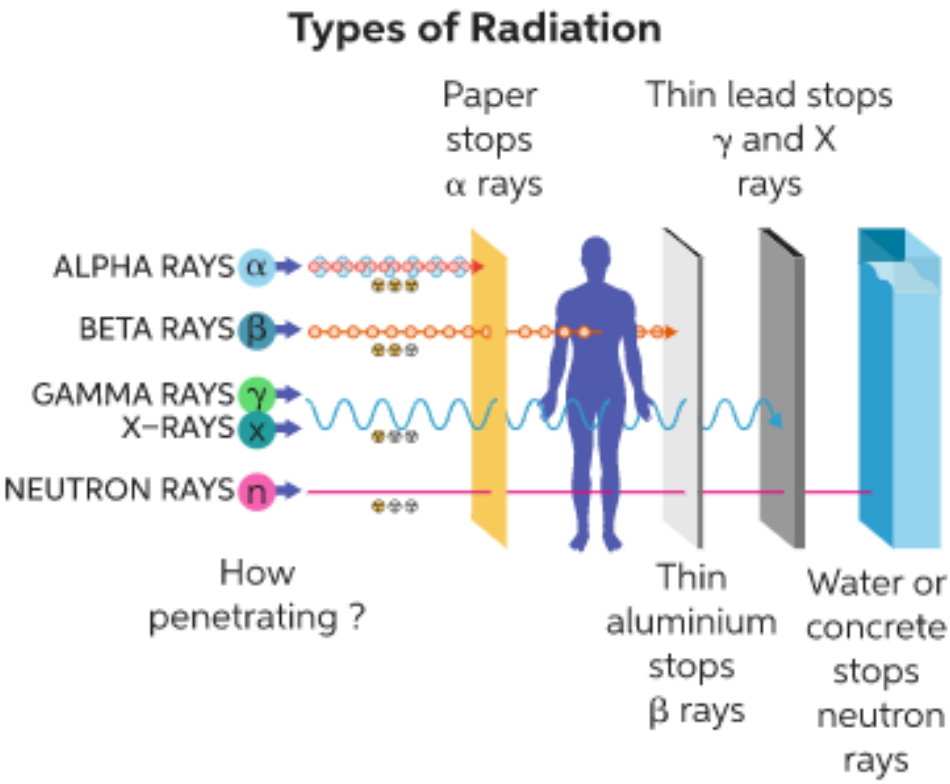

Figure 2. 5: Types of ionization radiation and penetration (Mirion, 2015).

2.3.1 Radioactive nuclei transformation

Non-ionizing radiation is energy which does not have enough energy to remove electrons from an atom. Ionizing radiation on the other hand have enough energy which can remove electrons from atom, resulting in electrically charged ions. This type of radiation can affect changes in the genetic make-up of the cells and tissues. The ions generated by ionizing radiation alter the chemical balance and reactions in the cells, thereby negatively affecting the cells. Ionizing radiations are either electromagnetic waves (gamma or X-rays) or particles (neutrons, beta or alpha), released by atoms, and travels in a medium or space (Zakariya and Kahn, 2014). All these radiations, with the exception of X-rays, are emitted from radioactive decay of unstable elements/nuclides, known as radionuclides/radioisotopes, which undergo a process known as disintegration. Radioactivity is defined as a spontaneous disintegration of an unstable nuclide to form one or lighter daughter particles.

Generally, only a few atoms are stable in nature. Radioactivity is a continuous transmutation process of unstable atoms forming new stable daughter particles/atoms. The term radioactive decay is a sub-process of radioactivity, deduced from the word ‘radiate’, which means to emit energy. Therefore, energies produced from hundreds of various types of unstable atoms are known as nuclear radiations. These are referred to as alpha (α), beta (β), neutron (n), protons (p) and gamma (γ) radiation (Murray and Holbert, 2014). They are all ionizing radiations, which can cause damage when they interact with a living tissue after spontaneous decompositions (radioactive decay) of various radionuclides. All ionizing radiations produced by radioactive decay are known as nuclear radiations.

2.3.1.1 Alpha decay

An alpha particle is a highly energetic, positively charged particle equivalent to a helium nucleus. The alpha particle is more hazardous internally if inhaled or ingested (Awwad *et al*., 2015). Each particle consists of two protons and two neutrons. Its emission results from nuclear fission of natural elements such as uranium and radium atoms, as well as some of artificially manufactured transuranic elements. Alpha decay process occurs

because of low neutron-to-proton ratio in nuclei of heavy isotopes. They cannot penetrate the skin, and pose high risks to sensitive body organs such as the lungs and the bones. Thus alpha particle is radiotoxic only if emitted inside the human body (Zakariya and Kahn, 2014). Therefore, the alpha health hazards result from ingested and inhaled radioactive elements (alpha emitters) such as radon.

Heavy unstable radioactive isotopes undergo radioactive decay process, losing two protons and two neutrons. This simply means a decrease of four in the mass number (A) and loss of two in the atomic number (Z). For illustration, nuclear equations, (2.2a) and (2.2b), show the alpha decay. Because alpha particle has 2 neutrons and 2 protons then the mass number is 4, which is the same as that of helium atom. Therefore, equations (2.2a) and (2.2b) are the same (Cember, 2008).

$$ {}^{\mathrm{A}}_{\mathrm{Z}}\mathrm{X} \rightarrow {}^{\mathrm{A}-4}_{\mathrm{Z}-2}\mathrm{Y} + \alpha + \mathrm{E} \qquad (2.2a) $$

Similarly, equation 2.2a can be written as:

$$ {}^{\mathrm{A}}_{\mathrm{Z}}\mathrm{X} \rightarrow {}^{\mathrm{A}-4}_{\mathrm{Z}-2}\mathrm{Y} + {}^{4}_{2}\mathrm{He} + \mathrm{E} \qquad (2.2b) $$

where, *E* is the total energy emitted due to alpha decay. The total kinetic energy is also referred to as a decay energy (Q_α), shared between the produced daughter nucleus, helium nucleus and gamma radiation emitted (L'Annunziata, 2012). Therefore, the decay energy is expressed as:

$$ \mathrm{Q}_\alpha = \mathrm{E} = \mathrm{E}_\mathrm{d} + \mathrm{E}_\alpha + \mathrm{E}_\gamma \qquad (2.3) $$

where, E_d is the kinetic energy of the daughter nucleus after recoil, E_α is the kinetic energy of alpha particle and E_γ is the energy loss of the gamma rays released from the daughter atom. An example of alpha particle decays is the radioactive decay of uranium-238 into thorium-234 (^{234}Th) shown in Equation 2.4:

$$ {}^{238}_{92}\mathrm{U} \rightarrow {}^{234}_{90}\mathrm{Th} + {}^{4}_{2}\mathrm{He} + 4.25\ \mathrm{MeV} \qquad (2.4) $$

In this case, the energy Q_α released by the alpha decay of ^{238}U is 4.25 MeV.

2.3.1.2 Beta (β^-) decay

Radioactive decay process of beta particle is a type of isomeric transition. Neutron rich isotopes are unstable with high neutron-to-proton ratios, and thus they release beta (β^-) particle through the transition process, producing a daughter nuclide of the same atomic number, A, as that of the parent. Similarly to alpha, beta particles are also considered hazardous only if a beta-emitter is ingested or inhaled (Awwad *et al*., 2015). During this isomeric transition (beta decay), a radionuclide emits a β-particle in the form of an electron (denoted β^- or ${}_{-1}^{0}e$). Equation (2.5a) shows β^- decay of a radioisotope. A beta (β^-) particle is a charged particle that is indistinguishable from an ordinary electron (Cember, 2008), and therefore, is negatively charged. A beta particle can effectively be absorbed by thin layers of metals such as aluminum, and wood, or plastic material. In beta decay process for a negatron emission, the total decay energy released is shared both by beta particle and the antineutrino, expressed as maximum energy (E_{max}) of the decay process (L'Annunziata, 2012).

2.3.1.3 Positron (β^+) decay

Another isomeric transition process can occur when an unstable radioisotopes of high proton-to-neutron ratios, emitting a positron (β^+), a decay in equation (2.5b). A positron particle is denoted by symbols β^+ or ${}_{+1}^{0}e$. Beta particles move fast and penetrate more compared to alpha particles (see Figure 2.5). These particles traverse a short distance into human flesh and are generally less harmful to people than alpha because of their low linear energy transfers (LET). During β^- decay the atomic number, Z, increases by 1, whilst for β^+decay the atomic number decreases by 1.

$$ {}_{Z}^{A}X \rightarrow {}_{Z+1}^{A}Y + \beta^- + \bar{\nu}_e \quad \text{or} \quad {}_{Z}^{A}X \rightarrow {}_{Z+1}^{A}Y + {}_{-1}^{0}e + \bar{\nu}_e \qquad (2.5a) $$

$$ {}_{Z}^{A}X \rightarrow {}_{Z-1}^{A}Y + \beta^+ + \nu_e \quad \text{or} \quad {}_{Z}^{A}X \rightarrow {}_{Z-1}^{A}Y + {}_{+1}^{0}e + \nu_e \qquad (2.5b) $$

The antineutrino, $\bar{\nu}_e$, is an antiparticle of neutrino, ν_e. Both have no electrical charge, with negligible (zero) masses. These particles produce very little observable effects when passing through biological matter (Young and Freedman, 2008). For a positron decay

process, the total energy released is shared between the positron and the neutrino. The positron loses its kinetic energy in a material via ionization, when it comes into contact with an electron, its antiparticle, and annihilates (L'Annunziata, 2012). During annihilation, two gamma photons with energy of 0.511 MeV each are simultaneously produced in opposite directions.

2.3.1.4 Electron capture

Electron capture (EC) is another type of decay, where a nucleus captures an inner shell electron. This nuclear reaction has the same effect as that of the positron decay. A spontaneous reaction of the nucleus of nuclide ${}^{A}_{Z}X$ undergoing electron capture is written as (Equation 2.6):

$${}^{A}_{Z}X + e^{-} \rightarrow {}_{Z+1}{}^{A}Y + v_e \qquad (2.6)$$

2.3.1.5 Neutron capture

Neutrons are neutral particles that are emitted as a result of nuclear fission. Nuclear fission is a splitting of atoms into smaller or lighter daughter products. These uncharged radiation particles are encountered inside the nuclear reactor. Neutrons make non-radioactive materials become radioactive, and when they interact with the human tissue, may cause severe damage.

Neutron decay is known as electron capture process. This emission process may not energetically possible only for a few radionuclides. Here, a combination of the orbital electron with a proton in the nucleus result in a production of a neutron and neutrino (Young and Freedman, 2008). The neutrons produced remain in the nucleus and only the neutrinos are being emitted. As result, this neutron decay (Equation 2.6) occurs when a mass of a parent uncharged nuclide is greater than mass of the daughter atom.

$$p + {}_{-1}{}^{0}e \rightarrow n + v_e \qquad (2.7)$$

Six forms of radioactive decay such as the alpha, electron, proton, neutron and gamma decays are summarized in Table 2.1.

Table 2.1: Fundamental properties of radiations (Mahmood and Haider, 2015; Takigawa and Washiyama, 2017).

Characteristics	Symbol	Identity	Charge	Mass (amu)	Energy Equivalent (MeV)
Alpha particle	$^{4}_{2}\mathrm{He}^{+2}$ or α	Helium nucleus	+2	4.00280	3727
Proton	$^{1}\mathrm{H}^{+}$, p	Positive particle	+	1.007593	938
Beta particle, electron	$^{0}_{-1}\mathrm{e}$ or β^{-1}	electron	-1	0.000548	0.511
Beta particle, positron	$^{0}_{+1}\mathrm{e}$ or β^{+1}	positron	+1	0.000548	0.511
Gamma ray	γ	Electromagnetic radiation	0	0	$< 6 \times 10^{-23}$
Neutron	n^{0}	Neutral particle	0	1.008982	940

2.3.1.6 Gamma decay

This decay occurs in most all the unstable radioactive isotopes. Gamma ray is a high-energy electromagnetic wave known as a photon. This wave behaves the same as X-rays but differ in origin. Gamma rays are very penetrating and require more substantial shielding for radiation protection reasons. Gamma decay is also known as the radioactive transformation associated with electrostatic forces are categorized into two forms, namely; (1) isomeric transition or nuclear isomerism, and (2) internal conversion (Mayles *et al*., 2007). Example of this is shown in the Equation 2.8 as:

$$^{99m}_{43}Tc \rightarrow {}^{99m}_{43}Tc + \gamma \qquad (2.8)$$

No change in both mass and atomic numbers of a nuclide undergoing gamma radioactivity transition. These photons are best absorbed by thick layers of dense materials and considered externally hazardous to human bodies (Awwad *et al*., 2015). When alpha or beta decays of radionuclides occur, there may still be some energy remaining in an atom of the daughter nuclide formed. This energy is released in the form of gamma rays for a daughter nuclide to become stable. Gamma rays are also hazardous

to personnel dealing with sealed and unsealed radioactive materials. Occupational exposure occurs often in industrial gauges for process control and elemental analysis in the mining industry (Faanu *et al*., 2010), and radiotherapy machines used in an imaging and treatment of patients (Motevalli and Borhanazad, 2015).

2.3.2 Half-life and radioactive decay kinetics

The decay kinetic is a process such that a radioactive nuclide undergoes transmutation to form new particles and emit some radiations in the form of particulate matter or electromagnetic waves called photons (Du Preez, 2018). During such transition, the intensity or strength of radiation is reduced to a half. Half-life ($t_{1/2}$), is therefore, defined as the time elapsed during radioactive decay of a nuclide to reduce its intensity of radiations to one half of its initial value (Du Preez, 2018). This is also known as a physical half-life (t_p) of a radionuclide, generally used for environmental radioactivity. Figure 2.6 shows the exponential decay of a radionuclide with time. The initial activity, A_o, in percentage (100%) reduces to a half (50%) of the initial value. Again, for 50% of the activity will reduce to its half (25%) for the second half-life, etc.

When associating half-life with biological decay and the surrounding (environment), the term biological half-life (t_b) is also important. Generally, there are radioisotopes that are taken into the body by way of ingestion or other pathways and get removed through respiration, perspiration, bowels and kidneys (Henriksen, 2009). The time taken before half of the isotope is removed by biological processes is called the biological half-life.

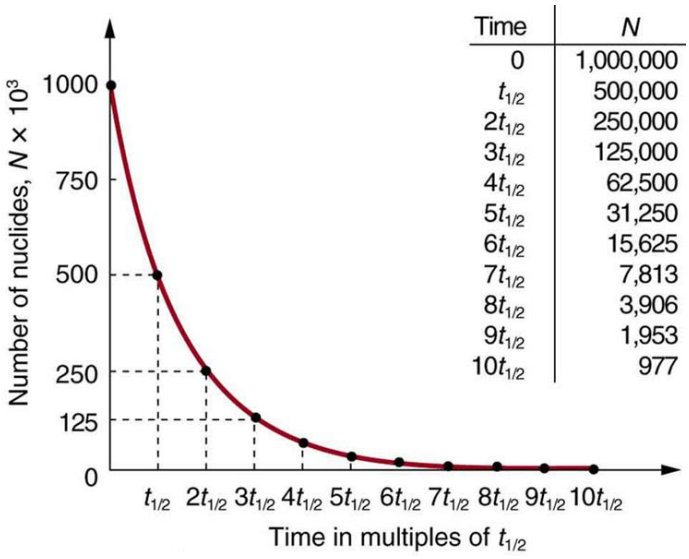

Time	*N*
0	1,000,000
$t_{1/2}$	500,000
$2t_{1/2}$	250,000
$3t_{1/2}$	125,000
$4t_{1/2}$	62,500
$5t_{1/2}$	31,250
$6t_{1/2}$	15,625
$7t_{1/2}$	7,813
$8t_{1/2}$	3,906
$9t_{1/2}$	1,953
$10t_{1/2}$	977

Figure 2. 6: A curve showing exponential decay the radiation intensity decreases with time (Bynum, 2012).

Activity is the rate of radioactive decay classified as an intrinsic property for every radioisotope that is non-dependent of chemical and physical form of the radioisotope (Zumdahl *et al*., 2020). For any given sample of a radioactive substance, the number of atoms, N, of a radioisotopes decrease with time, *t*, as their atomic nuclei transmute to stable nuclei. The law of radioactive decays states that the number of disintegrations per second, simply the activity (A), of a radioisotope source in Becquerel (Bq) is given as (Martin, 2013):

$$A = -\frac{dN}{dt} = \lambda . N \qquad (2.9)$$

where, λ is the disintegration constant and it is unique for each radionuclide, *N* is the number of nuclei that undergo integration process, *dt* is the time interval/elapsed during change in number of particles *dN*. The negative sign indicates that the number of particles is decreasing with time.

Integration is performed to determine the number of atoms N decreasing with time, *dN* is summed over time elapsed. Generally, rearranging and integrating Equation 2.7 above gives:

$$\frac{dN}{N} = -\lambda dt$$

$$\int_{N_o}^{N} \frac{dN}{N} = -\lambda \int_{t_o}^{t} dt; \text{ where } t_o = 0$$

$$lnN - lnN_o = -\lambda t$$

$$\ln\left(\frac{N}{N_o}\right) = -\lambda t$$

$$N = N_o e^{-\lambda t} \quad (2.10)$$

It is also important to know that there is a relationship between half-life ($t_{1/2}$) and the decay constant (λ) by setting $N = \frac{1}{2}N_o$ (Knapp and Dash, 2016). Therefore, this gives:

$$t_{1/2} = \frac{ln2}{\lambda} \quad (2.11)$$

Therefore, putting into consideration radionuclide injected into a body, for known physical (t_p) and biological (t_b) half-lives the formula to calculate the effective half-live (t_{ef}) is thus (Murray and Holbert, 2014):

$$\frac{1}{t_{ef}} = \frac{1}{t_p} + \frac{1}{t_b} \quad (2.12a)$$

$$t_{ef} = \frac{t_p.t_b}{t_p+t_b} \quad (2.12b)$$

The expression in Equation 2.12a can be written as: $\lambda_{ef} = \lambda_p + \lambda_b$, where, λ_{ef}, λ_p and λ_b are effective, physical and biological decay constants, respectively, of a unique radionuclide in use. In terms of activity in a sample, divide Equation 2.10 with time t to get:

$$A = A_o e^{-\lambda t} \quad (2.13)$$

where, A, A_o, λ, t are final activity, initial activity, rate of decay of a sample and time elapsed to reach final activity.

2.3.3 Radioactive equilibrium with daughters

A radionuclide decays by transforming into a new nuclear species of lower energy. Radioactive equilibrium is achieved only when a daughter radionuclide decays at the same rate as the parent (Cetnar, 2006). This state is reached after a transition period of a nuclide, and can never be reached when a half-life of the daughter nuclide is greater than the half-life of the parent nuclide, i.e., not possible when $t_{1/2,daughter} > t_{1/2,parent}$. There are two types of radioactive equilibrium, namely; secular and transient equilibrium. For the radioactive equilibrium, the samples should be sealed for at least 30 days to allow the rate of decays (activities) of the parent nuclide and that of the daughter nuclide to equal, as shown in Figure 2.6 below, i.e., $\lambda_p N_p = \lambda_d N_d$.

Secular equilibrium is achieved such that the physical half-life of the parent nuclide is much greater (above 100 times) in comparison to that of the daughter nuclide ($t_{1/2,parent} >> t_{1/2,daughter}$) (Velikyan, 2015). ^{238}U nuclide with a half-life of 4.5 x 10^9 years may reach secular equilibrium with its daughter products, such as ^{234}Th ($t_{1/2}$ = 24.1 days), or ^{234}Pa ($t_{1/2}$ = 1.18 minutes) with the exception of the final stable element in the decay chain, lead-206 (^{206}Pb). Transient equilibrium is achieved when the physical half-life of the parent nuclide is about 10 times greater than the physical half-life of the daughter nuclide ($t_{1/2,parent} > t_{1/2,daughter}$) (Knapp and Dash, 2016). A parent radionuclide X decays into a daughter Y and if the daughter nuclide is still not stable it will decay into a new nuclide Z, and so on. Therefore, a chain is observed: 1 → 2 → 3 to represent a decay for nuclides X → Y → Z. Each of these nuclides have different half-lives ($t_{1/2,a}$, $t_{1/2,b}$ and $t_{1/2,c}$), so their decay constants are: λ_1, λ_2 and λ_3.

The time evolution of a nuclide concentrations undergoing decay can be modelled using the equations of Ernest Rutherford (1905) and Harry Bateman (1910) (Martin, 2013; Levy, 2018). The appearance or disappearance of a nuclide results into three balance equations: one for the heavy nuclei, a second for fission products and a third for activation products (Marguet, 2018). The solution for transient (Figure 2.7 (a)) and secular (Figure 2.7 (b)) equilibria using Bateman equations are given by (Levy, 2018):

$$\frac{dN_1}{dt} = -\lambda_1 N_1 \quad (2.13)$$

$$\frac{dN_2}{dt} = \lambda_{i-1} N_{i-1} - \lambda_i N_i \quad (i = 2, n) \quad (2.14)$$

Assuming that there is zero concentrations of all daughter nuclides at time zero, we get:

$N_1(0) \neq 0$ and $N_i(0) = 0$ when $i > 1$

Solving for the n[th] nuclide after time t, we get:

$$N_n(t) = \frac{N_1(0)}{\lambda_n} \sum_{i=1}^{n} \lambda_i \alpha_i \, e^{(-\lambda_i t)} \quad (2.15)$$

where, $\alpha_i = \prod_{\substack{j=1 \\ j \neq i}}^{n} \frac{\lambda_j}{\lambda_j - \lambda_i}$ (2.16)

with λ_1 being the decay constant of the first radionuclide in the decay chain, λ_2 being the decay constant of first daughter radionuclide in the chain, λ_{i-1} is the $(i-1)$th decay constant with $i > 1$, N_1 and N_2 are numbers of atoms of a parent and daughter nuclides, respectively.

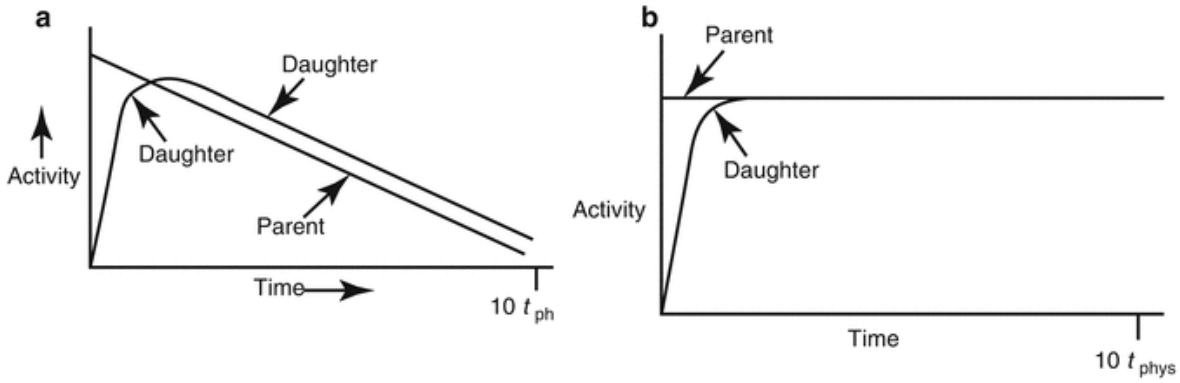

Figure 2. 7: An illustrative diagram of (a) transient and (b) secular equilibrium of parent and daughter radionuclides (Knapp and Dash, 2016).

The above equations give the activity of nuclides in the form:

$$A_p = \lambda_p N_p \text{ and } A_d = \lambda_d N_d \quad (2.17)$$

$$A_d(t) = A_p(0) \frac{\lambda_d}{\lambda_d - \lambda_p} \left(e^{-\lambda_p t} - e^{-\lambda_d t} \right) + A_d(0) e^{-\lambda_d t} \quad (2.19)$$

The term $A_d(0)e^{-\lambda_d t}$ in the activity equation is the residual daughter product activity remaining at t = 0, which is simpler if we set this value to zero and just examine the first

term (Equation 2.19). The Bateman equation of the daughter activity during a secular equilibrium condition, where $\lambda_d > \lambda_p$, is of the form (Levy, 2019):

$$A_d(t) = A_p(0)\frac{\lambda_d}{\lambda_d - \lambda_p}\left(e^{-\lambda_p t} - e^{-\lambda_d t}\right) \quad (2.20)$$

In transient radioactive equilibrium, the half-life of the daughter nuclide is negligibly smaller than that of the parent nuclide. The Bateman equation of a daughter during transient equilibrium condition, where $\lambda_d \gg \lambda_p$ becomes:

$$A_d(t) \approx A_p(0)\left(1 - e^{-\lambda_d t}\right) \quad (2.21)$$

2.3.4 Decay chains of ^{238}U, ^{226}Ra, ^{232}Th and ^{40}K

Radioactivity contributes to heat production on the core of the earth (Cowart and Burnett, 1994). This energy may be experienced during volcanic eruptions, heat produced by hot springs, movement of tectonic boundaries and so on. Most of the naturally occurring radioactive elements are members of one of the radioactive series of uranium (^{238}U), actinium (^{235}U), thorium (^{232}Th) (Martin, 2013). Members of the decay series of two uranium isotopes, ^{235}U ($t_{1/2}$ = 7.13 x 10^8 years) and ^{238}U ($t_{1/2}$ = 4.50 x 10^9 years), and also ^{232}Th ($t_{1/2}$ = 1.41 x 10^{10} years) nuclides produce much of this energy by radioactive decay (Cowart and Burnett, 1994; Halliday *et al*., 2013). Radionuclides that are within the ^{235}U decay series are neglected as they do not contribute much to total dose from natural background environment (UNSCEAR, 1988). One of the decay product of ^{238}U is ^{226}Ra, which eventually emits ^{222}Rn, with a half-life of four days, in the ground. The other radioactive isotope of radon is thoron (^{220}Rn) with a half-life of 55 seconds and is daughter product of ^{232}Th. On Figure 2.8, the daughter products from the three-decay series are radium, radon and thoron, polonium, bismuth, and lead isotopes. All the three parent radionuclides of ^{238}U, ^{235}U and ^{232}Th have low solubility. The most soluble isotopes ^{224}Ra, ^{228}Ra, and ^{226}Ra can be used to determine the concentrations of radionuclides in fluids, particularly water. Hence, among the daughter products of radium isotopes, only radon-222 and radon-220 are soluble radionuclides. Other radioactive isotopes which may possibly be soluble in water, but in small amounts, are thorium, actinium and polonium.

Naturally occurring radionuclides have three decay chains such as ^{232}Th decay chain (4n), ^{238}U decay chain (4n+2) and ^{235}U decay chain (4n+3) (L'Annunziata, 2012). ^{235}U decay chain is well known as actinium series. Of all the representations 4n, 4n+2 and 4n+3 series of decay chains of those radionuclides, n is a natural number value which falls in the range of, and exclude, 50 – 60.

The radioactive noble gas ^{222}Rn is continuously produced from ^{226}Ra decay (Mohammadi, 2010). Underground natural rock which contains uranium ore bodies would continuously emit radon in high concentrations via water in contact with it (groundwater) (WHO, 2011b). The noble gas ^{222}Rn which is soluble in fluids, dissolves into underground water, like borehole water, which then get carried away in high concentrations and possibly transferred to areas inhabited by the human population. It also escapes through the cracks and spaces within the soil into the atmosphere. This is the reason that radon concentration is often within the air and water at levels dictated by local geology and atmospheric sciences (meteorology) (Mohammadi, 2010). ^{222}Rn gas enters a human body when inhaled and attack- the lungs.

For ^{232}Th, ^{238}U and ^{235}U decay series, the respective mass numbers are 4n = A, 4n+2 = A and 4n+3 = A. Some of the radionuclides within the decay chains have very short half-lives. Lead isotopes which have atomic number of 82 (82 protons) are the heaviest stable elements and endpoint of radioactive transformation of uranium and thorium (Halliday *et al*., 2013). All three discussed decay chains end with stable lead isotopes, such that thorium, uranium and actinium terminate with ^{208}Pb, ^{206}Pb and ^{207}Pb, respectively. Generally, ^{226}Ra in natural undisturbed soil is in equilibrium with ^{238}U and in disturbed soils they might not necessarily be in equilibrium (Faanu *et al*., 2010). Therefore, studies that considered ^{226}Ra to quantify activity levels for ^{238}U in samples are based on assumptions of equilibria between these radionuclides.

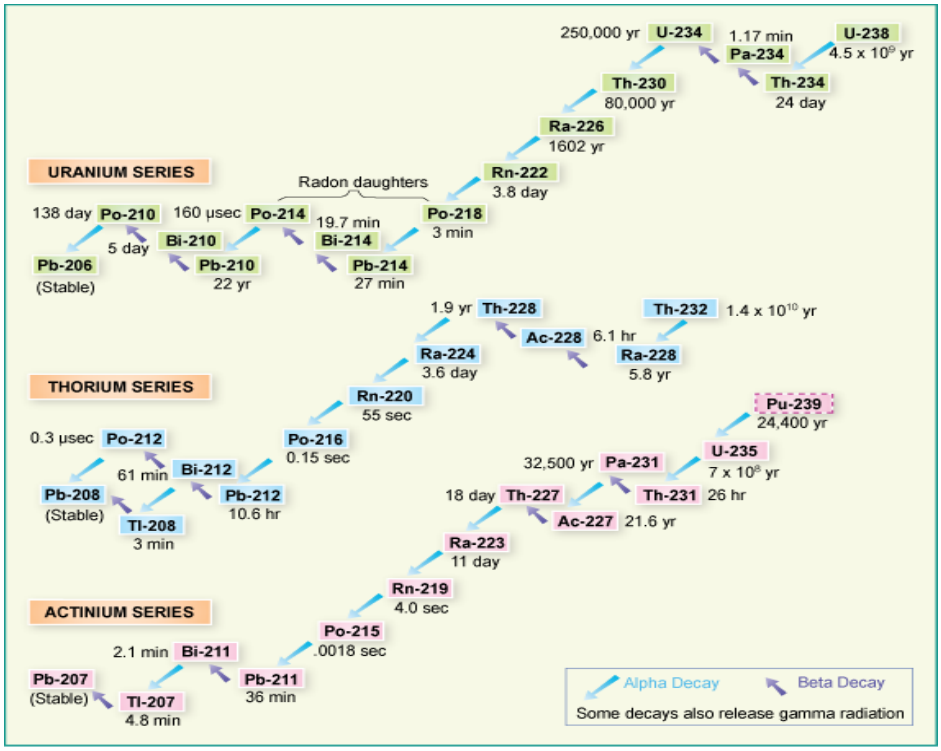

Figure 2. 8: Radioactive decay chains of uranium, thorium and actinium series (Ferreira *et al*., 2015).

Out of 24 known isotopes of potassium, only three occur naturally, namely: ^{39}K (93.3%), ^{40}K (0.0117%) and ^{41}K (6.7%). Potassium-40 ($t_{1/2}$ = 1.28 x 10^9 years) is the only natural occurring radionuclide under study which has no decay-series. The disintegration of this nuclide occurs with 89.5% release of a beta particles with endpoint energy Q(β^-) = 1330 keV transforming into ground state calcium-40 (^{40}Ca). Also, at energy of 490 keV, 0.001% occurs through positron decay (β^+) into argon-40 (^{40}Ar) before releasing gamma-ray of energy 1020 keV into ground state. The most important decay for ^{40}K is by electron capture (EC) with a probability of 10.4% (50 keV) into ^{40}Ar before it releases a gamma-ray of energy of 1460 keV into stable noble gas ^{40}Ar (Pradler *et al*., 2013). Another possible EC (0.16%) decay process releases an endpoint energy 1510 keV. One can easily observe that for all three ^{40}K decay processes into ^{40}Ar the endpoint energy (Q) is the same, about 1510 keV. The diagrammatic illustration for ^{40}K decay is shown on Figure 2.9.

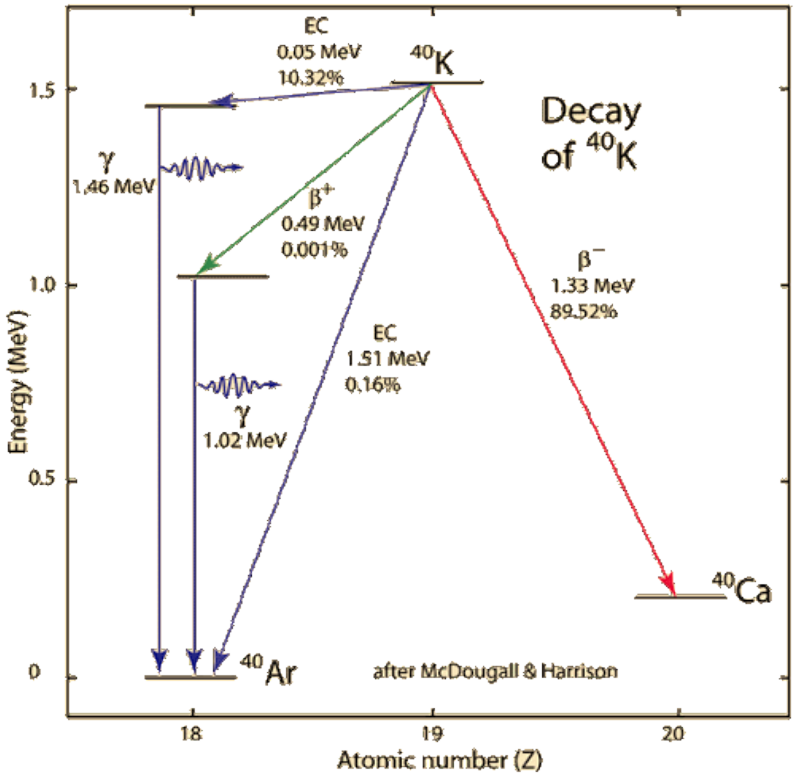

Figure 2. 9: The decay diagram of ^{40}K (McDougall et al., 1999).

It is also important to understand that potassium is not soluble in water but it is only found in the form of minerals such compounds and chlorine minerals of carnalite and sylvite which are soluble. The high concentrations of chloride give a salty taste to water (WHO, 2011b). It is present between 400 ppm (in sea water) because of its relatively high concentrations in oceanic basalts to about 2-3 ppm in river waters in the form K^+ (aq) ions.

2.4 Interaction of radiation with matter

When a quantum of radiations interacts with a medium, they may be scattered, absorbed and/or transmitted through. Scattering and absorption may cause some energy of quanta being left inside the medium. For interaction by ionization radiation, a medium is left ionized (Gazis, 2019). An example, a beam of mono-energetic photons is directed onto a material of thickness x and the intensity of the beam decreases exponentially with increase in depth. The process by which intensity of a beam decreases is called

attenuation, which occurs when there is scattering and absorption. Figure 2.10 illustrates the attenuation of photons traversing through a material.

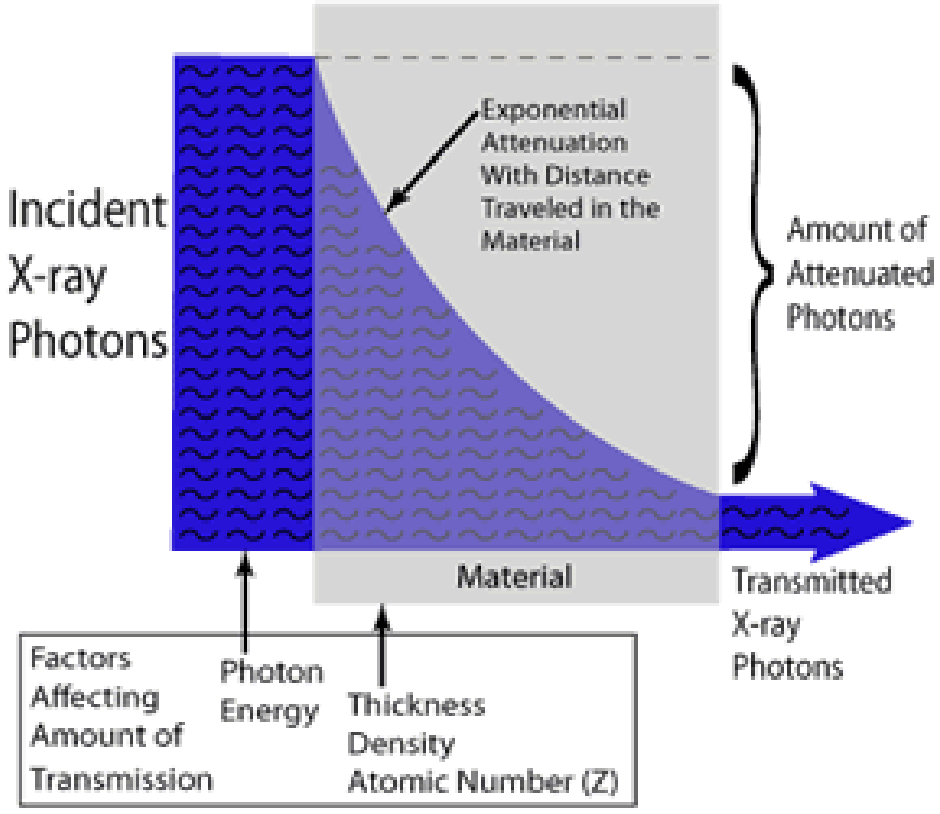

Figure 2. 10: Attenuation of beam intensity of photons (NDE-Ed.org, 2021).

Factors that affect attenuation of the beam are photon energy, thickness of material, atomic number and density of a material. Knowing the magnitude of the incident intensity (I_o) of a beam, thickness and attenuation coefficient of a material, one can approximate the transmitted intensity (I) by the formula (Martin, 2013):

$$I = I_o e^{-\mu x} \tag{2.22}$$

where, μ and x are the coefficient of absorption and thickness of a material, respectively. The equation applies to all different types of radiation. Zooming inside the material, there is a fundamental particle of matter called an atom which consists of electrons, protons and neutrons. In a case where a photon is transmitted, no interaction of radiation with

matter occurs and therefore contributes to the number of transmitted photons. Eventually, energy of an incident photon does not change and will be the same as that of the transmitted photons, $E_o = E_R$.

2.4.1 Rayleigh/simple scattering

Simple scattering is an elastic scattering process from atoms within a medium through which a quantum of radiations known as photons passes. A photon that interacts with and does not remove an electron on the atom, as a result it changes the direction with same the energy, in a process known as Rayleigh scattering (C). Neither energy is exchanged and nor electron is released in this process. Therefore, energy (E_o) of the incoming photon is the same as energy (E_s) of the scattered photon (Gazis, 2019).

2.4.2 Photoelectric effect

An X-ray photon is being completely absorbed by knocking off an electron from the inner shell leaves a hole and a secondary electron of energy less than that of the incident photon being produced. The process is known as photoelectric absorption (B). The electron produced, known as photoelectron, is released with energy less than that of the incident photon ($E_{ph} < E_o$). An electron from the upper level shell fills up the vacancy, releasing a secondary photon called characteristic X-ray, in this case, a K-characteristic X-ray if the electron transition is from L-shell to K-shell (Murray and Holbert, 2014).

2.4.4 Compton scattering

There is an inelastic scattering from quasi-free electrons, with a threshold for each shell of bound electrons corresponding to ionization energy of that particular shell (Basdevant and Rich, 2005). A photon may cause inelastic collision with weakly bound outer shell electrons, known as Compton scattering (D). During inelastic collision a photon is scattered with less energy ($E_s < E_o$) at an angle, θ, and a recoiled electron at a different angle, ϕ. Figure 2.11 shows dominant Compton scattering for energy from 400 keV to 5000 keV (Gazis, 2019).

2.4.3 Pair production

Most photons energies are in the range of kiloelectronvolts (keV) and pair production occurs only when energy of radiation is more than 1.02 MeV and dominant above 50 MeV. Therefore, it is rare that pair production occurs when a beam of photons penetrates a medium, especially when used for imaging. Figure 2.11 illustrates the atomic number of the material against photon energy ($E = hv$) (Hyun *et al*., 2018).

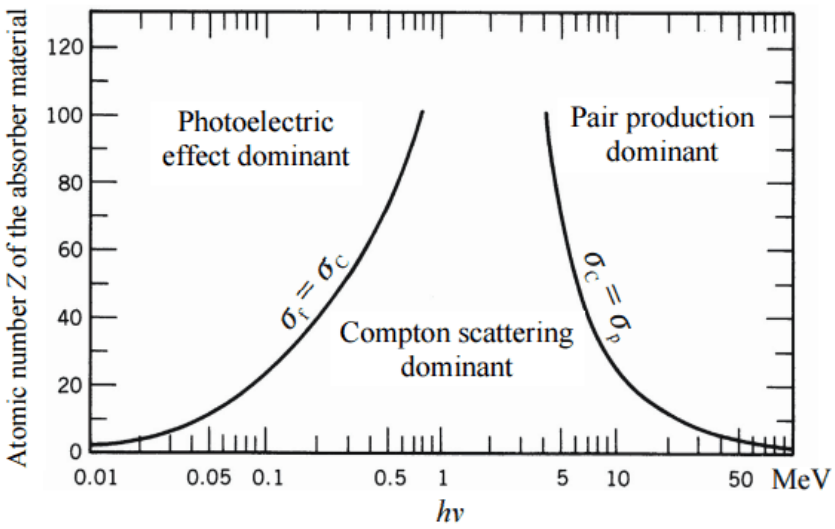

Figure 2. 11: Types of effects when radiation interact with a material (Hyun *et al*., 2018).

2.5 Biological effect of ionizing radiation

From the discovery of X-rays (1895) and radioactivity (1896), discussed in Section 2.3, their biological effects on both animals and humans cells are similar (Henriksen, 2009). Ionizing radiation causes change within the medium after interaction by excitation of atoms by deposition of its energy. Some of its energy is converted into heat. Zooming inside the human cell, there is smallest macroscopic structural and functional unit which contains a nucleus and cytoplasm enclosed within a membrane. This unit is called a cell. Inside the nucleus of the cell there is a complex genetic material known as a deoxyribonucleic acid (DNA). This is a long-chained molecule that encodes the genetic

characteristics of an organism. Its genes are responsible for the coding of proteins. When radiation interacts with a nucleus it breaks down a DNA strand resulting in a cell behaving in a strange way – wrong genetic encoding, bad coding for proteins, abnormal cell growth inheritance – and eventually coding for the genetic instruction guide for life and its processes are lost (Elgazzar and Kazem, 2015).

The fact that photons and particle radiations differ, their biological effects on living things depend on ionization density (Henriksen, 2009). When a human cell is irradiated above threshold, it dies subsequently. A linear quadratic (LQ) formula is used to describe a cell survival as a function of dose (Stewart *et al*., 2012). Equation 2.23 shows a linear-quadratic formula for dose response on a cell survival.

$$S = e^{-(\alpha D + \beta D^2)} \tag{2.23}$$

where, α is a constant describing the linearity for sensitivity of a cell's death on a plot and β describes that the sensitivity of cells to higher radiation doses may increase with high exposure.

In simple term, α is a non-repairable coefficient and β is a repairable coefficient of a cell due to radiation damage. A graph depicting the death of a cell due to radio-sensitivity on a semi-log plot of survival against the dose (D) is shown in Figure 2.12. The semi-log is given by:

$$-\log S = E \tag{2.24}$$

and $E = \alpha D + \beta D^2$ (2.25)

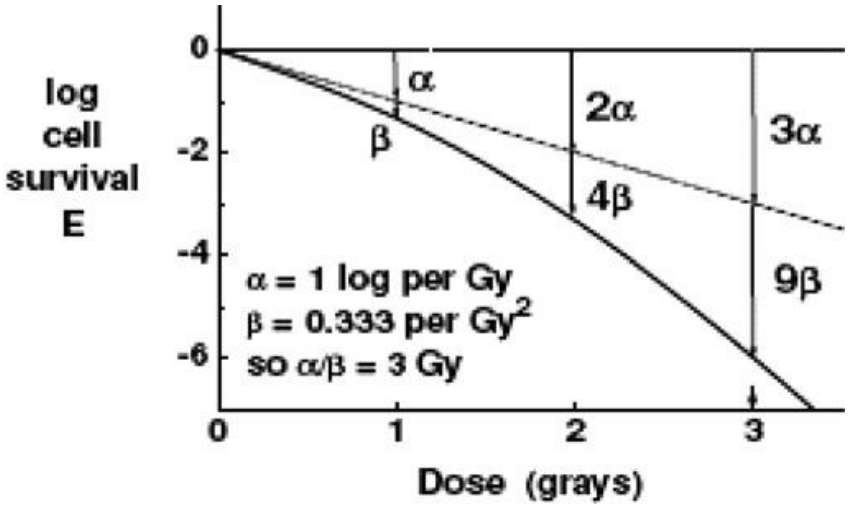

Figure 2. 12: A plot of semi-log (-log S = E) against the dose (D) (Fowler, 2006).

2.5.1 Basic radiation quantities and units

After the discovery of radiations at early stages (discussed in 2.3), the amount of radiations being emitted by a source should be approximated. The approach on this approximation, the estimation of radioactivity concentration in a sample, rather than single atoms, was the best option. The number of atoms of a radioactive element contained in a sample should be approximated. For a known mass (in grams) of a sample, with known atomic mass (m_A), the number of moles (n) is required. Activity (A_{Bq}) of a radionuclide is then computed from the following equation:

$$A_{Bq} = \frac{m}{m_A} N_A \frac{\ln(2)}{t_{\frac{1}{2}}} \tag{2.27}$$

where, N_A is a number of particles per mole in a sample called Avogadro's number (6.02214076×10^{23} mol^{-1}), a fraction $\frac{m}{m_A}$ is the number of moles (n) in a sample and $t_{\frac{1}{2}}$ is the half-life of radionuclide under study. A fraction $\frac{\ln(2)}{t_{\frac{1}{2}}}$ is called decay constant of the radionuclide denoted by *lambda* (λ), m is the mass of a sample and m_A is the atomic molar mass. Therefore, equation (2.27) can be re-written as:

$$A_{Bq} = nN_A\lambda \tag{2.28}$$

Units of Becquerel (Bq) and Curies (Ci) were introduced after the discovery. More importantly, the relationship between Bq and Ci was determined (1 Ci = 3.7×10^{10} Bq = 37 GBq) for computation of activity. Becquerel is defined as the number of nuclear disintegrations per unit time (1 Bq = 1 disintegration/sec), and it measures of actual radioactivity in a material (UNSCEAR, 2000). The rate of decay or disintegration rate of a radionuclide is directly proportional to the mass of the radionuclide in a sample. There are two major methods used to analyse radioactivity concentrations in samples. The first one is to determine the disintegration per second of radionuclide material by counting the number of atoms disintegrating per unit time using gamma spectrometric technique. Secondly, is by way of measuring a mass of a radionuclide in samples using mass spectrometric techniques, (i.e., ICP-MS, ICP-OES).

2.5.2 Sources of exposure

Above sixty (60) radioactive elements exist in the environment, that are categorized into primordial, cosmogenic, and human produced (Shahbazi-Gahrouei *et al*., 2013). Primordial nuclides are elements that were formed during the creation of the earth. Cosmogenic nuclides are those elements formed as a result of of cosmic rays (cosmic origin) interacting with atoms in the atmosphere. Anthropogenic radionuclides are minority amounts of elements formed as a result of human activities for different purposes, i.e., ^{60}Co for radiotherapy. These sources contribute to background radiations of which human beings are exposed to in everyday life. Soil, rocks, air, water and food in our environment are main exposure sources. In addition, industrial processes in our environments such as mining and medical procedures intensify exposure sources.

2.6 Radiation protection and permissible dose limits

The radiological protection system falls in the umbrella of experience science values (ESV). There are three radiological protection systems within this umbrella classified by principles such as justification, optimization and dose limits; situations such as planned, emergency and existing; and categories such as occupational, public, medical and environmental (Heron and Borrás, 2014). Protection and safety of humans to radiation sources stipulated in IAEA basic safety standards (BSS) document must be followed and

practiced all time (Heron and Borrás, 2014). This document prescribes maximum doses permitted and dose limits to humans, as established by International Atomic Energy Agency (IAEA). A radiation dose is described as the amount of radiation that is expected to be absorbed by a human. Radiation protection is necessary for the protection of humans due to exposures from any radiation source through application of the principle of justification, i.e. 'as low as reasonably achievable (ALARA)' (Rao *et al*., 2017; ICRP, 2012). ALARA is simply a process with the objective of attaining doses as far below the applicable limits as is reasonably achievable.

In the context of this study, the assessment of the external and internal radiological hazards of NORM in a study area is based on the calculation of radium equivalent activity (Ra_{eq}), internal and external hazard indices. The radium equivalent activity is assessed based on the assumption that 370 $Bq.kg^{-1}$ of radium, 259 $Bq.kg^{-1}$ of thorium and 4810 $Bq.kg^{-1}$ of potassium concentrations to produce same gamma dose (UNSCEAR, 1982). The Ra_{eq} activities are considered negligible when calculated values that are less than 370 $Bq.kg^{-1}$, an equivalence of gamma radiation public exposure level of 1 $mSv.y^{-1}$ from radioactivity in construction and building materials (UNSCEAR, 1982; OECD, 1979). The United Nations Scientific Committee on the Effects of Atomic Radiation (UNSCEAR) through evaluation data around the world in different materials recognized the need to propose radiation limits due to exposures by individual radionuclides. The world average values in soil are 33 $Bq.kg^{-1}$ for ^{238}U, 45 $Bq.kg^{-1}$ for ^{232}Th and 420 $Bq.kg^{-1}$ for ^{40}K, with median values of 30, 35 and 400 $Bq.kg^{-1}$, respectively, for three above-mentioned radionuclides (UNSCEAR, 2000). The world average values for ^{238}U, ^{232}Th and ^{40}K gives an absorbed dose in air indoors and outdoors of 84 $nGy.h^{-1}$ and 60 $nGy.h^{-1}$ from terrestrial gamma radiation, respectively (Birami *et al*., 2019). The national and international regulation stipulates that the annual inhalation doses to members of the public is 1 $mSv.y^{-1}$ (Stewart *et al*., 2012) and H_{ex} & H_{in} must be less than one (1) for the materials to be considered safe for building purposes (Ehsan *et al*., 2019). Exposure contributions from ^{222}Rn daughters inhalations are approximated at 0.92 Sv of indoor and 0.08 Sv of outdoor from ^{222}Rn inhaled exposures (UNSCEAR, 1982; UNSCEAR, 2000). These are the reference limits used by researchers to scientifically report findings based on the results.

The statement issued by International Commission of Radiological Protection (ICRP) in 2012 on dose limits due to tissue reactions in the human body, recommends that, for occupational exposures dose limit, the equivalent dose to the lens of the eye is 20 mSv in a year, averaged over defined periods of 5 years, with the dose in no single year exceeding 50 mSv (Huda *et al*., 2011; Vanhavere *et al*., 2011; Rao *et al*., 2017). ICRP 60 of 2007, reported also that the human exposure at 20 $mSv.y^{-1}$ for people at the age between 18 and 65 years can yield a maximum probability of cancer of about 1.0×10^{-3} and at 1 $mSv.y^{-1}$ as at birth can yield a probability of 1.5×10^{-4} in a year (ICRP, 2007). On situations of planned exposures, the ALARA principle is implored for these exposures and risks to ensure that the specified occupational and public exposure doses are within limits. Optimization is intended for attainment of desired level of protection and safety (IAEA, 1996). Table 2.5 shows the dose limits for planned exposure situations: occupational and public exposures (UNSCEAR, 2018; ICRP, 2012; Rao *et al*., 2017). In addition to that, recommendations by ICRP proposes that the dose limits for both pregnant women and public are similar. In the Japanese regulations, effective dose limit for workers is 100 mSv over a period of 5 years, with a maximum of 50 $mSv.y^{-1}$, with female workers the effective dose limit is 5 mSv in any three-month period (UNSCEAR, 2018; UNSCEAR, 2013). This values were derived for immediate adoption as "emergency dose limit" to be applied following Hiroshima accident for the workers responsible for emergency incidences. Table 2.2 summarizes the dose limits for occupational, and both public and pregnant groups.

Table 2. 2: The recommended dose limits to worker and the general public (ICRP, 2012; UNSCEAR, 2018).

Type of dose →	**Effective dose**	**equivalent dose**		
Type of exposure ↓	**whole body**	**lens of the eye**	**skin**	**extremities (hands and feet) or skin**
Occupational	20 mSv a year, averaged over defined periods of 5 years with no single year > 50 mSv	20 $mSv.y^{-1}$, averaged over defined periods of 5 years with no single year > 50 mSv	500 $mSv.y^{-1}$	500 $mSv.y^{-1}$

Public and pregnant women	1 $mSv.y^{-1}$ (higher values are permitted if the average over 5 years is not above 1 $mSv.y^{-1}$)	15 $mSv.y^{-1}$	50 $mSv.y^{-1}$	50 $mSv.y^{-1}$

Primarily, the uses of effective dose in radiological protection for the general population such as employees and the general public are mainly; the planning and optimization of protection on prospective dose assessment and the demonstration on compliances with limits of dose and/or comparisons with references levels or the dose constraints on retrospective dose assessments (ICRP, 2007). Generally, the effective dose is used for regulatory purposes and for managing of risks due to stochastic effects on employees and the general public. It is also important to note that effective doses are neither recommended evaluations of epidemiological studies, nor used for detailed retrospective investigations for exposures and risks to individuals.

2.7 Radiation detectors

Radiation monitoring instruments are very important and useful in monitoring exposures mostly from contaminated areas or areas likely to expose humans to radioactivity. In the industry, like nuclear power plants or radiotherapy centres, personal dosimeter badges are worn or carried by workers for the purpose of measuring radiation exposures. Radiation survey monitors are manufactured in the form of either solid state detectors or gas filled tube detectors. Environmental gamma radioactivity is measured by the use of portable scintillation or Geiger-Mueller (GM) counters. All instruments must be calibrated in terms of the appropriate quantities used in radiation protection (Rajan and Izewska, 2005). Other instruments are laboratory based, such as ion chambers, neutron survey meters, proportional counters and semiconductor detectors (Podgorsak, 2005). There are several criteria used for evaluating the performance of different types of radiation detectors such as sensitivity, energy resolution, efficiency and time resolution or pulse-resolving time of the detector (Loveland *et al*., 2017).

Other instruments known as personal monitors are used by employees working in high radiation risk environments. These instruments are thermo luminescence dosimetry (TLD), film, direct reading, optically stimulated luminescence, and radio-

photoluminescence glass badges (Podgorsak, 2005; Khan and Gibbons, 2014). They all measure cumulative doses of β and photons (X- and γ-rays) absorbed by the human body over time.

2.7.1 Geiger Muller counter

Geiger-Mueller (GM) counters were initially designed in 1928 by H. Geiger and E. W. Mueller as survey meters to measure environmental radioactivity. Their wall is made up of a thin metal cylinder acting as a cathode which surrounds the center electrode known as the anode. Their front part has a thin mica window sealed to the metal cylinder. Their thin mica window acts as passage that allows weak alpha particles to penetrate for detection. A GM tube, in Figure 2.13, is filled with gases such as neon, argon inclusive of halogens.

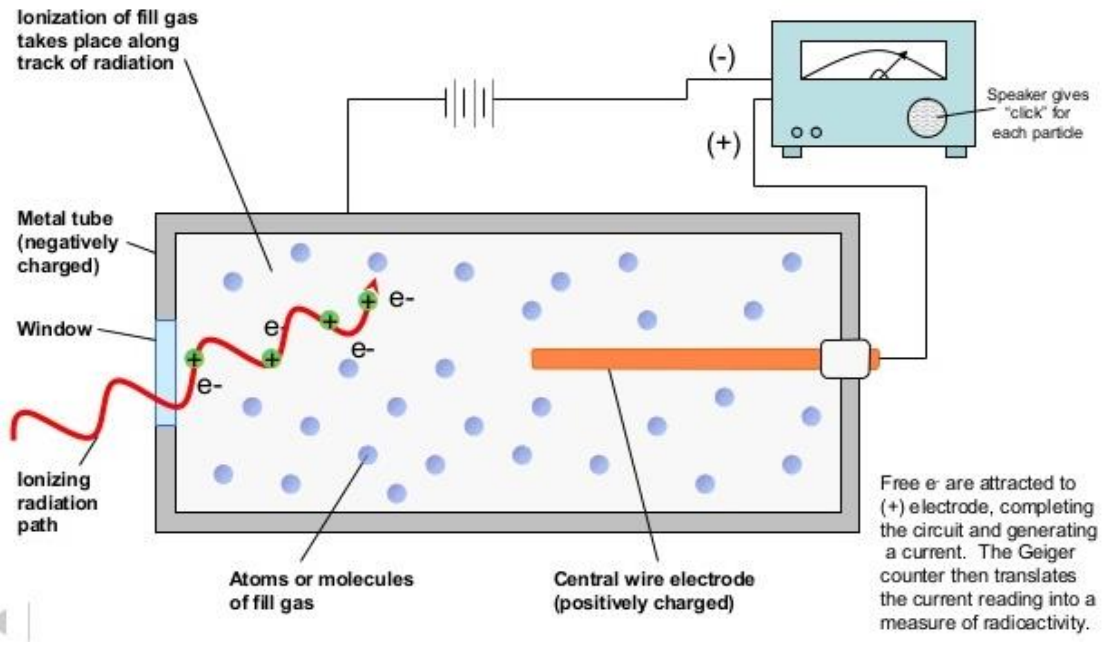

Figure 2. 13: An illustration of the inner structure of Geiger-Mueller counter (Quora, 2021).

The radioactive alpha particle passing through a mica window ionizes the molecules of gas confined in the tube and creates a conductive path within the gas. The liberated electron from an atom by the radioactive particle and the positively ionized atom move

rapidly towards the high potential electrodes with voltage of about +500 V. During that process, more collisions and ionizations with other gas atoms occur, which eventually creates an avalanche of ionized gas molecules. An electric current is produced which passes through the tube for particle detection (Obrenović *et al*., 2018).

2.7.2 Scintillation counter

A scintillation counter is similar to a GM-tube and ionization chamber which uses excitation effects to detect the resultant light pulses. It has scintillation crystals which produces light flashes when alpha, beta or gamma radiation interacts with them. The counter houses the scintillator and the photomultiplier tube (PMT). The flash of light produced by the scintillator is amplified by the photomultiplier tube. Each radiation interacting produces a pulse of the anode current at a photomultiplier output, counting each flash of light generated by the crystal. An illustrative diagram is shown on Figure 2.14.

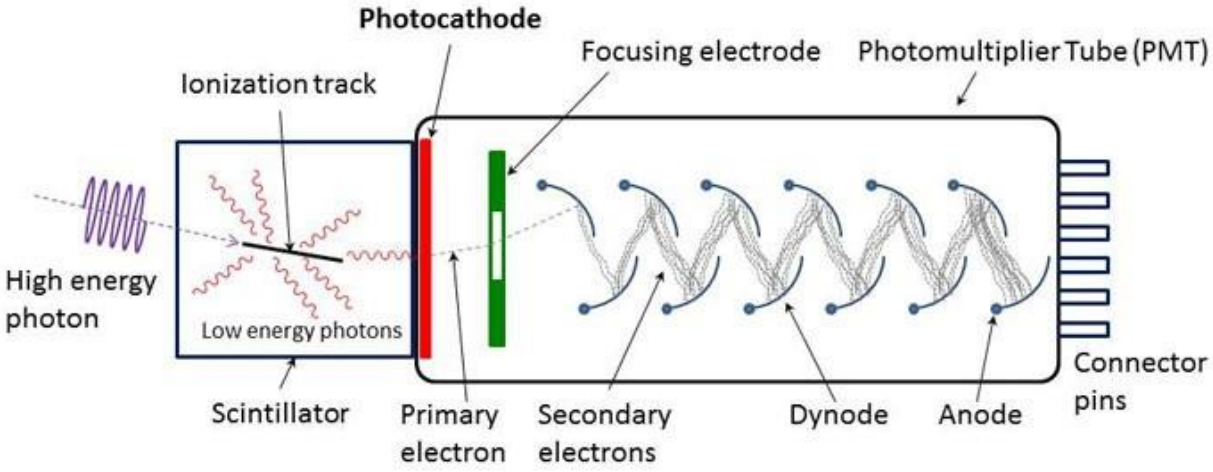

Figure 2. 14: The inside of a scintillation counter (Scionix, 2019).

2.8 Assessment of radiation

The aim of investigating and assessing radioactivity levels on various landscapes is to weigh the benefits and risks associated to human health. Assessment of radioactivity in

samples is done in laboratory by analytical techniques or on the site by means of survey meters as discussed on preceded topic on radiation monitors. The radiation statistics obtained is documented for future reference. Radiometric and mass spectrometric techniques (Sookdeo, 2015) are analytical methods used for determination of the toxic radionuclides and heavy metals in samples. Radiometric analytical (radioanalytical) methods are gross beta/alpha, alpha (α)-, beta (β)- and gamma (γ)-spectrometry, and mass spectrometric analytical methods using equipment such as inductively coupled-plasma mass spectrometry (ICP-MS) and optical emission spectrometry (ICP-OES), accelerator mass spectrometry (AMS), thermal ionization mass spectrometry (TIMS), resonance ionization mass spectrometry (RIMS), secondary ion mass spectrometry (SIMS), and glow discharge mass spectrometry (GDMS) (Sookdeo, 2015). This study only discusses gamma and ICP-MS analytical methods, which are used for analyses of samples under study.

2.8.1 Radiometric techniques

A number of radiometric techniques are discussed separately to understand the intended methods. These techniques include beta-alpha spectrometry, gamma spectrometry and liquid scintillation counter (LSC). These techniques are well-known for their use on the following areas: nuclear forensics, environmental radioactivity monitoring, minerology and geology, monitoring of industrial processes, NORM and/or TENORM, nuclear materials safeguards and security, nuclear reactor corrosion monitoring, radiopharmaceuticals and nuclear medicine, and health physics personnel monitoring

2.8.1.1 HPGe spectrometer detector

A high-purity germanium (HPGe) detector is a high resolution instrument used for spectrometry of gamma and X-rays. It operates at very low temperatures of liquid nitrogen. Liquid nitrogen (LN_2) is used for cooling the detector in a considerable environment at a temperature of 77 K (-195.79^{o}C). Most detectors that have been used in HPGe spectrometers are semiconductor detectors and sodium iodide thallium crystals (NaI (Tl)). Due to the high atomic number of germanium with its sensitive thickness of centimetres, it has larger attenuation coefficient which can create shorter mean free path

and can also be used as a total absorption of photons up to a few MeV. A complete gamma spectrometry system consists of important components such as the detector, cooling system and analysis software.

It is of high importance that the purity of the detector material be considered to provide tremendous gains in measurements capability (Mirion, 2015). Detectors are crystalline solids whose performance are mainly affected by three factors: (i) the lattice with interstitial atoms and vacancies with structural defects, (ii) semiconductor lattice with impurities, and (iii) interstitial atoms caused by the damage of radiation.

These structural defects, impurities and interstitial atoms that may ruin the detectors' performance are avoided when germanium crystals are eventually doped with lithium ions (Ge(Li)). Semiconductor detectors made of germanium or silicon compensated with lithium provide significantly better energy resolution. The peaks obtained by NaI(Tl) detectors are broader than those of germanium detectors by comparison, so peaks close together cannot be resolved by uncertainty and very difficult to separate at low-energy peaks. For successful operations of HPGe detectors requires use of liquid cryogens to reach cryogenic temperatures, i.e -196^{o}C for LN_2. Maximum efficiency of the semiconductor detectors was achieved only when operating on a very low temperatures, which avoids high noise caused by thermal excitation. Cryostat configurations and Dewar sizes with LN_2 are used to support radiation detectors (Figure 2.15). The detector and first stage of amplification circuit are enclosed in cryostat for noise reduction and cooling with liquid nitrogen to the required temperature (Loveland *et al*., 2017). Mirion Technologies formerly known as CANBERRA has manufactured slimline cryostats with detectors and electronics fitted in a cylindrical housing without protruding valves, flanges and preamplifier enclosures. The detectors have good resolution, and are used in measurements of radiation levels in a variety of applications such as environmental and personnel monitoring for contaminations, nuclear security, nuclear plant safety, radiometric essays and other medical applications. In gamma spectrometry, the high-purity germanium detectors that are being manufactured in the present day can achieve a net impurity concentration as low as 0.8 x 10^{10} cm^{-3} (Mirion, 2015). Hence, a large depletion depth, in Figure 2.16, is required to increase efficiency and for a complete

charge collection during measurements. It is also important to note that the thickness of the depletion depth (depletion region) d of the semiconductor detectors is given by the equation (Mirion, 2015):

$$d = (\frac{2\varepsilon V}{eN})^{\frac{1}{2}} \quad (2.29)$$

where, ε, V, e and N are dielectric constant, reverse bias voltage, electric charge and the net impurity concentration in the semiconductor detector, respectively.

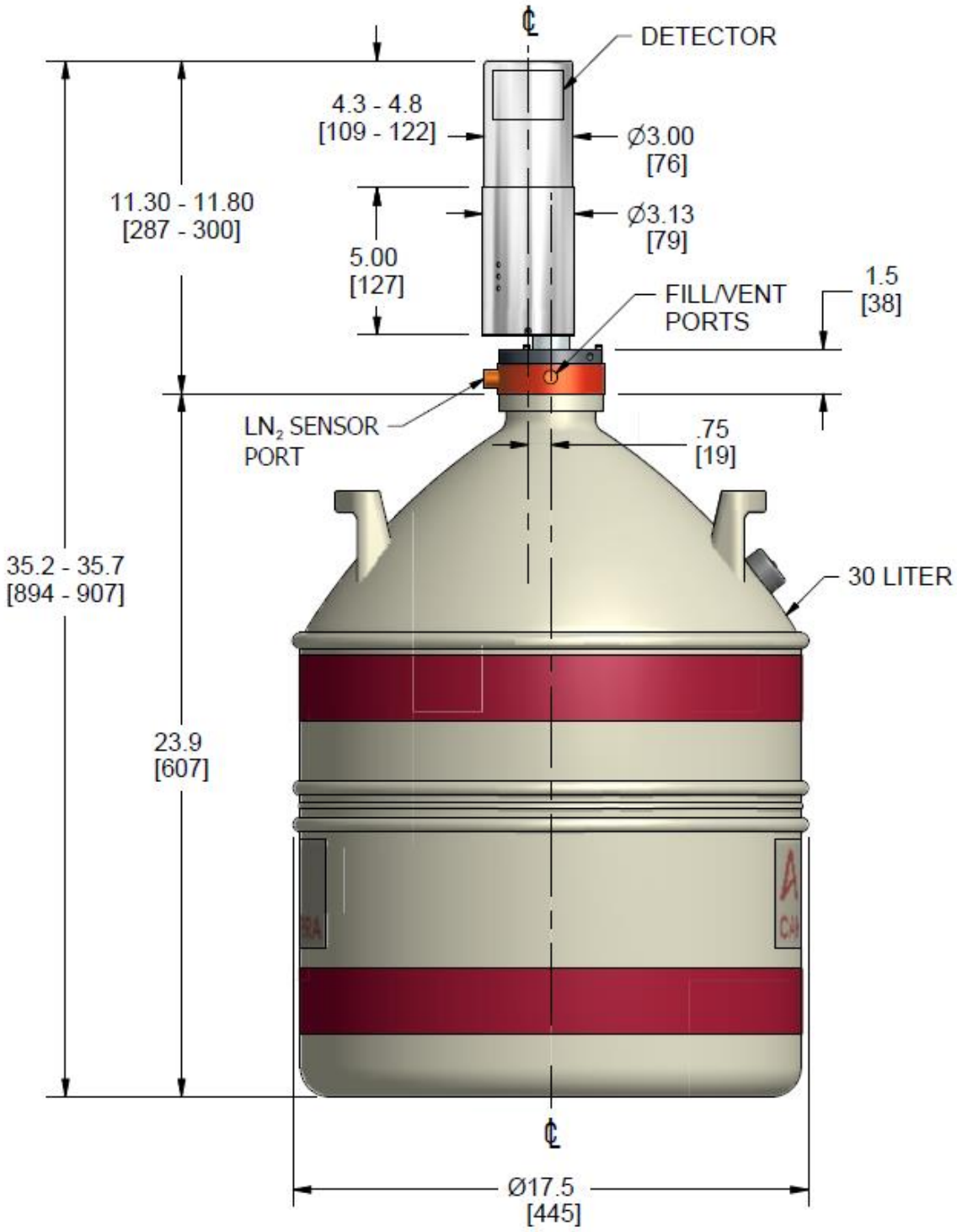

Figure 2. 15: 7500SL Vertical Dipstick in D-30 Dewar (Gene, 2000).

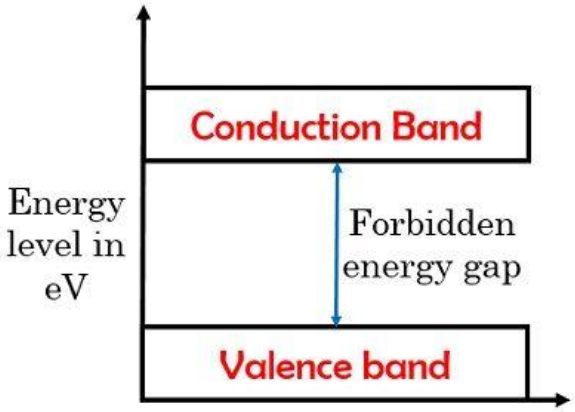

Figure 2. 16: The energy band diagram of a semiconductor detector (Globe, 2021).

The band gap is small for semiconductors, in comparison to that of insulators, such that the incident charged particles or applied electric field can impart energy that is enough for move electrons to move from the valence band to conduction band. Unlike conductors whose conductivity decreases due to increase in temperatures, conductivities for semiconductors rises with the rise in temperature which results in thermal increase of excited electrons (Trachanas, 2018). In addition, electrons carry current in conductors, whilst in semiconductors current also flows in the form of holes, empty spaces left behind in the valence band by thermally excited electrons. These holes created on the valence band behave as positively charged particles, contributing to overall conductivity in the semiconductor detector. The band gap energy (forbidden energy gap) for semiconductor detectors is approximately 1 eV ($E_g \approx 1$ eV). A germanium detector has the highest resolution of any direct ionization devices because of its small band gap energy of 0.73 eV and effective ionization potential of 2.95 eV (Loveland *et al*., 2017). The comparison between the valence and conduction bands are shown in Table 2.3.

Table 2. 3: Valence and conduction bands of semiconductor detectors (Mirion, 2015).

Basis	Valence Band	Conduction Band
Existence with respect to fermi-level	It is present below fermi-level.	Its existence is above fermi-level.
Effect of external excitation	Electrons move out of valence band	Electrons reaches the conduction band.
Energy state	Lower	Comparatively higher
Electron density	High	Low
Force by nucleus	Strong	Weak
Presence of electrons causes band to be filled	Partially or completely filled.	Empty or partially filled.

Multichannel analyzers (MCAs) are regarded as workhorse instruments in many approaches involving scientific measurements. They are designed purposefully to analyze streams of voltage pulses and arrange them into a spectrum against/versus pulse-height. Pulse heights often represents energy. The spectrum collected by the detector is displayed on the personal computer screen and eventually analyzed to identify and quantify the radionuclides of interest. Multichannel analyzers are categorized as; (i) basic analog for nuclear instrument module (NIM) Modular and standalone USB connected MCAs, (ii) integrated digital workstation MCAs for HPGe radiation detector systems, (iii) portable digital MCAs for scintillation and HPGe radiation detector systems, and (iv) digital photomultiplier tube (PMT) base MCAs containing digital signal processors and bias supply used in scintillation radiation detector systems.

2.8.1.2 The application of gamma spectrometry in radioactivity studies

Gamma spectrometry technique involves the identification and/or quantification of multiple radionuclides by analysis of the energy spectra produced in a γ-ray spectrometer, and may be applied in geochemical investigation, astrophysics and nuclear industry radioactivity. This technique is clearly and well understood for its use in radioactivity measurements of soil samples. Nagaraju *et al*. (2012) reported activity concentrations determined by gamma spectrometric technique on soil samples. The study indicated that

samples were stored in vials for measurements of mass and in polyethylene containers for liquids to allow for the equilibrium of ^{226}Ra with its decay products (^{214}Bi and ^{214}Pb) after sealing. The gamma ray measurements of samples were carried out using high-purity germanium (HPGe) detectors, containing a 10 cm lead (Pb) shielding, with a resolution of 1.8 keV, relative efficiency of 20.6% and an active volume of 250 and 100 cm^3 for liquid and solid samples, respectively (Nagaraju *et al*., 2012). For the analysis, the 186 keV gamma ray emitted by ^{226}Ra was used. The gamma ray spectra were analysed by using a software program which calculates the activity concentration of ^{226}Ra relative to the specific reference time and the density of the sample. As a tradition, the natural background level is always subtracted from each recorded spectrum (Durusoy and Yildirim, 2017). Gamma-ray spectrometry using HPGe gamma-ray detector and a PC-based MCA was applied in north of Malaysia to assess NORM (^{226}Ra, ^{232}Th, and ^{40}K) in agricultural and virgin soils (Alzubaidi *et al*., 2016). Except for potassium (^{40}K), the average activity concentrations ($Bq.kg^{-1}$) of ^{226}Ra and ^{232}Th in virgin and agricultural soils were higher than the world average values recorded in soils (UNSCEAR, 2000). For both samples, the mean value of gamma absorbed dose in air outdoor values were higher than the global average value of 60 $nGy.h^{-1}$ reported by UNSCEAR (2000).

Radiological aspects of soil samples from abandoned mine were investigated with the aim of investigating radiological levels and assessing the associated hazards in Serbia (Arafat *et al*., 2017). The aim of the study was to compare the results with those obtained in background area. Again here, samples collected were analysed using a Hyper-pure germanium detector to analyse the concentration of ^{226}Ra series, ^{232}Th series, ^{137}Cs radionuclides and ^{40}K (Arafat *et al*., 2017; Jayasheelan *et al*., 2013). The findings showed that from the calculated radiological hazard indices, there were no risks to people's health. However, people could be affected by radiation in one site, where the representative level index (1.052 $Bq.kg^{-1}$) and absorbed gamma dose rate (66.5 nGy^{-1}) exceeded the maximum permissible limits (Arafat *et al*., 2017).

Another assessment of radioactivity in the environment, done in the capital of Serbia, was performed using gamma-ray spectrometry (Mandić *et al*., 2010). In this study of 130 samples collected, the activity concentrations of uranium, potassium and thorium were

analysed again using HPGe gamma detector. Results of the soil samples collected from 45 locations were showing that the mean elemental concentration of uranium, thorium and potassium were 2.52±0.73 mg.kg^{-1}, 9.40±2.86 mg.kg^{-1} and 1.60±0.40%, respectively, which were compared with other studies worldwide (Mandić *et al*., 2010).

Furthermore, a study on assessment of radioactive materials and heavy metals in the surface soil was conducted in China (Bai *et al*., 2017). During this approach, both natural and anthropogenic radionuclides and heavy metals in 48 surface soil samples collected were analysed using HPGe spectrometry and ICP-MS (Bai *et al*., 2017). The aim was to estimate the average absorbed dose rate and annual effective dose rate, both external and internal hazard indices, and the radium equivalent activity.

Similar work was done in Nigeria on ^{226}Ra, ^{232}Th and ^{40}K radionuclides in soil (Isinkaye and Emelue, 2015). Their mean activity concentrations were found to be 47.89±18.67 Bq.kg^{-1}, 55.37±32.74 Bq.kg^{-1} and 1023±474 Bq.kg^{-1}, respectively. The radiological indices and dose rates obtained in this study were above the worldwide mean values but lower than their maximum recommended limits (Isinkaye and Emelue, 2015).

2.8.2 Mass spectrometry

Several mass spectrometric techniques such as inductively coupled plasma-optical emission spectrometry (ICP-OES) formerly known as atomic emission spectroscopy (ICP-AES), flame atomic emission (FAE), flame atomic absorption (FAA), graphite furnace atomic absorption (GFAA) and atomic absorption (AA) have been considered for use on various sample analysis recently (Wilschefski and Baxter, 2019). Mass spectrometers are more successful in different aspects, depending on what the researcher is looking for. This study discriminates other mass spectrometric techniques by specifically concentrating on ICP-MS as a mass spectrometric technique, which often is used by many researchers in Southern Africa in modern days.

2.8.2.1 Inductively coupled plasma-mass spectroscopy (ICP-MS)

The inductively coupled plasma-mass-spectrometry is a technique that determines elemental concentrations of samples by mass. It analyses low concentrations parts-per-

billions (ppb) and ultra-low-concentrations in parts-per-trillions (ppt). This is a technique which ionizes the sample by plasma, atomizes the sample and develops ions. These atomic and polyatomic ions are detected and recorded according to their masses. Also, regarded as best techniques which analyses metals and non-metals in a wide dynamic range of samples at very low concentrations by tracing elemental concentration of isotopes with a combination of precision, accuracy and analysis speed. There are several methods used to manage the acquisition of data; TotalQuant, quantitative, isotope ratio, isotope dilution and data only and these have been employed by softwares like ELAN and Syngistix.

The principle of the ICP-MS instrument is to determine multi-elements by mass of those particular trace elements. A pneumatic nebulization draws a solution into a radiofrequency plasma where energy transfer processes cause desolvation, atomization and ionization. The ions are extracted from the plasma through a differentially pumped vacuum interface and separated on the basis of their mass to-charge ratio by a quadrupole mass spectrometer having a minimum resolution capability of one atomic mass unit (1 amu) peak width at 5% peak height (Long and Martin, 1997; Caridi *et al*., 2019). An electron multiplier or Faraday detector receives and detects the ions transmitted through the quadrupole, and this ion information is processed by a data handling system.

There are interferences resulting from a combination of two or more elements/isotopes of different atoms that appear in the plasma with same mass, known as polyatomic interferences. Polyatomic interferences are encountered and have to be corrected by setting the instrument onto the appropriate mode for trace elements under investigation. Isobaric elements and polyatomic ions derived from the plasma gas, sample matrix and/or reagents contribute to these interferences.

The results from ICP-MS technique can be converted into activity concentration of specific radionuclides present in sample under study. ICP-MS technique was used to analyse heavy metal contents of chromium (Cr), nickel (Ni), copper (Cu), zinc (Zn), arsenic (As), cadmium (Cd), and lead (Pb) from the surface soil samples in China (Bai *et al*., 2017), and copper, zinc, lead, boron (B), arsenic and cadmium from red, rose and white wines

in Italy (Caridi *et al*., 2019). The main aim was to assess health risks. Except for lead which was about three times higher than that of China's mean, the rest of all other heavy metal showed that they did not exceed the average backgrounds of the country. The health risks estimated were falling within acceptable ranges/limits. The experimental results of wines in Italy show that they are lower than the contamination threshold values set by the Italian Legislation. Therefore, this research concluded that the concentrations of heavy metals in the surface soils and wines were at normal level.

In addition, ICP-MS can be used to determine levels of ^{238}U and ^{232}Th NORM in samples as assurance legitimate levels are achieved (PerkinElmer, 2017). During samples analyses, interferences on some elements are encountered. They are classified as spectroscopic and non-spectroscopic interferences. There are four types of spectroscopic interference in ICP-MS: isobaric elements, double charged ions, polyatomic ions and tailing interference (Wilschefski and Baxter, 2019). The determination of potassium by ICP-MS is limited by isobaric interferences of polyatomic species produced from argon in the plasma source (Nisi *et al*., 2017; Wilschefski and Baxter, 2019). This is a challenging task to perform on the instrument set on standard mode. Potassium-39 is the most abundant isotope and therefore regarded as the reference isotope during measurements. Also, the polyatomic species $^{38}Ar^{1}H$ (39 amu) is the most critical one since argon is the plasma gas and it is present at high concentrations (PerkinElmer, 2017). This applies to other two potassium isotopes, ^{40}K and ^{41}K, whose measurements have isobaric interferences of Ar species, ^{40}Ar (40 amu) and $^{40}Ar^{1}H$ (41 amu), respectively. Polyatomic ions form in the high-temperature plasma, either due to incomplete atomisation or from recombination reactions during the extraction of ions into the mass spectrometer (Wilschefski and Baxter, 2019). Reagents used for sample preparation, such as hydrochloric acids (Wilschefski and Baxter, 2019), plasma gas or sample matrix (Caridi *et al*., 2019) may also contribute to interferences. However, hydrochloric acid which is occasionally used stabilises mercury in a solution and only cause spectroscopic interference on vanadium and arsenic (Wilschefski and Baxter, 2019). In order to overcome these troubles, spectrometers are equipped with a collisions-reaction cell (CRC) with high resolutions.

NexION 2000 series of ICP-MS instrument is equipped with Universal Cell Technology™ (UCT) functionality for measurements of samples. Therefore, it can be operated in standard mode for routine analyses, dynamic reaction cell™ (DRC™) mode for ultimately low detection limits (compatible for oxygen and ammonia gases); or in easy-to-use Kinetic Energy Distribution (KED) mode for rapid analysis (PerkinElmer, 2017). Only collision-reaction cell mode is discussed on the next section for consideration of corrections of potassium interferences during measurements of samples.

2.8.2.2 Collision-reaction cell (CRC) mode

The kinetic energy distribution method does not need an in-depth knowledge of the sample before preparation and applies to all polyatomic interferences. This system discriminates between the kinetic energy of analyte ions and that of their interferences by creating a positively-biased voltage between the mass analyzer and the cell (PerkinElmer, 2017). Kinetic energy distribution (KED) occurs when an inert gas such as helium is used in the CRC, ions generated in the ICP undergo collisions with gas molecules causing a reduction in kinetic energy (Wilschefski and Baxter, 2019). Analyte ions are affected to a lesser extent than polyatomic ions. The probability of collisions of a helium inert gas with the polyatomic interferences is based on the relatively larger collisional cross-sections of the polyatomic ions. Collision reaction of gas with the sample solution occurs inside the plasma. Larger cross-sections of polyatomic ions discriminates them to undergo more collisions then analytes. The appropriate voltage difference between reaction cells and the analyser quadrupole is set to filter out the polyatomic ions, allowing analyte ions to prevail through this energy barrier. Figure 2.16 shows a diagram of an ICP-MS with inlets for samples through to the detector. The sample in a liquid form enters through a torch, then plasma housed in a coil, the sample and skimmer cones before being sprayed through to the electrostatic lenses in the form of ion beam (Figure 2.18).

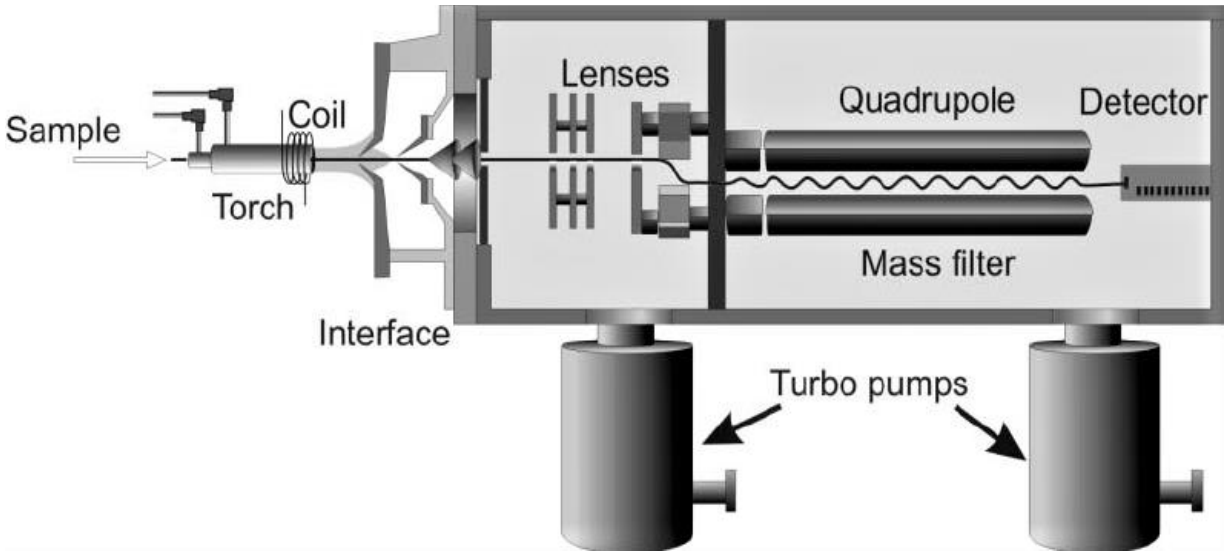

Figure 2. 17: The cross-sectional diagram of the ICP-MS (Košler and Sylvester, 2003).

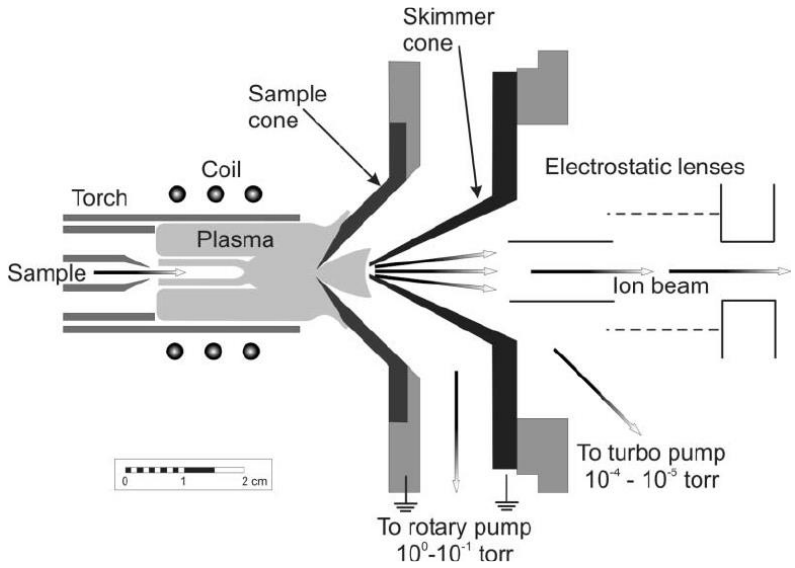

Figure 2. 18: The cross-sectional diagram of the interface on the ICP-MS (Košler and Sylvester, 2003).

In the process, analyte ions lose kinetic energy due to collision reaction cells and sudden reduction in polyatomic interference results in a much high signal to background ratio for the analyte (Wilschefski and Baxter, 2019). KED mode is especially useful in applications where moderate detection limits are required for multi-element analyses in complex matrices (PerkinElmer, 2017), unfortunately working only for polyatomic ions but not for both isobaric elements and double charged isobars (Wilschefski and Baxter, 2019). A

reactive gas in the CRC may chemically resolve isobaric ions by one of the following three important detection mechanisms (Wilschefski and Baxter, 2019):

(a) On-mass detection: the interfering ion reacts with the gas, forming a new polyatomic ion with a different mass to the analyte. The analyte can then be measured free of interference. This is the detection mechanism considered during measurements of concentrations for nuclides of interest in this study.

(b) Off-mass detection: the analyte reacts with the gas, forming a product ion with a different mass. The analyte can then be measured indirectly using the product ion mass.

(c) Neutralization: the interfering ion is neutralized via a charge exchange reaction with the gas.

2.9 Modelling software

It is generally difficult and cumbersome to manually determine the cancer risks of a population over a lifetime (NRC, 2006). Hence, a number of computer programmes are used for modelling the radiological impacts of radiations from a variety of sources on living organisms. Softwares such as RESRAD, Safran, Ecolego and Normalyssa can be used in the dynamic industry to approximate the risks associated with radiation exposures or intake of natural occurring radioactive materials to humans.

RESidual RADioactivity (RESRAD) is a computerized software inbuilt modelling code tool developed for deterministic/probabilistic analyses of doses and risks associated with residual radioactivity from NORM, at user's specified time (Yu *et al*., 2001). This in-built code incorporate default parameter distribution based on average input data. Figure 2.19 shows a schematic diagram of exposure pathways and RESRAD family of codes' web diagram used for different purposes, respectively. Upon running the tool, results are shown in the form of deterministic graphics such as interactive output, graphics and text reports (Kamboj *et al*., 2000). In this study, this modelling tool was used to estimate the potential radiologic annual doses and cancer risks to members of the public due to NORM from both mines and residential areas through a variety of exposure pathways defined in Chapter 3, Section 3.7. The estimation of total dose from all possible exposure pathways considered in RESRAD (Figure 3.30) can be done by utilising RESRAD-OFFSITE model,

which was considered for this study on samples collected from mining zones (Yu *et al*., 2001).

.

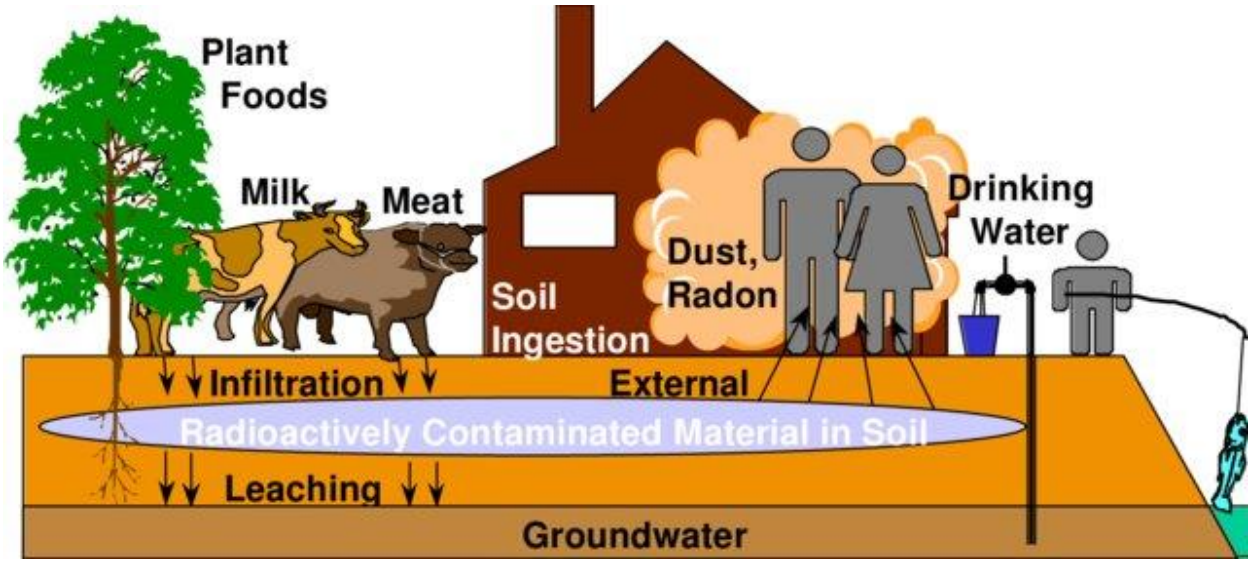

Figure 2. 19: Schematic diagram of exposure pathways (Kamboj *et al*., 2000).

The pathway analysis deriving the guidelines of concentrations from dose limits consists of four main parts: environmental transport, source, dose or exposure and scenario analysis (Yu *et al*., 2001). In terms of source analysis, source terms are derived to determine the rate of release of residual radioactivity into the environment. It depends on the concentrations of radionuclides under consideration, the geometry of a contaminated zone, ingrowth and decay rates of radionuclides as well as leaching and erosion rates. Analysis of environmental transport is based on pathways of nuclides to reach human exposure area and migration rate of this pathways. Dose or exposure analysis basically addresses on derivation issues of dose conversion factors (DCF) of radiation doses incurred during exposure to ionizing sources. Exposure scenarios determines patterns of human activities in consideration of parameters that control release rate of radionuclides into environment, with the severity and human exposure duration at given locality.

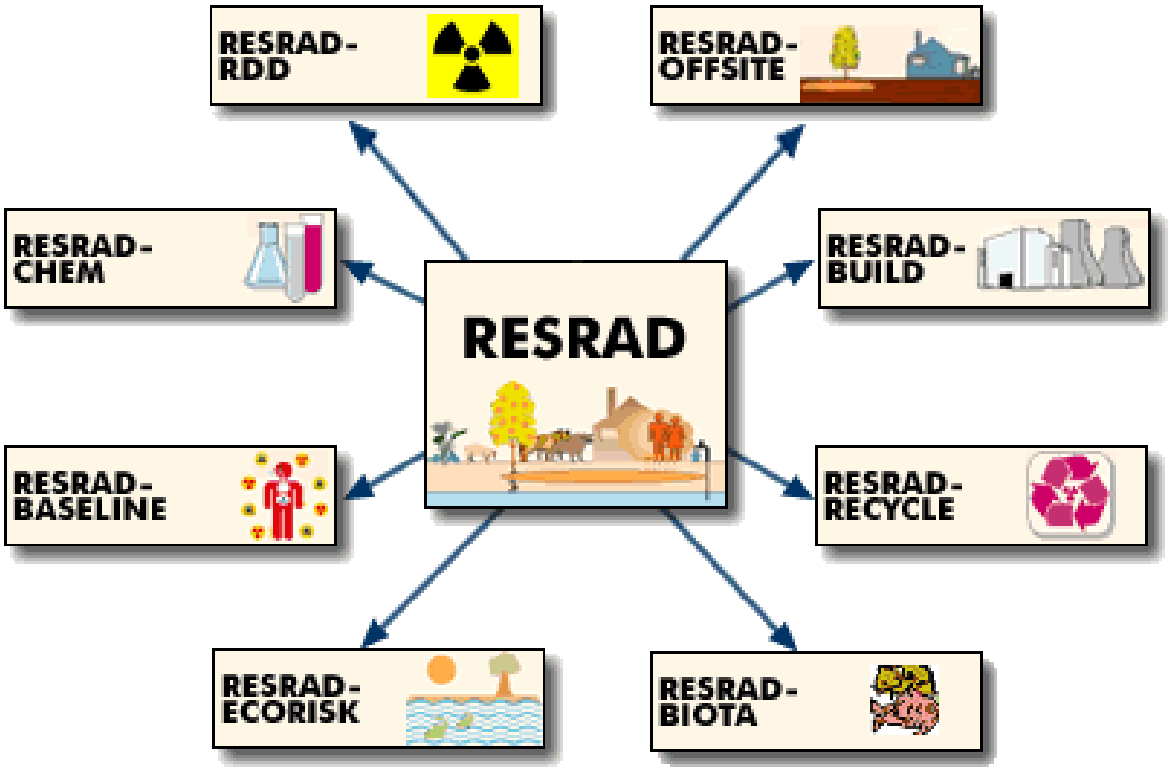

Figure 2. 20: The web diagram of RESRAD family of codes (Yu *et al*., 2001).

2.10 Exposure pathways

Gamma radiations from ^{220}Rn, ^{222}Rn, ^{235}U, ^{238}U, ^{232}Th and ^{40}K decays contributes to increased exposures of a human population. The most common exposure pathways in the environments are soil, water, crops or vegetation, animal and atmosphere (Yu *et al*., 2001). The transportation of radionuclides through these media in the environment may lead to their ingestion, inhalation and/or external exposures to humans. Figure 2.21 is an illustration of parameters for exposure pathways considered for comprehensive risk assessment analysis. A radioactive material may be inhaled, ingested or it enters through the bloodstream and these are referred to as internal exposures. One can only reduce this exposure when a radionuclide is fully eliminated from the body through excretion or by treatment. The main uptake pathway of uranium into the body is via the food chain (Faanu *et al*., 2010). Therefore, a knowledge about chemical behaviour of uranium

distribution and accumulation in a bio-system will make a good transition from geo-system to bio-system.

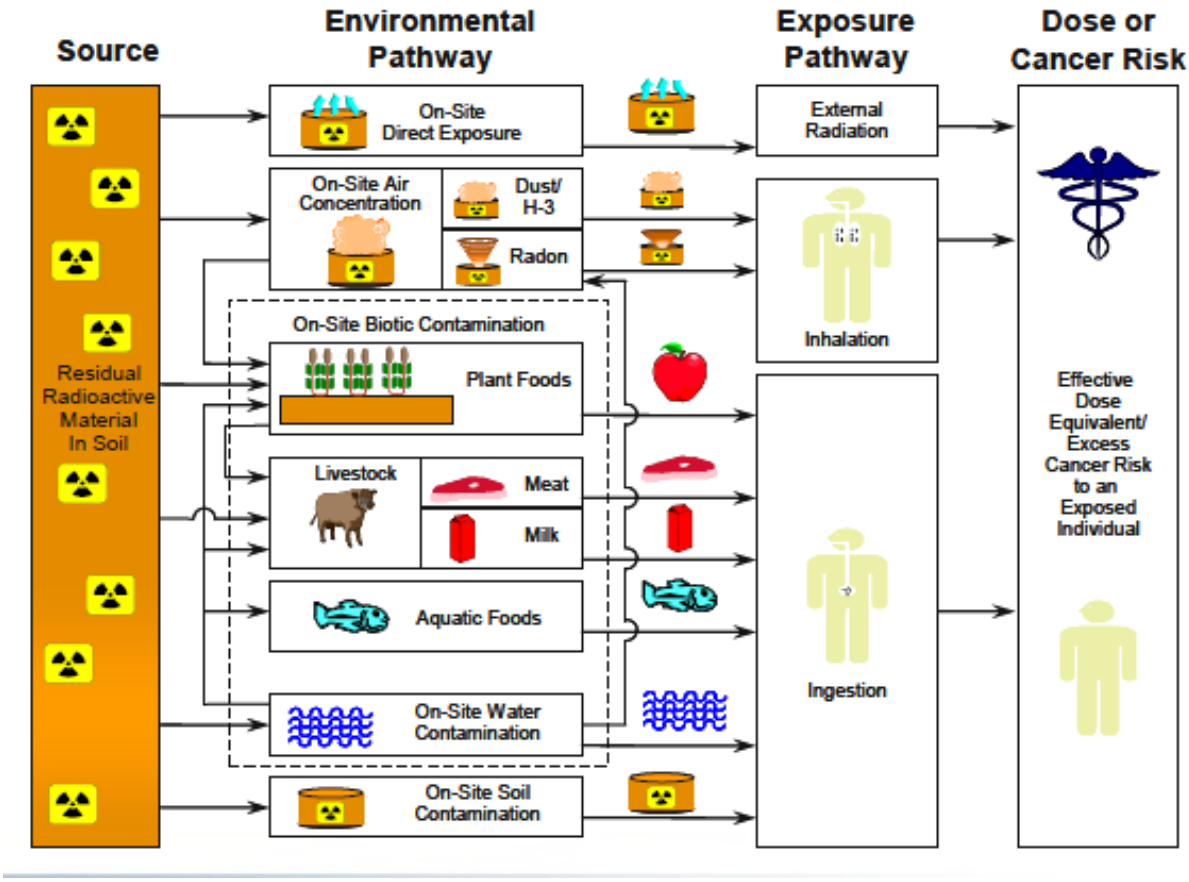

Figure 2. 21: Pathways for performing a comprehensive risk assessment analysis (Yu *et al*., 2015).

Thorium has exceptionally very low solubility in natural waters and is entirely transferred via dust and it is slightly in metallic form. Chemically, thorium corrodes slowly when it gets into contact with water and dissolves readily in hydrochloric acid, except other most common acids. It also dissolves in concentrated nitric acid containing a small amount of catalytic fluoride ion. Other thorium radioisotopes are observed in the thorium and uranium decay series. Thorium element is also found in small amounts in most rocks and soils, where it is about four times more abundant than uranium (Faanu *et al*., 2010). It occurs in a form of various minerals such as thorite ($ThSiO_4$), thorianite (ThO_2 +UO_2) and

monazite a phosphate mineral. It contributes readily to human exposures internally and externally. To reduce or avoid external exposure, a proper shielding is required.

2.10.1 Identification of pathways

There are three major exposure pathways by which radiations can enter the human body. Major pathways are identified as external radiations from radionuclides exposed to the body's skin, the inhalation of radionuclides through dust or radon itself, and the ingestion of contaminated soil, food, milk or water. With beta and gamma radiations from radionuclides being distributed within the contaminated zone, then external radiation pathways become dominant. External radiation dose for individuals is calculated with correction factors applied for the finite and thickness of contaminated zone (Kamboj *et al*., 2000; Yu *et al*., 2001).

In situations of contaminations by radon decay products and contaminated dust in the atmosphere, inhalation exposures occur. This inhalation pathway consists of an airborne exposure segment that links the source of radiation with airborne radionuclides exposed at locality of exposure (Mathuthu *et al*., 2016; Dudu *et al*., 2018). In addition to that, there is existence of a segment that links the airborne radionuclides with exposed individuals characterized by occupancy factor and inhalation rate factor (Yu *et al*., 2015).

2.10.2 Exposure situations

There are three situations that humans are exposed externally; (1) planned, (2) background (existing) and (3) emergency exposure situations. Planned exposure results from radiation sources used for specific purpose in authorised facilities and activities. Radiations used in medical procedures such as diagnostic imaging and radiotherapy, or used in research are examples of planned exposures. Existing exposure is a background radiation exposure which has been in continuous existence in the environment and requires that some regulatory decisions to be made following assessment of the situation. Gold mining residues, which had a quantity of uranium, in South Africa were dumped on open for approximately seventy (70) years, because uranium was not extracted from the milled ore (Winde and Sandham, 2004) and this could contribute more to both internal

and external exposures. Also, the presence of radon gas in buildings like homes, classrooms, offices and all buildings closed on the top contributes with poor ventillations could contribute to existing exposures. During situations of emergencies such as nuclear accidents, unexpected events occur and requires a prompt and immediate response – Fukushima (Tanigawa *et al*., 2012). It is also very crucial to know that most daughter radionuclides produced from a radioactivity decay, are transferred to the ecosystem and, eventually, to humans (Krisanangkura *et al*., 2013).

2.11 Conclusion

This chapter discussed about mining and milling activities which could increase radiation exposures in the environment. The discovery of radioactivity and types of radioactive decays by scientists, such as Curies, Roentgen, Becquerel and subsequent contribution by others was great annotations to build on for the main objective of this research. Radioactive equilibrium, which was applied in the identification and quantification of natural radionuclides in of NORM, was also discussed. Interactions of radiations with matter and their biological effects are of great importance during calculations of radiation hazards. The recommended radiation dose limits introduced by IAEA, ICRP and other organizations for the protection of humans due to radiations have also been discussed.

CHAPTER 3: METHODOLOGY

3.0 Introduction

This chapter focuses on all steps used or followed in order to achieve the main aim of the research, which was to evaluate the radiological impacts around the uranium mines in the Erongo Region. The analysed results were intended to contribute towards a database of radioactivity levels in the Erongo region. A descriptive research design was adopted for the study as it aimed to investigate the content of radionuclides released via various pathways to critical groups. Therefore, both quantitative and qualitative research methodologies were employed where applicable.

The study was carried out by collecting samples in the areas around the uranium mining activities of the Erongo region in Namibia where there are potentially high levels of pollution through the atmosphere (air and dust), soil and surface as well as ground water source. The sections include; description of the study area community, sample and sample preparations, and the principles of methods used in the analysis of the parameters.

3.1 Study area

Erongo region covers an area of 63,586 km^2, which comprises 7.7 per cent of Namibia's total landscape of about 823,680 km^2. It lies between -23.81 and -20.48 degrees latitude (south), and 13.64 and 16.55 degrees longitude (east) on the central coast of the country. The region is named after Mount Erongo, a well-known landmark in the region, and in particular Namibia. This region shares its borders with Kunene region (north), Otjozondjupa region (north-east), Khomas region (South-east), Hardap region (south) and then its coastline (west) with the Atlantic Ocean. There are two remarkable harbour towns of Namibia, namely; Swakopmund and Walvis Bay, found in the region. Other towns are found on the highlands such as Karibib, Usakos, Arandis, Henties Bay, Omaruru and Uis. The delineation of the region is shown in Figure 3.1, in the Namib desert regarded as a palaodrainage system with lots of palaochannels hosting calcrete-uranium deposits and prospects. Arandis town is located on the north-east of

Swakopmund, about 70 km inland along B2 road which networks from the harbour town of Walvis Bay, linking up with B1 road in Okahandja, Otjozondjupa region. On the north of Arandis, behind the Damara intrusive mountains is Trekkopje mine located about 25 km via B2 road. North-eastern side, on either sides of the Khan river which stretches from Usakos, are Rossing (west) and Husab (east) uranium mines, located about 15 km and 36 km from the Arandis town, respectively. Langer Heinrich uranium mine is located approximately 60 km on south-eastern mountains of Arandis.

An increase in exploration, mining and milling activities may pose a threat on exposures to residents of this region because of its high level of uniform uraniferous alaskitic meta-sediments. Since most of the mines are open pits, the chances of exposures are high because of blasting, loading and hauling of the raw ore grades from the pit before processing of the uranium bearing rock (von Oertzen, 2017). A recent population census statistic indicates continually increase of residents over the past few years (NPC, 2012). Due to the increase in population in the area a possible increase on dwellings may occur. These residents are members of critical groups since they are at risk of being exposed to radioactive materials resulting from exploration, uranium mining and milling.

Arandis and Karibib towns are not only close to uranium mines but to other mineral activities. The exposures are not limited to only the mentioned towns but also reach to other towns. The likely exposures to critical groups are external (gamma) and internal (beta/alpha) radiation through atmosphere as exposure pathway (dust). Inside the mines, company employees and medical personnel also fall in the category of critical groups. Borehole water (aquatic pathway), soil along the river and around mines were collected and analysed during the study.

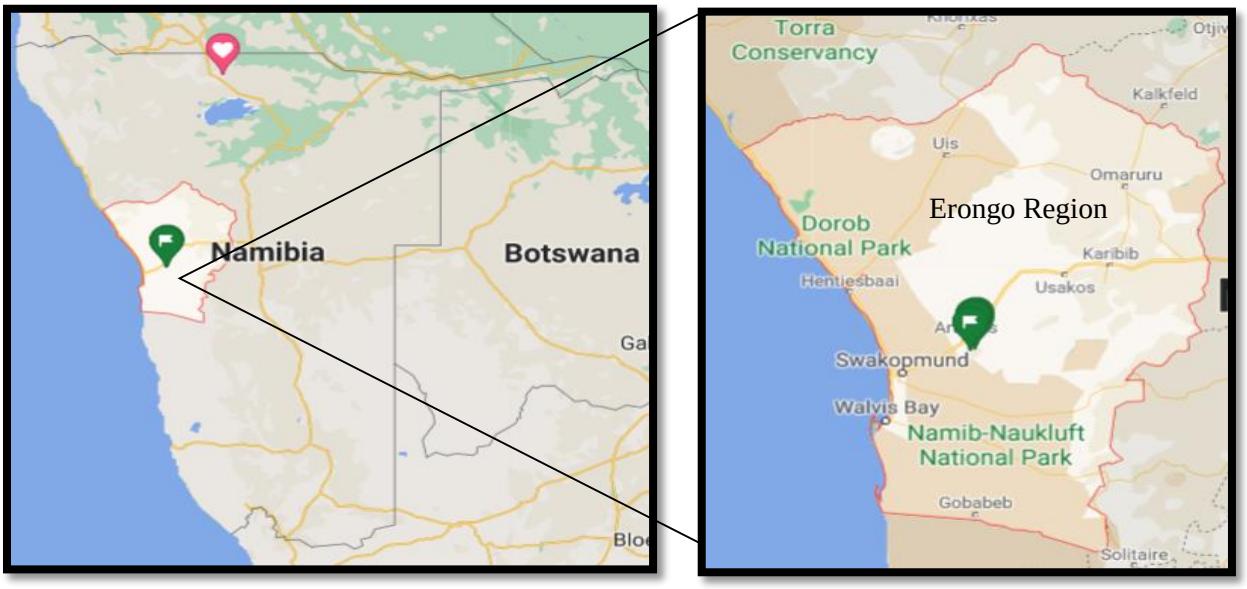

Figure 3. 1: The Erongo region map on (left) the central coastal and the (right) enlarged area of Namibia (Source: www.google.com/maps; accessed on 10 June 2021).

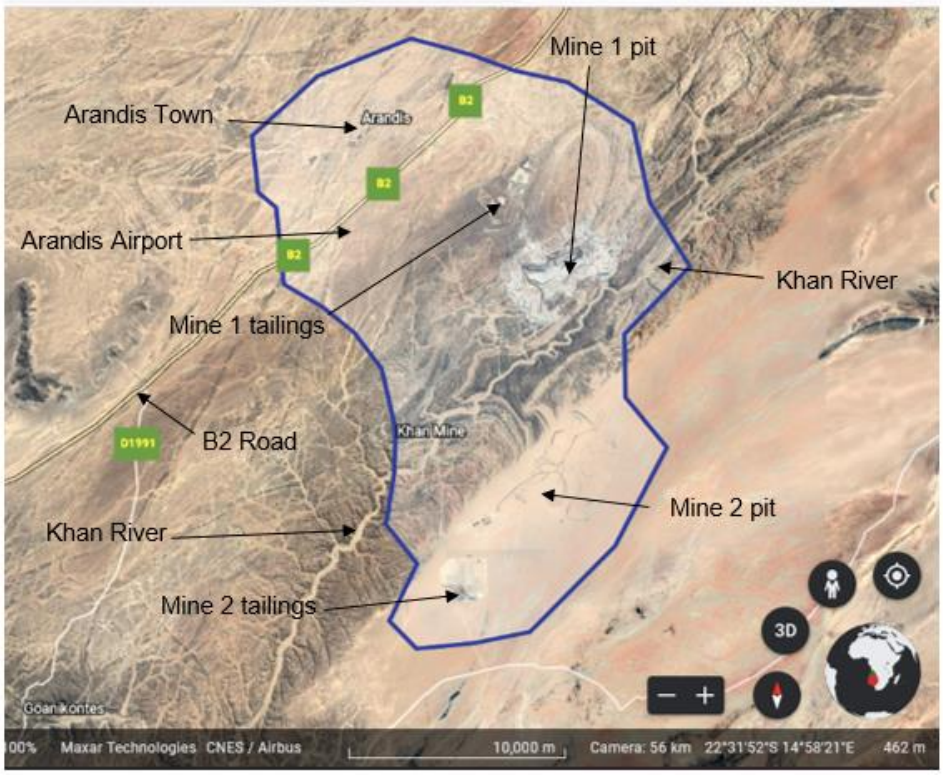

Figure 3. 2: The delineation of the study area boundary, with no collection points.

3.1.1 Geological structure and climate of Erongo region

Erongo region is a prominent mountainous landscape, blessed with uranium meta-sediments of schist, gneiss, quartzite and marble (CNNC, 2018), which is situated on the edge of the Namib Desert (Hegenberger, 1988). It is within this area where Erongo volcanic complex (EVC), one of a number of anorogenic complexes of the Damaraland alkaline province, is housed (Pirajno, 1990). The region is mineral rich in high grade of uranium hosted in a type of pegmatite granites called alaskites (Berning, 1986). It also endures arid climate with an average annual rainfall of 30 mm and alaskites is approximated between 70% – 90% (CNNC, 2018; Goudie and Viles, 2014). There are primarily two uranium rich minerals; the autunite ($Ca(UO_2)_2(PO_4)_2$*10-12(H_2O) and carnotite ($K_2(UO_2)_2(VO_4)_2 \cdot 3H_2O$) (Dickinson and Sullivan, 1976). Autunite minerals are hydrated calcium uranyl phosphates.

In the anarogenic complexes of the Damaland, uranium composite is found within carnotite, an oxide that contains uranium and vanadium within granitic rocks. The carnotite occurs as thin films lining grains, fracture planes and cavities or as disseminations (Marsh, 2009). Minerals are also largely found within calcium carbonate cemented conglomerates belonging to the tertiary period. Uraninite (H_4O_2U), formerly known as pitchblende, dominates with 55%, followed by secondary uranium mineral with 40% and the rest is refractory uranium minerals (CNNC, 2018). Erongo is no exemption to increase in exposure rate due to the presence of primordial radionuclides and their progenies, heavy and toxic metals which are of serious stochastic and deterministic effects, which may lead to cancer in the short and long run. The region receives an average annual rainfall of 50 mm and average temperature of 24^{o}C (MME, 2010). The region experiences also thick fog every morning, resulting in high humidity in the atmosphere and very strong winds capable of moving sand off the desert surface and tailings surface heaps. Wind is predominantly in the south-westerly in summer and also north-easterly to easterly during winter seasons (RE, 2018).

3.1.2 Population

Erongo region has a population of about 150 800, according to Namibia 2011 population and housing census preliminary results (NPC, 2012). This human population is considered for sample study, which includes persons accessing the mines, living in the vicinity and/or working in offices.

3.2 Sampling in study area

The sample collection from the study area was aimed at acquiring meaningful analytical results. First, the volume of samples of interest is important for satisfaction and filling of geometric containers used for counting on the analytical instrument. Random sampling strategy was employed to select the sampling sites in Arandis town and two operational uranium mines closer to Arandis; coded as sections A (Arandis), B (mine 1), C (Khan river) and D (mine 2) for confidentiality reasons. Sections B and D are the currently operating uranium mines in the region considered in this research as possible sources of radiation exposures to population and the potential radiological health hazards associated risks to the workers and the general public. Section A (Arandis town) is a residential area with residences of the nearest town in the region. For each sample collected the global positioning system (GPS) was recorded. The GPS values and names of the mines under study will not be published in this thesis because of the confidentiality agreements signed with the mines. Figure 3.2 shows some of the samples packed in their containers for transportation to the laboratory for analysis.

Figure 3. 3: Sampling process and well-coded plastics used for transportation to CARST analytical laboratory.

3.3 Samples collection and preparation

About 1.5 kg soil (78), 1 L water (20), 1 kg granitic uranium ores (8), 10 g dust (11) samples each were randomly collected from the study areas A, B, C and D in Erongo region, Namibia and transported to the Centre of Applied Radiation Science and Technology (CARST), North-West University (NWU), South Africa. Table 3.1 shows the type and number of samples collected from each study area. For computation of activity concentrations of radionuclides of interests, the daughter products can be used for best interpretations with assumed secular equilibrium.

Table 3. 1: The specific number of samples collected per section of study area.

Study Area	Description	Samples collected
Section A	Residential zone and the surroundings – 46 samples	• Forty (40) soil samples collected from the streets, airport and peripheries of the town. • Six (6) samples from the garden and heaps of soil used in the gardens.
Section B	Mining zone (mine 1) – 42 samples	• Eight (8) crushed uranium (granitic) ore samples • Ten (10) tailings water (TW) samples. • Ten (10) borehole water (BW) samples • Fourteen (14) soil samples from tailings and surroundings of the mine
Section C	Khan river – 6 samples	• Forty-four (6) soil samples
Section D	Mining zone (mine 2) – 23 samples	• Twelve (12) tailing soils • Ten (11) dust samples

3.3.1 Preparation of Soil and crushed uranium ore samples

All soil samples were spread on cartons and left on the open to dry for seven (7) days at room temperature prior to packaging, to remove all possible moistures. They were then crushed for homogeneity, filtered through a 2.0 mm sieve, and about 500 g of weighed samples were individually packed and sealed in well coded 500 ml cylindrical plastic containers, shown in Figure 3.3. The mass (m_s) for each sample was measured and recorded for use during calculation of radioactivity concentrations. Each sample was sealed in a container and stored for about 30 days, to allow parent radionuclide and its progeny to reach radioactive secular equilibrium.

For ICP-MS analysis, accurately measured masses of each dust sample were prepared for PerkinElmer Microwave Sample Digestion System (Titan MPS, PerkinElmer Inc., USA). Standard vessels with a volume of 75 ml were used for the digestion. An

approximate mass of about 0.500 grams of samples were transferred to the well-marked vessels. For each vessel, 9 ml of 35% hydrochloric (HCL) acid and 3 ml of 70% nitric (HNO_3) acid were added and then placed in the digester. A standard or blank sample was prepared with the same volumes of both hydrochloric and nitric acids into a blank vessel, and transferred to the digester together with the vessels with soil and crushed uranium ore samples. After digestion, the vessels were let to cool down and homogeneous solutions were diluted with ultra-pure Mili-Q (25 Ω), distilled water to make 50 ml. To reduce the concentration, 1 ml of an aliquot was pipetted into 10 ml of distilled water. Safety measures were put in place, especially for handling nitric and hydrochloric acids which were reagents utilized for digestions of samples. This process was handled inside a fume hood. Also gloves, laboratory coat, mask and safety glasses were worn as part of radiation protection measures during preparation.

Figure 3. 4: Drying of samples and laboratory apparatus used in preparations of soil samples for HPGe analysis.

3.3.2 Preparation of water and dust samples

The collected dust samples were also dried, pulverized and prepared for digestion. The same preparation procedure used for soil and crushed uranium ores was employed. Water was filtered using a Whatman 42 filter paper, removing particles of bigger sizes such as soil and dust (Sethy *et al*., 2014).

3.4 Calibration of detectors

3.4.1 Energy and efficiency calibrations for HPGe detector

Calibrations for energy and efficiency of the Canberra HPGe detector well-type detector were performed using IAEA radiometric reference materials; RGU-1, RGTh-1 and RGK-1, of powder samples equivalent to soil, provided by IAEA in cylindrical plastic containers in Figure 3.5. IAEA-RGU-1 standard sample source was prepared by dilution with silica sand of Canadian Certified Reference Materials Programme (CCRMP) Uranium Ore BL-5 (7.09% U) and IAEA-RGTh-1 standard source sample was prepared by dilution with silica sand of OKA-2 (2.89% Th, 219 µg U/g) (IAEA, 1987). To calculate efficiency of the gamma spectrometry instrument, the following equation is used (Tedjani *et al*., 2016):

$$\varepsilon = \frac{C_{n,p}}{A\,(Bq)\;x\;I_{\gamma}\;x\;T(s)} \qquad (3.1)$$

where, $C_{n,p}$ is the total number of counts per peak area under calibration, I_{γ} is the gamma probability emission and T is total time of acquisition.

Efficiency calibration curve of the detector as a function of energy is a smooth curve which falls exponentially with increase in energy on the spectrum window. These calibrations were performed well prior to counting of samples, with known activities of radioactive nuclides. This is the most important quality control and quality assurance procedures which have to be performed on every analytical instruments for accuracy and performance. Calibrations of analytical instruments are done in accordance with recommended procedures by international standard agencies, and in this case, the IAEA. Figure 3.6 shows a schematic setup at CARST, and the linear channel vs energy graph is shown in Figure 3.7.

Figure 3. 5: The IAEA radiometric reference materials; RGU-1, RGTh-1 and RGK-1 for calibration of both energy and efficiency for HPGe detector at CARST.

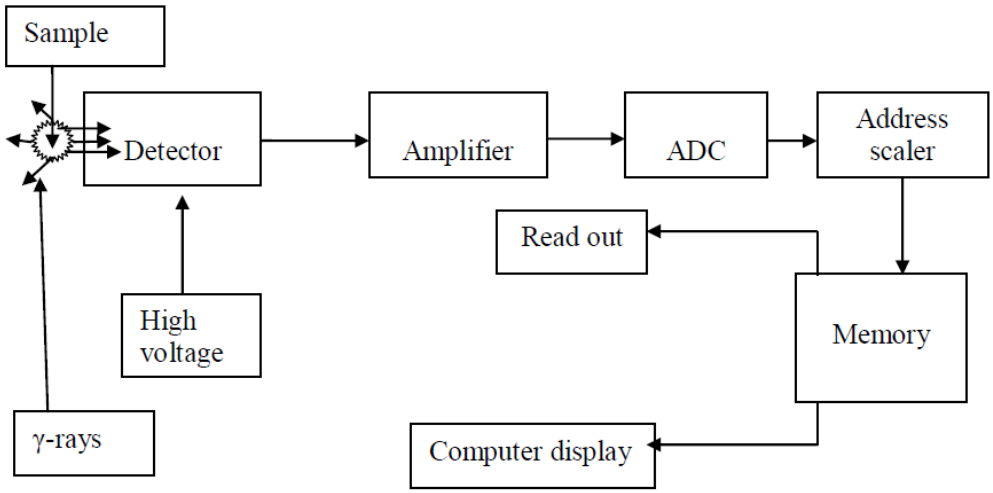

Figure 3. 6: A schematic setup of the gamma spectrometry in the CARST laboratory.

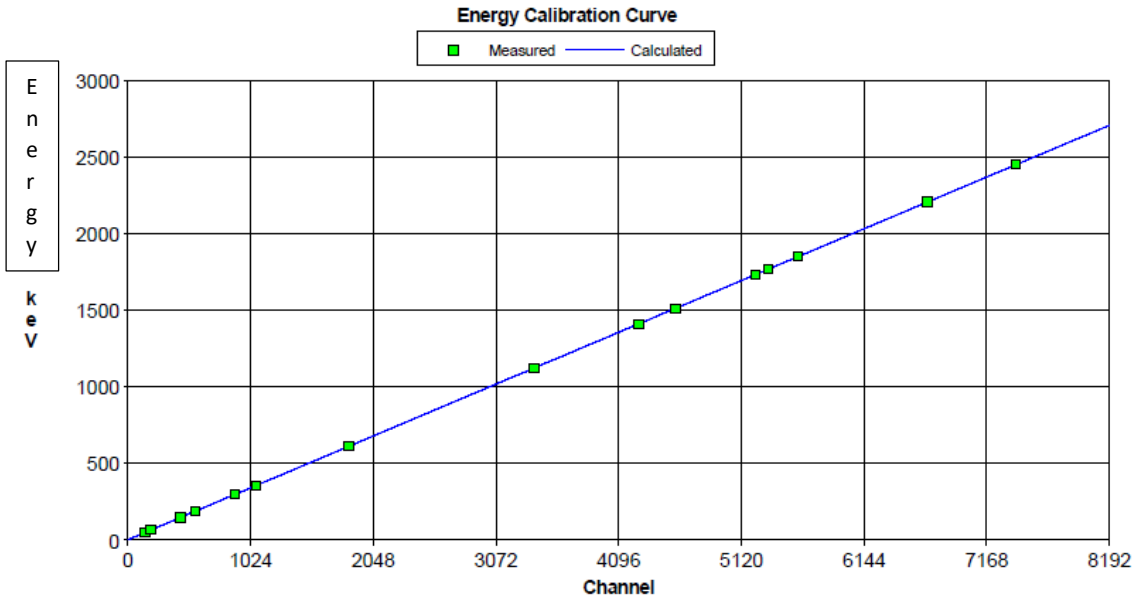

Figure 3. 7: Energy calibration, a linear graph, of the HPGe well-type detector.

Calibration for efficiency was recorded and saved for use during calculation during analyses of samples. The efficiency smooth curve is shown in Figure 3.7.

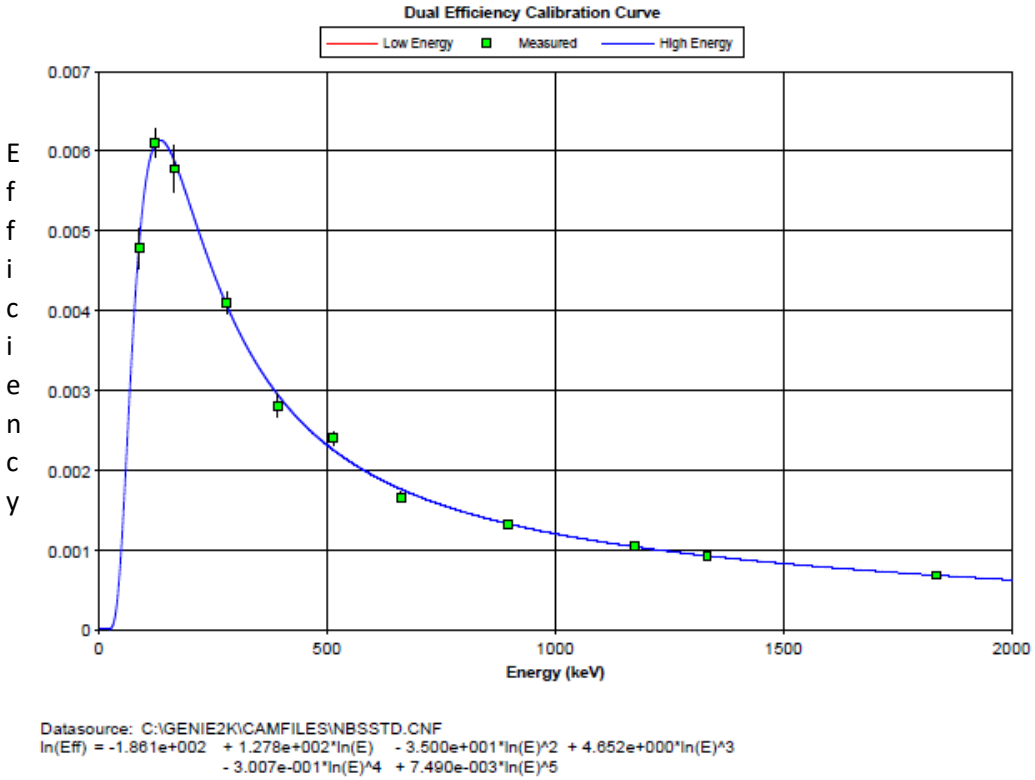

Figure 3. 8: Efficiency curve for the calibration of HPGe detector.

3.4.2 ICP-MS calibration

External calibration was performed on the ICP-MS using a multi-element calibration solution 5% of nitric acid (HNO_3) for total quantitative (TotalQuant) methods. The solution has 10 $mg.L^{-1}$ concentrations of silver (Ag), aluminium (Al), arsenic (As), barium (Ba), beryllium (Be), bismuth (Bi), calcium (Ca), cadmium (Cd), cobalt (Co), chromium (Cr), caesium (Cs), copper (Cu), iron (Fe), gallium (Ga), indium (In), potassium (K), lithium (Li), magnesium (Mg), manganese (Mn), sodium (Na), nickel (Ni), lead (Pb), rubidium (Rb), selenium (Se), strontium (Sr), thallium (Tl), uranium (U), vanadium (V) and zinc (Zn). Calibration prepares analytical instruments for anticipated measurements.

There were two important objectives for this exercise, namely; to check the accuracy of the instrument, and to determine the traceability of measurements. It also included the correction of instrument when out of calibration. A report was generated showing the errors in measurements. In this case, the concentration of each element was expected to be around 10 $mg.L^{-1}$, with acceptable errors for the instrument to pass the test. The mode of analyses was put into consideration. For these analyses, a helium gas for kinetic energy distribution (KED) was used for collisions on the cells. Also daily optimization for the instrument was performed on [KED] QID, [Helium KED] Cell Entrance Voltage, [Helium KED] Cell Exit Voltage, [Helium KED] CRO, and [Helium KED] Performance Check of the ICP-MS.

3.5 Determination of minimum detectable activity (MDA)

A minimum detectable activity of MDA on HPGe detector can be calculated for both the radionuclides which have not been found in the spectrum and those that have been found (Gene, 2000). MDA is defined as a lowest quantity of radioactivity measurable by the instrument under specified conditions (Faanu *et al*., 2010). Curie (1968) developed good acceptable methods and have been implored in this study. One of his concepts was critical level (L_C), a point by which a net signal cannot be reliably significant. The other one is detection limit (L_D), which is the smallest net signal which can be quantified. Detection limit parameters for all radioactive elements under study, peak to Compton ratio (PCR) and the peak shape parameters are crucial to be known. Expectation is that the

minimum detection limit (MDL) varies for each element. A most common formula used to compute the efficiency (ε) for equipment calibration of a detector is written as:

$$\varepsilon = \frac{N}{\varepsilon_\gamma . T . \mathrm{A} . P} \tag{3.3}$$

where, *N* is the peak area in number of counts at that particular energy, ε_γ is the geometric efficiency of a detector, *A* is the absolute activity of the standard [Bq], *T* is the elapsed time of measurement and *P* is the gamma probability of disintegration of the radionuclide under consideration. The activity detection limit used in gamma spectrometry, MDA per unit mass or volume is calculated as (Genie, 2000):

$$MDA = \frac{L_D}{T\varepsilon'\gamma V K_c K_w U_f S_{cf}} \tag{3.4}$$

where, T is the live time in seconds, V is the volume or mass of sample, γ is the gamma probability of the energy under consideration, ε' is the coefficient of attenuation, S_{cf} is the sample conversion factor, K_c is counting correction factor of a nuclide decay, K_w is nuclide decay correction factor starting from the time that a sample was collected.

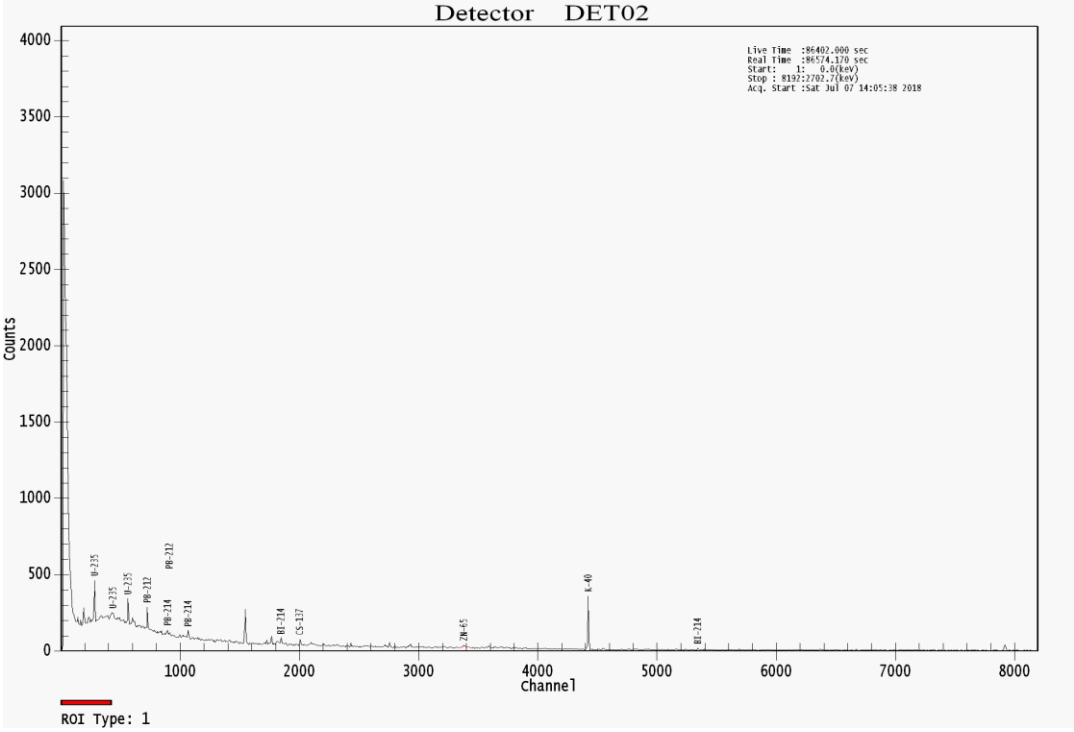

Figure 3. 9: The background peaks measured by HPGe showing counts against channel number.

The minimum detectable limits obtained should be put into consideration during samples analyses and discussions. Firstly, the background measurement was executed and run for a time of 43200 seconds, with no sample mounted on the detector. Counts were collected and the data were analysed. Re-arranging Equation 3.4 above, one can calculate the minimum detectable activity of each radionuclide under study interest as:

$$MDA\left(\frac{Bq}{unit\ weight}\right) = \frac{(2.71+4.66(\sigma))}{T.\varepsilon_{\gamma}.P.wt} \quad (3.5)$$

where, T, ε_{γ} and P are as defined above and σ is the standard deviation of the background corrected during time T over the energy range of interest calculated as:

$$\sigma = \sqrt{Net\ Peak\ Area} \quad (3.6)$$

Figure 3.9 shows a spectrum of the background peaks of radionuclides measured on the gamma spectrometer for determination of MDA.

3.6 Data analyses (elemental and activity concentrations)

Analyses of all radionuclides of interest in this study was performed for both the gamma spectroscopy and the ICP-MS. The gamma detector used, Figure 3.10, was manufactured by Canberra Industries (Meriden, CT, USA). It has a detector model GCW2021 and relative efficiency of 36.4% and resolution of 1.842 keV at 1332 keV γ-ray emission of ^{60}Co. The high-purity germanium system computer has Genie 2000 version 3.3 software installed for quantitative and qualitative analysis. A digital based multi-channel analyser (MCA 1000) couples the detector to the software. The counts per peak area at a specified energy, shown in Table 3.2, recorded and computed to obtain activity concentrations for each radionuclide under study.

For the determination of elemental concentrations,the samples were also counted using inductively coupled plasma-mass spectroscopy (ICP-MS) technique. For this technique, attention was focused on water and dust samples, even though soil was also analysed by this technique for quality assurance purposes. Analyses on ICP-MS data were computered in a special method such that the mass of sample used during sample preparation is considered.

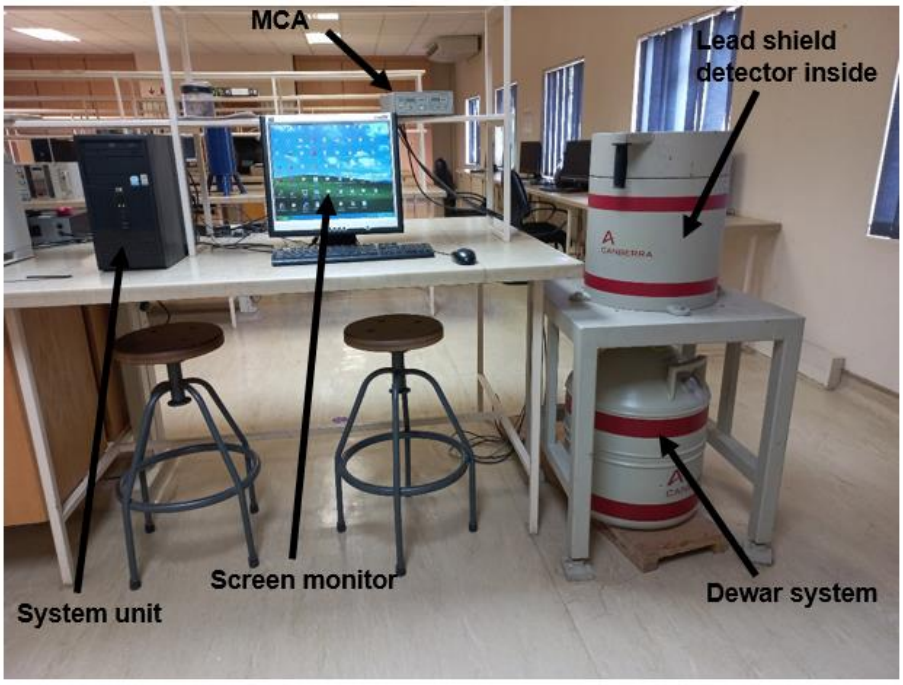

Figure 3. 10: The HPGe system at CARST used in this study showing the MCA, Dewar cooling system (with LN2), lead shield, computer monitor and data display.

3.6.1 Radioactivity measurements of ^{226}Ra, ^{238}U, ^{232}Th and ^{40}K

3.6.1.1 HPGe technique

Gamma spectrometry is a non-destructive technique that uses HPGe (or Na(Tl)I detector for identification and quantification of all gamma emitting radionuclides present in the sample based on energies and peak area of full energy peaks of their respective gamma rays. The acquisitions of all samples data were performed on a Genie 2000 version 3.3 computerized software, under low-background conditions achieved by a detector using lead shielding. The gamma spectra were obtained by measuring radioactivity counts for a period 12 hours (43200 s) per sample. One good and important advantage for non-destructive method of HPGe instruments is that it allows many gamma-emitting nuclides to be measured simultaneously.

The calculations of activity concentrations for radionuclides of interests were obtained from results of daughter products assuming secular equilibrium have been achieved. In

order to avoid interferences and keep accuracy of counts energy tolerance and nuclide confidence index threshold were 3.00 keV and 0.30, respectively. Analysis from the spectrum was performed using energy lines with their respective gamma emission probability and efficiency. On HPGe detector ^{238}U, ^{226}Ra and ^{232}Th cannot be determined directly because of gamma emission probability for ^{238}U and ^{232}Th with low yield and ^{226}Ra emits gamma at energy of 186 keV (3.6%), which is interfered with that from ^{235}U at 185.9 keV of emission probability of 57.2% and hence difficult for a system to separate them. Table 3.2 shows a list of daughter nuclides, with their half-lives and probability of emissions (yield), under consideration during analyses. The energy lines of 63.20 keV and 92.60 keV for ^{234}Th, and 1001.03 keV for ^{234m}Pa were used to determine ^{238}U concentrations in samples. To calculate the ^{226}Ra activity concentration, both energy lines 295.22 keV and 351.93 keV for ^{214}Pb, and other three energies 609.31 keV, 1120.29 keV and 1764.49 keV for ^{214}Bi were used, provided that the samples are in radiochemical equilibrium. Gamma photons emitted with energy of 238.63 keV for ^{212}Pb, and other two energy lines 338.32 keV and 911.20 keV for ^{228}Ac were used to calculate the activity concentrations of ^{232}Th. The gamma emission with energy of 1460.63 keV was used for natural decay of ^{40}K to stable ^{40}Ar (with photon intensity of 10.4%) by electron capture.

Table 3. 2: Analysed nuclides with their half-lives and energy spectra.

Target nuclide	Analysed nuclide	Half-life ($t_{1/2}$)	Energy spectrum (keV), with gamma intensity/yield (%)
^{238}U (4.468×10^9 years)	^{234}Th	14.10 d	63.20 (3.70%) and 92.60 (5.21%)
	^{234m}Pa	6.74 h	1001.03 (0.83%)
^{226}Ra (1650 years)	^{214}Pb	26.80 min	295.22 (18.28%); 351.93 (35.34%),
	^{214}Bi	19.70 min	609.31 (45.16%); 1120.29 (14.78%) and 1764.49 (15.17%)
^{232}Th (1.405×10^{10} years)	^{228}Ac	6.15 h	338.32 (11.27%) and 911.20 (25.80%)
	^{212}Pb	10.60 h	238.63 (43.60%)
Non-series (1.25×10^9 years)	^{40}K	The daughter ^{40}Ar is stable nuclide	1460.63 (10.66%)

The activity concentrations of all radionuclides of interest were computed using net peak counts (C_{NP}) for a particular energy line, after correction for a background and Compton contributions, of the respective nuclides. The formula utilized for calculation of activity concentration (A_c) at each spectral gamma energy is shown in Equation 3.7 (Durusoy and Yildirim, 2017; IAEA, 1989):

$$\mathrm{A}_c(\mathrm{Bq.kg^{-1}}) = \frac{\mathrm{C_{NP}}}{B_I \times \varepsilon(\mathrm{E_\gamma}) \times \mathrm{m}} \tag{3.7}$$

where, N_{CP} is the net peak counts per second under the peak area of interest corrected for background effects in Equation 3.8 as:

$$N_{CP} = N_S - N_B \tag{3.8}$$

N_S is the total number of counts per second (cps) under the peak area of interest in the spectrum, N_B is the gross background counts per second (cps) under the peak of interest, B_I is branching ratio intensity, $\varepsilon(E\gamma)$ is the absolute photo-peak efficiency (%) of the

detector, and m is the mass of the sample in kg. Figure 3.11 shows the spectral lines with their respective radionuclides obtained for analyses of sample ORE 8. Again, the uncertainty was calculated using a formula:

$$\sigma_{A_c} = 100 x A_c x \sqrt{(\frac{\sigma_S}{S})^2 + (\frac{\sigma_{\varepsilon_i}}{\varepsilon_i})^2 + (\frac{\sigma_\gamma}{\gamma})^2 + (\frac{\sigma_q}{q})^2} \quad (3.9)$$

where, σ_{A_c} is the combined uncertainty, ε_i is the efficiency of the *i*th energy line considered, σ_S is the net area efficiency, σ_γ is the branching ratio efficiency, σ_{ε_i} is the *i*th energy line efficiency, and q is the sample quantity with σ_q as the sample quantity efficiency.

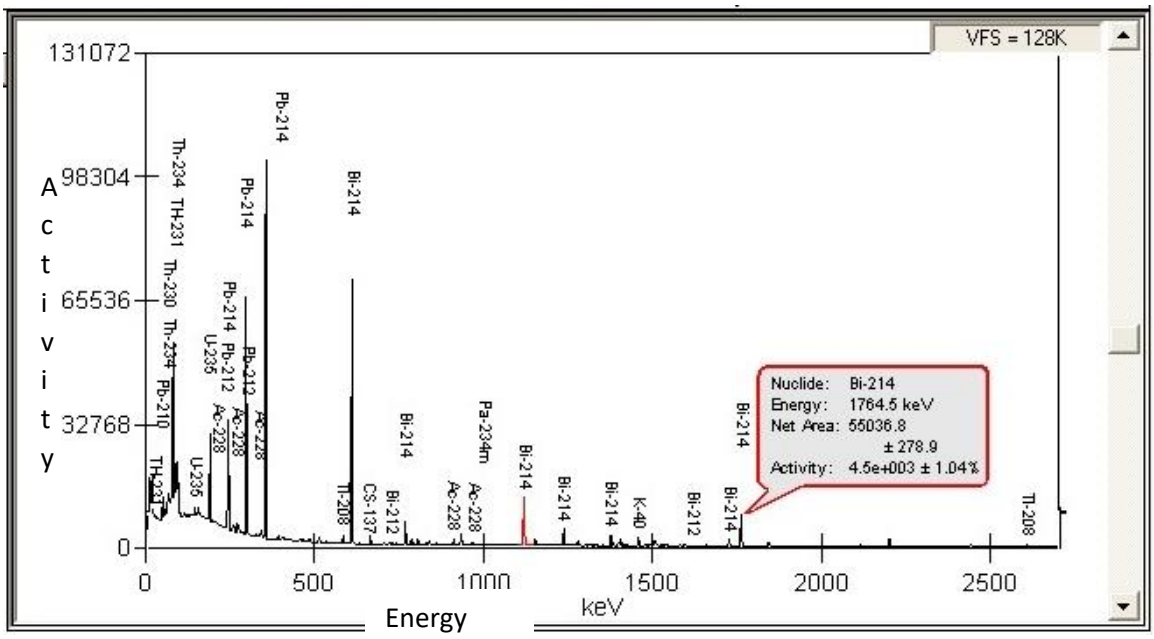

Figure 3. 11: Spectral lines obtained for sample ORE 8.

The concentrations of the radionuclides were calculated from the average weighted mean activities of each of their energy lines (A_{av}) as illustrated by the formula:

$$A_{av} = \frac{\sum_{i=1}^{N} \frac{A_{c_i}}{\sigma^2 A_{c_i}}}{\sum_{i=1}^{N} \frac{1}{\sigma^2 A_{c_i}}} = \frac{\sum_{i=1}^{N} \frac{A_{c_i}}{\sigma^2 A_{c_i}}}{\sigma_{A_{av}}} \quad (3.10)$$

where, A_{c_i} is the activity concentration as obtained for the *i*th energy line,

$\sigma_{A_{c_i}}$ is uncertainty in activity concentration of the i^{th} energy line, and

$\sigma_{A_{av}}$ is uncertainty of the weighted average activity concentrations of all energy lines.

From Equation 3.10 above, the uncertainty of weighted average activity ($\sigma_{A_{Av}}$) from multiple selected was calculated as:

$$\sigma_{A_{Av}} = \sqrt{\frac{1}{\sum_{i=1}^{N} \frac{1}{(\sigma_{A_i})^2}}} \quad (3.11)$$

3.6.1.2 ICP-MS technique

The NexION ICP-MS (2000C series) instrument, manufactured by Perkin Elmer, CT, USA, with Syngistix version 2.5 software was used to perform elemental concentration for a variety of samples. This is a mass spectroscopic instrument which can be-operated in four modes, such as standard (argon), helium kinetic energy distribution (KED), both Oxygen and Ammonia dynamic reaction cell (DRC) modes. Helium KED uses collision-reaction cell to reduce interferences on atoms in the cells. Radionuclides of interests are uranium, thorium and potassium, and potassium, which have interferences with argon species when the instrument is set on standard mode, under argon. Therefore, the instrument was operated on helium KED mode for reduction of polyatomic interferences for potassium, namely; ^{40}K and ^{41}K, with isobaric interferences of argon species, ^{40}Ar and $^{40}Ar^{1}H$, respectively.

The multi-element determination of radionuclides was then performed when a solution was introduced by pneumatic nebulization into a radiofrequency plasma where energy transfer processes cause desolvation, atomization and ionization. With the mass and dilution factors included to obtain the concentrations of samples, in ppb ($\mu g.kg^{-1}$) or ppm ($mg.kg^{-1}$). The following two approaches can be used to get activity concentrations for ^{238}U, ^{232}Th and ^{40}K in $Bq.kg^{-1}$:

(1) The activity per unit mass were calculated by adopting the formula:

$$A = -dN/dt = \lambda.N \quad (3.12)$$

where, λ is the disintegration constant and it is unique for each radionuclide, *N* is the number of particles/atoms that undergo integration process, *dt* is the time interval/elapsed during change in number of particles *dN*. Utilizing the natural isotopic abundances, half-life ($t_{1/2}$) in seconds, atomic weight (isotopic molar mass) of the nuclide of interest, the following formula has been adopted to calculate activity concentrations for radioisotopes in samples (Pilakouta *et al*., 2017):

$$A_c = \lambda N * k * C_s = \frac{\ln(2)}{t_{\frac{1}{2}}} * \frac{N_A}{M_A} * \ k \ * \ C_s \qquad (3.13)$$

where, N_A is Avogadro's number, 6.022 x 10^{23} atoms per mol., *k* is the natural abundance (^{238}U: 99.27%; ^{232}Th: 99.98% and ^{40}K: 0.0117%) (Murray and Holbert, 2014) of the nuclide of interest, M_A is isotopic molar mass (^{238}U: 238.05079 g.mol^{-1}; ^{232}Th: 232.03805 g.mol^{-1}; ^{40}K: 39.963998 g.mol^{-1}), the decay constant is a fraction natural logarithm (*ln* (2)) and half-life of each radionuclide (^{238}U: 1.41 x 10^{17} s; ^{232}Th: 4.43 x 10^{17} s and ^{40}K: 3.95 x 10^{16} s) and C_s is a total concentration of a nuclide in a samples as measured ICP-MS.

(2) It is noted from the IAEA Techniczl Report Series No 295 of 1989 that the conversion factors of the three radionuclides of ^{238}U, ^{232}Th and ^{40}K used to convert the obtained concentrations in ppm to Bq.kg^{-1}. Considering also that 1% = 10 000 ppm = 10 000 mg.kg^{-1} these factors are as follows:

- 1 ppm = 12.35 Bq.kg^{-1} for ^{238}U;
- 1 ppm = 4.06 Bq.kg^{-1} for ^{232}Th and
- 1% = 313 Bq.kg^{-1} for ^{40}K (IAEA, 1989). (3.14)

Either of the two methods discussed above would reach to the final and correct activity concentrations for the radionuclides of interest in the study.

3.6.2 Radiological health hazards indices due to NORM

3.6.2.1 Absorbed dose (D)

Absorbed dose is crucial to assess the potential for biochemical changes in specific tissues or organs. It is a concentration of energy deposited in tissue as a result of an exposure to ionizing radiation. This energy (E) deposition in a medium per unit mass (m),

D (Gy) = E/m, is applicable to human tissue. It is therefore necessary to assess the rate of energy deposition (D_R) in air at 1 m above the ground, resulting from ^{238}U series, ^{232}Th series and ^{40}K (Bai *et al*., 2017). Some researchers call it absorbed gamma dose rate of radioisotopes as distributed uniformly in the soil (Bai *et al*., 2017; Amanjeet *et al*., 2017). This is computed using Equation 3.15:

$$D_R(nGy.h^{-1}) = 0.0417A_K + 0.462A_U + 0.604A_{Th} \quad (3.15)$$

where, A_K, A_U and A_{Th} are activity concentrations for potassium, uranium and thorium respectively. The factors 0.0417, 0.462 and 0.604 are dose conversion factors for A_K, A_U and A_{Th}, respectively (Amanjeet *et al*., 2017).

3.6.2.2 Radium equivalent (Ra_{eq})

There is a high possibility for builders and contractors to utilize some radioactive materials for constructions of houses and dwellings. The design and ventilation systems for these buildings strongly influence indoor levels of the radioactive gas radon and its decay products, which contribute significantly to doses through inhalation (UNSCEAR, 2017) Therefore, radium equivalent activity has been introduced to assess the gamma rays emitted from materials containing ^{226}Ra (^{238}U-series), ^{232}Th and ^{40}K in Bq.kg^{-1} when used for building constructions. It is well documented that these radionuclides emit gamma doses in differing number of activities even when they are of the same amount in any material. The radium equivalent is calculated depending on the basis that the activity concentrations A_{Ra} (Bq kg^{-1}) for ^{226}Ra, 1.43 of A_{Th} (Bq.kg^{-1}) for ^{232}Th and 0.077 of A_K (Bq.kg^{-1}) of ^{40}K produce similar gamma dose rate. The Ra_{eq} activity of the sample in Bq.kg^{-1} is achieved using equation (3.16) (Thabayneh, 2012)

$$\mathrm{Ra_{eq}} = \mathrm{A_{Ra}} + 1.43\mathrm{A_{Th}} + 0.077\mathrm{A_K} \leq 370\ \mathrm{Bq.kg^{-1}} \quad (3.16)$$

where A_{Ra}, A_{Th} and A_K are activity concentrations of ^{226}Ra, ^{232}Th and ^{40}K, respectively. The values 1.43 and 0.077 are dose conversion factors for ^{232}Th and ^{40}K, respectively. The dose conversion factor for ^{226}Ra is a unit. Therefore, researchers have commended radium equivalent as one crucial reference standard used in the regulation of radiation protection for public (UNSCEAR, 2013). Activity concentration as a result radium

exposure is limited to 370 Bq.kg^{-1}, which produces equivalent to maximum permissible limit of 1 mSv.y^{-1} of exposure from building materials to inhabitants.

3.6.2.3 Annual effective dose (AED)

The annual effective dose is the sum of the dose from external exposure in that year plus the committed dose from intakes by inhalation and ingestion in that year (UNSCEAR, 2017). Estimation of the annual effective dose due to external ionizing radiation need more attention today for health care. Researchers have introduced annual effective dose in the field, as received by a member of the public, and is calculated by the formula (Munyaradzi *et al*., 2018):

$$AED\ (mSv.y^{-1}) = D_R \times DCF \times F_2 \times T \quad (3.17)$$

where, D_R is the absorbed dose rate (in nGy.h^{-1}) as computed using Equation 3.16 above, dose conversion factor (DCF) from dose rate above 1 m in air above the flat surface into effective dose, given as 0.9, 0.8 and 0.7 Sv.Gy^{1} for categorized age group of infants (0 – 5 years), children (6 – 15 years) and adults (≥ 16 years), respectively (UNSCEAR, 2000). It is noted that individuals spend about 80% (19 hours) of their time indoors and 20% (5 hours) outdoors daily. Therefore, indoor and outdoor radiation exposures from building materials contribute to a prolonged exposure situations (Onjefu *et al*., 2021), and hence F_2 denotes the external outdoor 0.2 or indoor 0.8 occupancy factors (Samreh *et al*., 2015). T is the total exposure time in a year (in hours per year), which is 8760 h.y^{-1}. Therefore, Equation 3.17 can be rewritten as (Issa *et al*., 2013):

$$AED_{out}\left(\frac{mSv}{yr}\right) = D_R\left(\frac{nGy}{h}\right) x\ 8760\,\frac{h}{yr}\ x\ DCF\ \left(\frac{Sv}{Gy}\right) x\ 0.2\ x\ 10^{-6} \quad (3.18)$$

$$AED_{in}\left(\frac{mSv}{yr}\right) = D_R\left(\frac{nGy}{h}\right) x\ 8760\,\frac{h}{yr}\ x\ DCF\ \left(\frac{Sv}{Gy}\right) x\ 0.8\ x\ 10^{-6} \quad (3.19)$$

where, AED_{out} and AED_{in} are outdoor and indoor annual effective doses determined with respect to absorbed dose into the human body. It is recommended that the effective dose efficiency of material used in building constructions should not exceed 1 mSv.y^{-1} with respect to both radiation exposures (Joel *et al*., 2018).

3.6.2.4 The total annual effective dose

The total annual effective dose (AED_T) is calculated for each age group as a sum of external exposures due to outdoor (Equ. 3.18) and indoor (Equ. 3.19). This is the exposures to each age group on members of the public, and only employees of the uranium mines (age group ≥ 16 years) due to gamma radiation from NORM in soils. Therefore, the total annual effective dose for a human's exposure living at a particular area in a year is calculated as a sum of indoor and outdoor occupancies:

$$AED_{Total}\left(\frac{mSv}{yr}\right) = AED_{in} + AED_{out} \quad (3.20)$$

3.6.2.5 Internal and external exposure indices

Internal and external hazard indices are used to compare the radiological exposures to international standards. The measured activity concentrations of ^{238}U, ^{232}Th and ^{40}K are used to calculate radiological parameters and these are radium equivalent, indoor doses, annual effective dose and excess lifetime cancer risk.

After radioactive decay, radiations emitted may either expose human beings internally or externally (Amwaalanga *et al*., 2019). External (H_{ex}) and internal hazard indices (H_{in}) were introduced to account for external and internal exposures by photons (gamma rays) from radon (^{222}Rn) and thoron (^{220}Rn) together with their short-lived products (Amanjeet *et al*., 2017; UNSCEAR, 1988). The aims were to determine whether exposure is comparable to maximum permissible limit of 1 $mSv.y^{-1}$ due to NORM (Kamunda *et al*., 2016). The approximation of external radiation doses as measured by gamma spectrometry from building materials is known as external hazard index shown by Equation 3.21. Since ^{222}Rn and ^{220}Rn nuclides are products of NORM in the soil, they pose a high risk of lung cancer when inhaled by humans and therefore Equations 3.21 and 3.22 were used for external and internal hazard indices, respectively (Amanjeet *et al*., 2017):

$$H_{ex} = \frac{A_{Ra}}{370} + \frac{A_{Th}}{259} + \frac{A_K}{4810} \leq 1 \quad (3.21)$$

$$H_{in} = \frac{A_{Ra}}{185} + \frac{A_{Th}}{259} + \frac{A_K}{4810} \leq 1 \quad (3.22)$$

where, A_U, A_{Th} and A_K are the activity concentrations of ^{238}U (^{226}Ra), ^{232}Th and ^{40}K in $Bq.kg^{-1}$ in the soil samples, respectively. The value of each of the hazard indices must be less than a unit for the radiation hazard to be negligible and this value corresponds to upper limit of 370 $Bq.kg^{-1}$ (UNSCEAR, 2017).

3.6.2.6 Gamma index (I_γ)

The gamma-radiation hazards from the radionuclides under study is calculated using Equation 3.23 (Joel *et al*., 2018). Gamma index is known as the evaluation of radioactivity level index on samples under investigation. Therefore, this index is calculated as (Samreh *et al*., 2015; Issa *et al*., 2013):

$$I_\gamma = \frac{A_{Ra}}{300\ Bq.kg^{-1}} + \frac{A_{Th}}{200\ Bq.kg^{-1}} + \frac{A_K}{3000\ Bq.kg^{-1}} \quad (3.23)$$

Based on the values calculated for annual effective dose efficiency values (in section 3.7.2.3), the gamma activity index values should not exceed a unit. Therefore, all gamma index above 1 indicates that AED values for the particular samples under investigation are above the recommended 0.3 $mSv.y^{-1}$ protection level (Thabayneh, 2012).

3.6.2.7 Alpha index (I_α)

Internal health hazards are represented by alpha index as a consequence of exposure from alpha emitting radionuclides when inhaled or ingested. Carcinogenetic substances such as radon (^{222}Rn), thoron (^{220}Rn) and their progenies are natural radioactive gases that are emitted in outdoor and indoor environments which contribute to human health hazards. Human exposures of these radioactive gases increase the risk of lung cancers (Giri and Pant, 2018). Therefore, indoor environmental exposures may depend on the type of materials used, like bricks, concrete, etc. Assessment of alpha index is another aspect to estimate excess alpha radiation emitted from samples which may possibly be used for building constructions. The equation that denotes alpha activity index is given as (Joel *et al*., 2018; Righi and Bruzzi, 2006):

$$I_\alpha = \frac{A_{Ra}}{200\ Bq.kg^{-1}} \quad (3.25)$$

where, A_{Ra} is activity concentration for radium-226 (Bq.kg^{-1}), regarded to be in building materials. The International Commission on Radiation Protection recommends that alpha index should not exceed the level of activity concentration of 200 Bq.kg^{-1} in building materials for dwellings (Righi and Bruzzi, 2006). The level of ^{226}Ra activity concentration below 200 Bq.kg^{-1} is a clear reflection of radon inhalation in dwellings below 200 Bq.m^{-3} (ICRP, 1994). In conclusion, radon concentration upper limit for alpha index recommended is 1 (Joel *et al*., 2018).

3.6.2.8 Excess lifetime cancer risk (ELCR)

Cancer risks associated with radiation have been estimated for various organs and tissues, including bone marrow, thyroid, lung, breast and gastrointestinal organs in human beings (NRC, 2006). Excess lifetime cancer risk (ELCR) represents the chances that cancer may develop over a lifetime at any given exposure level due to radiation. This is presented as a value representing the number of extra cancer cases expected in a population exposed to a carcinogen at a given dose, calculated by considering the average life expectancy of a human being estimated at 70 years (Samreh *et al*., 2015):

$$ELCR = AED_T \times HLD_A \times CRF \quad (3.26)$$

where, AED_T is the total annual effective dose equivalent, HLD_A is the average human's lifetime duration (estimated to be 70 years) and *CRF* is the cancer risk factor (Sv^{-1}) i.e. fatal cancer risk per Sievert. For stochastic effects, which may occur due to low background radiation, the ICRP 60 stipulates a threshold value of 0.05 for the public exposure (Samreh *et al*., 2015). The world average value for cancer risk factor is 0.29 x 10^{-3} (Taskin *et al*., 2009). Therefore, equation 3.26 above can be written in the form:

$$ELCR = AED_{tot}(mSv.y^{-1})\ x\ 70\ y\ x\ 0.05\ Sv^{-1} \quad (3.27)$$

3.7 Modelling the absorbed doses and cancer risks using RESRAD model

The modelling was based on the assumption that, the levels of radioactivity concentrations of ^{238}U, ^{232}Th and ^{40}K primordial radionuclides in samples collected from the mining zones may have long term effect to residents within a specified radius. The consideration was on residential dwellings and the town of Arandis which has an

estimated population of about 10 000 and a residence surface area approximated at 1.484 km^2. The objective was to estimate the radiological cancer risks to members of the public due to NORM using RESRAD modelling tool. In this study, RESRAD-OFFSITE (vs 4.0) was performed on parameters of the samples collected from mining and residential areas, respectively.

3.7.1 Intake and risks of radionuclides

RESRAD modelling tool has built-in default model to generate the quantity of intake QINT(i,p,t) of each individual radionuclide (i) as well as the exposure pathways (p) on a specified time (t) in years. The model also can estimate total cancer risks CNRS(i,p,t) based on the radionuclide, pathways and total risk time of intake. The intake summed up for individual radionuclides to estimate absorbed doses and lifetime cancer risks were performed at intervals of 25 years for a period of 200 years, i.e., 0 year, 25 years, 50 years, 75 years, …, 150 years, 175 years and 200 years.

The lifetime cancer morbidity risks were estimated from the average activity concentrations determined in samples from all sections (A, B, C and D), discussed in Table 3.1, in the study area using equation 3.28 shown as:

$$LCR = A_r \; x \; ED \; x \; k_{rc} \qquad (3.28)$$

where, A_r, ED and k_{rc} are the estimated average activity concentration ($Bq.g^{-1}$) in samples integrated over time, the duration of exposure and the specific coefficient of cancer risk of individual radionuclides in the environment (y^{-1} per $Bq.g^{-1}$) (Yu *et al*., 2001).

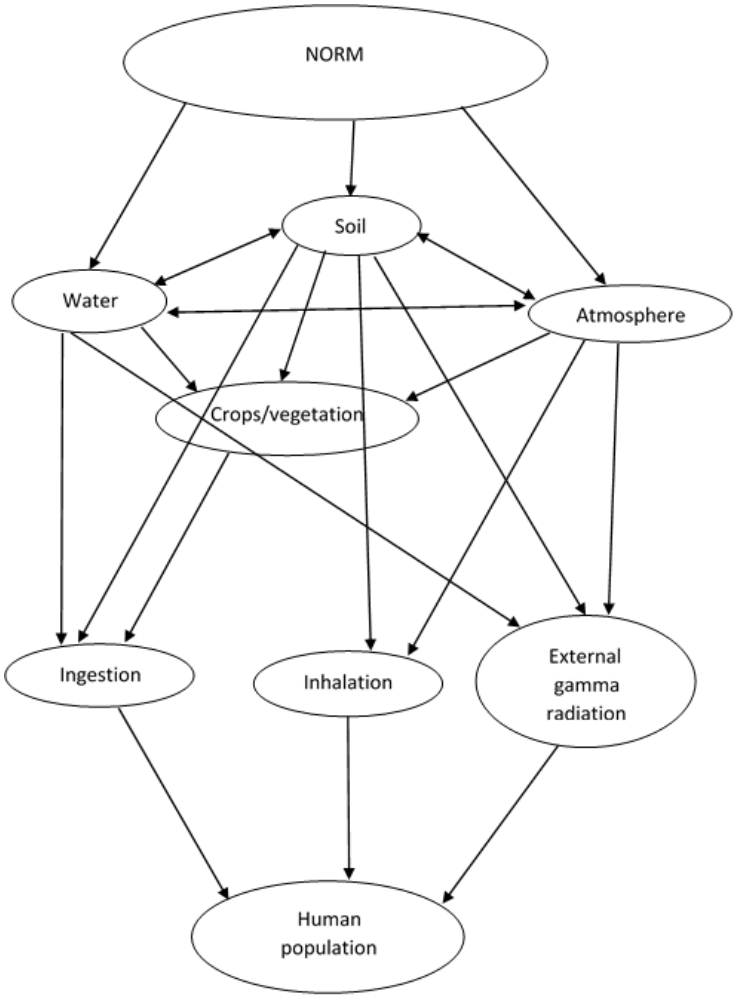

Figure 3. 12: Schematic diagram of the exposure pathways considered during RESRAD modelling of annual effective doses and morbidity risks.

The exposure pathways considered were atmosphere, crops, surface and ground water, as well as soil which may be in contact with humans by external gamma exposures, inhalation and ingestion shown in Figure 3.12 adopted from Figure 2.20. Some site and default values of specific characteristics and parameters used as inputs were entered in the model for the estimation of lifetime cancer risks (LCR) in samples. These values together with activity concentrations determined are shown in Tables 6.1 and 6.2, in Chapter 6.

3.8 Specific activity

The researcher also had an interest to know an important characteristic of nuclides well-known as the specific activity (SpA) in a unit mass (g) or volume (ml) of a pure radionuclide block or container. This is a measure which allows comparisons between the strength or quantity – *activity per unit mass* – of different radionuclides in a unit mass of sample (Murray and Holbert, 2014). It can simply be defined as activity per unit mass of a pure material. For a pure ^{226}Ra sample of 1 g, the specific activity is approximately 1.0 Ci/g. Taking into consideration of the half-lives of all radionuclides under study, the activity formula was employed to calculate specific activities of each. Table 3.3 shows the calculated specific activities (considering their respective half-lives) of ^{238}U (4.47 x 10^9 y), ^{226}Ra (1.65 x 10^3 y), ^{232}Th (1.41 x 10^{10} y) and ^{40}K (1.28 x 10^9 y) (Halliday *et al*., 2013; Serway and Jewett, 2012). There are proportionality factors such as Avogadro's number (6.022 x 10^{23} g.mol^{-1}) and the decay constant ($\lambda = \frac{\ln(2)}{t_{1/2}}$) which relates the number of constituent particles in a sample with the amount of substance in that sample, and the rate at which the amount decreases. Therefore, the amount of disintegration per unit mass of a pure sample is given by equation 3.28:

$$SpA = \lambda N = \frac{\ln(2)}{t_{1/2}} x \frac{m}{M_A} N_A \qquad (3.28)$$

where, N_A is Avogadro's number and M_A is a unique molar mass of an atom under consideration. The number of particles/atom, *N,* is calculated as a fraction of Avogadro's number to atomic molar mass ($N = \frac{mN_A}{m_A}$).

Table 3. 3: Specific activities in mass of each NORM under this study (Martin, 2013).

Nuclide	Half-life (s)	Atomic molar mass (g.mol^{-1})	Specific Activity		
			Bq.g^{-1}	Ci.g^{-1}	Bq.kg^{-1}
Ra-226	5.05E+10	226.0250	3.66E+10	9.89E-01	3.66E+13
U-238	1.42E+17	238.0508	1.24E+04	3.34E-07	1.24E+07
Th-232	4.45E+17	232.0381	4.05E+03	1.09E-07	4.05E+06
K-40	4.04E+16	39.9640	2.59E+05	6.99E-06	2.59E+08

The main aim of calculating the specific activities was to ensure that all activity concentrations of radionuclides of interest in this study did not exceed those of pure materials.

3.9 Conclusion

The data obtained in this chapter were used to draw graphical representations of nuclide distributions in samples and tabulated data in the next chapters (Chapter 4: HPGe, Chapter 5: ICP-MS) and Annexures, respectively. Discussions on activity distributions and radiological hazards as well as RESRAD code results are in Chapter 6.

CHAPTER 4: GAMMA SPECTROSCOPY RESULTS

4.0 Introduction

This chapter discusses the results of the radioactivity concentrations of NORM (^{238}U, ^{226}Ra, ^{232}Th and ^{40}K) determined in samples from the study areas using the High-purity germanium detector. It includes; the absorbed dose rates, radium equivalent activity annual effective doses and radiological health hazard indices, such as external and internal hazards, alpha and gamma indices, of soil measured in area of study. The determined results were also discussed in comparison with public and occupational exposure levels as well the world average values documented by the international standards organizations on radiological protection and safety (ICRP, 2012; UNSCEAR, 2018). The world average radiation exposure level documented by United Nations Scientific Committee on the Effects of Atomic Radiation of 1988 is 0.07 $mSv.y^{-1}$.

4.1 Minimum detectable activity of the HPGe detector

Equation 3.5 in Chapter 3 was used to calculate the minimum detectable activity of the radionuclides of interest in this study. Table 4.1 shows details of all the variables required to determine the minimum detectable activity (MDA) for ^{238}U, ^{226}Ra, ^{232}Th and ^{40}K on the gamma spectrometer detector. Most importantly, some of the samples analyzed in this study were natural samples such as uranium granitic ores, and therefore their activity concentrations should not exceed specific activities of pure materials shown in Table 3.3 of Chapter 3.

Table 4. 1: The MDA calculated on the HPGe detector used in this study.

Minimum detectable activity (MDA)							
Nuclide of interest	Measured daughter	Energy (keV)	Net Peak area	Sigma (σ)	Efficiency	Gamma yield (%)	MDA ($Bq.wt^{-1}$)
	^{214}Pb	351.77	73.30	8.56	0.01260	35.34	0.22
		609.00	90.20	9.50	0.00806	45.16	0.30
		1119.66	35.00	5.92	0.00533	14.78	0.89
^{226}Ra	^{214}Bi	1763.79	31.70	5.63	0.00410	15.17	1.08
		63.15	216.00	14.70	0.01150	3.70	3.87
	^{234}Th	92.54	592.00	24.33	0.01920	5.21	2.69
^{238}U	^{234m}Pa	1001.13	60.70	7.79	0.00571	0.83	19.06
		338.51	72.80	8.53	0.01300	11.27	0.67
	^{228}Ac	911.18	107.00	10.34	0.00607	25.80	0.75
^{232}Th	^{212}Pb	238.59	174.00	13.19	0.01700	43.60	0.20
^{40}K	-	1460.53	961.00	31.00	0.00457	10.66	6.99

4.2 Radioactivity concentrations

Activity concentrations for daughter radionuclides with shorter half-lives are presented in tables of Annexures, except for ^{40}K, used to quantify these NORM of interest in this study determined using Equation 3.7 with their uncertainties (Equation 3.9). The levels of weighted radioactivity concentrations with their respective weighted uncertainty were calculated using Equations 3.10 and 3.11, respectively. The results determined were reported separately for each study section in the study area. The tables of results are presented in Annexure B and graphical representations were shown on each section. Only four radionuclides such as ^{226}Ra, ^{238}U, ^{232}Th and ^{40}K, of NORM were considered for discussions of activity concentrations and all presented on tables in Annexure B.

4.2.1 Section A: Arandis town

4.2.1.1 NORM in garden samples

In the Arandis town, there are few gardens which are not really for commercial purposes but purposefully set up for domestic food consumptions. The gardens' samples were coded DG-S1, DG_S2, DG_S3, DG_S4 and DG_S5, and the other two samples coded AR_S_T1 and AR_S_T2 were collected from soil heaps from where the soil samples used in garden is collected. The weighted activity concentrations for these samples are shown in Table B1 on Annexure B and graphically represented in Figure 4.1.

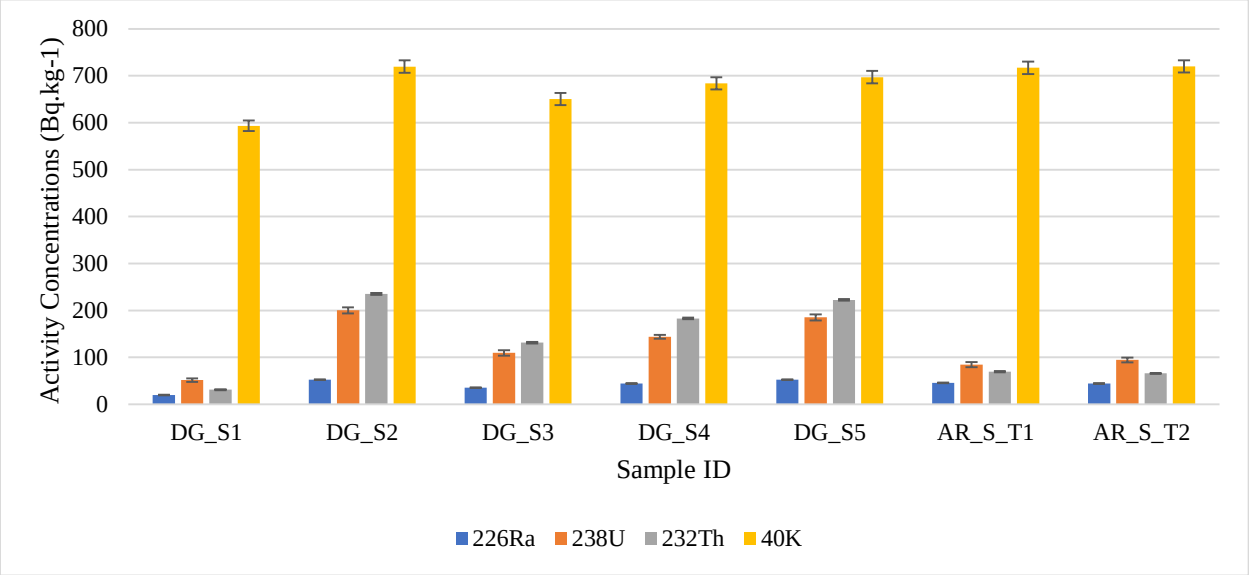

Figure 4. 1: The weighted mean concentrations of ^{226}Ra, ^{238}U, ^{232}Th and ^{40}K determined in samples of Arandis town gardens.

The soil samples collected have shown weighted activity concentrations for ^{226}Ra ranging from 19.73±0.47 to 52.58±0.87 Bq.kg^{-1} with an average of 42.22±0.73 Bq.kg^{-1}. The weighted radioactivity concentrations for ^{238}U ranged from 51.60±4.00 to 200.28±6.57 Bq.kg^{-1} with an average of 124.29±5.33 Bq.kg^{-1}. The fact that the samples were sealed and incubated for thirty (30) days does not mean ^{238}U and ^{226}Ra would be in radioactive equilibrium and this is due to the fact that their respective half-lives are longer. The results of these two nuclides had shown that their activity concentrations completely differ. ^{232}Th was determined with a weighted radioactivity concentrations ranging from 29.96±1.59 to

235.40±1.98 Bq.kg^{-1} with an average of 133.11±1.74 Bq.kg^{-1}. The non-series radionuclide ^{40}K had a weighted activity concentration calculated as 593.40±11.15 to 720.00±13.24 Bq.kg^{-1} with an average of 683.06±12.88 Bq.kg^{-1}. The activity concentrations for ^{238}U, ^{232}Th and ^{40}K are greater than the world averages levels and limits reported by UNSCEAR (2000). However, all minimum of activity concentrations were above average levels and limits, except for ^{226}Ra. The lowest and highest activity concentrations were observed for ^{226}Ra and ^{40}K, respectively. The average activity concentrations for ^{238}U, ^{226}Ra, ^{232}Th and ^{40}K in the garden samples were found to be above the world averages levels of 35, 33, 45 and 420 Bq.kg^{-1}, respectively (UNSCEAR, 2018; UNSCEAR, 2000).

4.2.1.2 NORM in soils of Arandis streets

The forty soil samples collected from the streets of Arandis town were coded AR 1, AR 2, AR 3, AR 4, …., AR 38, AR 39 and AR 40. The results for these representative samples were representatively reliable in providing the average background radiations of the town. The determined weighted activity concentrations were tabulated and graphically shown in Table B2 on Annexure B and Figure 4.2 in this chapter, respectively.

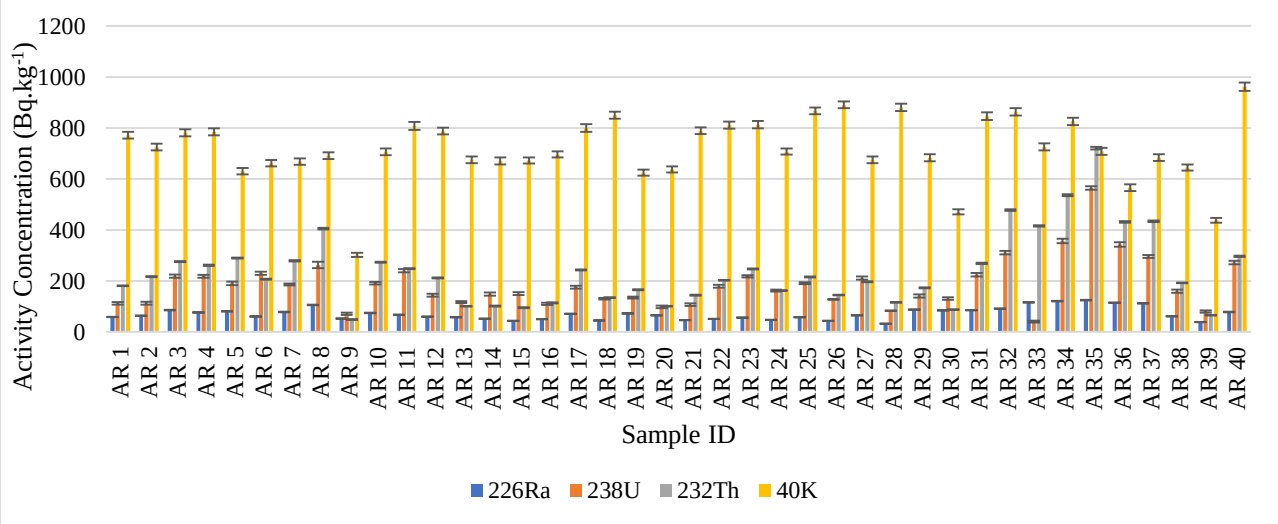

Figure 4. 2: The weighted mean concentrations of ^{226}Ra, ^{238}U, ^{232}Th and ^{40}K determined in samples around Arandis town.

The weighted activity concentrations calculated indicated a range of 32.59±0.53 to 124.19±1.30 Bq.kg^{-1} and an average of 70.84±0.87 Bq.kg^{-1} for ^{226}Ra, 40.54±3.71 to

564.80±7.33 Bq.kg^{-1} with an average of 186.22±5.49 Bq.kg^{-1} for ^{238}U, 49.34±0.68 to 720.98±4.48 Bq.kg^{-1} with an average of 237.16±1.98 Bq.kg^{-1} for ^{232}Th and 302.40±8.27 to 962.00±16.10 Bq.kg^{-1} with an average of 720.16±12.85 Bq.kg^{-1} for ^{40}K. ^{40}K had shown highest concentrations in all samples except sample AR 35. All calculated weighted activities in the samples were higher than both the world averages and world limits of all NORM. Only ^{226}Ra and ^{40}K were determined with minimum activity concentrations below the world averages. ^{226}Ra was observed with low weighted activity concentration in sample AR 28 and ^{40}K was determined with highest weighted activity concentration in sample AR 40, doubling both its world's average and limit values. The low values of ^{226}Ra concentration could be attributed to the fact that this radionuclide is soluble and therefore, could have drained into the soil with seasonal rain water. The high concentration of ^{40}K is attributed to the fact that the study was carried in as an arid region with minimal plants to absorb this radionuclide as fertilizer. The averages of the weighted activity concentrations for NORM in soil samples from Arandis streets were above the world's average values of 33, 35, 45 and 420 Bq.kg^{-1} for ^{238}U, ^{226}Ra, ^{232}Th and ^{40}K, respectively.

4.2.2 Section B: mine 1

4.2.2.1 Uranium ore sediments (granitic ores)

The crushed uranium ore sediments are fine particles in solid form obtained from the hard granitic rock shown in Figure 2.1. It is a silver-grey in colour in metallic form and dark grey to black as discussed in section 2.1

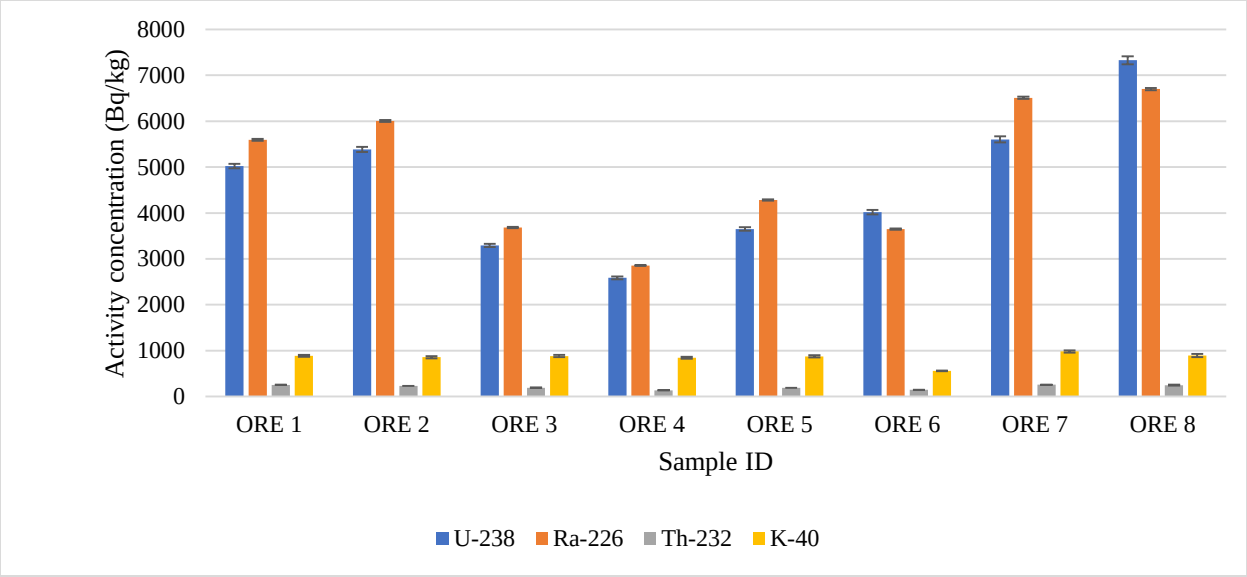

Figure 4. 3: The weighted activity concentrations associated with granitic uranium ore samples.

Uranium granitic ore samples were coded ORE 1, ORE 2, ORE 3, …, ORE 7 and ORE 8. Their activity concentrations are shown in Table B3 in the Annexure B and graphically represented in Figure 4.3. The weighted mean activity concentrations for ^{226}Ra ranged between 2855.84±11.02 Bk.kg^{-1} and 6700.44±24.02 Bq.kg^{-1}, with an average of 4909.39±18.13 bq.kg^{-1}. ^{238}U was determined with weighted mean activity concentrations ranging between 2585.38±28.48 Bq.kg^{-1} and 7325.38±84.42 Bq.kg^{-1}, with an average of 4610.29±50.57 Bq.kg^{-1}. The ratio for activity concentration for ^{226}Ra (4909.39±18.13 Bq.kg^{-1}) to that of ^{238}U (4610.29±50.57 Bq.kg^{-1}) was approximately 1.06. The weighted mean activity concentrations for ^{238}U were quantitatively approximated by those of ^{226}Ra, and therefore results had shown that the samples were collected from undisturbed natural soil. Only in natural soil can the concentration of ^{238}U be estimated by that of ^{226}Ra because of existence of secular equilibrium between the two nuclides.

^{232}Th and ^{40}K had weighted mean activities concentrations ranging from 136.62±3.23 Bq.kg^{-1} to 258.72±3.19 Bq.kg^{-1} with average of 207.51±3.93 Bq.kg^{-1}, and 561.90±8.49 Bq.kg^{-1} to 984.10±23.62 Bq.kg^{-1}, with an average of 849.09±23.20 Bq.kg^{-1}, respectively. Among all the determined radionuclides in NORM, ^{232}Th has been found with lower activity concentration in the samples, followed by ^{40}K and the dominant ^{238}U nuclide.

These results indicated that the activity concentrations due to all three primordial radionuclides of ^{238}U, ^{232}Th and ^{40}K in crushed uranium ores were significantly higher than the world's average values of 35, 45 and 420 $Bg.kg^{-1}$, respectively (UNSCEAR, 2018). Uranium concentration is expected to be high because the samples were collected in a uranium mining area. The samples originated from the calcerate-granitic rocks underground and therefore, an expectation of primordial radionuclides with high concentrations was inevitably feasible. In addition to the high concentrations, the ore samples originated from intrusive igneous rock which had been proven to strongly contain an average content of uranium and thorium at 5 ppm and 15 ppm, respectively (Onjefu *et al*., 2021).

4.2.2.2 Samples of mine tailings and surroundings

The activity concentrations for samples collected from mine 1 are shown in Table B4 in the Annexure B and graphically represented in Figure 4.4. These soil samples were collected from uranium mines' tailings and the surroundings, coded S01, S02, S03, …, S13 and S14. The weighted activity concentrations were used during analyses and discussions.

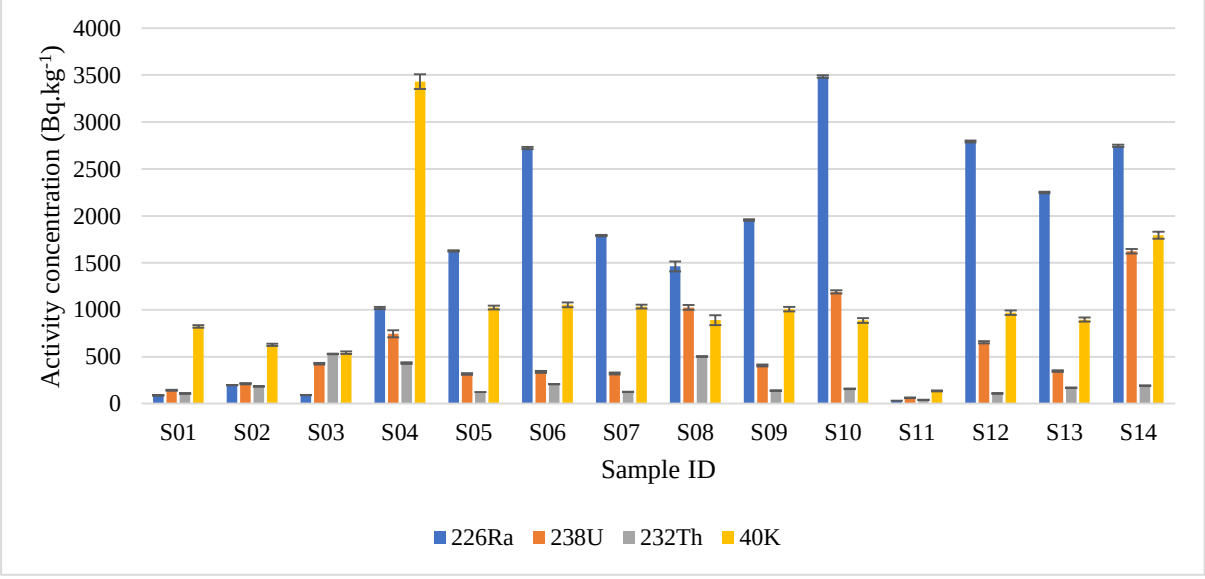

Figure 4. 4: The NORM from soil samples from study area B.

The weighted activity concentrations for ^{226}Ra ranged from 31.38±0.35 Bq.kg^{-1} to 3484.04±12.30 Bq.kg^{-1} with an average of 2546.56±10.38 Bq.kg^{-1}. The weighted activity concentrations for ^{238}U were ranging between 60.80±3.57 Bq.kg^{-1} and 1622.95±23.04 Bq.kg^{-1} with an average of 557.36±13.45 Bq.kg^{-1}. The calculated weighted average concentrations for ^{238}U and a daughter ^{226}Ra were incomparable. Human activities and other natural factors such as mining, milling, wind blowing and rainfall were possible causes of the disequilibrium between these two nuclides. Hence, this was considered a disturbed soil in the mining zone and therefore the weighted activity concentration for ^{238}U could not be quantified using its daughter nuclide ^{226}Ra. This was reflected by the ratio for activity concentration for ^{226}Ra (1131.52±7.47 Bq.kg^{-1}) to that of ^{238}U (421.58±10.98 Bq.kg^{-1}) which was approximately 3. ^{232}Th had weighted activity concentrations measured between 39.81±0.46 Bq.kg^{-1} and 530.09±3.42 Bq.kg^{-1} with an average of 215.59±2.37 Bq.kg^{-1}. The non-series ^{40}K radionuclide was activity concentration was calculated to be in a range of 135.60±3.48 Bq.kg^{-1} and 3429.00±78.63 Bq.kg^{-1}, and an average of 1079.12±26.60 Bq.kg^{-1}. Activity concentrations calculated for all three primordial radionuclides in NORM were higher than the world's average and limit levels on the earth's crust (UNSCEAR, 2018).

The weighted activity concentrations of ^{226}Ra was determined to be lowest in sample S11 and highest in sample S10. Only samples coded S1, S2, S3 and S14 were collected at a considerable distance from the tailings. Except S14, the samples which were not collected from tailings had shown significantly low concentrations in comparison to the values for tailings. Sample S14 recorded activity concentrations for both ^{226}Ra and ^{238}U at 3484.04±13.30 Bq.kg^{-1} and 1188.92±17.05 Bq.kg^{-1}, respectively. The high concentrations may be attributed to the facts that radionuclides may have been carried by wind-blown dusts, containing uranium and radium deposits, from tailings towards the sample locus point. Therefore, S14 collection point was considered a ^{238}U hotspot. Another sample of interest was S11, collected from tailings but recorded low activities ranging from a minimum of 31.38±0.35 Bq.kg^{-1} for ^{226}Ra to 135.60±3.48 Bq.kg^{-1} for ^{40}K. This evidence could be attributed to leaching of radionuclides in the soil, especially the soluble ^{226}Ra nuclide resulting into radon accumulation underground. The weighted activity concentrations for these nuclides were found to be above the world's average values of

35, 33, 45 and 420 Bq.kg^{-1} for ^{238}U, ^{226}Ra, ^{232}Th and ^{40}K, respectively. This concluded that the prevalence of cancers amongst miners working in these sites where possible.

4.2.3 Study area C: Khan river

The activity concentrations for samples collected from Khan river are shown in Table B5 in the Annexures and graphically represented in Figure 4.5. Six samples collected from nearby non-perennial Khan river, coded KHN1, KHN2, …, KHN6 were analyzed. This river is geographically running down to south-westerly between the two mines meeting up with the Swakop river. According to the SEMP report (2014), Khan river valley is regarded as an area with valuable deposits of uranium and may be affected by explorations in the near future for mining activities (GSN, 2014).

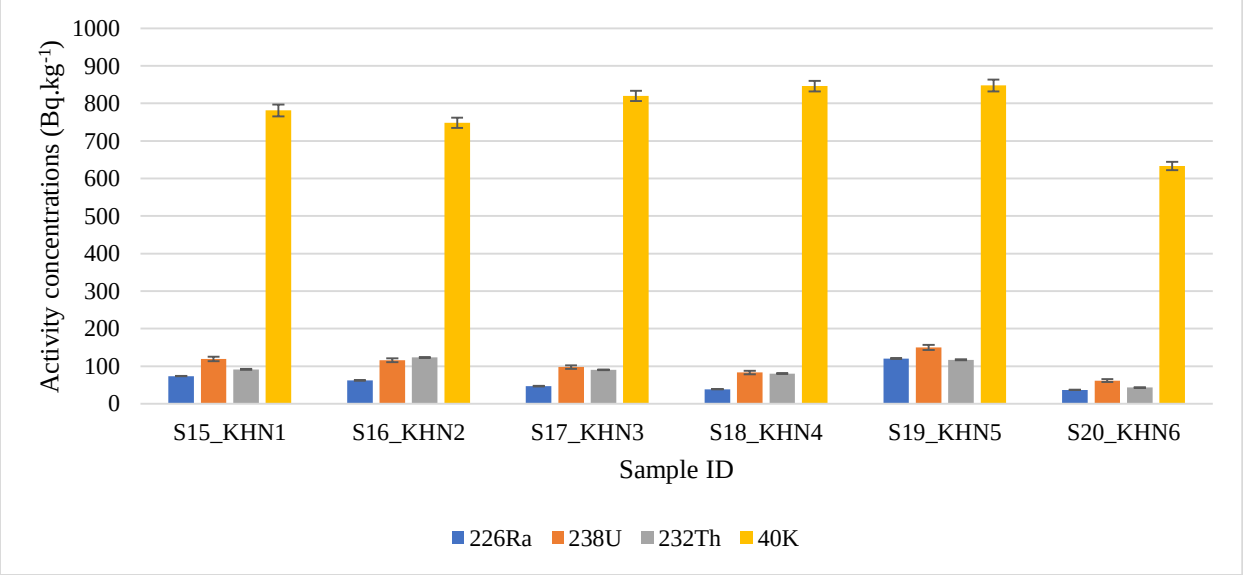

Figure 4. 5: Graphical representation of weighted mean concentrations of NORM determined in samples from Khan river.

The weighted activity concentrations were ranging from 36.96±0.46 to 120.60±0.99 Bq.kg^{-1} with an average of 63.27±0.69 Bq.kg^{-1} for ^{226}Ra, 61.91±4.07 to 150.13±6.73 Bq.kg^{-1} with an average of 104.77±5.23 Bq.kg^{-1} for ^{238}U, 43.34±0.57 to 123.29±1.55 Bq.kg^{-1} with an average of 91.02±1.09 Bq.kg^{-1} for ^{232}Th, and 633.40±11.06 to 847.90±15.83 Bq.kg^{-1} with an average of 779.58±13.93 Bq.kg^{-1} for ^{40}K. In exclusion of

^{40}K, the radioactivity levels of ^{226}Ra, ^{238}U and ^{232}Th determined in samples collected from this study area were significantly lower than those of measured in Arandis town samples. The water soluble ^{226}Ra was recorded with low activity concentration of 36.96±0.46 Bq.kg^{-1} and ^{40}K with a highest of 847.90±15.83 Bq.kg^{-1} in samples S20_KHN6 and S19_KHN5, respectively. The lower activity concentration was not only significantly comparable to, but the highest doubles both world's average values for ^{226}Ra and ^{40}K, respectively. The low concentrations could have been attributed to seasonal flow of water from highlands towards the sea.

4.2.4 Section D: mine 2

Tailings contribute to an increase in background radiation in the environment due to the reason that they are uncovered and deposited in the open environment, and can presumably be blown away by wind into the atmosphere, and also to nearby residential dwellings. Mining companies decrease windblown atmospheric exposure by using water tanks mounted on mining equipment to sprinkle on top of the soil. The samples collected from mine 2 were coded SU_T1, SU_T2, SU_T3, …, SU_T11 and SU_T12. Figure 4.6 and Table B6 (in Annexure B) represent the activity concentration of NORM in soils from uranium mine 2.

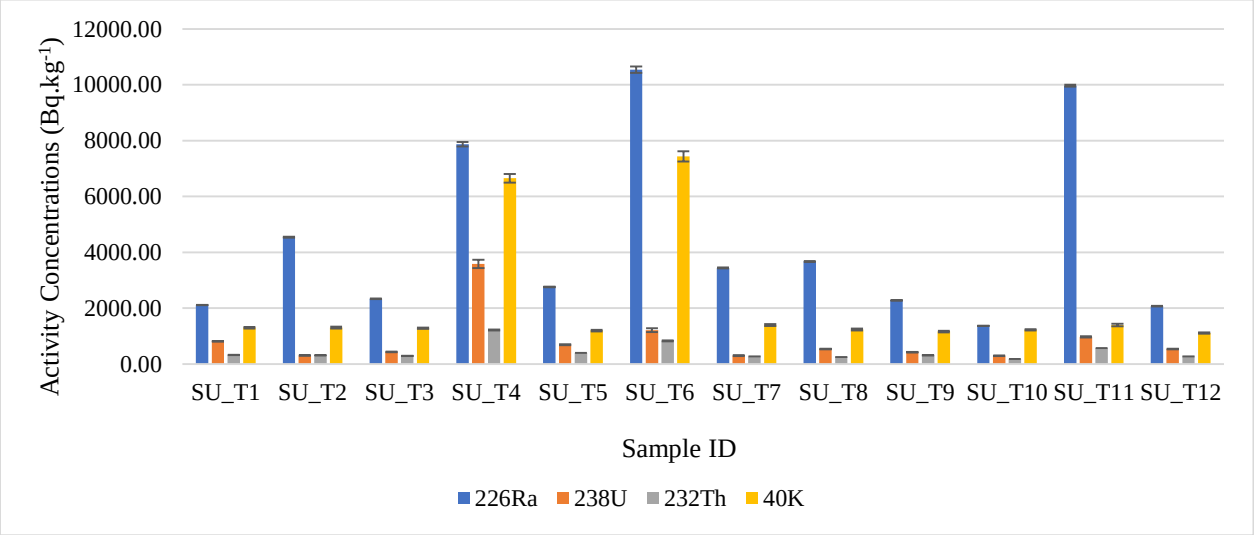

Figure 4. 6: The weighted mean concentrations of NORM determined from tailings samples from uranium mine 2.

The results captured using gamma spectroscopy had shown significantly high radioactivity concentrations. These analyses had shown ^{226}Ra calculated weighted activity concentrations between 1371.82±5.69 Bq.kg^{-1} and 10538.08±113.09 Bq.kg^{-1}, with an average of 4414.15±27.42 Bq.kg^{-1}. ^{238}U level was calculated and found to vary from 296.28±9.71 Bq.kg^{-1} to 3583.22±150.13 Bq.kg^{-1}, with an average of 842.59±29.31 Bq.kg^{-1}. As is the case with disturbed soil, a ^{226}Ra to ^{238}U ratio was approximated at 5, the disequilibrium exists between the nuclides. The concentrations are illustrated on the graph by the heights of their respective bars. The calculated radioactivity concentrations for both ^{232}Th and ^{40}K were 178.83±1.61 Bq.kg^{-1} to 1217.42±20.24 Bq.kg^{-1} and 1111.00±25.96 Bq.kg^{-1} to 7435.00±180.00 Bq.kg^{-1}, respectively. Their average values calculated were 436.74±5.16 Bq.kg^{-1} for ^{232}Th and 2225.00±52.65 Bq.kg^{-1} for ^{40}K. The concentrations of ^{238}U, ^{232}Th and ^{40}K in the samples were higher than world's average levels 35, 45, 420 Bq.kg^{-1}, respectively.

The minimum and maximum activity concentrations recorded were 178.83±1.61 Bq.kg^{-1} in SU_T10 and 10538.08±113.09 Bq.kg^{-1} in SU_T6 for ^{232}Th and ^{226}Ra, respectively. It was revealed by this study that the lowest determined activity concentration in tailing's soil was higher than the world average reported by UNSCEAR. Thorium series consists of thoron and other two soluble isotopes of radium which can be dangerous to humans if inhaled or ingested. Radium concentrations contribute to high rate of radon emanation into the atmosphere, ground and surface water as well and if the necessary measures are not put in place, may contribute to plants, animals and eventually human exposures.

4.2.5 Comparisons of determined average activity concentrations of NORM for samples from sections A, B, C and D

The minimum and maximum values for measured radioactivity concentrations of NORM in samples for this study and compared to other studies as well to world's average values are shown in Table 4.2.

Table 4. 2: The tabulated average values of activity concentrations (Bq.kg^{-1}) associated with samples from current study and those of other parts of the world.

Study area		Activity concentrations (Bq.kg^{-1})				References
		^{226}Ra	^{238}U	^{232}Th	^{40}K	
Arandis garden soil	Min	19.73±0.47	51.60±4.00	31.14±1.01	593.40±11.15	Current study
	Max	52.58±0.85	200.28±6.57	235.40±1.98	720.00±13.24	
	Ave	**42.22±0.73**	**124.29±5.33**	**134.13±1.56**	**683.06±12.88**	
Arandis streets soil	Min	32.59±0.53	40.54±3.71	49.34±0.68	302.40±8.27	Current study
	Max	124.19±1.30	564.80±7.33	720.98±4.48	962.00±16.10	
	Ave	**70.84±0.87**	**186.22±5.49**	**237.16±1.98**	**720.16±13.17**	
Arandis Average		**56.53±0.80**	**155.26±5.41**	**185.65±1.77**	**701.61±13.03**	Current study
Mine 1 granitic ore	Min	2855.84±11.02	2585.38±28.48	136.62±3.23	561.90±8.49	Current study
	Max	6700.44±24.02	7325.38±84.42	258.72±3.19	984.10±23.62	
	Ave	**4909.40±18.13**	**4610.29±50.57**	**207.51±3.92**	**849.09±23.20**	
Mine 1 soil	Min	31.38±0.35	60.80±3.57	39.81±0.46	135.60±3.48	Current study
	Max	3484.04±13.30	1622.95±23.04	530.09±3.42	3429.00±78.63	
	Ave	**1589.35±10.38**	**557.36±13.45**	**215.59±2.38**	**1079.12±26.60**	
Khan River	Min	36.96±0.46	61.91±4.07	43.34±0.57	633.40±11.06	Current study
	Max	120.60±0.99	150.13±6.73	123.29±1.55	847.90±15.83	
	Ave	**63.27±0.69**	**104.77±5.23**	**91.02±1.09**	**779.58±13.93**	
Mine 2 soil	Min	1371.82±5.69	296.28±9.71	178.83±1.61	1111.00±25.96	Current study
	Max	10538.08±113.10	3583.22±150.10	1217.42±20.24	7435.00±180.00	
	Ave	**4414.15±27.42**	**842.59±29.31**	**436.74±5.16**	**2225.00±52.65**	
Gold Mine, RSA		-	785.3 ± 13.7	43.9 ± 1.0	427.0 ± 13.1	(Kamunda *et al*., 2016)
Tin Mine, Bangka Island	Range	2.47 – 4231.06	5.41 – 5411.27	2.91 – 7543.46	2.79 – 217.43	(Murniasih *et al*., 2021)
Walvis Bay, Namibia	Ave	99.59±24.39	-	90.90±31.99	553.07±107.17	(Njinga *et al*., 2016)
Henties Bay, Namibia	Ave	175.59±0.92	-	40.17±27.00	349.66 ± 8.00	(Onjefu *et al*., 2017)
bauxite ore deposit, Cameroon	Ave	125	99	157	671	(Nguelem *et al*., 2016)
World	Ave (Range)	33 (16 – 110)	35	45 (11 – 64)	420 (140 – 850)	(UNSCEAR, 2000)

The average radioactivity concentrations measured for ^{226}Ra measured in the whole study area had shown a minimum value of 42.22±0.73 Bq.kg^{-1} determined in Arandis garden. This average value was greater than the world average. Significantly higher values for ^{226}Ra concentrations were determined at mine 1 with 4909.40±18.13 Bq.kg^{-1} in granitic ore samples and 1589.35±10.38 Bq.kg^{-1} in tailings samples, and tailings samples of mine 2 recorded 4414.15±27.42 Bq.kg^{-1}. The mining area 1 has shown high concentration of potassium-40, up to 3429.00±78.63 Bq.kg^{-1}, about ten times higher than the world average value for radionuclide. The high level of potassium is likely to significantly contribute to the high rate of increase of deterministic effects on people living in the region in the future.

The concentration of ^{238}U in samples from the study area were recorded with minimum level in samples of Khan river at 104.77±5.23 Bq.kg^{-1} and very high level in granitic ore samples of mine 1, about 130% higher than the world average of 35 Bq.kg^{-1}. ^{232}Th nuclide was recorded with a minimum of 91.02±1.09 Bq.kg^{-1} in Khan River and a maximum of 436.74±5.16 Bq.kg^{-1} in mine 2, almost ten times higher than the world average value of 45 Bq.kg^{-1}. ^{40}K concentration ranged from 683.06±12.88 Bq.kg^{-1} to 2225.00±52.65 Bg.kg^{-1}, as high as five times in comparison with the world average value of 420 Bq.kg^{-1}. All determined activity concentrations of NORM in samples, except the minimum average of ^{40}K, were above the worldwide ranges of 11 to 64 Bq.kg^{-1} for ^{238}U, 17 to 60 Bq.kg^{-1} for ^{232}Th and 140 to 850 Bq.kg^{-1} for ^{40}K (UNSCEAR, 2017). Figure 4.7 shows the average weighted activity concentrations of soil samples from the whole study area.

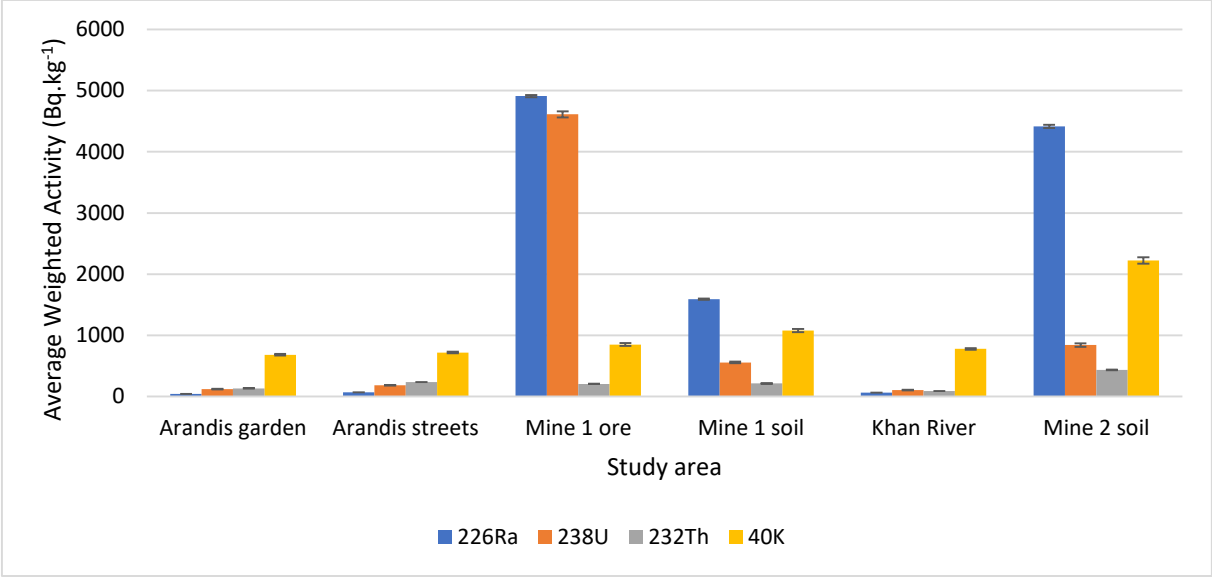

Figure 4. 7: The average weighted mean activity concentrations associated with samples from study area A, B, C and D.

The averages of all weighted activity concentrations of NORM calculated for Arandis town and Khan river in this study were insignificantly higher but comparable to those in a study by Njinga *et al*., (2016) covered on selected areas around uranium mines in Erongo region. ^{238}U and ^{226}Ra concentrations were found to be high in uranium mines (mine 1 and 2) tailings' soil samples and were comparable to those measured in a tin mine of Bangka Island by Murniasih *et al*. (2021). The concentrations were also significantly higher than those of a bauxite ore deposits in Cameroon studied by Nguelem *et al*. (2019). With exception of soil samples of uranium mine 2, the level of ^{232}Th concentrations were found to be significantly higher than both world's average and range, and comparable to that of bauxite ore deposits in Cameroon. Uranium mine 2 (section D) had also shown very high concentration of ^{40}K, above the world ranges.

4.3 Radiological hazards associated with samples from the study area

The activity concentrations obtained in section 4.2 were used to estimate the radiological health related hazards to the residents of Arandis town as a control area due to ^{226}Ra, ^{238}U, ^{232}Th and ^{40}K primordial radionuclides. The radiological hazards estimated were the dose rate, radium equivalent, indoor and outdoor annual effective dose, gamma index,

alpha index and excess lifetime cancer risks. The radiological hazards were calculated using equations 3.15 – 3.27. The gamma absorbed dose rate in air at 1 m above the ground was estimated using the activity concentrations of ^{238}U, ^{232}Th and ^{40}K. Radium equivalent activity was obtained from the activity concentrations of ^{226}Ra, ^{232}Th and ^{40}K in samples. The annual effective doses were calculated for the age group above 16 years because they are adults who are likely exposed to ionizing radiations both at work and homes. External hazards were estimated by radium equivalent activity to assess external exposures by gamma dose from building materials. The alpha index was estimated from the activity concentrations of ^{226}Ra, ^{232}Th and ^{40}K associated with NORM in samples collected from sections A, B, C and D. Gamma index was calculated using activity concentration of ^{226}Ra only associated with soil samples used for this study. All estimates of radiological hazards should not be regarded as measures of health detrimental effects.

4.3.1 Study area A

4.3.1.1 Garden samples hazards

The radiological health hazards associated with NORM in soil samples from the garden and soil hips were calculated using Equations 3.15 to 3.27 in Chapter 3. The results are shown in Table C1 in the Annexures and graphically represented in Figures 4.8 – 4.12.

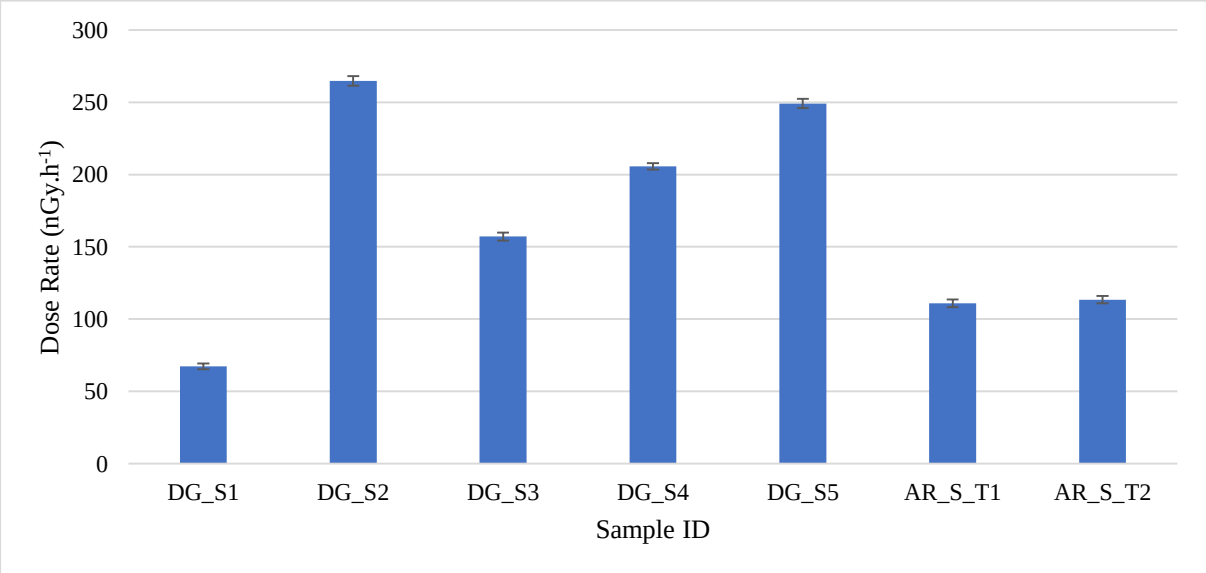

Figure 4. 8: Dose rates calculated from samples from gardens.

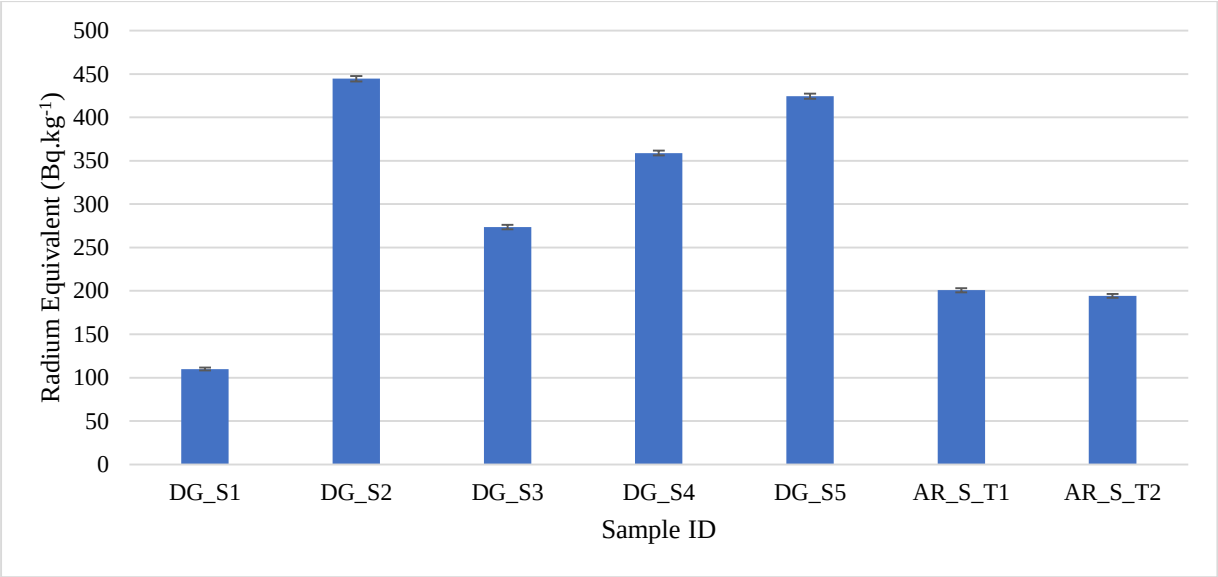

Figure 4. 9: Radium equivalent activity of soils in the gardens.

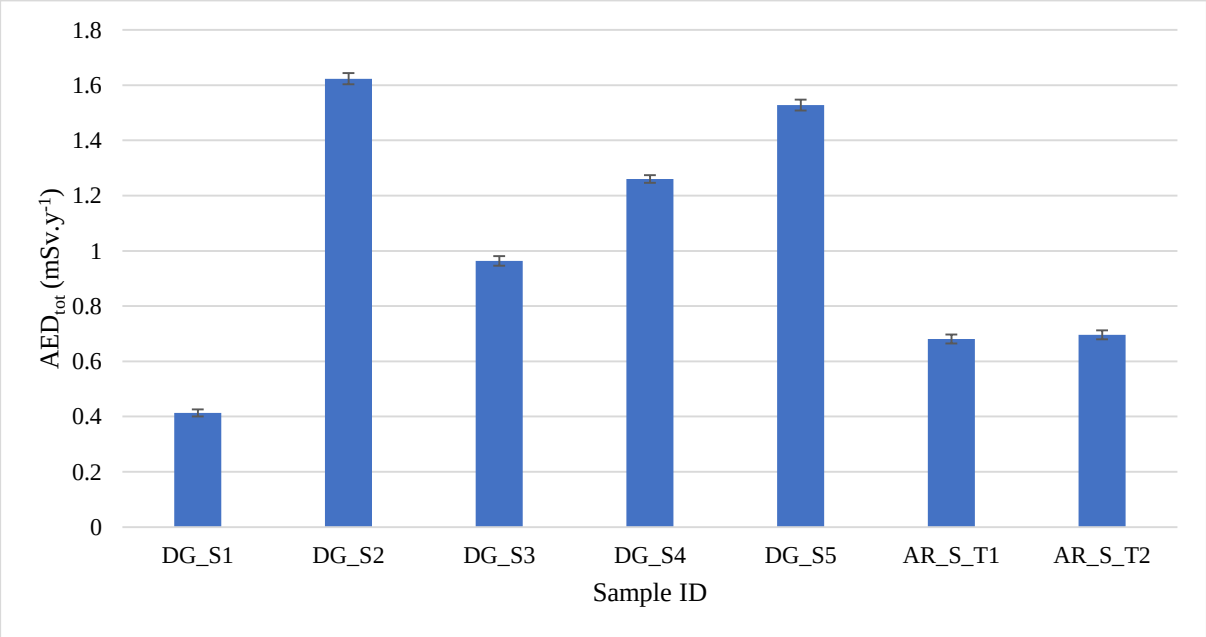

Figure 4. 10: Annual effective dose calculated in soil from gardens.

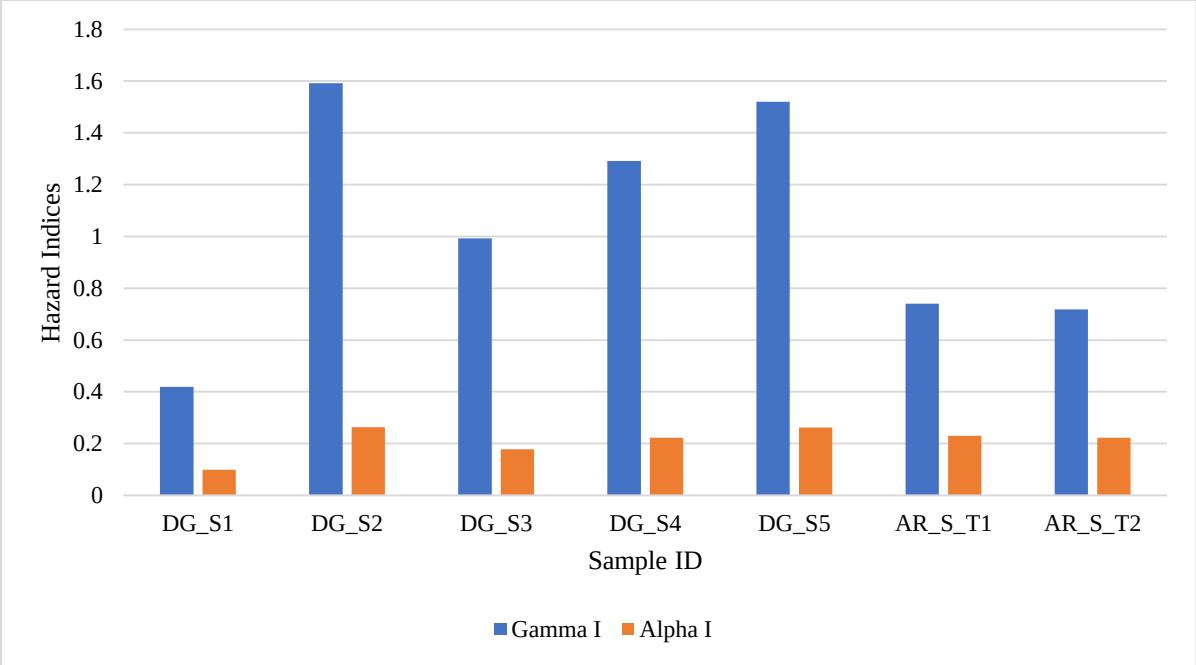

Figure 4. 11: Hazard indices in soil samples from the gardens.

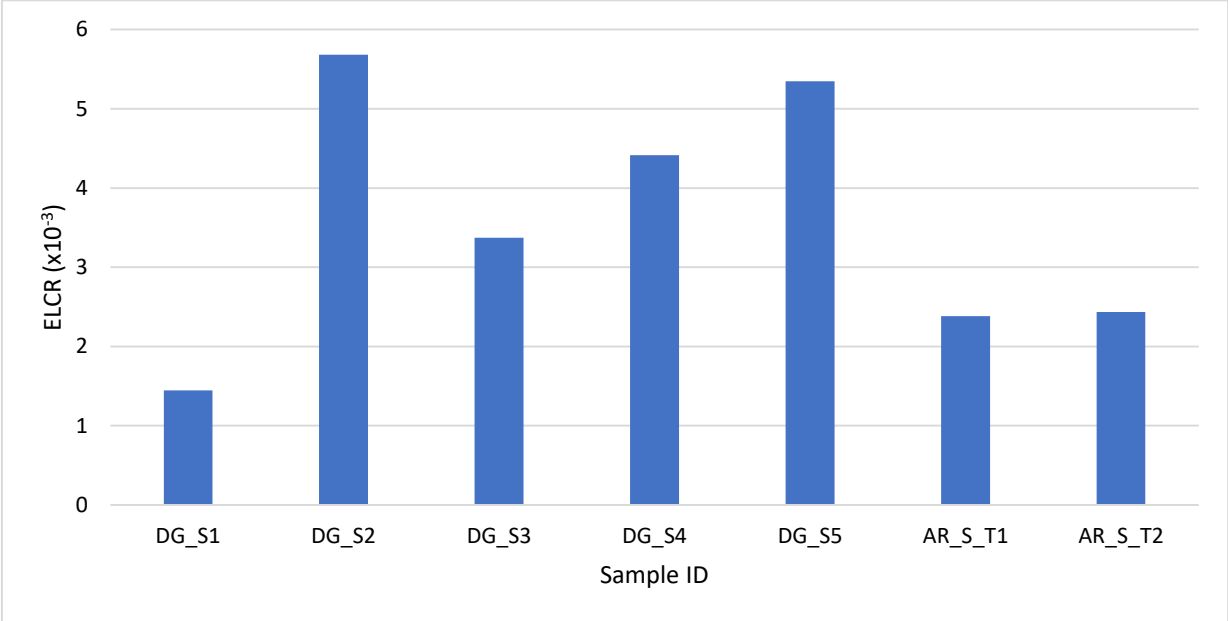

Figure 4. 12: Excess life cancer risks calculated in soil samples from the gardens.

Soil used for agricultural purposes such as animal grazing, crops and vegetables farming must be well investigated for radioactive hazards for the benefits of primary and secondary users in the food chain. Five samples from the garden and two samples from

the main heap soil in the gardens were analyzed for this purpose. The dose rate calculated from these samples ranged from 67.39±2.00 to 264.72±3.31 nGy.h^{-1} with an average of 166.30±2.70 nGy.h^{-1}. The annual effective dose ranged from 0.41 to 1.62 mSv.y^{-1} with an average of 1.02 nGy.y^{-1}. The radium activity calculated ranged from 109.95±1.74 to 444.60±3.14 Bq.kg^{-1} with an average of 286.63±2.55 Bq.kg^{-1}. The average radium equivalent activity for the samples was comparable to 370 Bq.kg^{-1} for building materials with gamma dose exposure of 1 mSv.y^{-1}.

The hazards indices; external, internal, annual effective dose, gamma, and alpha indices were presented in Annexure C ranging from 0.30 to 1.20, 0.35 to 1.34, 0.41 to 1.62 mSv.y^{-1}, 0.42 to 1.59 and 0.10 to 0.26 with averages of 0.77, 0.89, 3.58 mSv.y^{-1}, 1.04 and 0.21, respectively. These results had shown that the average absorbed dose calculated was significantly higher than both the world average outdoor exposure of 60 nGy.h^{-1} for global primordial radiation and standard limit of 84 nGy.h^{-1} (UNSCEAR, 2000). The average annual effective dose was comparable to 1 mSv.y^{-1} permissible limit value for public exposure (UNSCEAR, 2018). The excess life cancer risk (x 10^{-3}) determined in samples ranged from 1.45 to 5.68, with an average of 3.58. The cancer risk was higher than the world average of 0.29 x 10^{-3} (UNSCEAR, 2017).

4.3.1.2 Radiological health hazards of samples from the Arandis town

The radiological hazards of NORM in Arandis soil samples calculated and tabulated in Table C2 of Annexure C and graphical representations are shown in Figures 4.13 – 4.17.

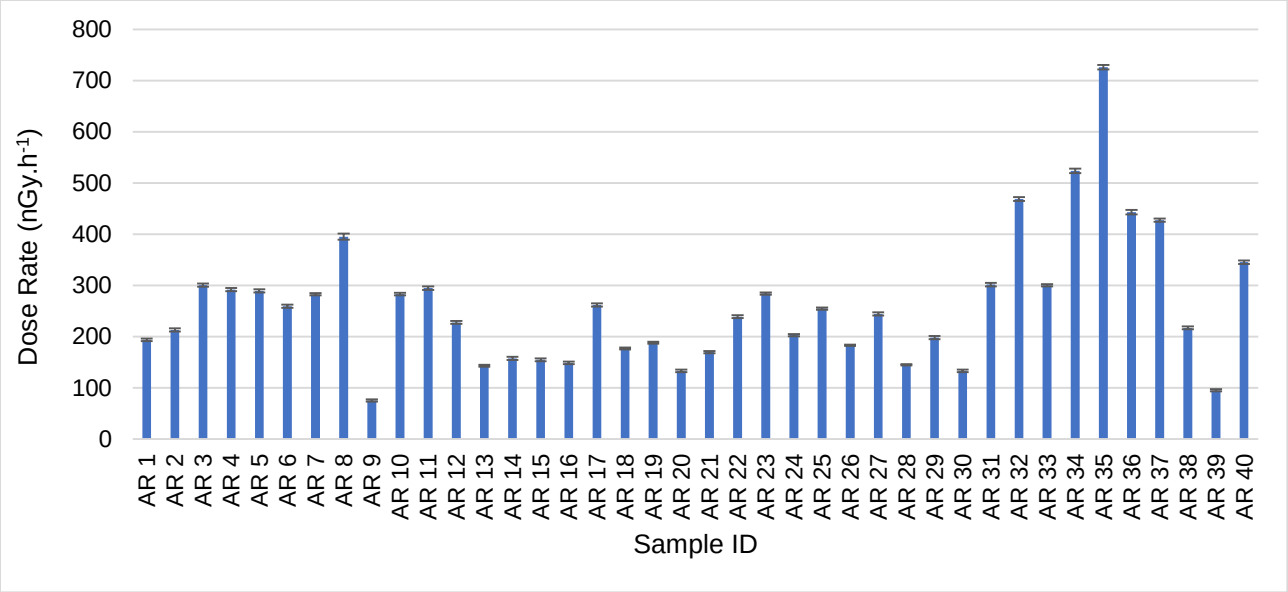

Figure 4. 13: The dose rates calculated from samples of Arandis town.

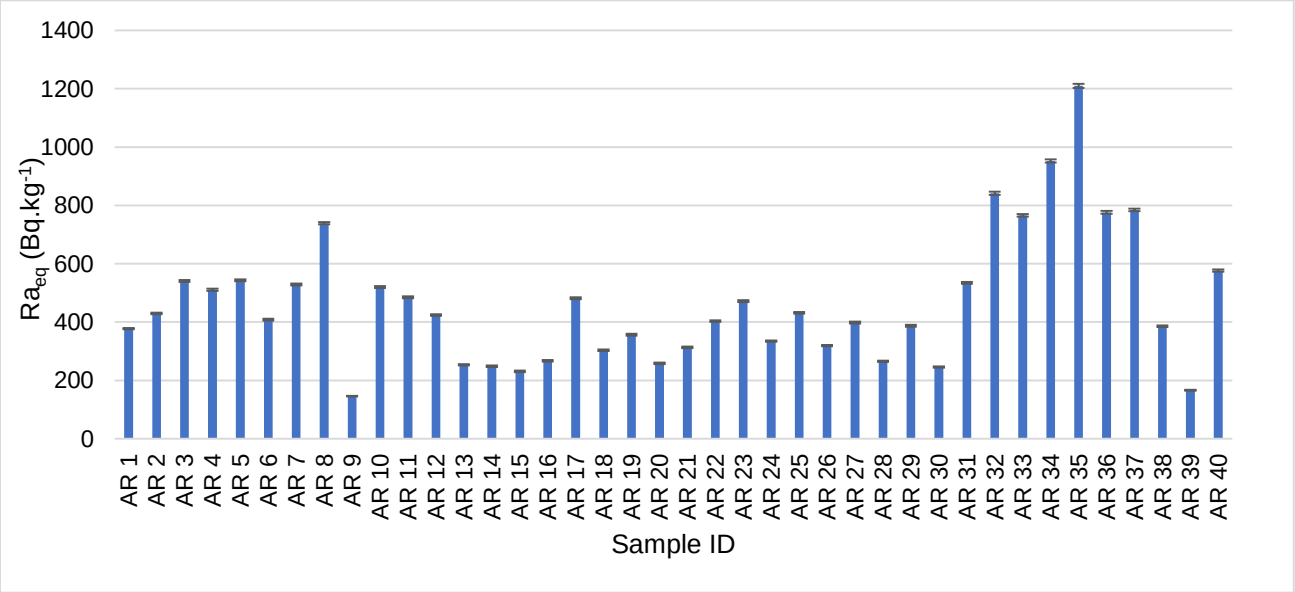

Figure 4. 14: The radium equivalent activity calculated from samples of Arandis town.

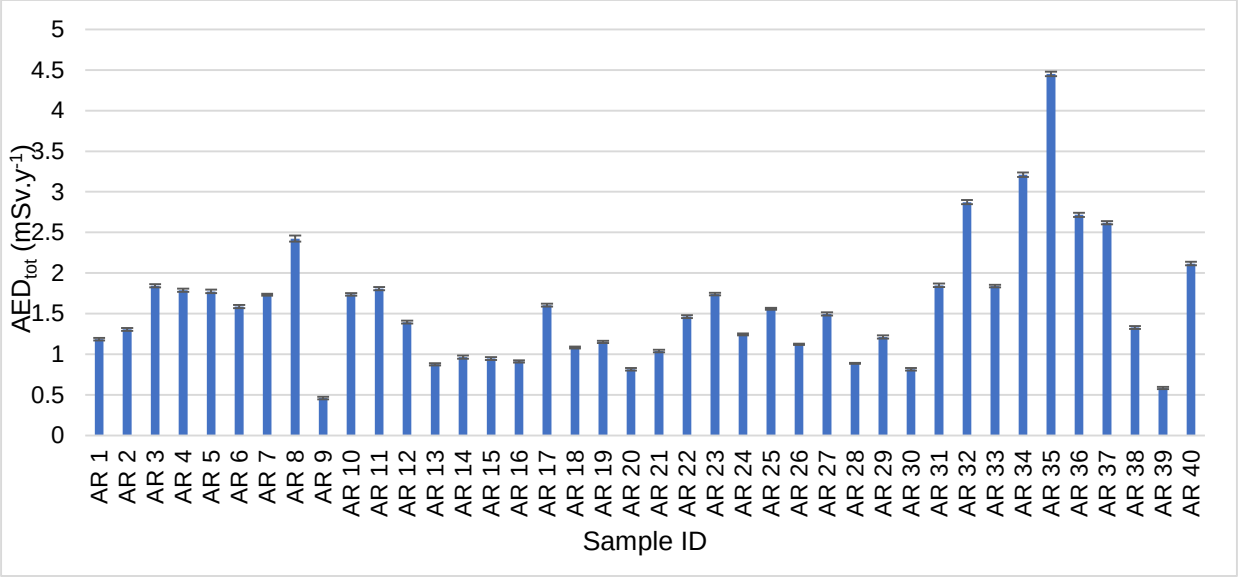

Figure 4. 15: The annual effective dose calculated from samples of Arandis town.

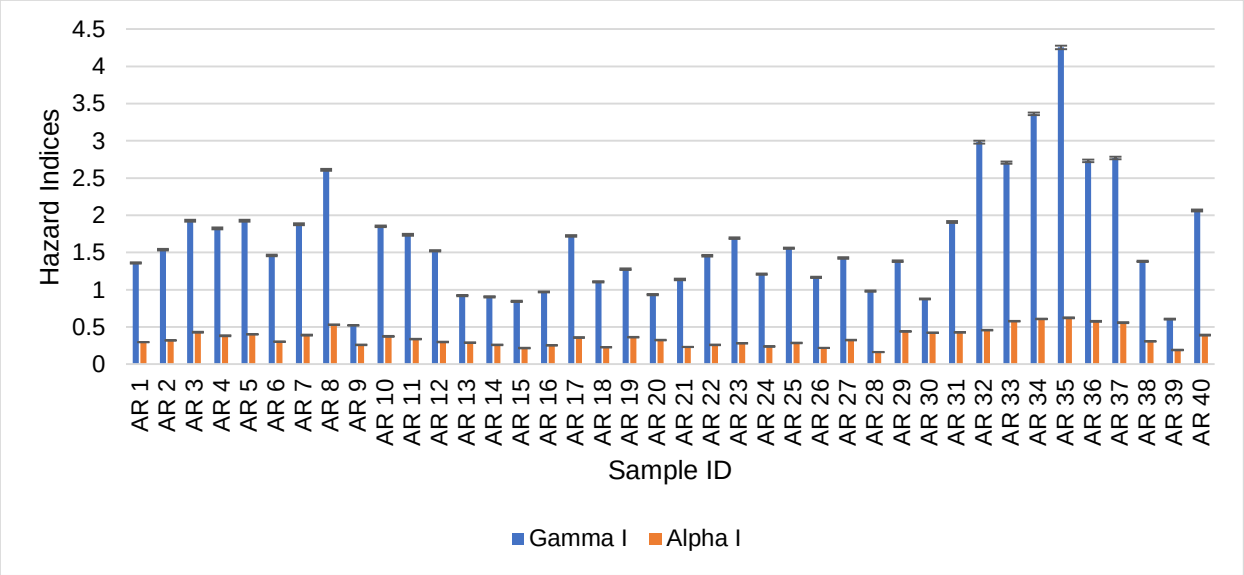

Figure 4. 16: Hazard Indices calculated from samples of Arandis town.

The activity concentrations of ^{238}U, ^{232}Th and ^{40}K were used in estimating the radiological hazards associated with soil samples collected from Arandis town. The estimated gamma dose rates in air at 1 m above the flat surface was determined to be between 75.31±2.31 and 725.95±4.38 nGy.h^{-1} with an average of 259.31±2.89 nGy.h^{-1}. The determined average gamma dose rate calculated for this study was higher than the world average of

59 nGy.h^{-1} (UNSCEAR, 2000). The radium equivalent activity calculated ranged from 145.78±1.34 to 1209.74±6.63 Bq.kg^{-1} with an average of 465.43±3.14 Bq.kg^{-1}.

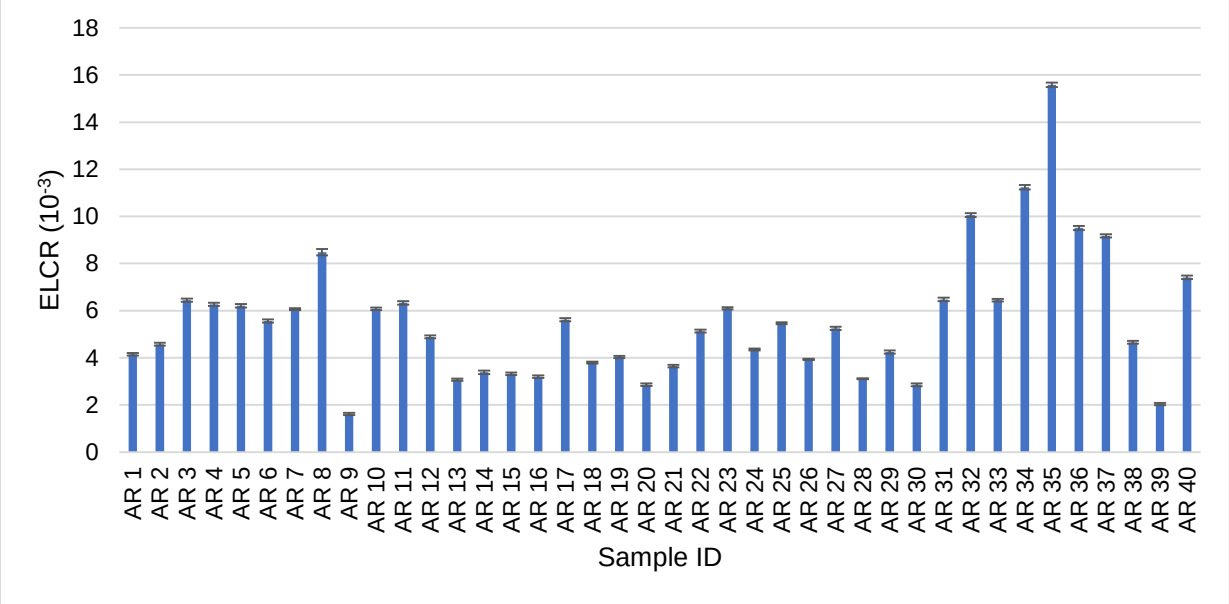

Figure 4. 17: Excess life cancer risks of soil samples from Arandis town.

Radium equivalent activity estimated the gamma dose exposed to humans from building materials and it is expected that the value should not exceed the maximum of 370 Bq.kg^{-1} for the material to be considered safe for building purposes. Hence, the reported radium equivalent activity for the samples was 26% higher than the recommended radioactivity concentration for external exposure safety criterion. The outdoor and indoor annual effective dose for adults (age above 16 years) was estimated at 92.36±2.83 to 890.30±5.37 µSv.y^{-1} and 369.45±11.34 to 3561.22±21.47 µSv.y^{-1}, with averages of 318.02±3.54 µSv.y^{-1} and 1272.08±14.16 µSv.y^{-1}, respectively. The total annual equivalent doses were estimated from the absorbed dose ranging between 0.46 and 4.45 mSv.y^{-1} with an average of 1.59 mSv.y^{-1}. The average annual effective dose was lower than the averages both for Erongo region and world, but about five times higher than recommended dose constraint for the public of 0.3 mSv.y^{-1} for each source (ICRP, 2013). The radiological indices such as alpha and gamma were estimated from activity concentrations for ^{226}Ra, ^{238}U and ^{40}K, and ^{226}Ra, respectively. Alpha index was estimated to be in a range of 0.52 to 4.26 with an average of 1.66. Gamma index was determined

and it varied from 0.16 to 0.62±0.01 with an average of 0.35. The excess life cancer risks (x 10^{-3}) at average life-time of 70 years was estimated and the values range from 1.62x10^{-3} to 15.58x10^{-3} with an average of 5.57x10^{-3}. This basically means the excess life cancer risk calculated for the current study in Arandis was about twenty times (x20) higher than the world average. A study by Munyaradzi *et al*. (2018) reported the average excess life cancer due to external exposure from terrestrial radiations in Karibib and Arandis towns at 0.36x10^{-3} and 0.49x10^{-3}, respectively (Munyaradzi *et al*., 2018). In addition to that, the current study discovered excess life cancer risk in Arandis to be ten times higher than those reported by Munyaradzi *et al*. (2018) in both Arandis and Karibib.

4.3.2 Study Area B

4.3.2.1 Crushed uranium ore sediments

The radioactivity concentrations of NORM in granitic ore samples from uranium mine 1 (section B), coded ORE1, …, ORE8, were again utilized in calculations of radiological related hazards to humans. The results are shown in Table C4 (in Annexure C) and graphically in Figures 4.18 – 4.22.

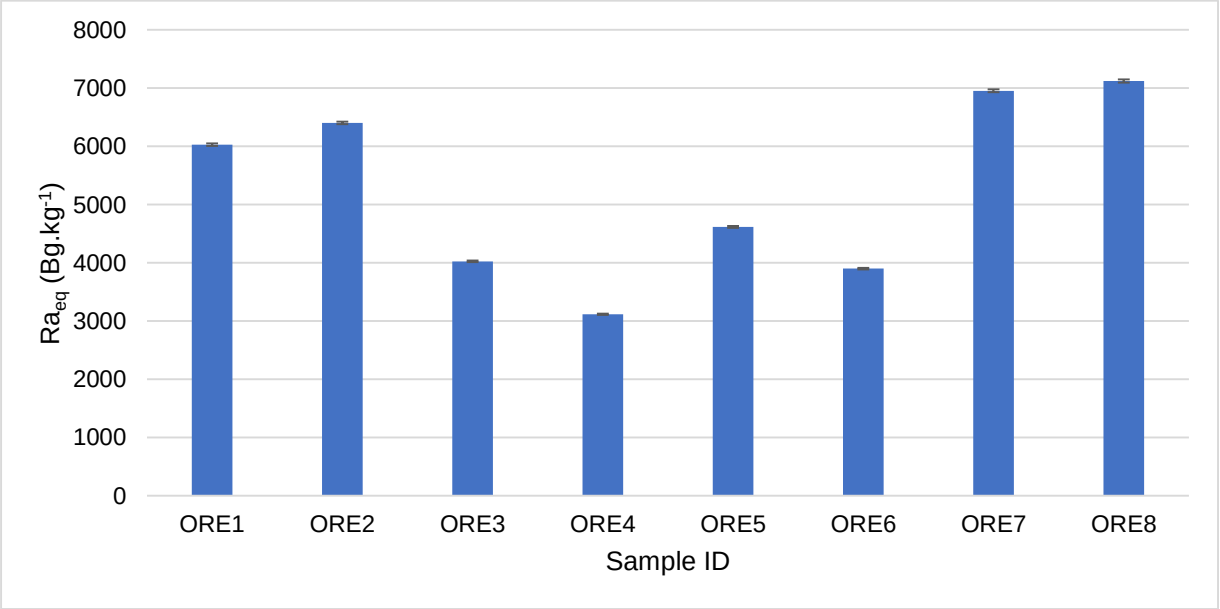

Figure 4. 18: The radium equivalent activity concentrations of the crushed ores due to NORM.

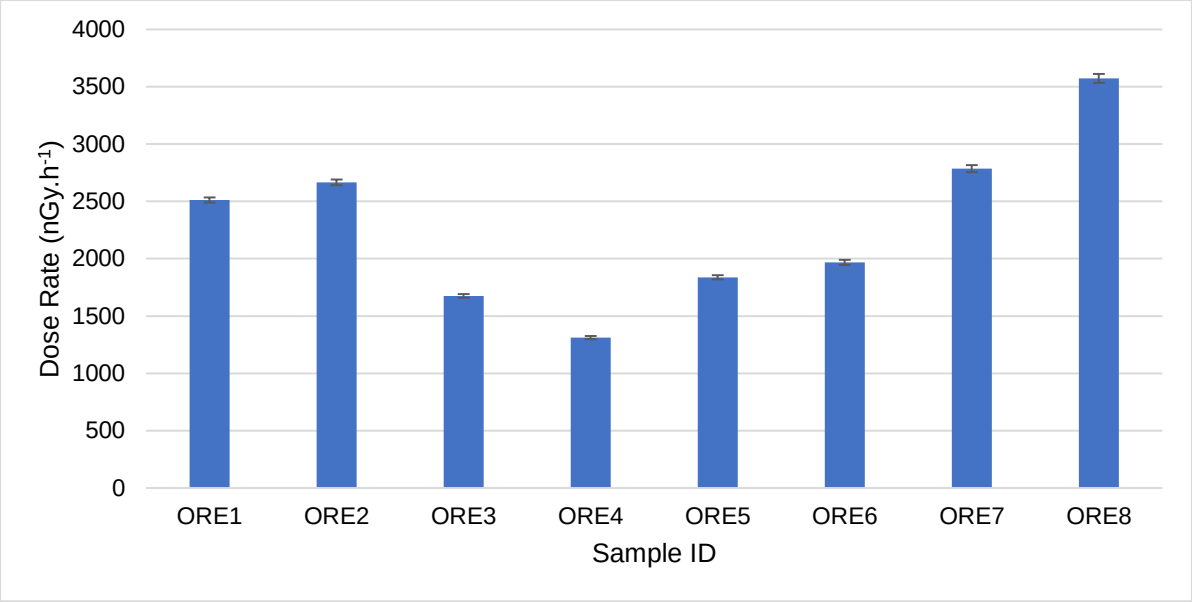

Figure 4. 19: The calculated dose rates, at 1 m above the ground, of crushed granitic ore due to NORM concentrations in samples.

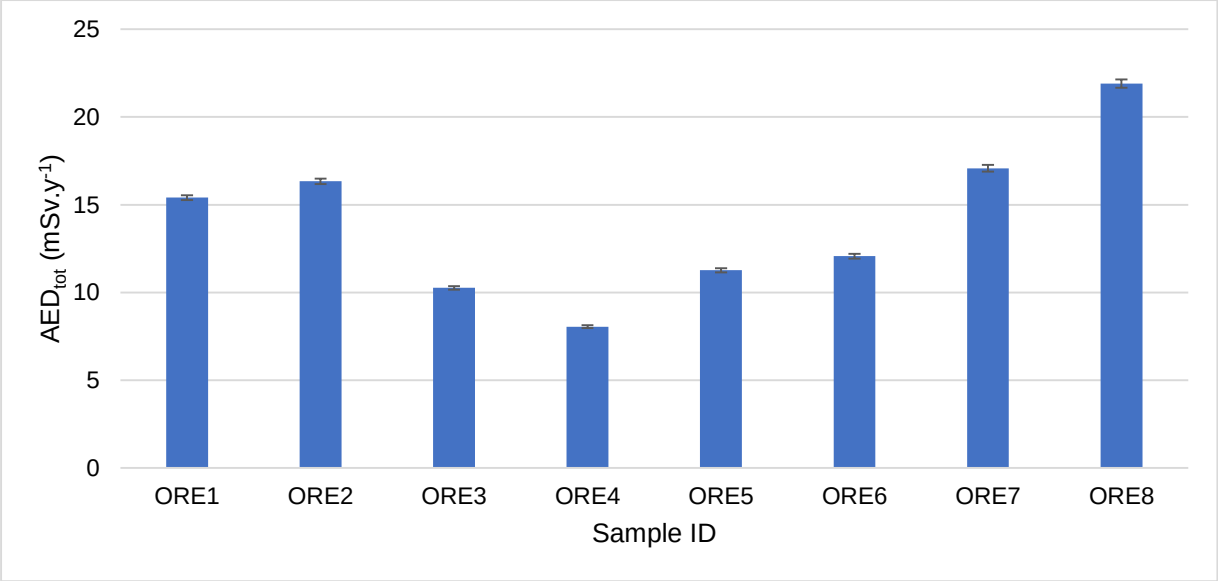

Figure 4. 20: The annual effective dose determined in the crushed granitic ores samples.

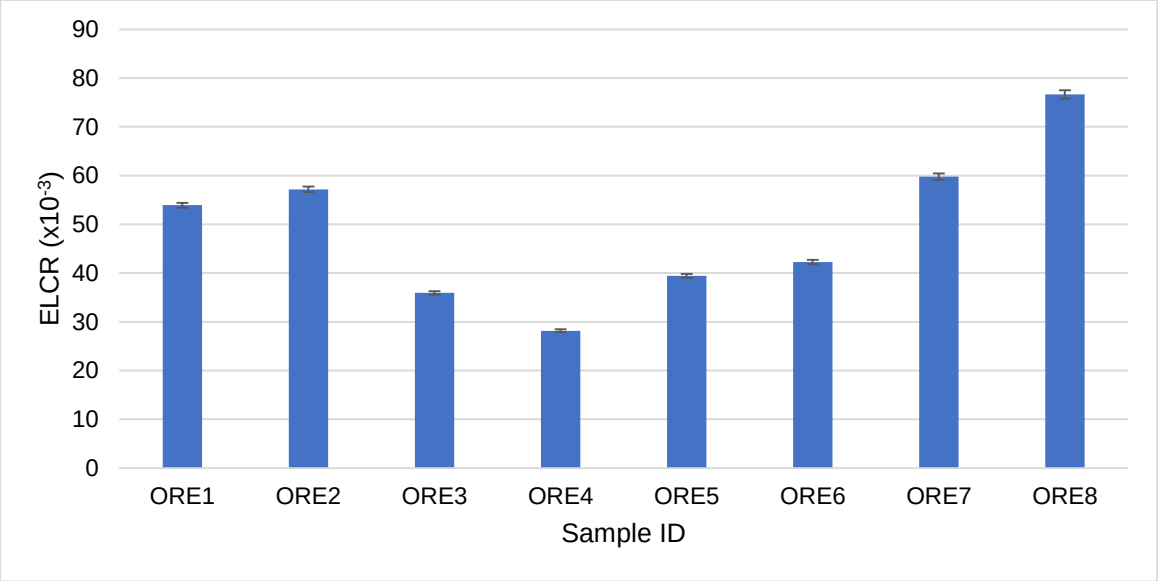

Figure 4. 21: Excess life cancer risks (ELCR) calculated from crushed ore samples.

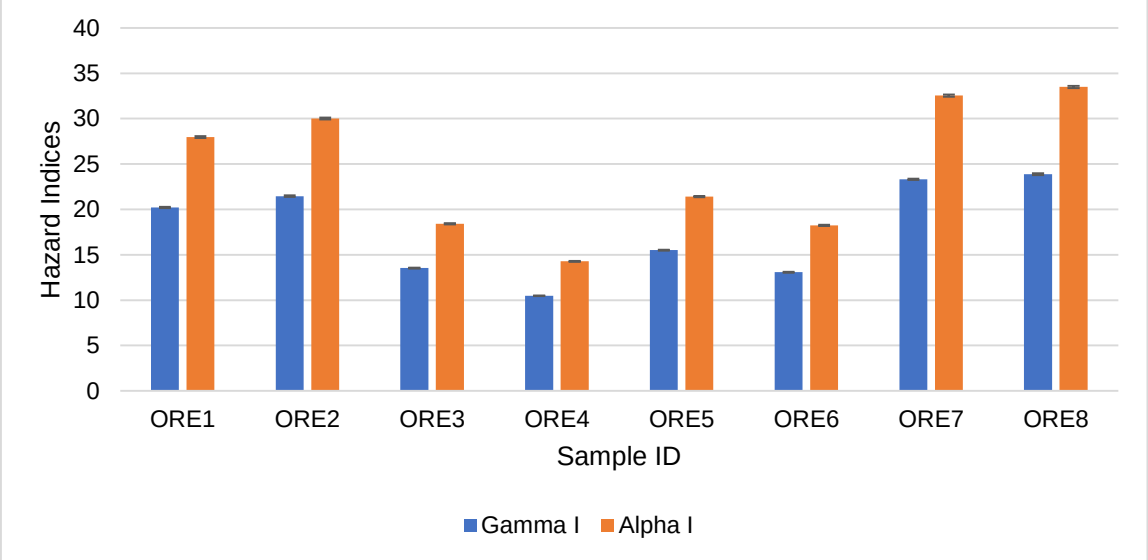

Figure 4. 22: Alpha and gamma hazard indices due to NORM, with their respective errors, as calculated from crushed granitic ore samples.

The calculated results for dose rates are shown in Table C3 in Annexure C. The values for absorbed dose rates ranged between 1312.23±13.34 and 3571.74±39.54 nGy.h^{-1} with an average of 2290.70±23.53 nGy.h^{-1}. Also, the absorbed dose rates were significantly higher than the world average outdoor and indoor exposures of 60 nGy.h^{-1} and 84 nGy.h^{-1} for global primordial radiation, respectively, recommended by UNSCEAR (2000). Both

indoor (AED_{in}) and outdoor (AED_{out}) annual effective dose calculated were significantly higher than the recommended limit of 1 $mSv.y^{-1}$ for public. The total annual effective dose (AED_{Tot}) had shown a weighted mean and average errors with minimum of 8.05±0.08 $mSv.y^{-1}$ and maximum of 21.90±0.24 $mSv.y^{-1}$ with an average of 14.05±0.14 $mSv.y^{-1}$. AED_{Tot} values were about six times higher than the average effective dose reported Ministry of Mines and Energy (2010) in a year. Both the outdoor and indoor annual effective dose efficiency values were significantly higher than the world permissible limit value of 70 $\mu Sv.y^{-1}$ (UNSCEAR, 1988). This could be a result of a geological background area of collection of samples under the study.

The radium equivalent activities calculated for the samples of uranium ore deposits analysed were very high. The lowest value calculated was 2845.86±28.91 $Bq.kg^{-1}$ and the highest being calculated was 7749.60±85.77 $Bq.kg^{-1}$. All other values are shown in Table 3C of Annexure C. These values were very high, almost ten times higher, compared to the safely defined level of 370 $Bq.kg^{-1}$ for building materials (UNSCEAR, 2000). This indicates that gamma dose exposures expected from uranium ores when used as building materials was approximated at 150 $mSv.y^{-1}$ in excess of the permitted value to the public, but less than the occupational exposure provided that none of annual exposure exceeds 50 mSv. Therefore, it is advisable that management of the mine should not allow a small fraction or portion of uranium ore deposits to get in contact with building materials used for construction inside and outside the mine, region and the whole country at large. Therefore, preventative measures should be put in place to avoid any contact or transfer of these ore deposits to construction materials.

The external exposures (external hazard index, H_{ex}) by photons (gamma rays) from radon (^{222}Rn) and thoron (^{220}Rn) accumulations, together with their short-lived products (Amanjeet *et al*., 2017), were calculated with a minimum of 7.93 ± 0.10 and maximum of 18.59 ± 0.20 recorded. Table D3 in Annexure D shows clearly that sample ORE 8 could probably pose the highest hazardous effects to human health. The external hazard index of uranium ore samples was higher than the maximum permissible limit of 1 $mSv.y^{-1}$ due to natural radioactive materials in the mine. All diagrams for radiological hazards calculated in this study are shown on Figures 4.18 – 4.22. The calculated gamma index

values in this study shows that internal annual effective dose to employees was extremely high, ranging between 10.48±0.04 and 23.88±0.10, with an average of 17.69±0.07. The values of the alpha index falls between 14.28±0.06 and 33.50±0.12, with average of 24.55±0.09. Both the gamma and alpha indices calculated were approximately ten times higher than a unit prescribed by International Commission on Radiation Protection in homes and at work (ICRP, 1994). Excess lifetime cancer risk calculated for uranium ore samples ranged from $28.16x10^{-3}$ to $33.50x10^{-3}$ with an average of $24.55x10^{-3}$. The excess lifetime cancer risks determined in this study were significantly approximated to a hundred times in excess than the world average of $0.29x10^{-3}$ (UNSCEAR, 2017). Expectation of high radiological health related hazards were inevitable because granitic rocks were sources of these ore samples.

4.3.2.2 Tailings soil and mining licensed area

The radiological hazards calculated for samples collected in Mine 1 were recorded in Table C4 in Annexure C and graphically represented in Figures 4.23 – 4.27.

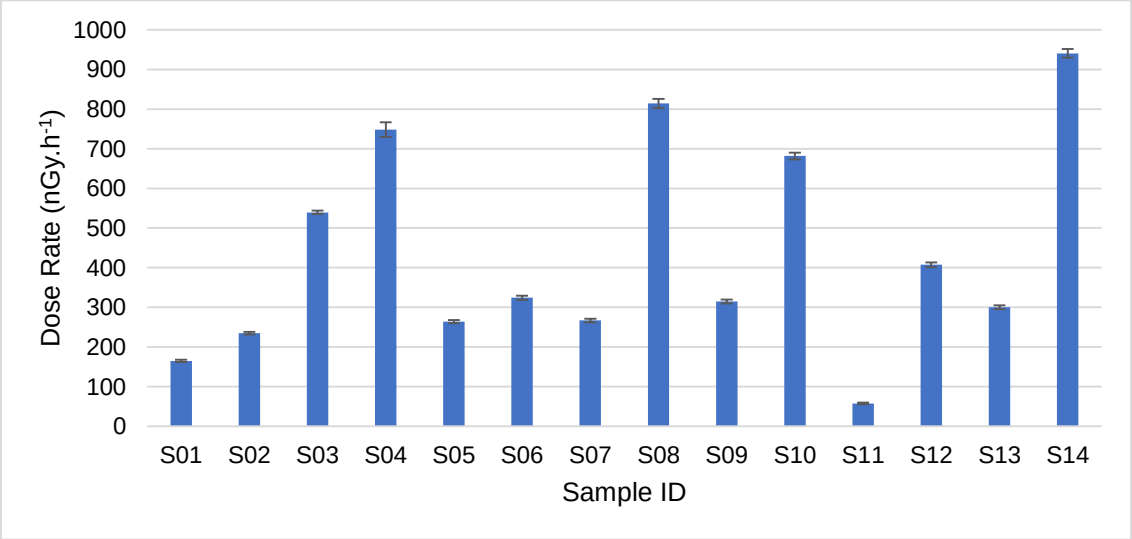

Figure 4. 23: The calculated dose rates of soil samples from mine B.

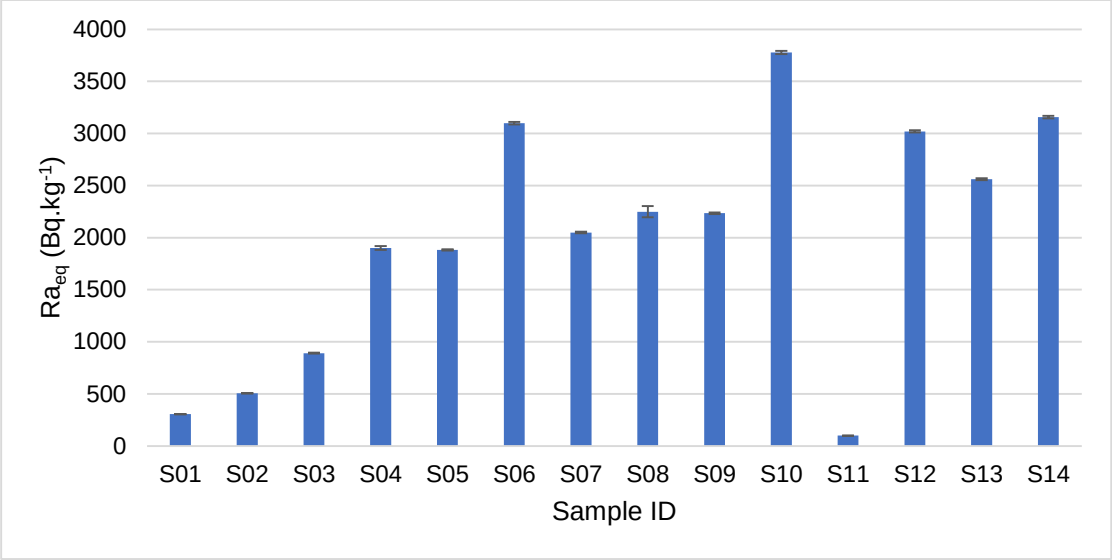

Figure 4. 24: The calculated radium equivalent activity for sample in mine B.

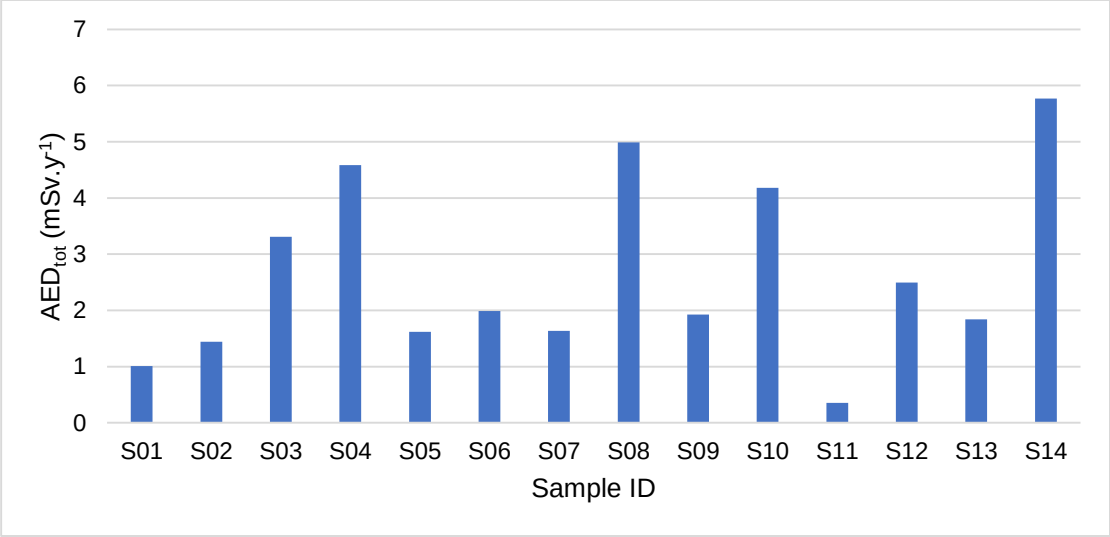

Figure 4. 25: The calculated annual effective dose measured in samples of mine 1.

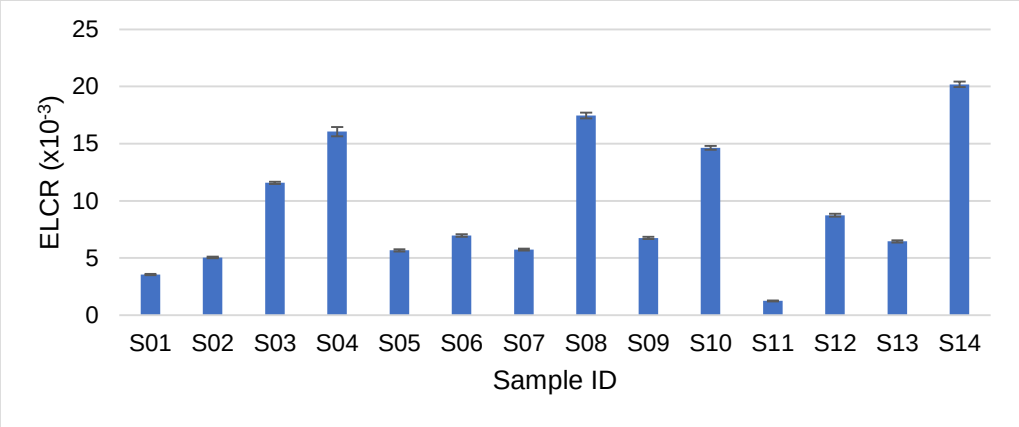

Figure 4. 26: Excess lifetime cancer risks calculated in samples from mine 1.

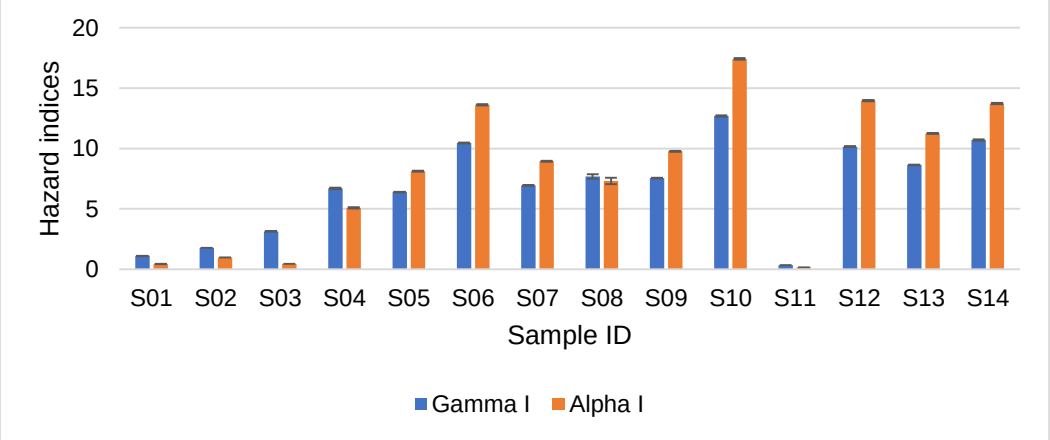

Figure 4. 27: The hazard indices due to ^{226}Ra, ^{232}Th and ^{40}K in samples of mine 1.

The radium equivalent activity concentration for soil samples from uranium mine 1 ranged from 98.74±0.79 $Bq.kg^{-1}$ to 3777.93±14.1 $Bq.kg^{-1}$ with an average of 1980.73±11.7 $Bq.kg^{-1}$. The radium equivalent was reported to be about five times higher than the permissible limit of 370 $Bq.kg^{-1}$, an equivalence to gamma dose exposure level higher than 1 $mSv.y^{-1}$. The absorbed dose rates were calculated to be in the range of 57.79±1.68 to 940.48±10.80 $nGy.h^{-1}$ with an average of 432.71±6.50 $nGy.h^{-1}$. This study reported that the calculated data for dose rate of these soil samples was higher than the world average outdoor exposure of 60 $nGy.h^{-1}$ for global primordial radiation and standard limit of 84 $nGy.h^{-1}$ (UNSCEAR, 2000).

The annual effective dose to humans was reportedly ranging between 0.35 and 5.77 $mSv.y^{-1}$ with an average of 2.65 $mSv.y^{-1}$. The determined total effective dose to humans was significantly higher than both the average effective doses of 0.7 $mSv.y^{-1}$ reported both for Namibia (MME, 2010) and the world of 0.48 $mSv.y^{-1}$ (UNSCEAR, 2017). Only soil samples from tailings and/or possibly radiation hotspots in the section B had shown high effective dose efficiency. Also, occupational exposure was significantly lower than the permissible annual limit of 20 mSv published by ICRP.

Radiation exposure to the humans (employees) externally, internally, as well as alpha and gamma indices hazards ranged as 0.27 to 10.21, 0.35 to 19.63, 0.16 to 17.42 and 0.35 to 12.70 (with averages of 5.35, 9.65, 7.95, and 6.74), respectively. All the health hazards calculated had reported values greater than a unit. Since random sampling was performed in this area, there was no fundamental and scientific findings which could evidently prove that the samples contributed to high risks of radiological hazards to humans. Eventually, these results had shown significantly high variations of health hazards calculated in all samples.

4.3.3 Study area C

Figures 4.28 – 4.32 represent the radiological hazards for the Khan river samples, coded S15_KHN1, …, S20_KHN6. These graphs were drawn from tabulated values in Table C5 in the Annexure C.

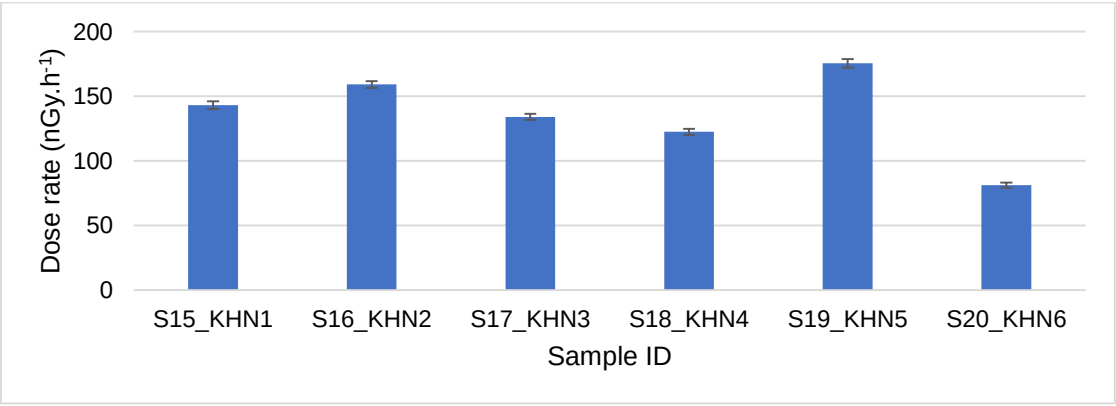

Figure 4. 28: The calculated dose rates at 1 m in air above the ground due to NORM concentrations for Khan river samples.

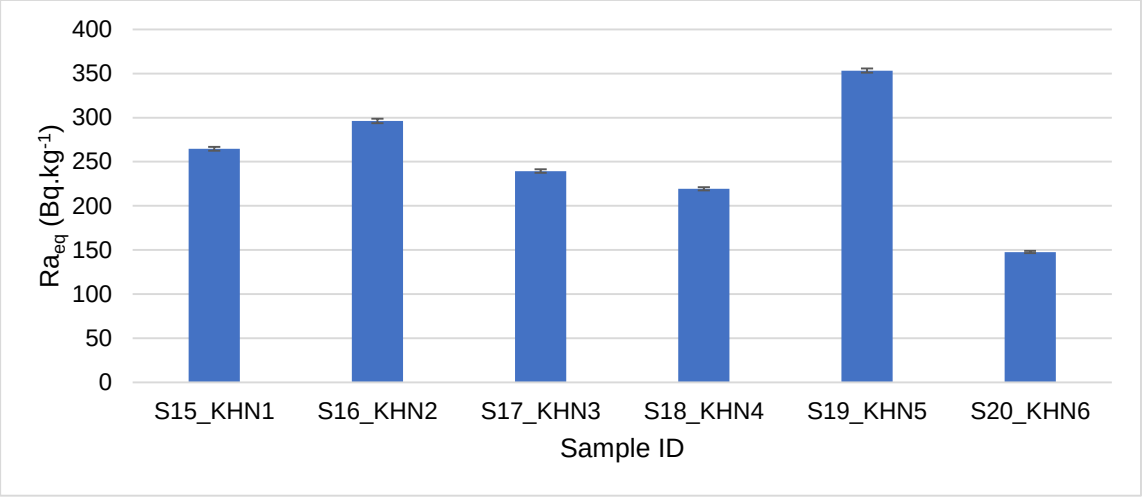

Figure 4. 29: The radium equivalent activity due to NORM concentrations for Khan river samples.

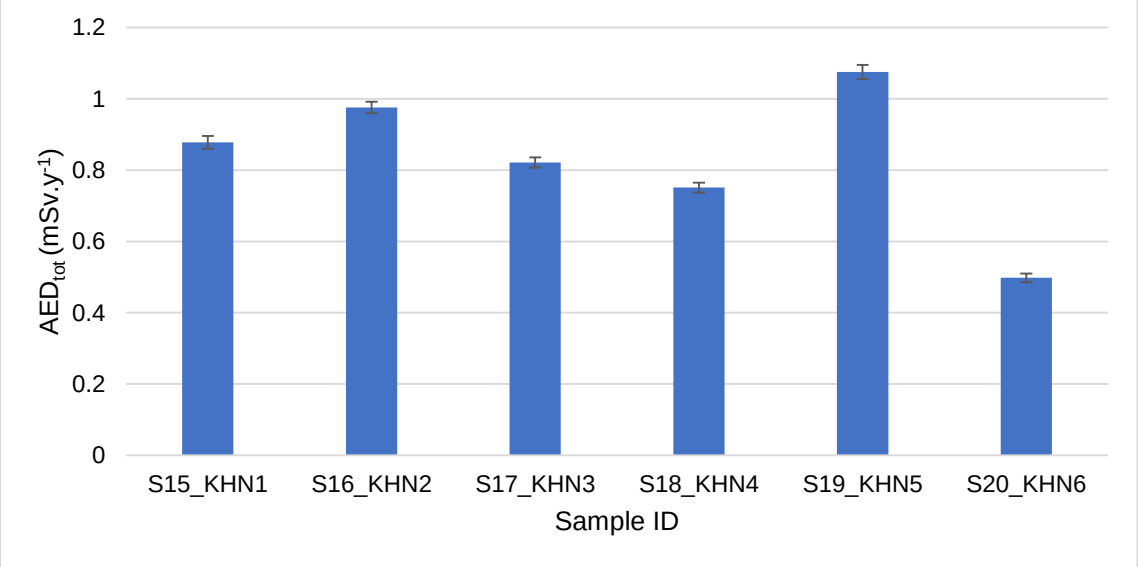

Figure 4. 30: The annual effective dose (AED) for Khan river samples.

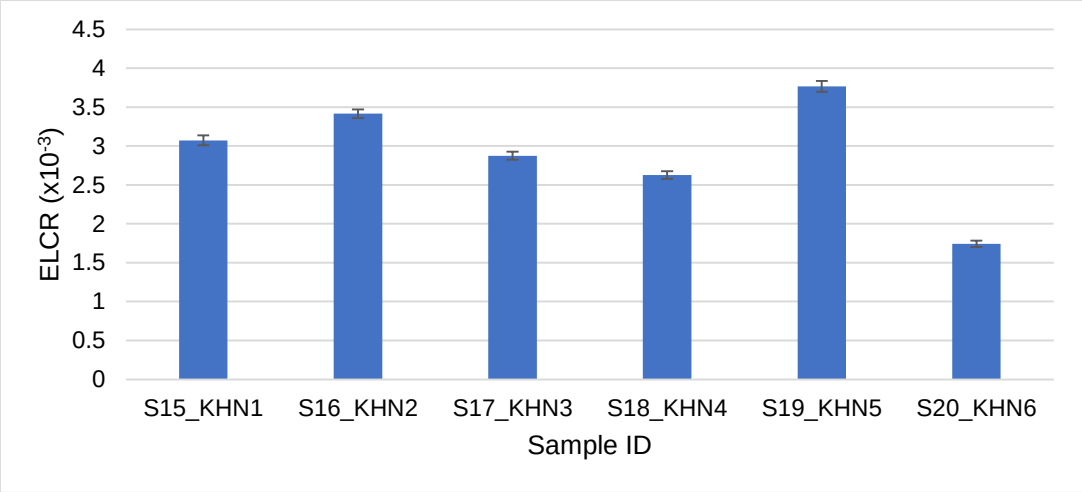

Figure 4. 31: Excess lifetime cancer risk (ELCR) graph for Khan river samples.

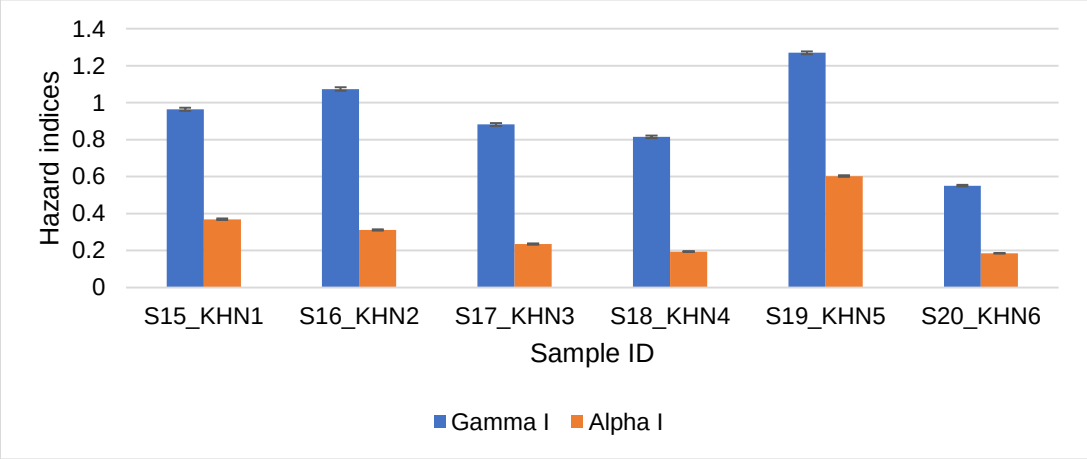

Figure 4. 32: The hazard indices for Khan river soil samples.

Sediments of soil samples collected from a small portion of the Khan river stream had indicated average radiological health related hazards. The indoor absorbed dose to the public was high, ranging from 81.19±1.97 to 175.43±3.25 nGy.h^{-1}, with an average of 135.89±2.58 nGy.h^{-1}. Of all the six samples analyzed, only one (S20_KHN6) had shown absorbed dose rate at 1 m in air less than the world average (84 nGy.h^{-1}). The radium equivalent activity calculated to account for durability of materials to be used for building construction ranged from 147.71±1.26 to 353.29±2.25 Bq.kg^{-1} with an average of 253.45±2.03 Bq.kg^{-1} and found to be less than radiological safety level of 370 Bq.kg^{-1} for safe use. Annual exposures of the Khan river samples were obtained ranging from 0.50

to 1.08 mSv.y^{-1} with an average of 0.83 mSv.y^{-1}. Only sample coded S19_KHN5 had shown the total annual effective dose exposure greater than the world limit of 1 mSv.y^{-1}. Higher values above the world average (0.92x10^{-3}) for excess lifetime cancer risks were calculated for lifetime exposure of 70 years ranging from 1.74x10^{-3} to 3.77x10^{-3} with an average of 2.92x10^{-3}. Both the gamma and alpha indices ranging from 0.55 to 1.27 and 0.18 to 0.60 with averages of 0.93 and 0.32 were comparable to the gamma and alpha exposures of a unit. The results of sample study in the river had shown radiological levels below or comparable to permissible international standards for radiation safety to humans. Only the excess cancer risks calculated were to be high compared to the world average of 0.29x10^{-3}.

4.3.4 Study area D

The radiological hazards for soil samples collected from uranium mine 2 (section D) are shown in Table C6 in the Annexure C and graphically represented in Figures 4.33 – 4.36.

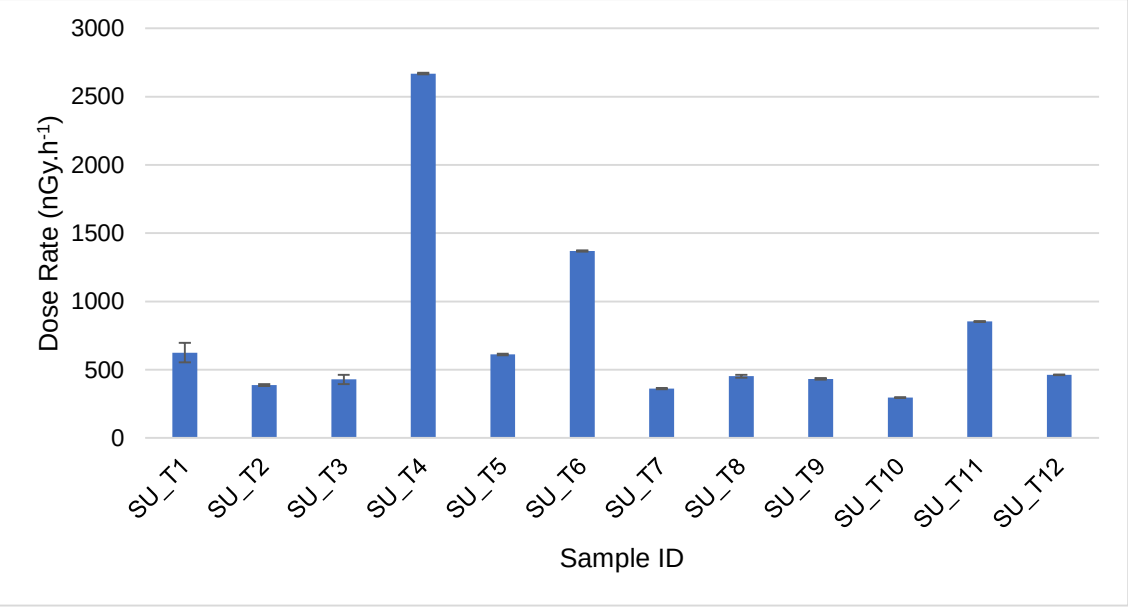

Figure 4. 33: The calculated dose rates of tailings in mine 2.

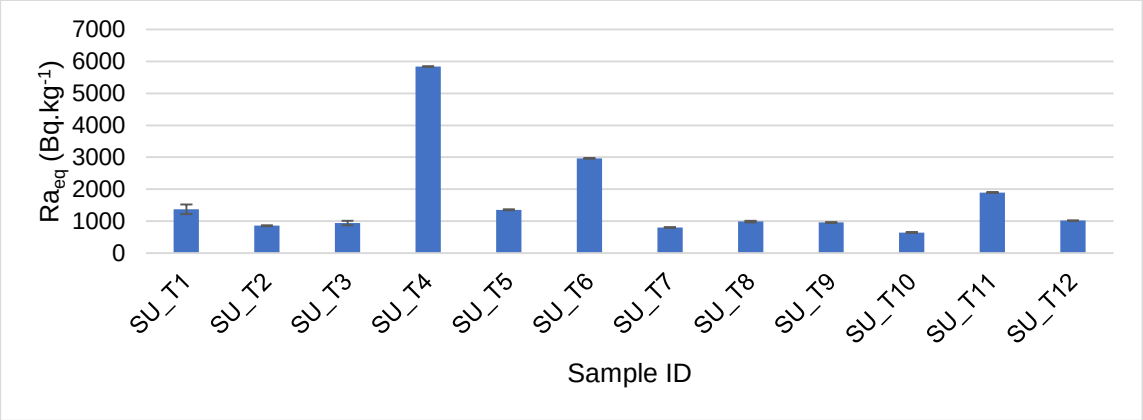

Figure 4. 34: The radium equivalent activity (Ra_{eq}) graph for soil of uranium mine 2.

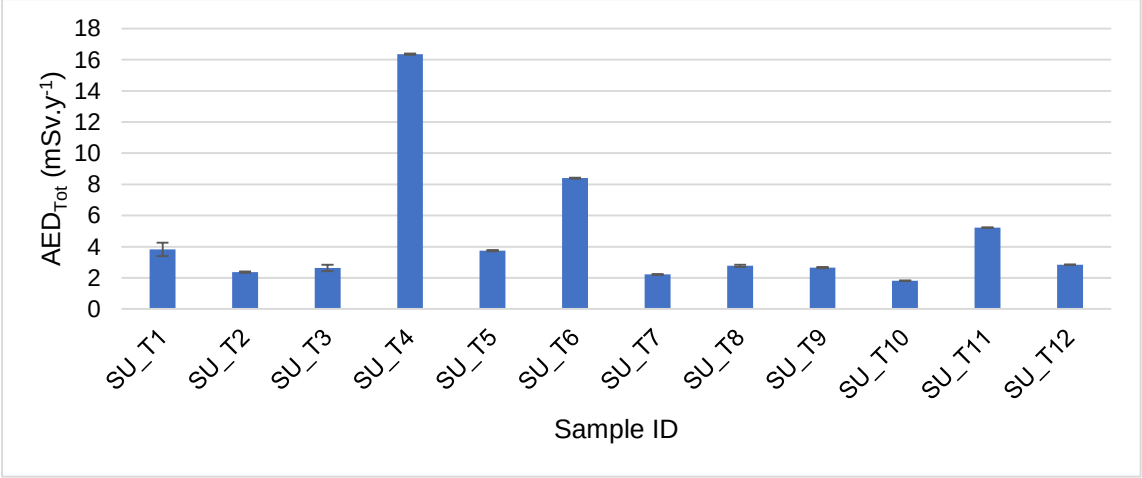

Figure 4. 35: The annual effective dose (AED) for soil from uranium mine 2.

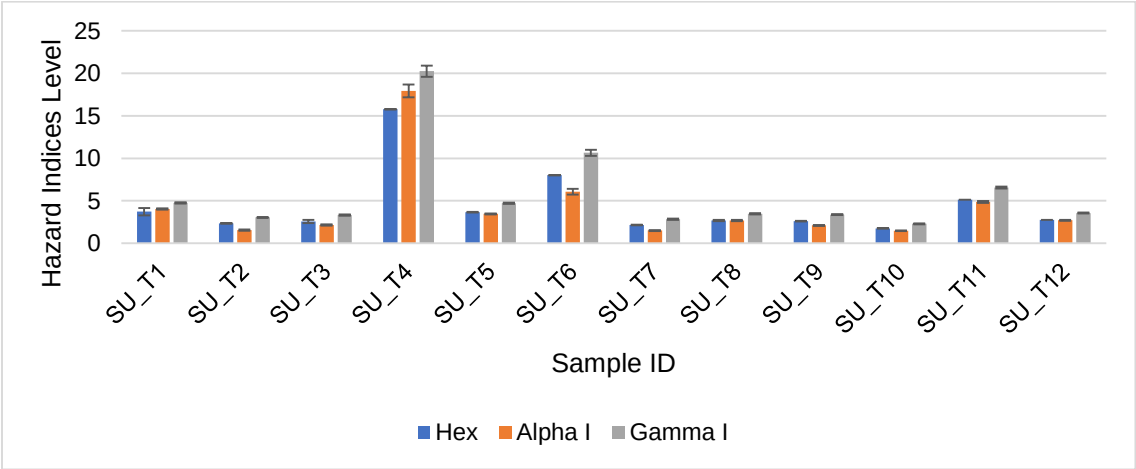

Figure 4. 36: External Hazard Index calculated from tailings of mine 2.

The radium equivalent activity, absorbed dose rates, annual effective dose, external hazards, alpha and gamma indices were calculated to assess radiological hazards. The dose rates calculated for tailing samples ranged from 291.22±4.70 to 2668.20±70.70 $nGy.h^{-1}$ with an average of 718.03±13.93 $nGy.h^{-1}$. The absorbed dose rates were significantly above the world average outdoor and indoor exposures of 60 $nGy.h^{-1}$ and 84 $nGy.h^{-1}$ for global primordial radiation, respectively, reported by UNSCEAR (2000). The annual effective dose calculated ranged from 1.1.79±0.03 to 16.36±0.43 $mSv.h^{-1}$ with an average of 4.40±0.09 $mSv.h^{-1}$. A few of the samples recorded the annual effective doses higher than the criterion recommended limit of 1 $mSv.y^{-1}$ to the public and lower than 20 $mSv.y^{-1}$ to the employees, there was a sign of good control on occupational exposures from tailings of the mine. The radium equivalent activity for these samples had shown a range of 1713.09±6.42 to 12290.04±116.30 $Bq.kg^{-1}$ with an average of 5129.61±28.51 $Bq.kg^{-1}$. The determined average radium equivalent activity was extremely higher than the recommended activity limit of 370 $Bq.kg^{-1}$ from building materials and an equivalence of annual exposure of 1 mSv is not exceeded. The external and internal hazards, alpha and gamma indices values for the samples ranged from 4.63±0.01 to 33.21±0.04, 8.34±0.01, 6.86±0.03 to 52.69±0.57 and 5.84±0.02 to 41.73±0.39, with averages of 13.86±0.01, 25.63±0.01, 21.76±0.14 and 17.37±0.10, respectively. The calculated values for hazard indices were above the reference level of a unit and therefore, indicated that tailings posed significant hazards to humans when used for building materials.

CHAPTER 5: ICP-MS RESULTS

5.0 Introduction

ICP-MS results for both borehole (BW), tailings (TW) water, as well as dust from study areas B and D, respectively, are discussed in this chapter. It was shown in Chapter 3 that both BW and TW consisted of 10 samples each collected for analysis. In addition to that, eleven dust samples were collected in study area D for counting on the ICP-MS. Measurements were not recorded in replicates due to time constraints and costs, which may have shown more accurate results in elemental and activity concentrations in samples. Results obtained in parts-per-billions (ppb), were converted into parts-per-millions (ppm) for ease and smooth conversion into activity concentrations ($Bq.kg^{-1}$) using Equations 3.13 or 3.14. Conversion factors presented in Equation 3.14 were used in this study.

5.1 Results of the contaminants

5.1.1 Borehole water of section B

The elemental concentrations of uranium, thorium and potassium total quantity obtained for borehole water samples collected from a uranium mine 1 are presented in Table D1 of the Annexure D. Total quantitative method presented data in ppm and calculations were performed to quantitatively analyze individual radionuclides of ^{238}U, ^{232}Th and ^{40}K in samples.

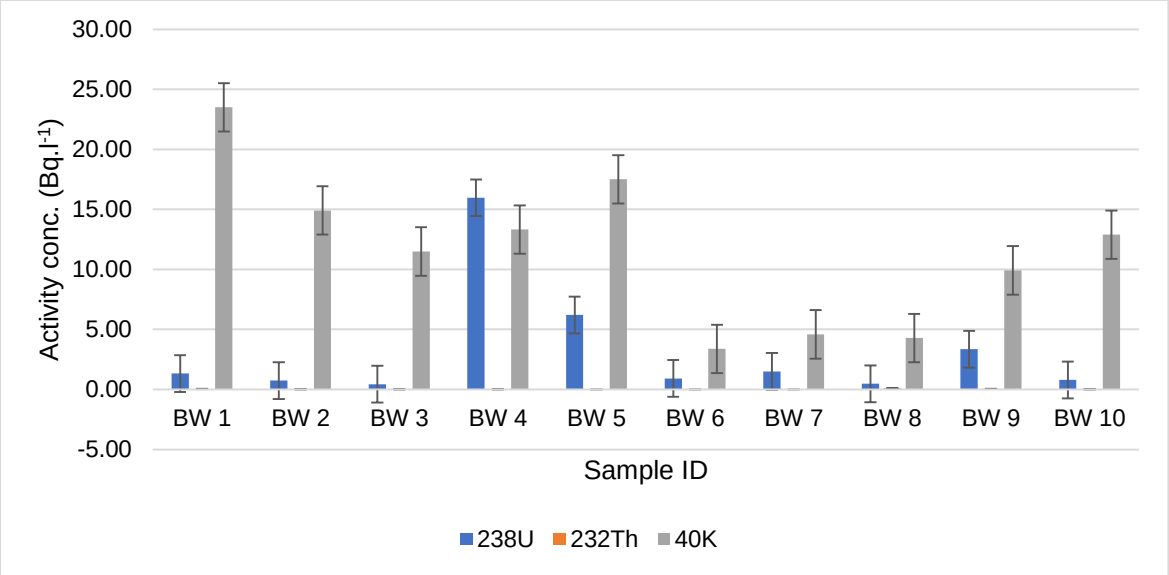

Figure 5. 1: Activity concentrations associated with NORM in borehole water from section B.

The activity concentrations were calculated using equation 3.14 from elemental concentrations measured by ICP-MS. The most sensitive detection method with low detection limits, had shown ^{40}K with the highest activity concentration of 23.5047 $Bq.l^{-1}$ and the lowest was ^{232}Th with 0.0020 $Bq.l^{-1}$. The uranium, thorium and potassium total quantitative concentrations recorded were 0.0351 to 1.2932 ppm, 0.00049 to 0.02522 ppm and 107.8256 to 750.9490 ppm with averages of 0.2566, 0.00581 and 369.9207 ppm, respectively. The concentrations measured (ppm), as shown above, were converted to activity concentrations and the values varied from 0.43 to 15.97 $Bq.l^{-1}$, 0.002 to 0.102 $Bq.l^{-1}$ and 3.37 to 23.50 $Bq.l^{-1}$ with averages of 3.17, 0.024 and 11.58 $Bq.l^{-1}$ for ^{238}U, ^{232}Th and ^{40}K, respectively. These values exceeded the drinking water quality guideline levels recommended by WHO for gross alpha screening and gross beta levels of 0.5 $mBq.l^{-1}$ and 1.0 $mBq.l^{-1}$, respectively (WHO, 2011b). The analysis shows that the water is not fit for human consumption.

5.1.2 Tailing water of section B

Elemental and activity concentrations for water from the lakes in the tailings site are shown in Table D2 in the Annexure D and graphically represented in Figure 5.2.

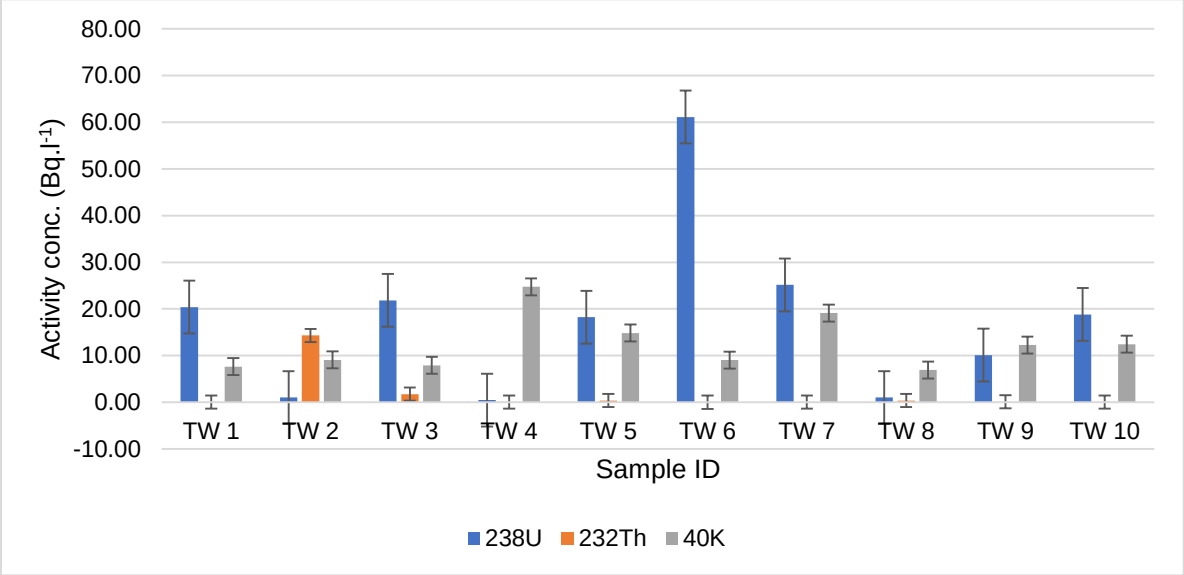

Figure 5. 2: The activity concentrations associated NORM in tailings lake water from section B.

The activity concentrations determined for NORM in tailing's water were ranging from 0.46 to 61.12 Bq.l^{-1} with an average of 17.81 Bq.l^{-1} for ^{238}U, 0.01 to 14.32 Bq.l^{-1} with an average of 1.72 Bq.l^{-1} for ^{232}Th and 6.90 to 24.74 Bq.l^{-1} with an average of 12.40 Bq.l^{-1} for ^{40}K. ^{238}U level was recorded with a maximum and highest average activity concentration. The distribution of radioactivity in water varies significantly and with minimum level at 0.01 Bq.l^{-1}. The calculated values for tailings' lake water exceed the drinking water quality guideline levels recommended by WHO for gross alpha screening and gross beta levels of 0.5 mBq.l^{-1} and 1.0 mBq.l^{-1}, respectively (WHO, 2011b). The significance of these analyses show that the radiologic concentration in water is to be used for human consumption and therefore contacts with edible foods must be avoided at all costs.

5.1.3 Dust from the uranium mine 2

The concentrations and activity concentrations determined in dust samples are numerically and graphically represented in Table D3 of the Annexure D and Figure 5.3, respectively.

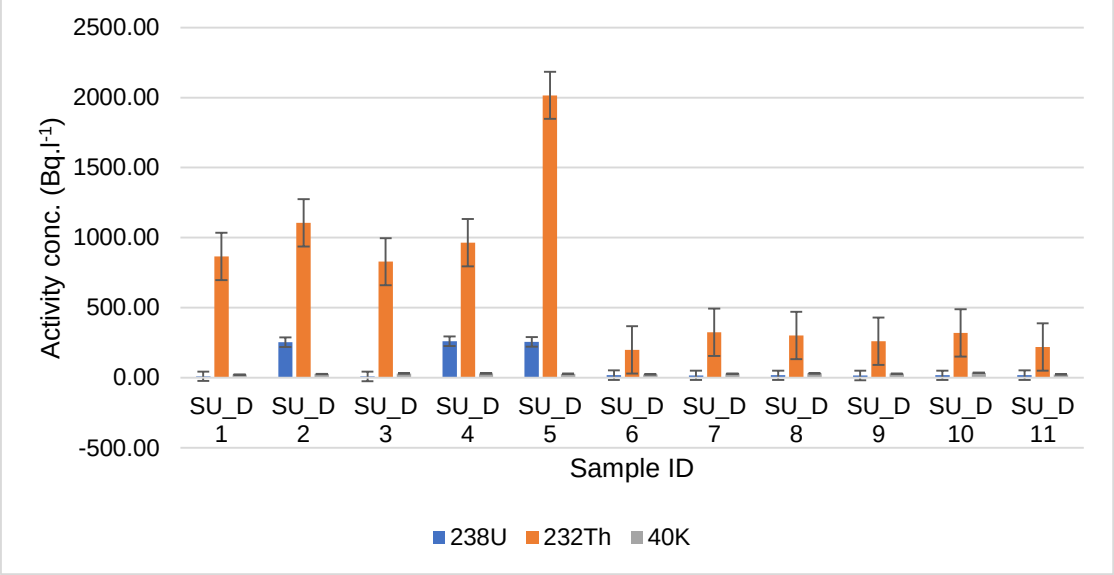

Figure 5. 3: The activity concentrations determined for NORM of ^{238}U, ^{232}Th and ^{40}K in dust from section D.

The activity concentration for NORM determined in dust from mine 2 ranged from 9.49 to 259.74 $Bq.m^{-3}$ with an average of 80.94 $Bq.m^{-3}$ for ^{238}U, 198.81 to 2015.99 $Bq.m^{-3}$ with an average of 673.12 $Bq.m^{-3}$ for ^{232}Th and 21.91 to 34.19 $Bq.m^{-3}$ with an average of 27.95 $Bq.m^{-3}$ for ^{40}K. The results had shown that thorium radionuclide is more transferrable through the atmosphere than uranium and potassium nuclides. In dust, ^{232}Th was recorded with significant high value of radioactivity concentration at 673.12 $Bq.m^{-3}$.

5.2 Radiological hazards determined in water and dust

There were only two radiological hazards considered for calculation depending on activity concentrations for ^{238}U, ^{232}Th and ^{40}K radionuclides in water and dust. The assumption was made such that the ^{238}U and its daughter ^{226}Ra nuclides were in equilibrium condition

and this would create a room for only calculating the dose rate and annual effective dose absorbed accordingly.

5.2.1 Absorbed dose

The absorbed dose at 1 meter above the ground was estimated for borehole water, tailing water and dust. The graphical representation of the dose rates are shown in Figures 5.4 – 5.6 and numerical values in Annexure (Table D4).

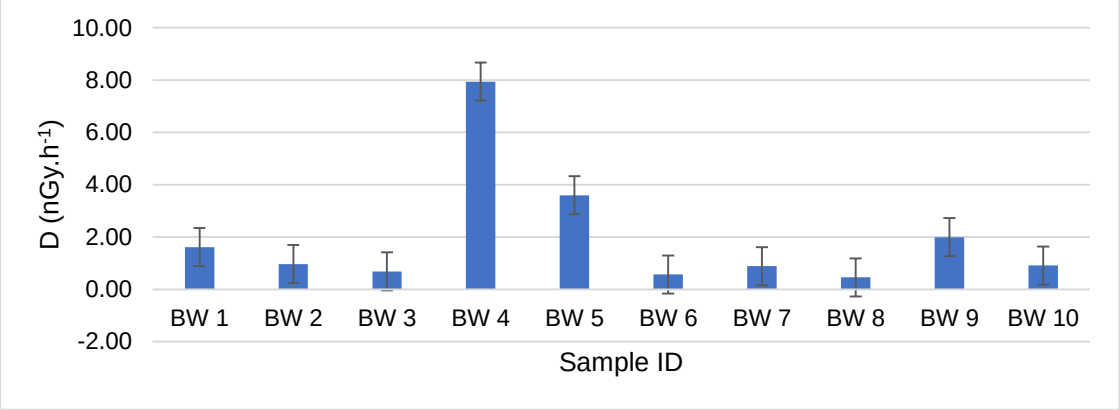

Figure 5. 4: The dose rate determined in borehole water.

The absorbed dose determined in borehole water ranged between 0.46 (BW 8) to 7.94 nGy.h^{-1} (BW 4) with an average of 1.96 nGy.h^{-1}. The absorbed dose was found to be less comparable to the world limit.

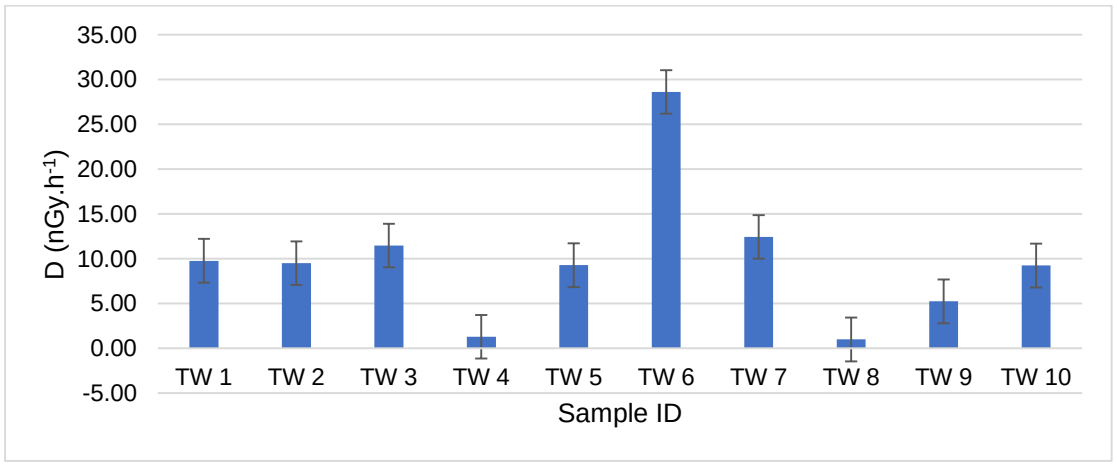

Figure 5. 5: The dose rate determined in tailings' lake water.

The absorbed dose in tailing's lake water were determined ranging from 0.99 (TW 8) to 28.6 nGy.h^{-1} (TW 6) with an average of 9.78 nGy.h^{-1}. The absorbed dose in water for the lakes were also less in comparison with the world limit.

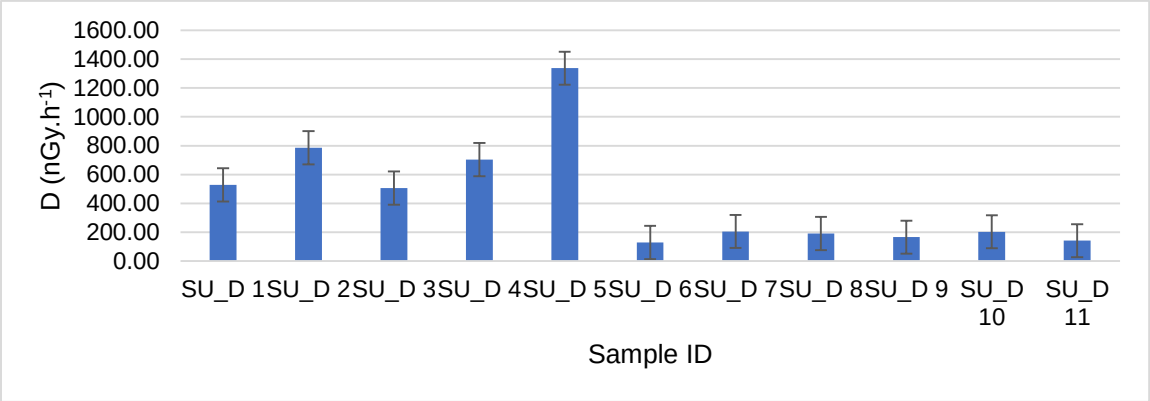

Figure 5. 6: The absorbed dose determined in dust.

In the case of dust samples the determined absorbed dose ranged between 129.00 and 1340.00 nGy.h^{-1} with an average of 445.00 nGy.h^{-1}. This health related hazard was higher than the world average and limit documented by ICRP (2012).

5.2.2 The Committed effective dose

The annual effective dose for water from the borehole and lakes of a uranium mine 1 and dust from mine 2 calculated are shown in Tables D4 – D6 on the Annexure D. The graphical representations of these radiological hazards are illustrated by Figures 5.7 – 5.9.

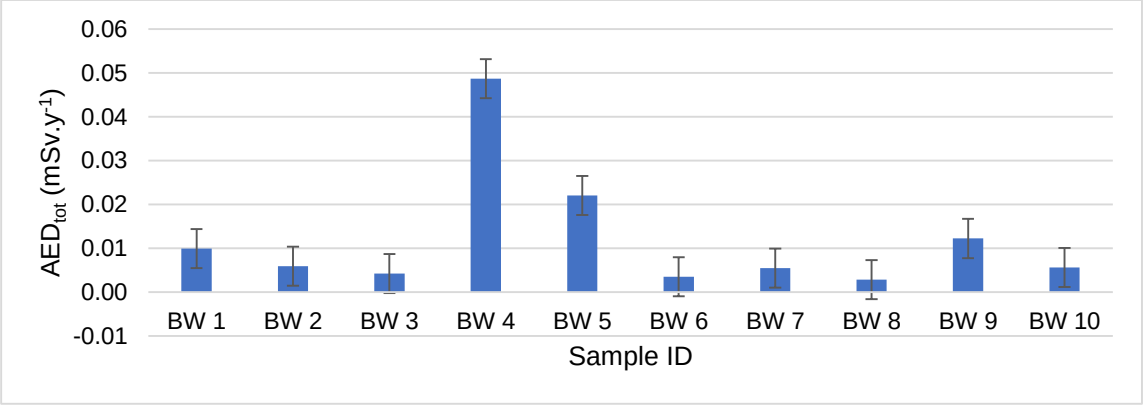

Figure 5. 7: Annual effective doses determined in water of the borehole.

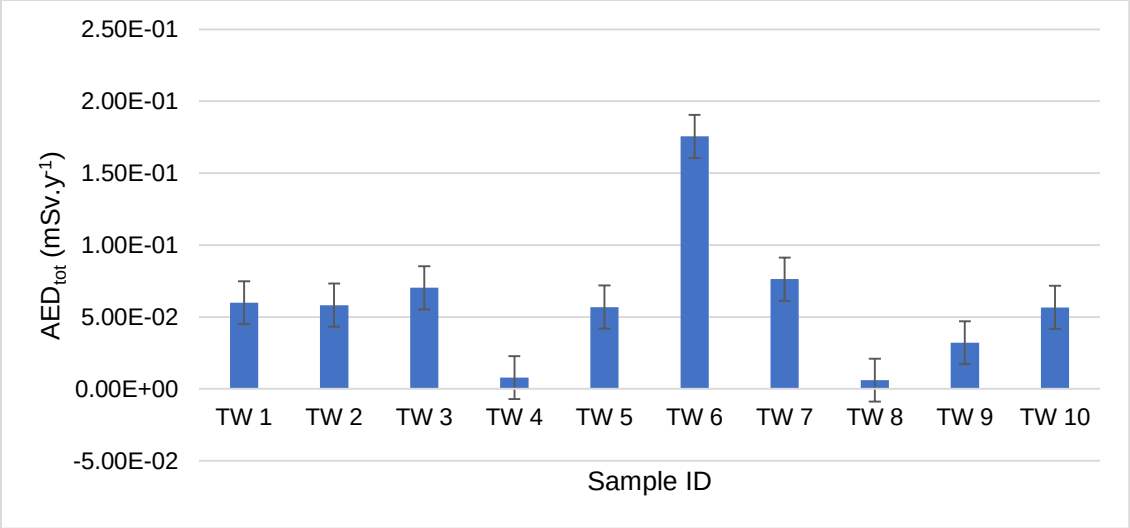

Figure 5. 8: Annual effective doses determined in water from the lakes on tailings.

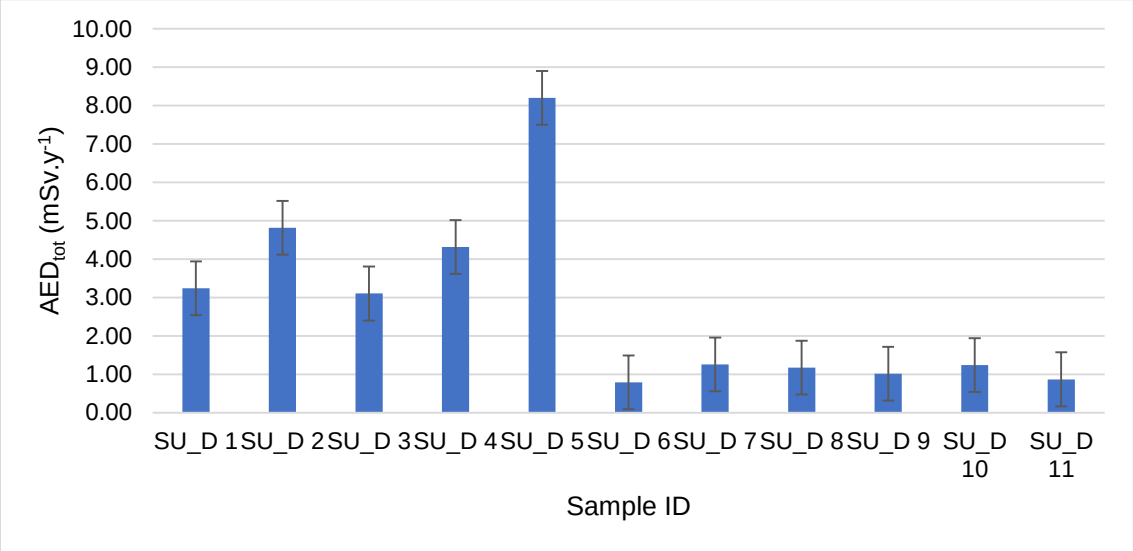

Figure 5. 9: The annual effective doses determined in dust.

The annual effective doses (AED) determined in boreholes, lakes and dust are shown in Tables D4 – D6 ranging from $2.80x10^{-3}$ to $4.87x10^{-2}$ mSv.y^{-1} with an average of $1.20x10^{-2}$ mSv.y^{-1}, $6.08x10^{-3}$ to $1.76x10^{-1}$ with an average of $6.00x10^{-2}$ and 0.79 to 8.20 mSv.y^{-1} with an average of 2.73 mSv.y^{-1}. This means that the annual effective dose measured using ICP-MS had shown less values in water and high average value in dust in comparison to the world limit documented by ICRP (2012).

CHAPTER 6: RESRAD MODELING TOOL RESULTS

6.0 Introduction

RESRAD-OFFSITE model 4.0 was performed with ICRP 107 based radionuclide transformations transfer factors and ICRP 60 external, inhalation and ingestion dose conversion factors. A block diagram of environmental and exposure pathways, is shown in Figure 3.12, for all possible transfers of all radionuclides of ^{226}Ra, ^{238}U, ^{232}Th and ^{40}K considered for this study. The assumption was made that environmental exposure pathways are the most likely conditions with high probability of transfers contributing to stochastic effects of cancer to members of the public in the region. The extent that possible health risks to the population within the study area has not been documented has led to the hypothetical scenario by method of modeling of risks using RESRAD computer program (developed by Argonne, Lemont, IL, USA).

Table 6. 1: The average activity concentrations determined in samples (top of table) actual values in $Bq.kg^{-1}$, and (bottom of table) as inputs on RESRAD-OFFSITE in $Bq.g^{-1}$.

RESidual RADioactivity (RESRAD) modeling activity concentration values					
		Actual average activity concentrations in $Bq.kg^{-1}$			
Study area	Samples	^{226}Ra	^{238}U	^{232}Th	^{40}K
A	Arandis soil	56.53	155.26	185.65	701.61
B	Uranium ore	4909.39	4610.29	207.51	847.09
B	Tailings soil	1589.35	557.36	215.59	1079.12
D	Tailings soil	4414.15	842.59	436.74	2225.00
		Input activity concentrations in $Bq.g^{-1}$ on RESRAD - OFFSITE			
B	Uranium ore	4.91	4.61	0.21	0.85
B	Tailings soil	1.59	0.56	0.21	1.08
D	Tailings soil	1.41	0.84	0.44	2.23

Table 6.2 shows the site and default values of specific characteristics and parameters entered as inputs on RESRAD model. The exposure media considered were water,

plants, soil and atmosphere. The site-specific mean values of estimated transfer factors for ^{238}U, ^{232}Th and ^{40}K radionuclides were obtained from a study conducted on some edible but not the only plants grown in the region such as beetroots, spinach and eggplants (Amakali, 2021).

Table 6. 2: The site-specific and default data of parameters considered in RESRAD-OFFSITE vs 4.0 modelling of doses and risks in sections A, B and D.

Parameters	**Interest**	**Site specific data**		**Default data**	**Reference**
Radionuclide:					
Distribution coefficients ($cm^3.g^{-1}$)	^{226}Ra			70	Yu *et al*., 2001
	^{238}U			50	Yu *et al*., 2001
	^{232}Th			60000	Yu *et al*., 2001
	^{40}K			5.5	Yu *et al*., 2001
Transfer factors (nonleafy and leafy vegetables)	^{226}Ra			0.04	Yu *et al*., 2001
	^{238}U	0.0038	0.014		Amakali, 2021
	^{232}Th	0.0065	0.020		Amakali, 2021
	^{40}K	1.37	2.77		Amakali, 2021
Exposure duration (years)	Arandis	70			Current study
	Section B, D			30	Yu *et al*., 2001
Possible contamination zone:					
Area (m^2)	Arandis	11000			Current study
	Section B, D	750 000			RUL, 2019
Precipitation (mm)		50			MME, 2010
Erosion rate ($m.y^{-1}$)				2	Yu *et al*., 2001
Density				1.55	Yu *et al*., 2001
Thickness (m)	Arandis			2	Yu *et al*., 2001
	Section B, D			100	RUL, 2019
Radon emanation coefficient	^{222}Rn			0.25	Yu *et al*., 2015
	^{220}Rn			0.15	Yu *et al*., 2015
Inhalation rate ($m^3.y^{-1}$)				8400	Yu *et al*., 2015
Modelled duration (years)	All sections	200			Current study

6.1 RESRAD-OFFSITE model

6.1.1 Estimation of summed absorbed dose

The absorbed dose summed for all radionuclides considered in modelling were estimated in RESRAD-OFFSITE, with inputs as shown in Tables 6.1 and 6.2 for sections B (mine 1) and D (mine 2). On mine 1, the deterministic results of individual radionuclides and sum are shown in Tables E1 and E2 in the Annexure E for uranium granitic ores and tailings, respectively, and the graphical representations are in Figure 6.1 and 6.2 in this chapter. For mine 2, the deterministic results are shown in Table E3 in the Annexure E and Figure 6.3 of this chapter.

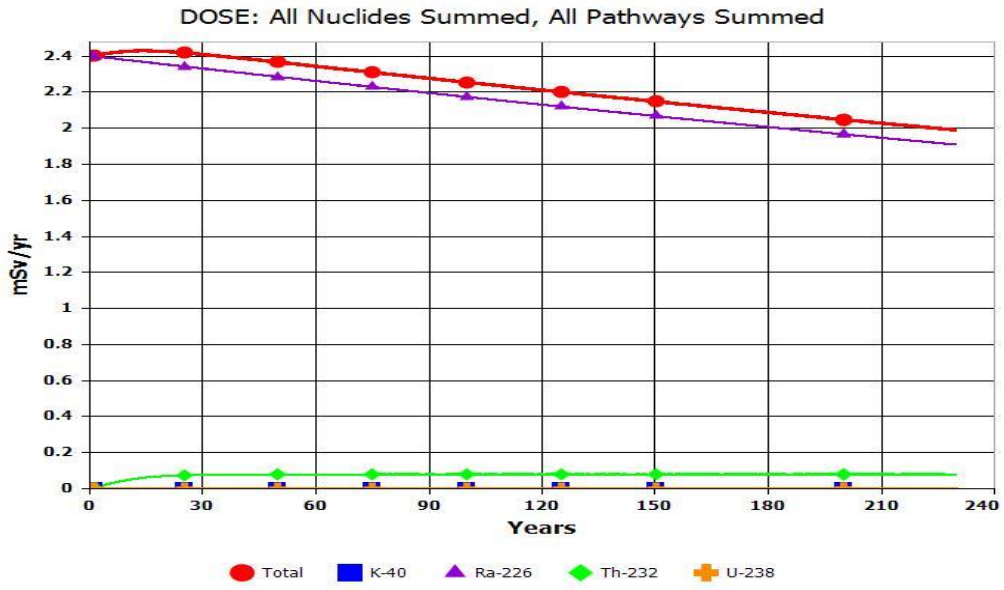

Figure 6. 1: The modelled annual effective dose, individual and summed, for uranium granitic ore samples from section B (mine 1).

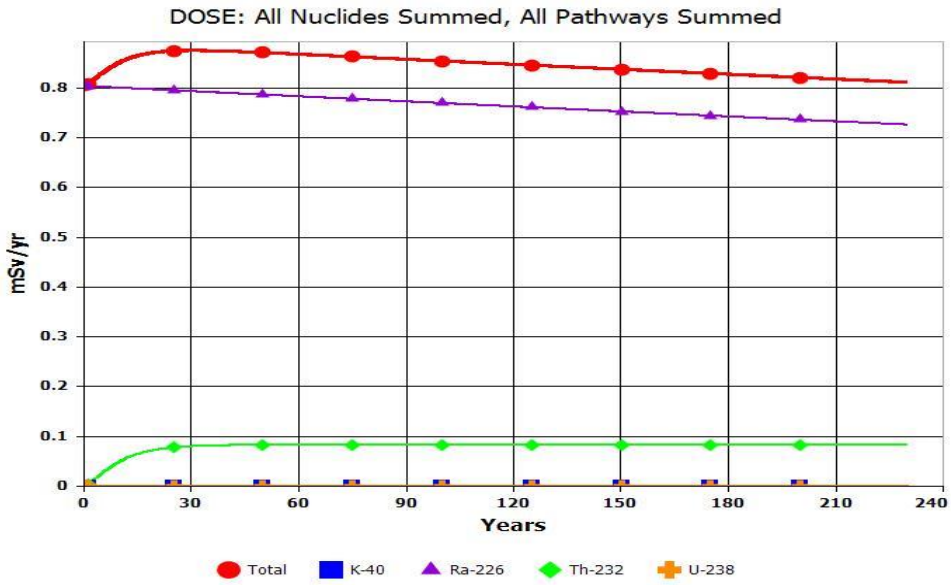

Figure 6. 2: The modelled annual effective dose, individual and summed, for tailings soil samples from section B (mine 1).

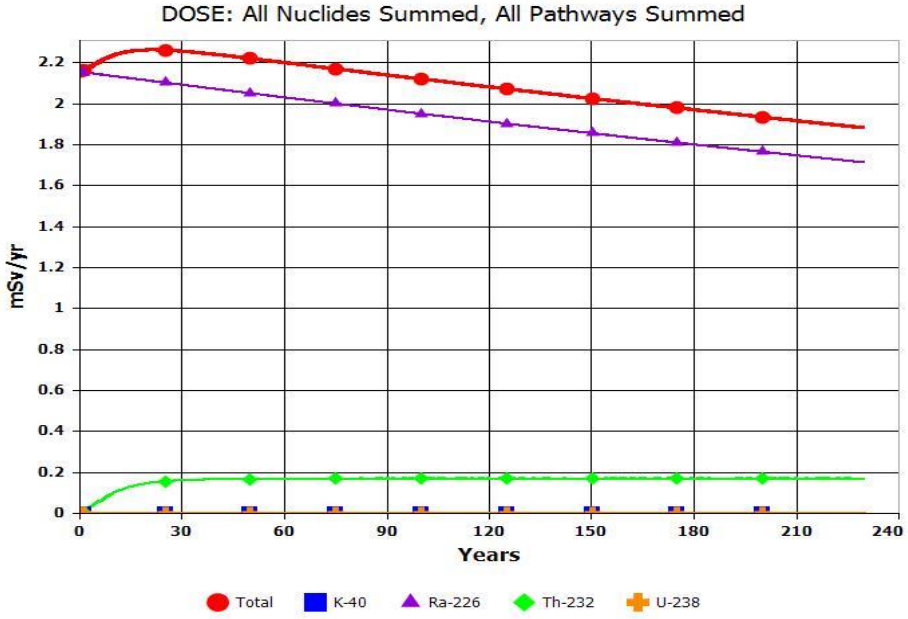

Figure 6. 3: The modelled annual effective dose, individual and summed, for soil samples from section D (mine 2).

The annual effective doses modelled for granitic ore samples, in Figure 6.1, from individual radionuclides of ^{226}Ra, ^{238}U, ^{232}Th and ^{40}K was highest with a value 2.4 mSv for ^{226}Ra which was significantly high compared to world average for all natural sources

(terrestrial and cosmological) of radiation and with absorbed dose from other three is significantly closer to zero. A significant increase in annual effective dose was observed for ^{232}Th at 8.6x10^{-4} to 8.0x10^{-2} mSv.y^{-1} between 0 year and 30 years. This has contributed to the increase in total absorbed dose to 2.43 mSv.y^{-1}, recorded between 10 and 20 years of exposure to granitic ore samples. The annual effective dose from ^{226}Ra decreased linearly as follows: 2.40 mSv (0 year), 2.34 mSv (25 years), 2.28 mSv (50 years), 2.23 mSv (75 years), 2.17 mSv (100 years), 2.12 mSv (125 years), 2.07 mSv (150 years), 2.02 mSv (175 years) and 1.97 mSv (200 years). Radionuclides of ^{238}U and ^{40}K were recorded high at 0 year with 1.07x10^{-3} and 6.37x10^{-3} and low at 200 years with 9.22x10^{-4} mSv and 1.62x10^{-4} mSv, respectively.

The modelled effective doses, in Figure 6.2, for NORM in samples from uranium mine 1 (section B), had shown initial value of effective doses at 8.06x10^{-1} mSv a year. It was ^{232}Th with an increase from 8.95x10^{-4} at 0 year to 8.06x10^{-2} mSv.y^{-1} in 30 years, and that contributed significantly to the increase of total annual effective dose from 8.06x10^{-1} to 8.76x10^{-1} mSv.y^{-1} in the same range of years. ^{238}U did not really contribute change to the total effective dose as it remained with almost constant values (at 1.29x10^{-4} at 0 year to 1.30x10^{-4} at 200 years). ^{40}K was modelled with 8.13x10^{-4} mSv.y^{-1} at 0 year to 8.00x10^{-4} mSv.y^{-1} at 200 years. The total effective doses recorded 8.21x10^{-1} mSv.y^{-1} at 200 years were still greater than the initial value (at 0 year), and again greater than the average level of 0.48 mSv.y^{-1} from terrestrial sources documented by WHO (2011).

The annual effective doses modelled for activity concentrations of NORM in tailings samples from mine 2 were recorded with a total of 2.16 mSv at 0 year with ^{226}Ra dominating among all other radionuclides, in Figure 6.3. An increase in total effective dose was recorded to a maximum of 2.26 mSv.y^{-1} due to a buildup of ^{232}Th doses between 0 and 20 years.

6.1.2 Estimation of summed cancer risks

The cancer morbidity risk results modelled on RESRAD-OFFSITE are shown in Table E4 and Figures 6.4 – 6.7 in Annexure E and this chapter, respectively. The World Health Organization (WHO) report of 2011 recommends acceptable effective lifetime radiation

attributable risks which may result in one additional cancer case per 100 000 of a exposed population, that is $1x10^{-5}$, and one cancer case per 1000 ($1x10^{-3}$) of a subpopulation (Simon, 2019). USNCEAR has determined the world average cancer risks at $0.29x10^{-3}$.

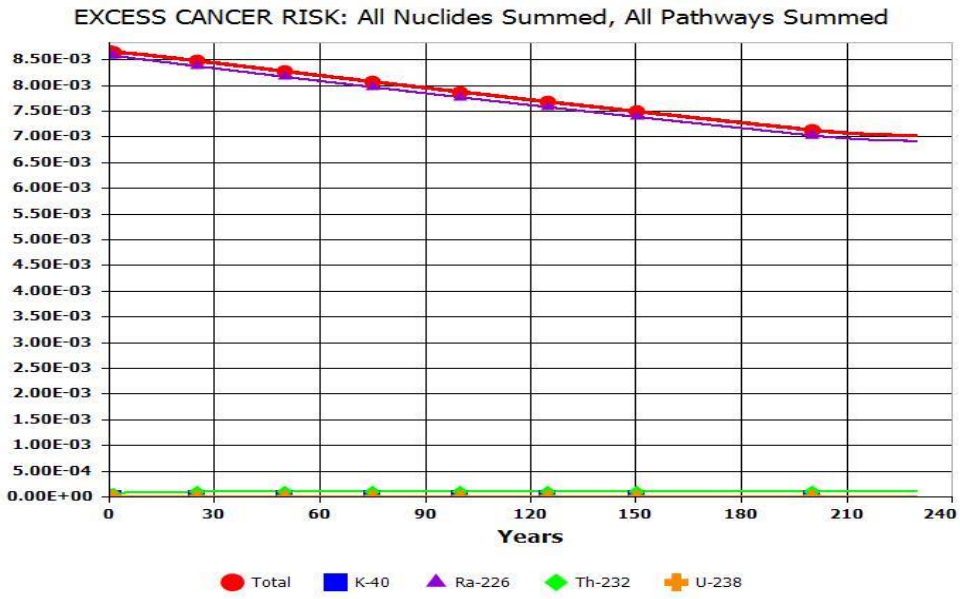

Figure 6. 4: The modelled morbidity cancer risks, individual and summed, for ^{40}K, ^{226}Ra, ^{232}Th and ^{238}U in ore samples from section B (mine 1).

The cancer morbidity risks for individual radionuclides of ^{40}K, ^{226}Ra, ^{232}Th and ^{238}U were estimated at: 0 year as $1.39x10^{-6}$, 8.5910^{-3}, $6.75x10^{-5}$, $2.34x10^{-6}$ with a total of $8.66x10^{-3}$; 50 years as $9.80x10^{-7}$, $8.17x10^{-3}$, $1.04x10^{-4}$, $2.25x10^{-6}$ with a total of $8.28x10^{-3}$; and at 200 years as $4.45x10^{-7}$, $7.03x10^{-3}$, $1.05x10^{-4}$, $2.01x10^{-6}$ with a total of $7.14x10^{-3}$, respectively. This means that ^{226}Ra contributed highly to cancer morbidity risk magnitudes in the range of $1x10^{-3}$ and total cancer cases of a person in 1000 of a subpopulation. This was greater than the world average cancer risks of $0.29x10^{-3}$ documented by UNSCEAR (2008) and WHO (2011).

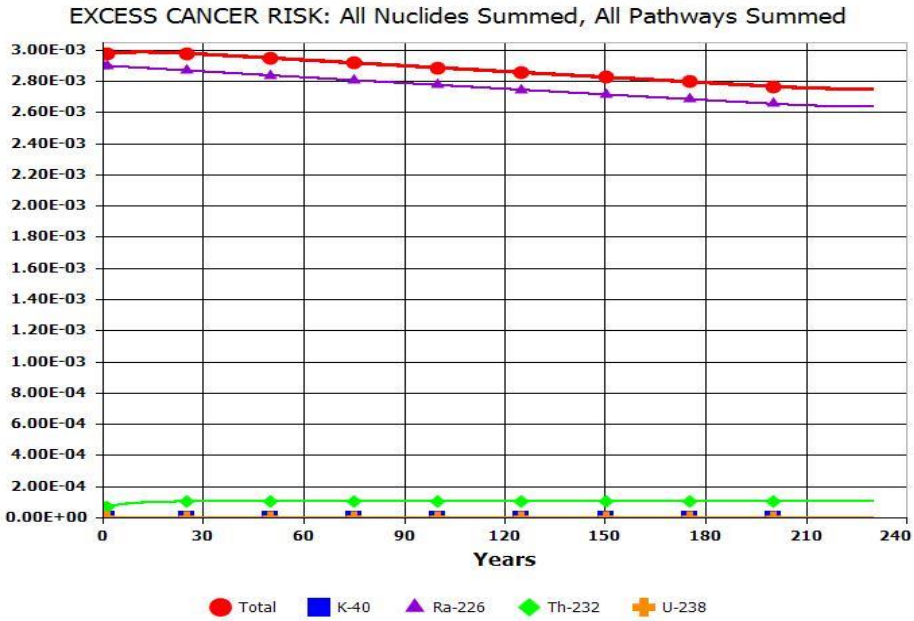

Figure 6. 5: The modelled morbidity cancer risks, individual and summed, for ^{40}K, ^{226}Ra, ^{232}Th and ^{238}U in soil samples from section B (mine 1) stockpiles and surrounding.

Soils from the tailings and surrounding of mine 1 had shown the modelled morbidity cancer risks for ^{40}K, ^{226}Ra, ^{232}Th and ^{238}U at 0 year as: $1.96x10^{-6}$, $2.90x10^{-3}$, $7.03x10^{-5}$ and $2.85x10^{-7}$; at 50 years as $1.95x10^{-6}$, $2.84x10^{-3}$, $1.09x10^{-4}$ and $2.86x10^{-7}$ with a total of $2.95x10^{-3}$; and at 200 years as: $2.04x10^{-6}$, $2.66x10^{-3}$, $1.09x10^{-4}$ and $2.86x10^{-7}$ with a total of $2.77x10^{-3}$. The total cancer risks determined was greater than the world limit of $1.45x10^{-3}$ documented by ICRP (2012).

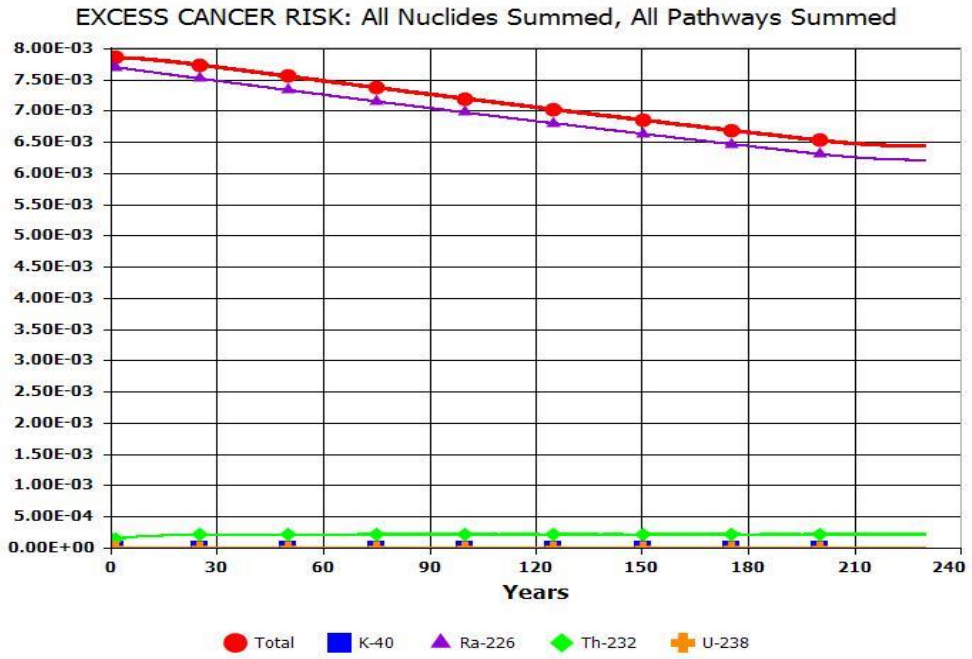

Figure 6. 6: The modelled morbidity cancer risks, individual and summed, for ^{40}K, ^{226}Ra, ^{232}Th and ^{238}U in soil samples from section D (mine 2) stockpiles.

The initial morbidity cancer risks determined for ^{40}K, ^{226}Ra, ^{232}Th and ^{238}U in samples of mine 2 reported at 0, 50 and 200 years are: $3.64x10^{-6}$, $7.72x10^{-3}$, $1.42x10^{-4}$, $4.27x10^{-7}$ with a total of $7.86x10^{-3}$; $2.57x10^{-6}$, $7.34x10^{-3}$, $2.20x10^{-4}$ and $4.12x10^{-7}$ with a total of $7.56x10^{-3}$; and $1.17x10^{-6}$, $6.32x10^{-3}$, $2.20x10^{-4}$ and $3.67x10^{-7}$ with a total of $6.54x10^{-3}$, respectively. Samples from the tailings had, as well, shown high probability of cancer cases in humans. A maximum of 8 persons per 1000 human population had a chance of developing cancer in the region and this chance of cancer case may decrease to 6 person after 200 years of exposure to these stockpiles.

6.1.3 Ingrowth progeny

The modelled cancer risks had shown high contribution from daughter products of NORM concentrations considered in the study. Of all modelled radioactivity concentrations in samples, ^{226}Ra was recorded with the highest cancer risk factors. A practical example was the cancer morbidity risks posed by individual radionuclides in tailings' soil samples of a uranium mine 1 (section B). Figure 6.7 shows the excess cancer risks from individual radionuclides with their respective ingrowth progenies. Cancer risks by ^{238}U radioactivity concentration over 200 years arises mostly from daughters of ^{234}U and ^{210}Po, with

negligible contributions from ^{230}Th, ^{226}Ra, ^{210}Pb as shown in Figure 6.7 (top left). The cancer risks from ^{226}Ra radioactivity concentration had aroused from ^{210}Po daughter, modelled and resulted with almost the same risks as parent, with a zero significant contribution from ^{210}Pb as shown in Figure 6.7 (top right). The morbidity risks modelled for both ^{238}U and ^{226}Ra had shown decreasing linear slopes over time. ^{232}Th ingrowth progenies that contributed to the cancer morbidity risks were ^{228}Ra and ^{228}Th over 200 years, shown in Figure 6.7 (bottom left). ^{40}K was the only radionuclide of NORM under this study with stable daughters and its cancer morbidity risks significantly increasing exponentially between 150 and 200 years as shown in Figure 6.7 (bottom right).

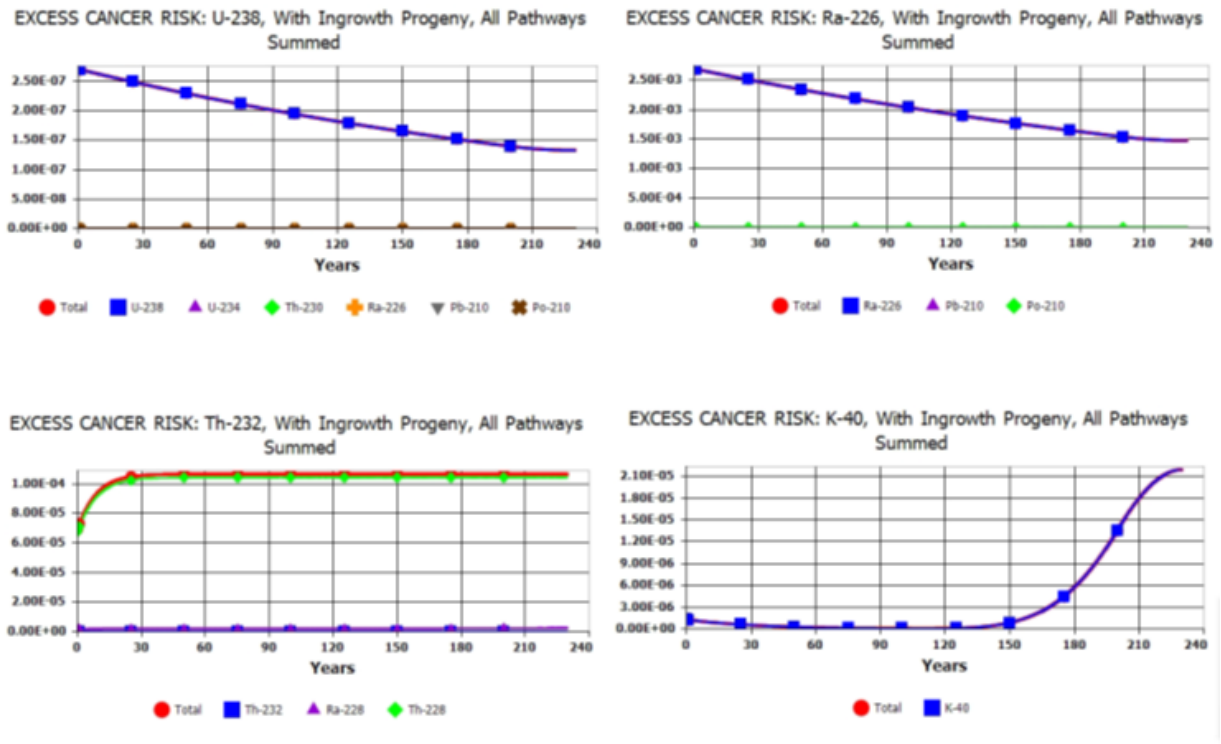

Figure 6. 7: The excess cancer risks of individual radionuclides of ^{238}U (top left), ^{226}Ra (top right), ^{232}Th (bottom left) with their ingrowth progenies, except for ^{40}K (bottom right).

The cancer morbidity risks for individual radionuclide with their progeny (radon inclusive), considering water, plants, soil and atmosphere exposure pathways by external gamma, inhalations and ingestions were recorded in descending order as ^{226}Ra > ^{232}Th > ^{40}K > ^{238}U. In RESRAD-OFFSITE model code, the total cancer morbidity risks in descending

order were recorded as 3 persons per 1 000 populations ($3x10^{-3}$) by tailings (stockpiles) and surrounding soil samples from section B (mine 1) < 7 – 8 persons per 1 000 populations ($7x10^{-3}$ – $8x10^{-3}$) by tailings (stockpiles) soil samples in section D (mine 2) < 7 – 9 persons per 1 000 populations ($7x10^{-3}$ – $9x10^{-3}$) by uranium ore samples of section B (mine 1) were at risk of developing cancer. This could prove that the modelled cancer risks in the region was higher than the recommended level for a population ($1x10^{-5}$) and a subpopulation ($1x10^{-3}$) documented by the World Health Organization (2011) as well as the world average ($0.29x10^{-3}$) documented by the United Nations Scientific Committee on the Effects of Atomic Radiation. According to these findings on RESRAD-OFFSITE long term evaluation, the residents of the region who live closer to mining activity areas would be at high risks of developing cancer due prolonged exposures.

CHAPTER 7: CONCLUSION AND RECOMMENDATIONS

7.0 Introduction

This study, first of its kind in Namibia covering both Arandis town and the surrounding mines, investigated the background radiations of the controlled area and two active uranium mines in the region. This chapter covers the conclusion of the results obtained and discussed in Chapters 4, 5 and 6. The first objective was to determine the radioactivity concentrations of NORM in soil samples from Arandis and uranium mines using HPGe detector. The objective was to evaluate the potential radiological risks to critical groups, employee and residents of Arandis, due to these radioactivity concentrations obtained from both HPGe detector and ICP-MS instrument. The activity concentrations were used to model the possible radiological cancer risks in 200 years' time on RESRAD code (vs 4.0) on the third objective. The fourth objective was this study to provide reference data which may possibly be utilized in future for radiological assessment for improvement of decision making and formulation of useful policies on improvement of radiological protection in the region.

7.1 Gamma spectrometry results

All activity concentrations calculated for respective radionuclides in samples measured in the study area were greater than the minimum detectable activity (MDA) values in Table 4.1. The weighted average activity concentrations measured for NORM (^{226}Ra, ^{238}U, ^{232}Th and ^{40}K) in most samples were significantly higher than the recommended world average values documented by ICRP (2012) and UNSCEAR (2000).

The measured average radioactivity level of NORM in crushed granitic uranium ores from a uranium mine in Erongo region, Namibia, indicated that uranium mining activities posed a high risk of radiation hazards to employees. The activity concentrations for all respective primordial radionuclides were extremely higher than the global average limits of 33, 45 and 420 Bq.kg^{-1} for the earth's crust (UNSCEAR, 2000). All calculated values for radiation

hazards of natural radioactive materials were significantly higher than the world recommended values (UNSCEAR, 2017; UNSCEAR, 2000; WHO, 1994).

However, even though the presented results in this study confirmed that radiation exposures and all attributed health risk is high, the effect could be fairly reduced by enforcing strong controls of preventing members of the public gaining access into the mining operational areas as optimization measures of king radiation exposures ALARA. On the part of the employees of the mine, since the levels of 238U, 232Th and 40K are above the recommended exemption levels by the IAEA (IAEA, 2014), the management of the mines must institute appropriate radiation protection measures and these must be enforced by the Nuclear Regulatory Body of Namibia. The management of the mining companies shall als institute strong and collective protective measures by providing staff with appropriate PPEs and radiation monitoring gadgets to monitor radiation exposures to the workers. The world's average activity concentrations in soil reported by UNSCEAR ranged from 11 to 64 $Bq.kg^{-1}$, 17 to 60 $Bq.kg^{-1}$ and 140 to 850 $Bq.kg^{-1}$ for ^{238}U, ^{232}Th and ^{40}K. These were lower than the results determined in soil samples used in this study. Differences in the results could be attributed to the differences in geographical and geological structure of the region with those in the UNSCEAR reports. It is a mountainous area where most of the mining and explorations are conducted, and are regarded as sitting on alaskites uranium and other mineral rich plateau and hence the reasons for the high radioactivity.

The mountainous areas where most of the mining and explorations are conducted, are regarded as sitting on alaskites uranium and other mineral rich plateau and hence measure high radioactivity. The controlled area, Arandis town, where 46 samples were collected have shown significantly higher but optimal activity concentrations in comparison to 8 granitic ores and 14 soil samples from study area B (uranium mine) as well as section D with 12 tailing soil samples. This study has shown high radioactivity concentrations in NORM of the granitic ore as well as the tailings samples of mines 1 and 2, which of course contributes exposures to terrestrial radiations in the region.

The study also discovered that disequilibrium in the uranium series (^{238}U and its daughter ^{226}Ra) in majority of samples, except on the natural soil of uranium granitic ores. This

could be as a results of the influence of some physicochemical condition that resulted in the parent/daughter ratio to depart from its equilibrium state/value. These could be as result of chemical fractionation which occurs in natural settings like decomposition of rocks settling of sediment particles, magma formations and speleothem precipitations (Gascoyne, 1992).

Table 7. 1: The comparisons of the current research and other research studies.

Place	**Region /Area**	**Dose rate (nGy.h^{-1})**	**Ra_{eq} (Bq.kg^{-1})**	**AED (mSv.y^{-1})**	**H_{ex}**	**H_{in}**	**I_{γ}**	**I_{α}**	**ELCR (x10^{-3})**	**Reference**
Section A	Garden	166.92	286.63	1.02	0.77	0.89	1.04	0.21	3.58	Current study
	Streets	259.31	465.43	1.59	1.26	1.45	1.66	0.35	5.57	
Section B (mine 1)	Ore	2290.70	5271.51	14.05	14.25	27.51	17.69	24.55	49.16	
	Tail. and surr.	432.71	1980.73	2.65	5.35	9.65	6.74	7.95	9.29	
Section C (Khan River)	Khan River	135.89	253.45	0.83	0.68	0.86	0.93	0.32	2.92	
Section D (mine 2)	Tailings	718.03	5129.61	4.40	13.86	25.63	17.37	21.76	14.09	
Range	**All study area**	**135.89 – 2290.70**	**253.45 – 5271.51**	**0.83 – 14.05**	**0.68 – 14.25**	**0.86 – 27.51**	**0.93 – 17.69**	**0.21 – 24.55**	**2.92 – 49.16**	**Current study**
RSA	Gold Mine	407.10 ±6.4	880.90±13.8	0.50	2.40	4.50	-	-	-	(Kamunda *et al*., 2016)
India		112.5	-	-	-	-	0.96	-	0.65	(Kandari *et al*., 2021)
Iran		-	-	0.82	-	-	-	-	2.85	(Masoumi and Keshtkar, 2021)
Namibia	Erongo	105.95	213.85	0.13	0.29	0.58	-	-	1.82	(Onjefu *et al*., 2021)
Coastline, Namibia	Erongo	93.27 – 105.95	121.01 – 176.61	2.4	-	-	-	-	-	(Onjefu *et al*., 2016)
World ave	All sources	-	-	2.4	-	-	-	-	-	(UNSCEAR, 2017; WHO, 2011a)
	Terrest. sources	-	-	0.48	-	-	-	-	0.29	(UNSCEAR, 2008)
Limits	World	59	370	1	≤ 1	≤ 1	≤ 1	200	1.45	(ICRP, 2012)

It is important to recall that secular equilibrium is attained during incubation of samples. The half-life of ^{238}U is 4.47 x 10^9 years and that of ^{226}Ra is 1600 years, and therefore equilibrium between these radionuclides would be difficult to be attained in this situation, except for natural undisturbed soil. Hence, granitic ores were the only natural undisturbed samples used in this study.

Uranium mines 1 and 2 also had shown significantly high radioactivity concentrations and radiological hazards from soils from and around tailings. Other samples which were collected some distance from tailings had also shown slightly high radioactivity. Only samples collected from the Khan river had shown very low and safe radiological values. This is a non-perennial river, and the results had shown low level of primordial radionuclides which may have been carried by due to the seasonal flowing water on the river sediments.

The annual effective doses, external and internal hazards, gamma and alpha indices calculated for soil samples from Arandis streets, mine 1, mine 2 showed values above a unity, posing a health hazards to the people living in the area and the population at large. The absorbed doses calculated in all samples were recorded to be higher than the world's recommended level of 59 $nGy.h^{-1}$ for indoor exposure. The minimum absorbed dose was measured in Khan river by 135.89 $nGy.h^{-1}$, whilst a significantly higher magnitude was measured with a value of 2290.70 $nGy.h^{-1}$ for uranium granitic ore samples of mine 1. The absorbed dose calculated in mine 1 (section B) was significantly comparable to the level measured in a Gold mine in South Africa by Kamunda *et al*. (2016). The minimum absorbed dose recorded was 135.89 $nGy.h^{-1}$ for Khan river samples.

This study had also calculated the radium equivalent activity, and the levels were low signifying the materials in for Arandis town and Khan river could be safe. It was found that Khan river recorded the minimum value of 253.45 $Bq.kg^{-1}$, whilst the 5271.51 $Bq.kg^{-1}$ and 5129.61 $Bq.kg^{-1}$ were calculated mine 1 ore samples and mine 2 tailings, respectively. These values were greater than those found by other studies in the region, like Onjefu *et al*. (2021). The annual effective dose calculated ranging from 0.83 to 14.05 $nGy.h^{-1}$ in all samples were greater than the world's average level of exposure from terrestrial sources,

but significantly comparable to both the background level in the region and worldwide exposures from all sources at 2.4 $mSv.y^{-1}$. The excess lifetime cancer risks calculated for this study ranged between $2.92x10^{-3}$ – $49.16x10^{-3}$. The minimum ELCR value was significantly comparable to that found in Iran at $2.85x10^{-3}$, and higher than both the world average ($0.29x10^{-3}$) and limit ($1.45x10^{-3}$), as documented by UNSCEAR (2008) and ICRP (2012), respectively. Based on calculations performed on gamma spectroscopy results, the study had shown high radiological hazards on humans and therefore, there is high probability of cancer disease incidences in the region is inevitable.

7.2. ICP-MS results

ICP-MS results have shown significantly high level of radioactivity concentrations in dust samples. The calculated concentrations of NORM in water collected from boreholes and lakes in the uranium mining zone of section B exceeded the drinking water quality guidelines recommended by WHO for gross alpha screening and gross beta levels of 0.5 $mBq.l^{-1}$ and 1.0 $mBq.l^{-1}$, respectively (WHO, 2011b). According to this study, the results showed hazardous level to an extent that water was not fit for human consumption at the time.

The radioactivity concentrations of NORM in dust had shown that the ^{232}Th level was extremely high, with an average of 673.12 $Bq.l^{-1}$ and low ^{40}K with an average of 27.95 $Bq.l^{-1}$. This indicated a high accumulation of ^{232}Th in dust. If wind blowing is high and in the direction of residential areas in the region, residents would be exposed to alpha decaying radionuclides such ^{228}Th, ^{224}Ra and a short-lived ^{220}Rn. These are hazardous alpha and beta emitting nuclides, and therefore, hazardous both externally and internally if allowed into contact with the skin or ingested through food and water. The concentration of ^{40}K in dust is below the world's average. However, this is not of concern since the human body has a mechanism of regulating its concentration and the effective dose to the body. ^{238}U concentration with an average of 80.94 $Bq.m^{-3}$ in dust was found to be above the world's average and could as well increase the level of exposure in homes through wind blowing.

7.3 RESRAD modelling results

The cancer morbidity risks modelled for NORM in mine 1 and mine 2 samples had shown that ^{226}Ra was the main contributor to risk of exposure. Modelling code which was performed with a cut-off half-life of 30 years indicated that a high risk factor of ^{226}Ra attributed to the build-up of its daughter product, lead-210 (^{210}Pb). ^{210}Pb is a hazardous daughter with a half-life of 22 years and it decays by emitting a beta particle (β^-) to form a bismuth-210 (^{210}Bi). It is also crucial to understand that ^{226}Ra existence in tailings soils decays by emission of alpha to form radioactive gas ^{222}Rn ($t_{1/2}$ = 3.8 days) which escapes from tailings and may be inhaled and causes lung cancer in humans (Gadalla and El-Fawal, 2014). All other daughters in a uranium-238 decay chain have very less half-lives, almost less than a year, and therefore its activity concentrations are regarded as contributing less to cancer risks in the human body. The other contributing radionuclide to cancer risks is ^{232}Th with build-ups of ^{228}Ra ($t_{1/2}$ = 5.8 years) which decays by emitting a β^- particle to form a short-lived actinium-228 (^{228}Ac) ($t_{1/2}$ = 6.1 hours), and ^{228}Th ($t_{1/2}$ = 1.9 years) which decays by emitting an alpha (α) into a short-lived product radium-224 (^{224}Ra) with a half-life of 3.6 days. Although activity concentrations for ^{40}K were recorded to be high in the region, its significant contribution factor was recorded less but slightly higher than that of ^{238}U in all samples.

This study has shown that the modelled cancer risks in the Erongo region is higher than the recommended level of $1x10^{-5}$ for a population and $1x10^{-3}$ for a subpopulation documented by the World Health Organization (2011), as well as the world average value of $0.29x10^{-3}$ documented by the United Nations Scientific Committee on the Effects of Atomic Radiation (2008). According to these findings on RESRAD-OFFSITE long term evaluation, the residents of the region who live closer to mining activity areas would be at high risks of developing cancer over prolonged periods of exposures.

7.4 Recommendations

7.4.1 Arandis residents and employees of uranium mines

People of all categories, whether residents, occupationally exposed workers and employees may inhale, ingest an amount of dust or food or water which may be chemically or radioactively contaminated. Travellers, tourists and commuters may also get exposed to the dust or access to food in the region. Therefore, the exploration and mining zones have reportedly measured high radiation level of NORM and hence the need to have access control to the operational areas of the mine and also the regularly (yearly) monitoring of mines is recommended. Radioactive waste products, which came from mining, milling, in-situ and heap leaching should not be allowed to be accessible to the inhabitants of the area and locals needs to instituted on working in such control areas. Close contact with waste products as a result of these activities must be minimized to reduce the exposures mostly due to radon emanation, radioactive dust and eternal gamma radiation.

A continuous monitoring of radon contamination in homes and all dwellings both in mines and the surrounding must be put in place. It is advisable that residents of the town minimize the time of stay in the region in a year, in compliance with the two principles of radiation protection known as ALARA and time. It is also advisable for employees to maintain low level of exposure with time and also wear protective clothing with lead material at all time when on duty. Wind can also contribute to high risks of radiological health hazards. Wind blowing carries radioactive dust afar and dust can contaminate consumable food such as vegetables and drinking water if kept in the open environment. Therefore, it is advisable that all agriculture activities be kept and practiced further away from highly radioactive areas. Wind blowing from mining and milling zones can also be blocked towards agricultural crops and residential areas. In addition to all protocols and radiation safety measures that are already put in place by uranium mines in collaboration with the National Radiation Protection Authority (NRPA) and in compliance with IAEA, close check-ups and examinations for employees must be put in place and implemented on a regular basis. This research will help both the uranium mines and NRPA managements in strengthening the radiological emergency response guidelines.

7.4.2 Modelling tools

The modelling tool has shown relatively high morbidity cancer risks over 200 years. Therefore, mine managements must perform tests on both employees on the level of radioactivity in their urine. A programme on health assessment of residents of the region on the level of radioactivity in urines must be introduced and cancer tests be performed routinely every five (5) years.

8. REFERENCES

ALONSO-HERNÁNDEZ, C., BERNAL-CASTILLO, J., MORERA-GÓMEZ, Y., GUILLEN-ARRUEBARRENA, A., CARTAS-AGUILA, H. & ACOSTA-MILIÁN, R. 2013. Naturally occurring radioactive materials (NORM) in ashes from a fuel-oil power plant in Cienfuegos, Cuba, and the associated radiation hazards. *Radiation Protection Dosimetry,* 158**,** 421-426.

ALZUBAIDI, G., HAMID, F. & ABDUL RAHMAN, I. 2016. Assessment of natural radioactivity levels and radiation hazards in agricultural and virgin soil in the state of Kedah, North of Malaysia. *The Scientific World Journal*.

AMAKALI, G. 2021. *Evaluation of primordial radionuclides and health impacts in soil, groundwater and food crops from the lower Swakop river, Namibia.* PhD, North-West University.

AMANJEET, KUMAR, A., KUMAR, S., SINGH, J., SINGH, P. & BAJWA, B. 2017. Assessment of natural radioactivity levels and associated dose rates in soil samples from historical city Panipat, India. *Journal of Radiation Research and Applied Sciences,* 10**,** 283-288.

AMRANE, M. & OUFNI, L. 2017. Determination for levels of uranium and thorium in water along Oum Er-Rabia river using alpha track detectors. *Journal of Radiation Research and Applied Sciences,* 10**,** 246-251.

AMWAALANGA, M. N., ONJEFU, S. A., ZIVUKU, M. & HAMUNYELA, R. H. 2019. Assessment of natural radioactivity levels and radiation hazards in shore sediments from the Zambezi river, Namibia.

ARAFAT, A., SALAMA, M., EL-SAYED, S. & ELFEEL, A. 2017. Distribution of natural radionuclides and assessment of the associated hazards in the environment of Marsa Alam-Shalateen area, Red Sea coast, Egypt. *Journal of Radiation Research and Applied Sciences,* 10**,** 219-232.

AUMALIKOVA, M., BAKHTIN, M., KAZYMBET, P., ZHUMADILOV, K., ALTAEVA, N., IBRAYEVA, D. & SHISHKINA, E. 2020. Site-specific concentration of uranium in urine of workers of the hydrometallurgical plant of Stepnogorsk mining and chemical combine. *Radiation and Environmental Biophysics,* 59**,** 703-710.

AWWAD, N., ATTALLAH, M., EL-AFIFI, E., IBRAHIUM, H. & ALY, H. 2015. Overview about different approaches of chemical treatment of NORM and TE-NORM produced from oil exploitation. *Advances in Petrochemicals*, 85.

BAI, H., HU, B., WANG, C., BAO, S., SAI, G., XU, X., ZHANG, S. & LI, Y. 2017. Assessment of radioactive materials and heavy metals in the surface soil around the Bayanwula prospective uranium mining area in China. *International Journal of Environmental Research and Public Health,* 14, 300.

BASDEVANT, J.-L. & RICH, J. 2005. *Fundamentals in nuclear physics: From nuclear structure to cosmology*, Springer Science & Business Media.

BERNING, J. 1986. The Rössing uranium deposit, South West Africa/Namibia. *Mineral Deposits of Southern Africa. V. 1-2.*

BIRAMI, F. A., MOORE, F., FAGHIHI, R. & KESHAVARZI, B. 2019. Distribution of natural radionuclides and assessment of the associated radiological hazards in the rock and soil samples from a high-level natural radiation area, Northern Iran. *Journal of Radioanalytical and Nuclear Chemistry,* 322, 2091-2103.

BYNUM, W. 2012. Chapter 31. Radioactivity. *A Little History of Science.* Yale University Press.

CARIDI, F., PAPPATERRA, D., BELMUSTO, G., MESSINA, M., BELVEDERE, A., D'AGOSTINO, M. & SETTINERI, L. 2019. Radioactivity and heavy metals concentration in Italian (Calabrian) DOC Wines. *Applied Sciences,* 9, 4584.

CARVALHO, F. P. 2011. Environmental radioactive impact associated to uranium production. *Journal of American Journal of Environmental Sciences,* 7, 547.

CEMBER, H. J., E. THOMAS 2008. *Introduction to Health Physics,* New York, McGraw Hill Companies, Inc.

CETNAR, J. 2006. General solution of Bateman equations for nuclear transmutations. *Annals of Nuclear Energy,* 33, 640-645.

CNNC 2018. Annual Environmental Management Report: CNNC Rossing Uranium Working for Namibia.

CNSC 2014. Canadian Nuclear Safety Commission, Frequently asked questions: Tritium.

COWART, J. & BURNETT, W. 1994. The Distribution of Uranium and Thorium Decay-Series Radionuclides in the Environment—A Review. *Journal of Environmental Quality,* 23**,** 651-662.

DICKINSON, K. A. & SULLIVAN, M. W. 1976. Geology of the Brysch uranium mine, Karnes County, Texas. *US Geol. Survey Jour. Research,* 4**,** 397-404.

DOYI, I., ESSUMANG, D. K., DAMPARE, S. & GLOVER, E. T. 2016. Technologically enhanced naturally occurring radioactive materials (TENORM) in the oil and gas industry: a review. *Reviews of environmental contamination and toxicology***,** 107-119.

DU PREEZ, L. 2018. *Airborne radiometric surveys through the uses of a handheld spectrometer fitted to a UAV.* North-West University.

DUDU, V. P., MATHUTHU, M. & MANJORO, M. 2018. Assessment of heavy metals and radionuclides in dust fallout in the West Rand mining area of South Africa. *Clean Air Journal,* 28**,** 42-52.

DURUSOY, A. & YILDIRIM, M. 2017. Determination of radioactivity concentrations in soil samples and dose assessment for Rize Province, Turkey. *Journal of Radiation Research and Applied Sciences,* 10**,** 348-352.

EHSAN, M. S., RAHMAN, M. F., TABASSUM, N., PRODHAN, M. M. H., PERVIN, S., SIRAZ, M. M., RAHMAN, A. M., YEASMIN, S. & MAHAL, S. F. 2019. The Activity Concentration of Radionuclides (226Ra, 232Th and 40K) in Soil Samples and Associated Health Hazards in Natore, Kushtia and Pabna District of Bangladesh. *Journal of Bangladesh Academy of Sciences,* 43**,** 169-180.

ELGAZZAR, A. H. & KAZEM, N. 2015. Biological effects of ionizing radiation. *The pathophysiologic basis of nuclear medicine.* Springer.

FAANU, A., DARKO, E., AWUDU, A., SCHANDORF, C., EMI-REYNOLDS, G., YEBOAH, J., GLOVER, E. & KATTAH, V. 2010. Radiation Exposure Control from the Application of Nuclear Gauges in the Mining Industry in Ghana. *Health Physics,* 98**,** S33-S38.

FAO 2005. Atomic Energy and Radiation Protection Act, 2005. Food and Agriculture Organization of the United Nations.

FERREIRA, V. V., FONSECA, R. L., ROCHA, Z., OLIVEIRA, A. L., MOREIRA, R. M., LEMOS, N. C., CHAGAS, C. J., MENEZES, M. & SANTOS, T. O. 2015. Use of radon as water tracer at Juatuba Basin. *J. Geographical Geology,* 7**,** 49-60.

FOWLER, J. F. 2006. Development of radiobiology for oncology—a personal view. *Physics in Medicine & Biology,* 51**,** R263.

GADALLA, A. & EL-FAWAL, M. Uranium Mining and Extraction Industries, Environmental Impacts and Mitigation Techniques. PAPERS PRESENTED, 2014. 393.

GASCOYNE, M. 1992. Geochemistry of the actinides and their daughters. *Uranium-series disequilibrium: applications to earth, marine, and environmental sciences. 2. ed.*

GAZIS, E. 2019. The Ionizing Radiation Interaction with Matter, the X-ray Computed Tomography Imaging, the Nuclear Medicine SPECT, PET and PET-CT Tomography Imaging. *Medical Imaging: Principles and Applications***,** 41.

GENE 2000. Genie TM Spectroscopy Software, 2000: Customization Tools Manual. *Canberra Industires, Inc. USA,* 3.1-9233653F.

GEOLOGY.COM. 2005. *Geological news and information* [Online]. Available: https://geology.com/rocks/granite.shtml [Accessed].

GERWARD, L. 1999. Paul Villard and his discovery of gamma rays. *Physics in perspective,* 1**,** 367-383.

GIRI, A. & PANT, D. 2018. Inhalation dose due to Rn-222, Rn-220 and their progeny in indoor environments. *Applied Radiation and Isotopes,* 132**,** 116-121.

GLOBE, C. 2021. *Difference Between Valence Band and Conduction Band* [Online]. Available: https://circuitglobe.com/difference-between-valence-band-and-conduction-band.html [Accessed August 18, 2021 2021].

GOUDIE, A. & VILES, H. 2014. *Landscapes and landforms of Namibia*, Springer.

GSN 2014. Strategic Environmental Management Plan (SEMP) for the Central Namib Uranium Province, 2012 Annual Report. *In:* GEOLOGY, E. A. E. (ed.). Ministry of Mines and Energy, Windhoek, Republic of Namibia: Geological Survey of Namibia (GSN).

GSN 2017. Strategic Environmental Management Plan (SEMP) for the Central Namib Uranium Mining Province, 2016 Annual Report. Ministry of Mines and Energy, Windhoek, Republic of Namibia. *Geological Survey of Namibia*.

GUNHILD VON OERTZEN, D. V. O. 2011. Guide to Radiation in Namibia's Uranium Exploration and Mining Sectors. The Uranium Institute: Chambers of Mines.

HABASHI, F. 2001. Niepce de saint-Victor and the discovery of radioactivity. *Bull. Hist. Chem,* 26**,** 105.

HALLIDAY, D., RESNICK, R. & WALKER, J. 2013. *Fundamentals of physics*, John Wiley & Sons.

HASSAN, N. 2012. Assessment and GIS mapping of terrestrial Gamma radiation in Elfao area in Elgedaref states.

HEGENBERGER, W. 1988. Karoo sediments of the Erongo Mountains, their environmental setting and correlation. *Communications of the Geological Survey of South West Africa/Namibia,* 4**,** 51-57.

HENRIKSEN, T. 2009. *Radioactivity and x-rays: Applications and health effects*, University of Oslo.

HERON, J. L. & BORRÁS, C. 2014. The International Basic Safety Standards and Their Application in Medical Imaging. *Radiological Safety and Quality.* Springer.

HUDA, W., MAGILL, D. & HE, W. 2011. CT effective dose per dose length product using ICRP 103 weighting factors. *Medical physics,* 38**,** 1261-1265.

HYUN, J., PIOT, P. & SEN, T. 2018. Optics and bremsstrahlung estimates for channeling radiation experiments at FAST. *arXiv preprint arXiv:1802.06113*.

IAEA 1987. Preparation and certification of IAEA gamma-ray spectrometry reference materials RGU-1, RGTh-1 and RGK-1. International Atomic Energy Agency Vienna.

IAEA 1989. Measurement of Radionuclides in Food and the Environment. *Int. At. Energy Agency Vienna, Au, Technical Report Series***,** 295.

IAEA 1996. International basic safety standards for protection against ionizing radiation and for the safety of radiation sources.

ICRP 1994. Protection against radon at home and at work. *ICRP publication,* 65**,** 1-48.

ICRP 2007. ICRP publication 103: The 2007 Recommendations of the International Commission on Radiological Protection. *Ann ICRP,* 37**,** 2.

ICRP 2012. ICRP statement on tissue reactions/early and late effects of radiation in normal tissues and organs—threshold doses for tissue reactions in a radiation protection context. ICRP publication 118. *Ann. ICRP,* 41**,** 1-322.

ICRP 2013. Radiological protection in geological disposal of long lived solid radioactive waste. *ICRP Publication 122. Annals of the ICRP,* 42.

ISINKAYE, M. & EMELUE, H. 2015. Natural radioactivity measurements and evaluation of radiological hazards in sediment of Oguta Lake, South East Nigeria. *Journal of Radiation Research and Applied Sciences,* 8**,** 459-469.

ISSA, S., UOSIF, M. & ELSAMAN, R. 2013. Gamma radioactivity measurements in Nile River sediment samples. *Turkish Journal of Engineering and Environmental Sciences,* 37**,** 109-122.

JAYASHEELAN, A., MANJUNATHA, S., YASHODHARA, I. & KARUNAKARA, N. 2013. Study of natural radioactivity and estimation of radiation dose in the environment of Tumkur, Karnataka, India. *Radiation Protection Dosimetry,* 158**,** 73-78.

JOEL, E., MAXWELL, O., ADEWOYIN, O., EHI-EROMOSELE, C., EMBONG, Z. & OYAWOYE, F. 2018. Assessment of natural radioactivity in various commercial tiles used for building purposes in Nigeria. *MethodsX,* 5**,** 8-19.

KAMBOJ, S., LEPOIRE, D., GNANAPRAGASAM, E., BIWER, B., CHENG, J., ARNISH, J., YU, C., CHEN, S. & MO, T. 2000. *Probabilistic dose analysis using parameter distributions developed for RESRAD and RESRAD-BUILD codes*, Division of Risk Analysis and Applications, Office of Nuclear Regulatory.

KAMUNDA, C., MATHUTHU, M. & MADHUKU, M. 2016. An assessment of radiological hazards from gold mine tailings in the province of Gauteng in South Africa. *International Journal of Environmental Research and Public Health,* 13**,** 138.

KANDARI, T., SINGH, P., SEMWAL, P., KUMAR, A., BOURAI, A. & RAMOLA, R. 2021. Evaluation of background radiation level and excess lifetime cancer risk in Doon valley, Garhwal Himalaya. *Journal of Radioanalytical and Nuclear Chemistry***,** 1-13.

KENNY, A. 1977. *Nuclear power*, Cambridge, Massachusetts, Ballinger Publishing Co.

KHAN, F. M. & GIBBONS, J. P. 2014. *Khan's the physics of radiation therapy*, Lippincott Williams & Wilkins.

KHAN, M. F., WESLEY, S. G. & RAJAN, M. 2014. Polonium-210 in marine mussels (bivalve molluscs) inhabiting the southern coast of India. *Journal of Environmental Radioactivity,* 138**,** 410-416.

KNAPP, F. R. & DASH, A. 2016. Radionuclide generator systems represent convenient production systems to provide therapeutic radionuclides. *Radiopharmaceuticals for therapy.* Springer.

KOŠLER, J. & SYLVESTER, P. J. 2003. Present trends and the future of zircon in geochronology: laser ablation ICP-MS. *Reviews in Mineralogy and Geochemistry,* 53**,** 243-275.

KRISANANGKURA, P., ITTHIPOONTHANAKORN, T. & UDOMSOMPORN, S. 2013. Environmental dose assessment using Ecolego: case study of soil from Japan. *Journal of Radioanalytical and Nuclear Chemistry,* 297**,** 443-450.

L'ANNUNZIATA, M. F. 2012. Radiation physics and radionuclide decay. *Handbook of Radioactivity Analysis.* Elsevier.

LEVY, E. 2018. A matrix exponential approach to radioactive decay equations. *American Journal of Physics,* 86**,** 909-913.

LEVY, E. 2019. Decay chain differential equations: Solutions through matrix analysis. *Computer Physics Communications,* 234**,** 188-194.

LONG, S. E. & MARTIN, T. D. 1997. *Determination of Trace Elements in Marine Waters by On-line Chelation Preconcentration and Inductively Coupled Plasma-Mass Spectrometry*, United States Environmental Protection Agency, Office of Research.

LOVELAND, W. D., MORRISSEY, D. J. & SEABORG, G. T. 2017. *Modern nuclear chemistry*, John Wiley & Sons.

MAHMOOD, R. & HAIDER, Q. 2015. *Radiation Physics and its applications in diagnostic radiological techniques*.

MANDIĆ, L. J., DRAGOVIĆ, R. & DRAGOVIĆ, S. 2010. Distribution of lithogenic radionuclides in soils of the Belgrade region (Serbia). *Journal of Geochemical Exploration,* 105**,** 43-49.

MARGUET, S. 2018. *The physics of nuclear reactors*, Springer.

MARSH, D. 2009. Development and expansion of the Langer Heinrich Operation in Namibia. *IAEA Tecdoc Series***,** 160.

MARTIN, J. E. 2013. *Physics for radiation protection*, Wiley Online Library.

MASOUMI, H. & KESHTKAR, M. 2021. Assessment of Background Radiation, Annual Effective Dose and Excess Lifetime Cancer Risk in Gonabad City. *Frontiers in Biomedical Technologies,* 8**,** 170-174.

MATHUTHU, M., KAMUNDA, C. & MADHUKU, M. 2016. Modelling of Radiological Health Risks from Gold Mine Tailings in Wonderfonteinspruit Catchment Area, South Africa. *International Journal of Environmental Research and Public Health,* 13**,** 570.

MAXWELL, O., WAGIRAN, H., IBRAHIM, N., LEE, S. K. & SABRI, S. 2013. Comparison of activity concentration of 238U, 232Th and 40K in different Layers of subsurface Structures in Dei-Dei and Kubwa, Abuja, northcentral Nigeria. *Radiation Physics and Chemistry,* 91**,** 70-80.

MAYLES, P., NAHUM, A. & ROSENWALD, J.-C. 2007. *Handbook of radiotherapy physics: theory and practice*, CRC Press.

MCDOUGALL, I., MAC DOUGALL, I. & HARRISON, T. M. 1999. *Geochronology and Thermochronology by the 40Ar/39Ar Method*, Oxford University Press on Demand.

MIDZI, W., OYEDELE, J., SHIMBOYO, S. A. & TAAPOPI, E. E. 2019. Measurement of natural radioactivity and dose rate assessment of terrestrial gamma radiation in the soils of Karibib and Okahandja, Namibia.

MIRION, T. 2015. *Radiation Measurement & Detection Devices* [Online]. Mirion Technologies, Inc. Available: https://www.mirion.com/learning-center/radiation-safety-basics/types-of-ionizing-radiation [Accessed 17 June 2021].

MME 2010. Strategic Environmental Assessment for the central Namib Uranium Rush. Ministry of Mines and Energy Windhoek.

MOHAMMADI, S. 2010. Elements of natural radioactive decay series in Iranian drinking water and cigarettes. *Arhiv za higijenu rada i toksikologiju,* 61**,** 235-238.

MORRELL, J. S. & JACKSON, M. J. 2013. *Uranium processing and properties*, Springer.

MOTEVALLI, S. & BORHANAZAD, A. 2015. Assessment of occupational exposure in medical practice in Tehran, Iran. *Rom. Rep. Phys.,* 67**,** 431-438.

MUNYARADZI, Z., ANNA, K. N. & MAKONDELELE, T. V. 2018. Excess lifetime cancer risk due to natural radioactivity in soils: Case of Karibib town in Namibia. *African Review of Physics,* 13**,** 71-78.

MURNIASIH, S., PRABASIWI, D. S. & ROZANA, K. The impact of radioactivity from tin mining on Bangka island. AIP Conference Proceedings, 2021. AIP Publishing LLC, 020045.

MURRAY, R. & HOLBERT, K. E. 2014. *Nuclear energy: an introduction to the concepts, systems, and applications of nuclear processes*, Elsevier.

NABHANI, K. A., KHAN, F. & YANG, M. 2016. Technologically enhanced naturally occurring radioactive materials in oil and gas production: A silent killer. *Process Safety Environmental Protection,* 99**,** 237-247.

NAGARAJU, K., CHANDRASHEKARA, M., RANI, K. P. & PARAMESH, L. 2012. Measurement of gamma natural background radiation in Chamaraja Nagar district, Karnataka state, India. *Radiation Protection and Environment,* 35**,** 73.

NDE-ED.ORG. 2021. *Newton's Inverse Square Law* [Online]. Iowa State University: Nondestructive Evaluation Physics: X-Ray. Available: https://www.nde-ed.org/Physics/X-Ray/inversesquare.xhtml [Accessed 18 June 2021].

NELSON, C. 2014. *The age of radiance: the epic rise and dramatic fall of the atomic era*, Simon and Schuster.

NGUELEM, E. J. M., NDONTCHUENG, M. M. & MOTAPON, O. 2016. Determination of 226 Ra, 232 Th, 40 K, 235 U and 238 U activity concentration and public dose assessment in soil samples from bauxite core deposits in Western Cameroon. *SpringerPlus,* 5**,** 1-12.

NICHOLS, L. 2020. *Introductory Chemistry - Lecture Lab (Lumen)* [Online]. The LibreTexts libraries. Available: https://chem.libretexts.org/Courses/Lumen_Learning/Book%3A_Introductory_Ch

emistry__Lecture_Lab_(Lumen)/12%3A_Nuclear_Reactions/12.3%3A_Radioactive_Decay [Accessed 18 June 2021].

NIELSEN, S. P. Alpha, beta and gamma measurements of environmental radioactivity. NKS Workshop on Radioanalytical Chemistry, 2013. NKS Secretariat.

NIETO, L. 2020. *Marie Curie, international radiancy* [Online]. Available: https://curiokids.net/marie-curie-international-radiancy/?lang=en [Accessed 17 June 2021].

NISI, S., COPIA, L., DAFINEI, I. & DI VACRI, M. 2017. ICP-MS measurement of natural radioactivity at LNGS. *International Journal of Modern Physics A,* 32**,** 1743003.

NJINGA, R. L., TSHIVHASE, M. V., KGABI, N. A. & ZIVUKU, M. 2016. Hazards index analysis of Gamma emitting radionuclides in selected areas around the Uranium Mine sites at Erongo Region, Namibia.

NPC 2012. Namibia 2011 population and housing census preliminary results. *National Planning Commission (NPC), Windhoek, Namibia*.

NRC 2006. Health risks from exposure to low levels of ionizing radiation: BEIR VII phase 2. *National Research Council*.

OBRENOVIĆ, M. D., JANIĆIJEVIĆ, A. J. & ARBUTINA, D. S. 2018. Statistical review of the insulation capacity of the Geiger-Muller counter. *Nuclear Technology and Radiation Protection,* 33**,** 369-374.

OECD 1979. Exposure to radiation from the natural radioactivity in building materials. *In:* (NEA), N. E. A. (ed.) *Report by a Group of Expertsof the OECD.* Nuclear Energy Agency, Paris, France: Organization for Economic Co-operation and Development.

OJOVAN, M. I., LEE, W. E. & KALMYKOV, S. N. 2019. *An introduction to nuclear waste immobilisation*, Elsevier.

ONJEFU, S. A., IYAMBO, M. L., ABAH, J. & MWIYA, S. 2021. Radiological analysis of the suitability of Erongo granite for building material. *Geomatics, Natural Hazards and Risk,* 12**,** 181-197.

ONJEFU, S. A., KGABI, N. A., TAOLE, S. H., MTAMBO, O. P., GRANT, C. & ANTOINE, J. 2016. Occupancy factor model for exposure to natural

radionuclides along the coastline of Erongo Region, Namibia. *Journal of Geoscience and Environment Protection,* 4**,** 117-126.

ONJEFU, S. A., TAOLE, S. H., KGABI, N. A., GRANT, C. & ANTOINE, J. 2017. Assessment of natural radionuclide distribution in shore sediment samples collected from the North Dune beach, Henties Bay, Namibia. *Journal of Radiation Research and Applied Sciences,* 10**,** 301-306.

OVASKAINEN, R. 1999. The determination of minor isotope abundances in naturally occurring uranium materials. The tracing power of isotopic signatures for uranium. Helsinki Univ.(Finland). Lab. of Radiochemistry.

OYEDELE, J. 2006. Assessment of the natural radioactivity in the soils of Windhoek city, Namibia, Southern Africa. *Radiation Protection Dosimetry,* 121**,** 337-340.

OYEDELE, J. & SHIMBOYO, S. 2013. Distribution of radionuclides and radiation hazard assessment in soils of Southern Namibia, Southern Africa. *Radiation Protection Dosimetry,* 156**,** 343-348.

PERKINELMER 2017. Syngistix™ Software for ICP-MS v.2.2: Software Reference Guide. 710 Bridgeport Avenue, Shelton, CT 06484-4794, U.S.A.

PILAKOUTA, M., KALLITHRAKAS-KONTOS, N. & NIKOLAOU, G. 2017. Determining the 40K radioactivity in rocks using x-ray spectrometry. *European Journal of Physics,* 38**,** 055803.

PIRAJNO, F. 1990. Geology, geochemistry and mineralisation of the Erongo Volcanic Complex, Namibia. *South African Journal of Geology,* 93**,** 485-504.

PODGORSAK, E. B. 2005. *Radiation oncology physics*, IAEA Vienna.

PRADLER, J., SINGH, B. & YAVIN, I. 2013. On an unverified nuclear decay and its role in the DAMA experiment. *physics letters B,* 720**,** 399-404.

QUORA. 2021. *How do Geiger counters measure radiation?* [Online]. Quora. Available: https://www.quora.com/How-do-Geiger-counters-measure-radiation [Accessed 18 June 2021].

RAJAN, G. & IZEWSKA, J. 2005. Radiation monitoring instruments. *Podgorsak EB, Radiation Oncology Physics: A Handbook for teachers students. Vienna: International Atomic Energy Agency (IAEA)*.

RAO, N., HAGEMEYER, D. & MCCORMICK, Y. 2017. DOE 2016 Occupational Radiation Exposure. Oak Ridge Inst. for Science and Education (ORISE), Oak Ridge, TN (United States).

RE, H. 2018. Aannual report on environmental management at Orano, Namibia.

RIGHI, S. & BRUZZI, L. 2006. Natural radioactivity and radon exhalation in building materials used in Italian dwellings. *Journal of Environmental Radioactivity,* 88**,** 158-170.

SALOM, A. T. & KIVINEN, S. 2020. Closed and abandoned mines in Namibia: a critical review of environmental impacts and constraints to rehabilitation. *South African Geographical Journal,* 102**,** 389-405.

SAMREH, M. M. A., THABAYNEH, K. M. & KHRAIS, F. W. 2015. Measurement of activity concentration levels of radionuclides in soil samples collected from Bethlehem Province, West Bank, Palestine. *Turkish Journal of Engineering and Environmental Sciences,* 38**,** 113-125.

SCHNEIDER, G. 2018. Uranium, the Environment and Sustainable Development: Lessons from Namibia.

SCIONIX. 2019. *Scintillation light detection devices* [Online]. 3981 LA Bunnik: Scionix, Netherlands. Available: https://scionix.nl/read-out/ [Accessed 09 November 2021].

SERWAY, R. A. & JEWETT, J. W. 2012. *Principles of Physics: A Calculus-Based Text, Volume 2*, Cengage Learning.

SETHY, N., JHA, V., RAVI, P. & TRIPATHI, R. 2014. A simple method for calibration of Lucas scintillation cell counting system for measurement of 226Ra and 222Rn. *Journal of Radiation Research and Applied Sciences,* 7**,** 475-477.

SHAHBAZI-GAHROUEI, D., GHOLAMI, M. & SETAYANDEH, S. 2013. A review on natural background radiation. *Advanced Biomedical Research,* 2.

SHINDONDOLA-MOTE, H. 2009. *Uranium mining in Namibia: the mystery behind" low level radiation"*, Labour Resource and Research Institute.

SIMON, T. W. 2019. *Environmental risk assessment: a toxicological approach*, CRC Press.

SOOKDEO, A. 2015. *The Determination of ^{210}Pb by Accelerator Mass Spectrometry.* Université d'Ottawa/University of Ottawa.

STEWART, F., AKLEYEV, A., HAUER-JENSEN, M., HENDRY, J., KLEIMAN, N., MACVITTIE, T., ALEMAN, B., EDGAR, A., MABUCHI, K. & MUIRHEAD, C. 2012. ICRP publication 118: ICRP statement on tissue reactions and early and late effects of radiation in normal tissues and organs–threshold doses for tissue reactions in a radiation protection context. *Annals of the ICRP,* 41**,** 1-322.

TAKIGAWA, N. & WASHIYAMA, K. 2017. *Fundamentals of nuclear physics*, Springer.

TANIGAWA, K., HOSOI, Y., HIROHASHI, N., IWASAKI, Y. & KAMIYA, K. 2012. Loss of life after evacuation: lessons learned from the Fukushima accident. *The Lancet,* 379**,** 889-891.

TASKIN, H., KARAVUS, M., AY, P., TOPUZOGLU, A., HIDIROGLU, S. & KARAHAN, G. 2009. Radionuclide concentrations in soil and lifetime cancer risk due to gamma radioactivity in Kirklareli, Turkey. *Journal of Environmental Radioactivity,* 100**,** 49-53.

TEDJANI, A., MAVON, C., BELAFRITES, A., DEGRELLE, D., BOUMALA, D., RIUS, D. & GROETZ, J.-E. 2016. Well GeHP detector calibration for environmental measurements using reference materials. *Nuclear Instruments and Methods in Physics Research Section A: Accelerators, Spectrometers, Detectors and Associated Equipment,* 838**,** 12-17.

THABAYNEH, K. 2012. Natural radioactivity levels and estimation of radiation exposure in environmental soil samples from Tulkarem Province–Palestine.

THABAYNEH, K. M. 2018. Determination of radon exhalation rates in soil samples using sealed can technique and CR-39 detectors. *Journal of Environmental Health Science and Engineering,* 16**,** 121-128.

TRACHANAS, S. 2018. *An introduction to quantum physics: a first course for physicists, chemists, materials scientists, and engineers*, John Wiley & Sons.

TURNER, J. E. 2008. *Atoms, radiation, and radiation protection*, John Wiley & Sons.

UNSCEAR 1982. Ionizing radiation: sources and biological effects. 1982 report to the general assembly, with Annexes.

UNSCEAR 1988. *Sources, Effects and Risks of Ionizing Radiation: United Nations Scientific Committee on the Effects of Atomic Radiation* UN.

UNSCEAR 1993. *Sources and Effects of Ionizing Radiation, United Nations Scientific Committee on the Effects of Atomic Radiation (UNSCEAR) 1993 Report: Report to the General Assembly, with Scientific Annexes*, United Nations.

UNSCEAR 2000. Effects of Ionizing Radiation. *United Nations, New York***,** 453-487.

UNSCEAR 2010. UNSCEAR 2008 Report to the General Assembly, with Scientific Annexes. United Nations New York.

UNSCEAR 2013. Sources, effeccts, and risks of ionization radiation. *In:* ASSEMBLY, R. T. T. G. (ed.) *United Nations Scientific Committee on the Effects of Atomic Radiation.* United Nations.

UNSCEAR 2017. *Sources, Effects and Risks of Ionizing Radiation, United Nations Scientific Committee on the Effects of Atomic Radiation (UNSCEAR) 2016 Report: Report to the General Assembly, with Scientific Annexes*, United Nations.

UNSCEAR 2018. *Sources, effects and risks of ionizing radiation: UNSCEAR 2017 report to the general assembly with scientific annexes*, United Nations.

VANHAVERE, F., CARINOU, E., DOMIENIK, J., DONADILLE, L., GINJAUME, M., GUALDRINI, G., KOUKORAVA, C., KRIM, S., NIKODEMOVA, D. & RUIZ-LOPEZ, N. 2011. Measurements of eye lens doses in interventional radiology and cardiology: final results of the ORAMED project. *Radiation Measurements,* 46**,** 1243-1247.

VELIKYAN, I. 2015. 68Ga-based radiopharmaceuticals: production and application relationship. *Molecules,* 20**,** 12913-12943.

VON OERTZEN, G. 2017. Radiation exposures at uranium mines-what are the risks?

WACKERLE, R. 2009. Natural Terrestrial Radiation of the Erongo Region, Central Western Namibia Processing Report, October 2009. Windhoek, Namibia: Geointrepid Consulting Services Namibia.

WEBMASTER. 2000. *A Teacher's Guide to the Nuclear Science Wall Chart* [Online]. 2000 Webmaster. Available: https://www2.lbl.gov/abc/wallchart/chapters/02/3.html [Accessed 18 June 2021].

WHO 1994. International basic safety standards for protection against ionizing radiation and for the safety of radiation sources.

WHO 2011a. Guidelines for drinking-water quality. *World Health Organization, Geneva,* 216**,** 303-304.

WHO 2011b. Guidelines for drinking-water quality, Fourth Edition. *WHO chronicle,* 38**,** 104-108.

WILSCHEFSKI, S. C. & BAXTER, M. R. 2019. Inductively coupled plasma mass spectrometry: introduction to analytical aspects. *The Clinical Biochemist Reviews,* 40**,** 115.

WINDE, F., BRUGGE, D., NIDECKER, A. & RUEGG, U. 2017. Uranium from Africa–An overview on past and current mining activities: Re-appraising associated risks and chances in a global context. *Journal of African Earth Sciences,* 129**,** 759-778.

WINDE, F. & SANDHAM, L. 2004. Uranium pollution of South African streams–An overview of the situation in gold mining areas of the Witwatersrand. *GeoJournal,* 61**,** 131-149.

YOUNG, H. D. & FREEDMAN, R. A. 2008. Sears and Zemansky's university physics (Vol. 1). San Francisco. Pearson/Addison Wesley.

YU, C., KAMBOJ, S., WANG, C. & CHENG, J.-J. 2015. Data collection handbook to support modeling impacts of radioactive material in soil and building structures. Argonne National Lab.(ANL), Argonne, IL (United States).

YU, C., ZIELEN, A., CHENG, J.-J., LEPOIRE, D., GNANAPRAGASAM, E., KAMBOJ, S. A., WALLO III, A., WILLIAMS, W. & PETERSON, H. 2001. User's manual for RESRAD version 6. Argonne National Lab., IL (US).

ZAKARIYA, N. I. & KAHN, M. 2014. Benefits and biological effects of ionizing radiation. *Sch. Acad. J. Biosci,* 2**,** 583-591.

ZUMDAHL, S. S., ZUMDAHL, S. A. & DECOSTE, D. J. 2020. *Chemistry: An atoms first approach*, Cengage Learning.

9. ANNEXURES

Annexure A: Tables of coordinates from the study areas

Table A1: Coordinates and mass samples collected in Arandis town.

Sample Code	Position		Location (Erongo Region)	Sample mass counted (kg)
	Latitude	Longitude		
AR 1	-22.4169	14.98278	Arandis town	0.7402
AR 2	-22.4139	14.98333	Arandis town	0.7259
AR 3	-22.4094	14.98333	Arandis town	0.7230
AR 4	-22.4111	14.97917	Arandis town	0.7120
AR 5	-22.4103	14.97500	Arandis town	0.6568
AR 6	-22.4125	14.97278	Arandis town	0.5960
AR 7	-22.4156	14.96944	Arandis town	0.6984
AR 8	-22.4217	14.97167	Arandis town	0.7836
AR 9	-22.4192	14.96611	Arandis town	0.6019
AR 10	-22.4181	14.97111	Arandis town	0.7197
AR 11	-22.4222	14.96583	Arandis town	0.5298
AR 12	-22.4225	14.96944	Arandis town	0.7573
AR 13	-22.4250	14.97056	Arandis town	0.5633
AR 14	-22.4217	14.97139	Arandis town	0.4774
AR 15	-22.4278	14.96806	Arandis town	0.5966
AR 16	-22.4275	14.97306	Arandis town	0.6981
AR 17	-22.4281	14.97611	Arandis town	0.6723
AR 18	-22.4300	14.97389	Arandis town	0.7859
AR 19	-22.4261	14.97611	Arandis town	0.7231
AR 20	-22.425	14.97361	Arandis town	0.6821
AR 21	-22.4222	14.97250	Arandis town	0.7757
AR 22	-22.4203	14.97028	Arandis town	0.7304
AR 23	-22.4189	14.96944	Arandis town	0.7309
AR 24	-22.4189	14.96944	Arandis town	0.8080
AR 25	-22.4192	14.97222	Arandis town	0.6952
AR 26	-22.4172	14.97000	Arandis town	0.8115
AR 27	-22.4242	14.98167	Arandis town	0.6293
AR 28	-22.4242	14.98167	Arandis town	0.8264
AR 29	-22.4289	14.99167	Arandis town	0.5708
AR 30	-22.4244	15.01750	Arandis town	0.6322
AR 31	-22.4289	14.99333	Arandis town	0.6283

AR 32	-22.4317	15.00944	Arandis town	0.8294
AR 33	-22.4364	15.00750	Arandis town	0.6639
AR 34	-22.4369	15.02028	Arandis town	0.7889
AR 35	-22.4347	15.00250	Arandis town	0.7427
AR 36	-22.4403	14.99917	Arandis town	0.5966
AR 37	-22.4453	14.99194	Arandis town	0.6966
AR 38	-22.4258	14.98167	Arandis town	0.7028
AR 39	-22.4619	14.98333	Arandis Airport	0.7151
AR 40	-22.4631	14.97917	Arandis Airport	0.7238

Table A2: Coordinates positions and masses for mine 1 soil samples counted on HPGe detector.

Sample ID	Position		Location (Erongo Region)	Mass (kg) of sample
	Latitude	**Longitude**		
S01	-22.4826	15.03475	Soil	0.702413
S02	-22.4480	15.99110	Soil	0.659285
S03	-22.4401	15.00486	Soil	0.696733
S04	-22.4528	15.04997	Soil	0.651612
S05	-22.4605	15.02702	Tailings	0.647589
S06	-22.4589	15.02845	Tailings	0.574344
S07	-22.4573	15.03040	Tailings	0.633298
S08	-22.4582	15.03242	Tailings	0.440654
S09	-22.4611	15.02671	Tailings	0.625687
S10	-22.4553	15.02989	Tailings	0.600299
S11	-22.4565	15.03082	Tailings	0.620014
S12	-22.4579	15.02873	Tailings	0.641539
S13	-22.4599	15.02673	Tailings	0.637864
S14	-22.8154	15.91650	Soil	0.49108

Table A3: Coordinate positions and masses of ore samples counted on HPGe detector.

Sample ID	Position		Facility	Mass (kg) of sample
	Latitude	**Longitude**		
ORE1	-22.47252	15.04570	Course ore stock pile	0.62606
ORE2	-22.47252	15.04570	Course ore stock pile	0.62789
ORE3	-22.46743	15.04182	Fine crushing area	0.68486
ORE4	-22.46754	15.04190	Fine crushing area	0.67607
ORE5	-22.46725	15.04173	Fine crushing area	0.68518

ORE6	-22.56692	15.04170	Fine crushing area	0.66445
ORE7	-22.46736	15.04167	Fine crushing area	0.64013
ORE8	-22.46706	15.04154	Fine crushing area	0.68377

Table A4: Coordinate positions for water from both the tailings and boreholes.

Sample ID	Position		Location (Erongo Region)
	Latitude	**Longitude**	
TW1	-22.45481	15.03989	Paddy X station
TW2	-22.45519	15.04003	Flushing area
TW3	-22.44523	15.03656	Paddy Y2
TW4	-22.45658	15.02367	Empty 5
TW5	-22.45766	15.01983	DW5
TW6	-22.45766	15.03631	Heap leach area
TW7	-22.46223	15.03889	Station 5
TW8	-22.46061	15.03876	Lake Andrew
TW9	-22.46063	15.03889	Lake Prad
TW10	-22.47709	15.03543	Seepage dam 110
BW1	-22.43286	15.04405	Paddy CD3
BW2	-22.44027	15.02819	Paddy CD3
BW3	-22.47967	15.03506	Paddy CD3
BW4	-22.48258	15.03485	Paddy CD3
BW5	-22.48599	15.00976	Paddy CD3
BW6	-22.49053	15.08190	Paddy CD2
BW7	-22.47503	15.10767	Paddy CD2
BW8	-22.52835	15.02934	Paddy CD2
BW9	-22.47994	14.99211	Paddy CD2
BW10	-22.44013	14.00488	Paddy CD2

Table A5: Coordinate positions and masses used for Khan river samples counted on HPGe detector.

Sample ID	Position		Location (Erongo Region)	Mass (kg) of sample
	Latitude	**Longitude**		
KHN1	-22.8113	29.93972	Khan river	0.4911
KHN2	-22.8116	29.94000	Khan river	0.5667
KHN3	-22.8113	29.94053	Khan river	0.6676
KHN4	-22.8109	29.94103	Khan river	0.6483
KHN5	-22.8105	29.94102	Khan river	0.4403
KHN6	-22.8107	29.94155	Khan river	0.7034

Table A6: Coordinate positions and masses used for mine 2 soils of the stockpiles, counted on the HPGe detector.

Sample ID	Position		Location (Erongo Region)	Mass (kg) of sample
	Latitude	Longitude		
SU_T1	-22.6065	15.00531	Tailings	0.471573
SU_T2	-22.6155	15.00213	Tailings	0.477051
SU_T3	-22.6111	15.00385	Tailings	0.490143
SU_T4	-22.6151	15.00513	Tailings	0.535891
SU_T5	-22.6208	15.01019	Tailings	0.528416
SU_T6	-22.6207	15.01847	Tailings	0.474869
SU_T7	-22.6197	15.02166	Tailings	0.485731
SU_T8	-22.6180	15.02455	Tailings	0.50096
SU_T9	-22.6136	15.02548	Tailings	0.568372
SU_T10	-22.6044	15.02516	Tailings	0.549826
SU_T11	-22.6026	15.01922	Tailings	0.390461
SU_T12	-22.6116	15.01395	Tailings	0.498643

Annexure B: Tables of weighted activity concentrations in sections A – D.

Table B1: Activity concentrations for soil samples collected from gardens in Arandis town.

Sample ID	Weighted activity concentrations ($Bq.kg^{-1}$)			
	^{226}Ra	^{238}U	^{232}Th	^{40}K
DG_S1	19.73±0.47	51.60±4.00	31.14±1.01	593.40±11.15
DG_S2	52.58±0.87	200.28±6.57	235.40±1.98	719.60±13.44
DG_S3	35.54±0.70	109.62±5.63	131.40±1.54	650.40±12.67
DG_S4	44.62±0.78	144.10±4.19	182.95±1.73	683.90±12.91
DG_S5	52.47±0.85	185.39±6.44	222.53±1.89	697.00±13.49
AR_S_T1	46.00±0.72	84.54±5.28	69.59±1.51	717.10±13.24
AR_S_T2	44.63±0.69	94.50±5.22	65.90±1.26	720.00±13.24
Min	19.73±0.47	51.60±4.00	31.14±1.01	593.40±11.15
Max	52.58±0.85	200.28±6.57	235.40±1.98	720.00±13.24
Ave	42.22±0.73	124.29±5.33	134.13±1.56	683.06±12.88

Table B2: The determined ^{226}Ra, ^{238}U, ^{232}Th and ^{40}K activity concentrations associated with soil samples from Arandis town.

Sample ID	Weighted activity concentrations (Bq.kg^{-1})			
	^{226}Ra	^{238}U	^{232}Th	^{40}K
AR 1	59.13±0.77	112.72±5.00	180.88±1.40	771.60±13.38
AR 2	63.77±0.84	112.72±5.80	216.63±1.82	725.40±13.22
AR 3	85.77±0.99	218.57±6.30	276.32±2.17	781.80±13.74
AR 4	76.28±0.91	218.57±5.94	261.72±2.32	784.90±13.98
AR 5	80.48±0.93	190.85±6.61	289.61±2.26	630.70±12.78
AR 6	60.49±0.89	229.95±6.35	207.50±1.85	661.80±12.83
AR 7	77.99±1.05	186.37±3.37	279.33±2.15	667.80±12.55
AR 8	105.85±1.09	262.91±12.70	405.40±2.67	691.90±13.00
AR 9	51.94±0.66	71.21±4.87	49.34±0.68	302.40±8.27
AR 10	74.56±0.94	191.52±4.76	273.45±2.12	706.80±12.79
AR 11	67.51±0.99	240.31±6.68	248.67±2.15	808.30±15.20
AR 12	59.76±0.79	144.41±5.34	212.16±1.79	787.70±13.32
AR 13	57.46±0.82	117.40±3.97	100.49±1.42	675.20±13.14
AR 14	52.03±0.79	148.26±6.60	101.33±1.72	670.40±13.63
AR 15	43.21±0.71	150.06±5.60	95.03±1.50	673.10±11.89
AR 16	50.55±0.71	110.31±4.99	113.96±1.36	696.40±12.39
AR 17	71.32±0.90	175.89±5.93	243.50±2.22	800.20±14.58
AR 18	45.31±0.67	130.40±3.41	134.48±1.50	850.40±14.22
AR 19	72.43±0.74	135.00±3.71	165.00±1.77	625.40±11.83
AR 20	64.57±0.74	98.17±4.84	101.17±1.37	637.70±12.04
AR 21	46.09±0.67	107.42±4.75	144.36±1.56	789.30±13.50
AR 22	51.57±0.73	179.27±5.70	202.54±1.72	811.00±13.91
AR 23	55.91±0.80	218.40±4.38	247.11±1.95	813.0014.24
AR 24	47.51±0.71	162.40±3.69	162.76±1.43	707.60±12.22
AR 25	57.08±0.64	191.28±3.45	215.46±1.57	867.30±13.66
AR 26	43.86±0.51	127.63±1.85	144.45±1.36	891.10±13.47
AR 27	64.84±0.89	210.90±6.36	196.67±1.85	675.30±13.25
AR 28	32.59±0.53	82.72±1.24	115.78±1.31	881.00±14.00
AR 29	87.90±1.00	141.05±5.95	172.65±1.91	683.30±13.85
AR 30	84.37±0.90	130.82±5.35	87.51±0.91	471.20±10.51
AR 31	85.04±0.84	224.95±6.73	268.89±2.18	846.50±14.88
AR 32	91.43±1.00	311.37±7.05	477.99±3.57	863.60±14.70
AR 33	115.41±1.19	40.54±3.71	415.86±2.58	725.80±13.85
AR 34	121.32±1.13	357.48±8.69	536.68±3.44	825.90±14.95
AR 35	124.19±1.30	564.80±7.33	720.98±4.48	708.40±14.22
AR 36	114.90±1.36	343.11±8.26	431.93±3.09	566.30±12.96

AR 37	111.70±1.18	296.25±5.28	433.83±3.02	683.90±12.76
AR 38	61.27±0.80	159.87±5.66	192.37±1.67	645.50±11.96
AR 39	38.16±0.61	80.32±4.57	65.97±1.06	438.30±9.21
AR 40	77.96±0.97	272.58±6.89	296.78±2.26	962.00±16.10
Min	32.59±0.53	40.54±3.71	49.34±0.68	302.40±8.27
Max	124.19±1.30	564.80±7.33	720.98±4.48	962.00±16.10
Ave	70.84±0.87	186.22±5.49	237.16±1.98	720.16±12.85

Table B3: Activity concentrations, with their respective uncertainties, for uranium ore samples.

Activity Concentrations (Bq.kg^{-1})				
Sample ID	**^{226}Ra**	**^{238}U**	**^{232}Th**	**^{40}K**
ORE 1	5593.88±20.48	5023.15±49.50	255.85±3.83	889.30±20.65
ORE 2	6004.68±22.20	5385.94±54.75	232.20±2.05	858.60±24.69
ORE 3	3682.19±13.90	3291.90±35.44	192.89±3.30	881.30±24.81
ORE 4	2855.84±11.02	2585.38±28.48	136.62±3.23	845.60±23.50
ORE 5	4281.26±15.68	3649.86±38.95	189.09±1.69	874.60±24.47
ORE 6	3648.43±13.89	4019.11±47.90	146.35±3.74	561.90±8.49
ORE 7	6508.41±23.87	5601.64±65.16	258.72±3.19	984.10±23.62
ORE 8	6700.44±24.02	7325.38±84.42	248.35±10.44	897.30±35.40
Minimum	2855.84±11.02	2585.38±28.48	136.62±3.23	561.90±8.49
Maximum	6700.44±24.02	7325.38±84.42	258.72±3.19	984.10±23.62
Average	4909.39±18.13	4610.29±50.57	207.51±3.93	849.09±23.20

Table B4: The activity concentrations associated with soil samples from study area B.

Activity concentrations (Bq.kg^{-1})				
Sample ID	**^{226}Ra**	**^{238}U**	**^{232}Th**	**^{40}K**
S01	87.55±0.82	141.91±5.51	107.82±0.98	821.10±13.97
S02	195.85±1.31	211.56±6.54	183.48±1.36	626.10±12.91
S03	90.99±1.03	425.20±8.78	530.09±3.42	543.10±12.20
S04	1019.52±11.83	744.97±38.09	431.84±9.42	3429.00±78.63
S05	1625.74±6.47	316.24±8.78	124.11±1.21	1025.00±20.58
S06	2722.95±10.72	337.29±10.74	206.12±1.87	1053.00±25.27
S07	1789.98±7.25	321.58±9.25	124.83±1.30	1034.00±21.07
S08	1461.69±53.83	1024.36±24.82	502.71±3.97	889.70±52.92
S09	1955.77±7.67	406.48±9.97	140.29±1.40	1006.00±22.77
S10	3484.04±13.30	1188.92±17.05	157.81±2.87	886.00±25.12
S11	31.38±0.35	60.80±3.57	39.81±0.46	135.60±3.48

S12	2791.39±10.73	653.53±12.26	107.50±1.29	968.50±23.48
S13	2248.49±8.67	347.25±9.87	170.05±1.49	895.60±22.45
S14	2745.54±11.36	1622.95±23.04	191.76±2.24	1795.00±37.60
Min	31.38±0.35	60.80±3.57	39.81±0.46	135.60±3.48
Max	3484.04±13.30	1622.95±23.04	530.09±3.42	3429.00±78.63
Ave.	1589.35±10.38	557.36±13.45	215.59±2.38	1079.12±26.60

Table B5: Tabulated activity concentrations in Khan river.

	Activity concentrations (Bq.kg^{-1})			
Sample ID	**^{226}Ra**	**^{238}U**	**^{232}Th**	**^{40}K**
S15_KHN1	73.83±0.081	119.79±6.00	91.40±1.27	781.40±15.64
S16_KHN2	62.30±0.80	115.69±5.17	123.29±1.55	748.40±13.46
S17_KHN3	47.08±0.56	97.81±4.71	90.37±1.05	820.20±13.61
S18_KHN4	38.86±0.51	83.29±4.71	80.63±0.98	846.20±13.98
S19_KHN5	120.60±0.99	150.13±6.73	117.07±1.13	847.90±15.83
S20_KHN6	36.96±0.46	61.91±4.07	43.34±0.57	633.40±11.06
Min	36.96±0.46	61.91±4.07	43.34±0.57	633.40±11.06
Max	120.60±0.99	150.13±6.73	123.29±1.55	847.90±15.83
Ave.	63.27±0.69	104.77±5.23	91.02±1.09	779.58±13.93

Table B6: Activity concentrations for soil samples collected from first mine (section D).

Sample ID	**Activity Concentration (Bq.kg^{-1})**			
	^{226}Ra	**^{238}U**	**^{232}Th**	**^{40}K**
SU_T1	2112.38±8.78	810.06±14.23	325.54±2.58	1301.00±26.91
SU_T2	4547.14±17.41	310.74±13.61	314.61±2.69	1300.00±34.72
SU_T3	2337.78±9.50	430.84±11.64	291.75±2.40	1282.00±27.34
SU_T4	7867.48±81.73	3583.22±150.10	1217.42±20.24	6653.00±15.33
SU_T5	2755.47±10.97	691.66±13.70	400.58±2.80	1200.00±27.15
SU_T6	10538.08±113.10	1214.93±66.55	824.80±16.46	7435.00±180
SU_T7	3441.84±13.48	301.66±12.39	272.93±2.24	1397.00±33.05
SU_T8	3673.86±14.17	536.77±13.64	252.34±2.13	1236.00±29.49
SU_T9	2280.17±9.10	420.54±11.11	314.55±2.30	1162.00±24.26
SU_T10	1371.82±5.69	296.28±9.71	178.83±1.61	1228.00±24.88
SU_T11	9970.16±36.80	972.41±22.85	571.83±4.21	1395.00±44.72
SU_T12	2073.67±8.34	541.91±12.15	275.76±2.28	1111.00±25.96
Min	1371.82±5.69	296.28±9.71	178.83±1.61	1111.00±25.96
Max	10538.08±113.10	3583.22±150.10	1217.42±20.24	7435.00±180.00
Ave.	4414.15±27.42	842.59±29.31	436.74±5.16	2225.00±52.65

Annexure C: Tables of radiological hazards in sections A – D.

Table C1: Radiological hazards calculated for soils from the gardens.

Sample ID	D (nGy.h^{-1})	Ra_{eq} (Bq.kg^{-1})	AED_{tot} (mSv.h^{-1})	ELCR (10^{-3})	H_{ex}	H_{in}	I_γ	I_α
DG_S1	67.39±2.00	109.95±1.74	0.41	1.45	0.30	0.35	0.42	0.10
DG_S2	264.72±3.31	444.60±3.14	1.62	5.68	1.20	1.34	1.59	0.26
DG_S3	157.13±2.81	273.53±2.50	0.96	3.37	0.74	0.83	0.99	0.18
DG_S4	205.60±2.27	358.90±2.78	1.26	4.41	0.97	1.09	1.29	0.22
DG_S5	249.13±3.23	424.36±3.01	1.53	5.35	1.15	1.29	1.52	0.26
AR_S_T1	110.99±2.66	200.74±2.50	0.68	2.38	0.54	0.67	0.74	0.23
AR_S_T2	113.49±2.59	194.30±2.18	0.70	2.44	0.52	0.65	0.72	0.22
Min	67.39±2.00	109.95±1.74	0.41	1.45	0.30	0.35	0.42	0.10
Max	264.72±3.31	444.60±3.14	1.62	5.68	1.20	1.34	1.59	0.26
Ave.	166.92±2.70	286.63±2.55	1.02	3.58	0.77	0.89	1.04	0.21

Table C2: The radiological health hazards estimated due to ^{226}Ra, ^{238}U, ^{232}Th and ^{40}K concentrations in soil samples of Arandis.

Sample ID	D (nGy.h^{-1})	Ra_{eq} (Bq.kg^{-1})	AED_{tot} (mSv.h^{-1})	ELCR (10^{-3})	H_{ex}	H_{in}	I_γ	I_α
AR 1	193.51±2.52	377.21±2.38	1.19	4.15	1.02	1.18	1.36	0.30
AR 2	213.17±2.95	429.40±2.91	1.31	4.58	1.16	1.33	1.54	0.32
AR 3	300.48±3.25	541.10±3.43	1.84	6.45	1.46	1.69	1.93	0.43
AR 4	291.79±3.14	510.98±3.60	1.79	6.26	1.38	1.59	1.82	0.38
AR 5	289.40±3.38	543.19±3.50	1.77	6.21	1.47	1.68	1.93	0.40
AR 6	259.17±3.18	408.17±2.96	1.59	5.56	1.10	1.27	1.46	0.30
AR 7	282.67±2.10	528.86±3.39	1.73	6.07	1.43	1.64	1.88	0.39
AR 8	395.18±6.11	738.85±4.10	2.42	8.48	2.00	2.28	2.61	0.53
AR 9	75.31±2.31	145.78±1.34	0.46	1.62	0.39	0.53	0.52	0.26
AR 10	283.12±2.60	520.02±3.33	1.74	6.08	1.40	1.61	1.85	0.37
AR 11	294.92±3.41	485.34±3.43	1.81	6.33	1.31	1.49	1.74	0.34
AR 12	227.71±2.75	423.80±2.87	1.40	4.89	1.14	1.31	1.52	0.30
AR 13	143.09±2.10	253.15±2.41	0.88	3.07	0.68	0.84	0.92	0.29
AR 14	157.66±3.27	248.55±2.78	0.97	3.38	0.67	0.81	0.90	0.26
AR 15	154.79±2.78	230.93±2.43	0.95	3.32	0.62	0.74	0.84	0.22
AR 16	148.83±2.50	267.13±2.29	0.91	3.19	0.72	0.86	0.97	0.25
AR 17	261.70±3.05	481.14±3.30	1.60	5.62	1.30	1.49	1.72	0.36

AR 18	176.93±1.91	303.10±2.51	1.08	3.80	0.82	0.94	1.11	0.23
AR 19	188.11±2.08	356.54±2.79	1.15	4.04	0.96	1.16	1.27	0.36
AR 20	133.06±2.44	258.35±2.29	0.82	2.86	0.70	0.87	0.93	0.32
AR 21	169.74±2.45	313.30±2.54	1.04	3.64	0.85	0.97	1.14	0.23
AR 22	238.98±2.89	403.64±2.78	1.47	5.13	1.09	1.23	1.45	0.26
AR 23	284.06±2.42	471.88±3.11	1.74	6.10	1.27	1.43	1.69	0.28
AR 24	202.84±1.98	334.73±2.36	1.24	4.35	0.90	1.03	1.21	0.24
AR 25	254.68±1.94	431.97±2.56	1.56	5.47	1.17	1.32	1.56	0.29
AR 26	183.37±1.31	319.04±2.26	1.12	3.94	0.86	0.98	1.17	0.22
AR 27	244.39±3.19	398.08±2.97	1.50	5.25	1.07	1.25	1.42	0.32
AR 28	144.88±1.14	265.99±2.23	0.89	3.11	0.72	0.81	0.98	0.16
AR 29	197.94±3.04	387.40±3.10	1.21	4.25	1.05	1.28	1.38	0.44
AR 30	132.94±2.57	245.79±1.78	0.82	2.85	0.66	0.89	0.88	0.42
AR 31	301.64±3.43	534.73±3.43	1.85	6.47	1.44	1.67	1.91	0.43
AR 32	468.58±3.95	841.47±5.33	2.87	10.06	2.27	2.52	2.98	0.46
AR 33	300.18±2.39	765.98±4.02	1.84	6.44	2.07	2.38	2.71	0.58
AR 34	523.75±4.57	952.36±5.18	3.21	11.24	2.57	2.90	3.36	0.61
AR 35	725.95±4.38	1209.74±6.63	4.45	15.58	3.27	3.60	4.26	0.62
AR 36	443.02±4.28	776.18±4.73	2.72	9.51	2.10	2.41	2.73	0.57
AR 37	427.42±3.09	784.74±4.59	2.62	9.17	2.12	2.42	2.77	0.56
AR 38	216.97±2.85	386.05±2.68	1.33	4.66	1.04	1.21	1.38	0.31
AR 39	95.23±2.24	166.24±1.78	0.58	2.04	0.45	0.55	0.60	0.19
AR 40	345.31±3.53	576.43±3.59	2.12	7.41	1.56	1.77	2.06	0.39
Min	75.31±2.31	145.78±1.34	0.46	1.62	0.39	0.53	0.52	0.16
Max	725.95±4.38	1209.74±6.63	4.45	15.58	3.27	3.60	4.26	0.62
Ave.	259.31±2.89	465.43±3.14	1.59	5.57	1.26	1.45	1.66	0.35

Table C3: The computed values of D, AED, Ra_{eq}, and H_{ex}, I_γ and I_α of uranium ores.

Sample ID	**D ($nGy.h^{-1}$)**	**Ra_{eq} ($Bq.kg^{-1}$)**	**AED_{tot} ($mSv.y^{-1}$)**	**H_{ex}**	**H_{in}**	**ELCR ($x10^{-3}$)**	**I_γ**	**I_α**
ORE1	2512.31±23.00	6028.21±21.25	15.41±0.14	16.29±0.004	31.41±0.005	53.92±0.49	20.22±0.07	27.97±0.10
ORE2	2664.36±25.35	6402.84±22.47	16.34±0.16	17.30±0.005	33.53±0.005	57.18±0.54	21.46±0.08	30.02±0.11
ORE3	1674.12±16.53	4025.88±14.80	10.27±0.10	10.88±0.005	20.83±0.005	35.93±0.35	13.53±0.05	18.41±0.07
ORE4	1312.23±13.34	3116.32±12.08	8.05±0.08	8.42±0.005	16.14±0.005	28.16±0.29	10.48±0.04	14.28±0.06
ORE5	1836.92±18.05	4619.01±15.97	11.26±0.11	12.48±0.005	24.05±0.005	39.42±0.39	15.51±0.05	21.41±0.08
ORE6	1968.65±22.25	3900.97±14.90	12.07±0.14	10.54±0.002	20.40±0.002	42.25±0.48	13.08±0.05	18.24±0.07

ORE7	2785.26± 30.17	6954.16± 24.37	17.08±0.1 9	18.79± 0.005	36.38± 0.005	59.78±0 .65	23.32± 0.08	32.54± 0.12
ORE8	3571.74± 39.54	7124.66± 28.42	21.90±0.2 4	19.25± 0.008	37.36± 0.009	76.66±0 .85	23.88± 0.10	33.50± 0.12
Min	1312.23± 13.34	3116.32± 12.08	8.05±0.08	8.42±0. 005	16.14± 0.005	28.16±0 .29	10.48± 0.04	14.28± 0.06
Max	3571.74± 39.54	7124.66± 28.42	21.90±0.2 4	19.25± 0.008	37.36± 0.009	76.66±0 .85	23.88± 0.10	33.50± 0.12
Ave.	2290.70± 23.53	5271.51± 19.28	14.05±0.1 4	14.25± 0.005	27.51± 0.005	49.16±0 .50	17.69± 0.07	24.55± 0.09

Table C4: The calculated radiological hazards in soil samples of mine 1.

Sample ID	**D (nGy.h^{-1})**	**Ra_{eq} (Bq.kg^{-1})**	**AED_{tot} (mSv.y^{-1})**	**ELCR (x10^{-3})**	**H_{ex}**	**H_{in}**	**I_γ**	**I_α**
S01	164.93±2.6 8	304.96±1.94	1.01	3.54	0.82	1.06	1.10	0.44
S02	234.67±3.1 8	506.44±2.55	1.44	5.04	1.37	1.90	1.78	0.98
S03	539.26±4.5 8	890.84±5.08	3.31	11.57	2.41	2.65	3.13	0.45
S04	747.99±18. 8	1901.08±18. 90	4.59	16.05	5.14	7.89	6.70	5.10
S05	263.81±4.2 1	1882.14±6.8 8	1.62	5.66	5.09	9.48	6.38	8.13
S06	324.23±5.2 0	3098.78±11. 20	1.99	6.96	8.37	15.73	10.46	13.61
S07	267.09±4.4 3	2048.10±7.6 6	1.64	5.73	5.53	10.37	6.94	8.95
S08	813.99±11. 9	2249.07±54. 3	4.99	17.47	6.08	10.03	7.68	7.31
S09	314.48±4.7 8	2233.85±8.1 2	1.93	6.75	6.04	11.32	7.56	9.78
S10	681.54±8.1 4	3777.93±14. 10	4.18	14.63	10.21	19.63	12.70	17.47
S11	57.79±1.68	98.74±0.79	0.35	1.24	0.27	0.35	0.35	0.16
S12	407.24±5.8 0	3019.69±11. 00	2.50	8.74	8.16	15.70	10.16	13.96
S13	300.49±4.7 4	2560.62±9.0 9	1.84	6.45	6.92	13.00	8.64	11.24
S14	940.48±10. 80	3157.97±12. 20	5.77±0.0 7	20.18	8.53	15.95	10.71±0. 04	13.73±0. 06
Min	57.79±1.68	98.74±0.79	0.35	1.24	0.27	0.35	0.35	0.16
Max	940.48±10. 80	3777.93±14. 1	5.77	20.18	10.21	19.63	12.70	17.42
Ave.	432.71±6.5 0	1980.73±11. 7	2.65	9.29	5.35	9.65	6.74	7.95

Table C5: Radiological values calculated from Khan river.

Radiological hazards								
Sample ID	**D (nGy.h^{-1})**	**Ra_{eq} (Bq.kg^{-1})**	**AED_{tot} (mSv.y^{-1})**	**ELCR (x10^{-3})**	**H_{ex}**	**H_{in}**	**I_γ**	**I_α**
S15_KHN 1	143.13±2.95	264.69±2.32	0.88	3.07	0.71	0.91	0.96	0.37
S16_KHN 2	159.12±2.63	296.23±2.58	0.98	3.42	0.80	0.97	1.07	0.31
S17_KHN 3	133.98±2.34	239.47±1.91	0.82	2.88	0.65	0.77	0.88	0.24
S18_KHN 4	122.46±2.33	219.31±1.84	0.75	2.63	0.59	0.70	0.81	0.19
S19_KHN 5	175.43±3.25	353.29±2.25	1.08	3.77	0.95	1.28	1.27	0.60
S20_KHN 6	81.19±1.97	147.71±1.26	0.50	1.74	0.40	0.50	0.55	0.18
Min	81.19±1.97	147.71±1.26	0.50	1.74	0.40	0.50	0.55	0.18
Max	175.43±3.25	353.29±2.25	1.08	3.77	0.95	1.28	1.27	0.60
Ave.	135.89±2.58	253.45±2.03	0.83	2.92	0.68	0.86	0.93	0.32

Table C6: The radioactive hazards measured in soil of uranium mine 2.

	Radiological hazards							
Sample ID	**D (nGy.h^{-1})**	**Ra_{eq} (Bq.kg^{-1})**	**AED_{tot} (mSv.y^{-1})**	**ELCR (x10^{-3})**	**H_{ex}**	**H_{in}**	**I_γ**	**I_α**
SU_T 1	387.80±6.65	5097.13±18.03	2.38±0.04	7.61±0.13	13.77±0.01	26.06±0.01	17.16±0.06	22.74±0.09
SU_T 2	428.72±5.69	2853.70±10.32	2.63±0.04	8.41±0.11	7.71±0.01	14.03±0.01	9.68±0.04	11.69±0.05
SU_T 3	2668.20±70.70	10120.67±87.50	16.36±0.43	52.36±1.39	27.35±0.04	48.61±0.05	34.53±0.30	39.34±0.41
SU_T 4	611.54±6.65	3420.69±11.86	3.75±0.04	11.99±0.13	9.24±0.01	16.69±0.01	11.59±0.04	13.78±0.05
SU_T 5	1369.51±33.17	12290.04±116.30	8.40±0.20	26.87±0.65	33.21±0.04	61.69±0.05	41.73±0.39	52.69±0.57
SU_T 6	362.47±6.04	3939.69±14.09	2.22±0.04	7.11±0.12	10.65±0.01	19.95±0.01	13.30±0.05	17.21±0.07
SU_T 7	451.95±6.55	4129.88±14.67	2.77±0.04	8.87±0.13	11.16±0.01	21.09±0.01	13.92±0.05	18.37±0.07
SU_T 8	432.73±5.41	2819.45±9.85	2.65±0.03	8.49±0.11	7.62±0.01	13.78±0.01	9.56±0.03	11.40±0.05
SU_T 9	296.10±4.71	1722.10±6.43	1.82±0.03	5.81±0.09	4.65±0.01	8.36±0.01	5.88±0.02	6.86±0.03
SU_T 10	852.81±11.02	10895.29±37.45	5.23±0.07	16.73±0.22	29.44±0.01	56.39±0.01	36.56±0.13	49.85±0.18

SU_T 11	463.25±5.88	2553.55±9.17	2.84±0.04	9.09±0.12	6.9±0.01	12.50±0.01	8.66±0.03	10.37±0.04
SU_T 12	291.22±4.70	1713.09±6.42	1.79±0.03	5.71±0.09	4.63±0.01	8.34±0.01	5.84±0.02	6.86±0.03
Min	291.22±4.70	1713.09±6.42	1.79±0.03	5.71±0.09	4.63±0.01	8.34±0.01	5.84±0.02	6.86±0.03
Max	2668.20±70.70	12290.04±116.30	16.36±0.43	52.36±1.39	33.21±0.04	61.69±0.05	41.73±0.39	52.69±0.57
Ave.	718.03±	5129.61±28.51	4.40±0.09	14.09±0.27	13.86±0.01	25.63±0.01	17.37±0.10	21.76±0.14

Annexure D: Tables of concentrations and activity concentrations determined using ICP-MS.

Table D1: Concentrations of NORM in borehole water.

Concentrations						
	TotalQuant (ppm)			**Bq.l^{-1}**		
Sample ID	**U**	**Th**	**K**	**^{238}U**	**^{232}Th**	**^{40}K**
BW 1	0.1073	0.00885	750.949	1.33	0.036	23.50
BW 2	0.0595	0.00174	476.399	0.73	0.007	14.91
BW 3	0.0351	0.00181	367.0569	0.43	0.007	11.49
BW 4	1.2932	0.00151	425.5607	15.97	0.006	13.32
BW 5	0.5023	0.00075	559.4425	6.20	0.003	17.51
BW 6	0.0745	0.00061	107.8256	0.92	0.003	3.37
BW 7	0.1219	0.00049	146.5109	1.51	0.002	4.59
BW 8	0.0379	0.02522	136.8029	0.47	0.102	4.28
BW 9	0.2710	0.01341	316.7913	3.35	0.054	9.92
BW 10	0.0639	0.00375	411.8680	0.79	0.015	12.89
Min	0.0351	0.00049	107.8256	0.43	0.002	3.37
Max	1.2932	0.02522	750.949	15.97	0.102	23.50
Ave.	0.2566	0.00581	369.9207	3.17	0.024	11.58

Table D2: Concentrations of NORM in tailing's lake water.

Concentrations TotalQuant				**Concentrations**		
	ppm			**Bq.l^{-1}**		
Sample ID	**U**	**Th**	**K**	**^{238}U**	**^{232}Th**	**^{40}K**
TW 1	1.6506	0.0130	244.4243	20.38	0.05	7.65

TW 2	0.0819	3.5273	290.2191	1.01	14.32	9.08
TW 3	1.7674	0.4281	253.2067	21.83	1.74	7.93
TW 4	0.0374	0.0181	790.2584	0.46	0.07	24.74
TW 5	1.4769	0.0940	474.5551	18.24	0.38	14.85
TW 6	4.9490	0.0036	288.6580	61.12	0.01	9.04
TW 7	2.0367	0.0082	610.5718	25.15	0.03	19.11
TW 8	0.0819	0.0962	220.5740	1.01	0.39	6.90
TW 9	0.8176	0.0237	391.8336	10.10	0.10	12.26
TW 10	1.5225	0.0152	397.8551	18.80	0.06	12.45
Min	0.0374	0.0036	220.5740	0.46	0.01	6.90
Max	4.9490	3.5273	790.2584	61.12	14.32	24.74
Ave.	1.4422	0.4227	396.2156	17.81	1.72	12.40

Table D3: Concentrations of NORM in dust.

	Concentrations TotalQuant			**Concentrations**		
	ppm			**Bq.l^{-1}**		
Sample ID	**U**	**Th**	**K**	**^{238}U**	**^{232}Th**	**^{40}K**
SU_D 1	0.7915	213.2768	70014.4442	9.77	865.90	21.91
SU_D 2	20.5003	272.2294	84258.0073	253.18	1105.25	26.37
SU_D 3	0.7692	204.1049	97581.1934	9.49	828.67	30.54
SU_D 4	21.0314	237.4930	97422.9412	259.74	964.22	30.49
SU_D 5	20.7051	496.5481	89454.5721	255.71	2015.99	27.99
SU_D 6	1.4041	48.9675	74217.9828	17.34	198.81	23.23
SU_D 7	1.3600	79.9237	93095.6517	16.79	324.49	29.14
SU_D 8	1.3937	74.2546	101004.8777	17.21	301.47	31.61
SU_D 9	1.3355	64.0420	91287.9795	16.49	260.01	28.57
SU_D 10	1.3951	78.8139	109249.0174	17.23	319.98	34.19
SU_D 11	1.4075	54.0811	74748.2696	17.38	219.57	23.39
Min	0.7692	48.9675	70014.4442	9.49	198.81	21.91
Max	21.0314	496.5481	109249.0174	259.74	2015.99	34.19
Ave.	6.5539	165.7941	89303.1761	80.94	673.12	27.95

Table D4: The dose rate and annual effective dose in borehole water.

Sample ID	**D (nGy.h^{-1})**	**AED$_{out}$ (mSv.y^{-1})**	**AED$_{in}$ (mSv.y^{-1})**	**AED$_{tot}$ (mSv.y^{-1})**
BW 1	1.61E+00	1.98E-03	7.92E-03	9.90E-03
BW 2	9.65E-01	1.18E-03	4.74E-03	5.92E-03
BW 3	6.84E-01	8.38E-04	3.35E-03	4.19E-03

BW 4	7.94E+00	9.73E-03	3.89E-02	4.87E-02
BW 5	3.60E+00	4.41E-03	1.77E-02	2.21E-02
BW 6	5.67E-01	6.96E-04	2.78E-03	3.48E-03
BW 7	8.88E-01	1.09E-03	4.36E-03	5.44E-03
BW 8	4.57E-01	5.61E-04	2.24E-03	2.80E-03
BW 9	1.99E+00	2.44E-03	9.77E-03	1.22E-02
BW 10	9.11E-01	1.12E-03	4.47E-03	5.59E-03
Min	4.57E-01	5.61E-04	2.24E-03	2.80E-03
Max	7.94E+00	9.73E-03	3.89E-02	4.87E-02
Ave.	1.96E+00	2.41E-03	9.62E-03	1.20E-02

Table D5: The dose rate and annual effective dose in tailings lake water.

Sample ID	D (nGy.h^{-1})	AED$_{out}$ (mSv.y^{-1})	AED$_{in}$ (mSv.y^{-1})	AED$_{tot}$ (mSv.y^{-1})
TW 1	9.77	1.20E-02	4.79E-02	5.99E-02
TW 2	9.50	1.16E-02	4.66E-02	5.82E-02
TW 3	11.46	1.41E-02	5.62E-02	7.03E-02
TW 4	1.29	1.58E-03	6.32E-03	7.90E-03
TW 5	9.28	1.14E-02	4.55E-02	5.69E-02
TW 6	28.62	3.51E-02	1.40E-01	1.76E-01
TW 7	12.44	1.53E-02	6.10E-02	7.63E-02
TW 8	0.99	1.22E-03	4.86E-03	6.08E-03
TW 9	5.23	6.42E-03	2.57E-02	3.21E-02
TW 10	9.24	1.13E-02	4.53E-02	5.67E-02
Min	0.99	1.22E-03	4.86E-03	6.08E-03
Max	28.62	3.51E-02	1.40E-01	1.76E-01
Ave	9.78	1.20E-02	4.80E-02	6.00E-02

Table D6: The dose rate and annual effective dose in dust.

Sample ID	D (nGy.h^{-1})	AED$_{out}$ (mSv.y^{-1})	AED$_{in}$ (mSv.y^{-1})	AED$_{tot}$ (mSv.y^{-1})
SU_D 1	528.44	6.48E-01	2.59E+00	3.24E+00
SU_D 2	785.64	9.64E-01	3.85E+00	4.82E+00
SU_D 3	506.18	6.21E-01	2.48E+00	3.10E+00
SU_D 4	703.66	8.63E-01	3.45E+00	4.31E+00
SU_D 5	1336.96	1.64E+00	6.56E+00	8.20E+00
SU_D 6	129.06	1.58E-01	6.33E-01	7.91E-01
SU_D 7	204.97	2.51E-01	1.01E+00	1.26E+00
SU_D 8	191.36	2.35E-01	9.39E-01	1.17E+00
SU_D 9	165.86	2.03E-01	8.14E-01	1.02E+00

SU_D 10	202.66	2.49E-01	9.94E-01	1.24E+00
SU_D 11	141.63	1.74E-01	6.95E-01	8.68E-01
Min	129.06	1.58E-01	6.33E-01	7.91E-01
Max	1336.96	1.64E+00	6.56E+00	8.20E+00
Ave.	445.13	5.46E-01	2.18E+00	2.73E+00

Annexure E: Tables of effective doses and cancer morbidity risks modelled on RESRAD-OFFSITE (vs 4.0)

Table E1: The annual effective dose for uranium ore samples from section B.

EFFECTIVE DOSE ($mSv.y^{-1}$): All Nuclides Summed, All Pathways Summed for ore samples					
Year	**^{40}K**	**^{226}Ra**	**^{232}Th**	**^{238}U**	**Total**
0	6.37E-04	2.40E+00	8.61E-04	1.07E-03	2.40E+00
1	6.33E-04	2.40E+00	3.63E-03	1.07E-03	2.40E+00
5	6.16E-04	2.39E+00	2.45E-02	1.07E-03	2.42E+00
10	5.95E-04	2.38E+00	4.79E-02	1.06E-03	2.43E+00
15	5.75E-04	2.37E+00	6.21E-02	1.06E-03	2.43E+00
20	5.55E-04	2.35E+00	7.04E-02	1.06E-03	2.43E+00
25	5.37E-04	2.34E+00	7.48E-02	1.05E-03	2.42E+00
50	4.50E-04	2.28E+00	7.99E-02	1.03E-03	2.37E+00
75	3.78E-04	2.23E+00	8.02E-02	1.02E-03	2.31E+00
100	3.17E-04	2.17E+00	8.02E-02	9.96E-04	2.25E+00
125	2.66E-04	2.12E+00	8.02E-02	9.77E-04	2.20E+00
150	2.23E-04	2.07E+00	8.02E-02	9.58E-04	2.15E+00
175	1.87E-04	2.02E+00	8.03E-02	9.40E-04	2.10E+00
200	1.62E-04	1.97E+00	8.03E-02	9.22E-04	2.05E+00

Table E2: The annual effective dose, individual and summed, for NORM in samples from section B.

EFFECTIVE DOSE ($mSv.y^{-1}$): All Nuclides Summed, All Pathways Summed for tailings soil (mine 1)					
Year	**^{40}K**	**^{226}Ra**	**^{232}Th**	**^{238}U**	**Total**
0	8.13E-04	8.04E-01	8.95E-04	1.29E-04	8.06E-01
1	8.13E-04	8.04E-01	3.78E-03	1.29E-04	8.09E-01
5	8.14E-04	8.03E-01	2.55E-02	1.30E-04	8.29E-01
10	8.14E-04	8.01E-01	4.99E-02	1.30E-04	8.52E-01
15	8.14E-04	7.99E-01	6.47E-02	1.30E-04	8.65E-01

20	8.14E-04	7.98E-01	7.33E-02	1.30E-04	8.72E-01
25	8.13E-04	7.96E-01	7.80E-02	1.30E-04	8.75E-01
30	8.13E-04	7.94E-01	8.06E-02	1.30E-04	8.76E-01
50	8.11E-04	7.87E-01	8.34E-02	1.30E-04	8.72E-01
75	8.08E-04	7.79E-01	8.37E-02	1.30E-04	8.63E-01
100	8.05E-04	7.70E-01	8.37E-02	1.30E-04	8.55E-01
125	8.02E-04	7.62E-01	8.38E-02	1.30E-04	8.46E-01
150	8.00E-04	7.53E-01	8.38E-02	1.30E-04	8.38E-01
175	8.00E-04	7.45E-01	8.38E-02	1.30E-04	8.30E-01
200	8.00E-04	7.37E-01	8.38E-02	1.30E-04	8.21E-01

Table E3: The annual effective dose, individual and summed, for NORM in samples from section D.

DOSE: All Nuclides Summed, All Pathways Summed for soil (mine 2)					
Year	**^{40}K**	**^{226}Ra**	**^{232}Th**	**^{238}U**	**Total**
0	1.67E-03	2.16E+00	1.81E-03	1.96E-04	2.16E+00
1	1.66E-03	2.15E+00	7.65E-03	1.96E-04	2.16E+00
5	1.61E-03	2.15E+00	5.15E-02	1.95E-04	2.20E+00
10	1.56E-03	2.14E+00	1.01E-01	1.95E-04	2.24E+00
15	1.51E-03	2.12E+00	1.31E-01	1.94E-04	2.26E+00
20	1.46E-03	2.11E+00	1.48E-01	1.93E-04	2.26E+00
25	1.41E-03	2.10E+00	1.57E-01	1.93E-04	2.26E+00
30	1.36E-03	2.09E+00	1.63E-01	1.92E-04	2.26E+00
50	1.18E-03	2.05E+00	1.68E-01	1.89E-04	2.22E+00
75	9.91E-04	2.00E+00	1.69E-01	1.86E-04	2.17E+00
100	8.31E-04	1.95E+00	1.69E-01	1.82E-04	2.12E+00
125	6.97E-04	1.90E+00	1.69E-01	1.79E-04	2.07E+00
150	5.85E-04	1.86E+00	1.69E-01	1.75E-04	2.03E+00
175	4.91E-04	1.81E+00	1.69E-01	1.72E-04	1.98E+00
200	4.24E-04	1.77E+00	1.69E-01	1.68E-04	1.94E+00

Table E4: The cancer morbidity risks, individual and summed, for NORM in uranium ore samples.

EXCESS CANCER RISK: All Nuclides Summed, All Pathways Summed					
Year	**^{40}K**	**^{226}Ra**	**^{232}Th**	**^{238}U**	**Total**
0	1.39E-06	8.59E-03	6.75E-05	2.34E-06	8.66E-03
1	1.38E-06	8.58E-03	7.08E-05	2.34E-06	8.66E-03
5	1.34E-06	8.55E-03	8.26E-05	2.33E-06	8.63E-03

10	1.30E-06	8.50E-03	9.23E-05	2.32E-06	8.60E-03
15	1.25E-06	8.46E-03	9.77E-05	2.31E-06	8.56E-03
20	1.21E-06	8.42E-03	1.01E-04	2.30E-06	8.52E-03
25	1.17E-06	8.38E-03	1.02E-04	2.30E-06	8.48E-03
50	9.80E-07	8.17E-03	1.04E-04	2.25E-06	8.28E-03
75	8.23E-07	7.97E-03	1.04E-04	2.21E-06	8.08E-03
100	6.90E-07	7.77E-03	1.04E-04	2.17E-06	7.88E-03
125	5.79E-07	7.58E-03	1.05E-04	2.13E-06	7.69E-03
150	4.86E-07	7.39E-03	1.05E-04	2.09E-06	7.50E-03
175	4.13E-07	7.21E-03	1.05E-04	2.05E-06	7.32E-03
200	4.45E-07	7.03E-03	1.05E-04	2.01E-06	7.14E-03

Table E5: The excess morbidity cancer risks estimated for NORM in soil of uranium mine 1.

EXCESS CANCER RISK: All Nuclides Summed, All Pathways Summed					
Year	**^{40}K**	**^{226}Ra**	**^{232}Th**	**^{238}U**	**Total**
0	1.96E-06	2.90E-03	7.03E-05	2.85E-07	2.97E-03
1	1.96E-06	2.90E-03	7.38E-05	2.85E-07	2.98E-03
5	1.96E-06	2.90E-03	8.61E-05	2.86E-07	2.98E-03
10	1.96E-06	2.89E-03	9.62E-05	2.86E-07	2.99E-03
15	1.95E-06	2.88E-03	1.02E-04	2.86E-07	2.99E-03
20	1.95E-06	2.88E-03	1.05E-04	2.86E-07	2.98E-03
25	1.95E-06	2.87E-03	1.07E-04	2.86E-07	2.98E-03
50	1.95E-06	2.84E-03	1.09E-04	2.86E-07	2.95E-03
75	1.94E-06	2.81E-03	1.09E-04	2.86E-07	2.92E-03
100	1.93E-06	2.78E-03	1.09E-04	2.86E-07	2.89E-03
125	1.93E-06	2.75E-03	1.09E-04	2.86E-07	2.86E-03
150	1.92E-06	2.72E-03	1.09E-04	2.86E-07	2.83E-03
175	1.92E-06	2.69E-03	1.09E-04	2.86E-07	2.80E-03
200	2.04E-06	2.66E-03	1.09E-04	2.86E-07	2.77E-03

Table E6: The excess morbidity cancer risks estimated for NORM in soil for section D (mine 2).

EXCESS CANCER RISK: All Nuclides Summed, All Pathways Summed					
Year	**^{40}K**	**^{226}Ra**	**^{232}Th**	**^{238}U**	**Total**
0	3.64E-06	7.72E-03	1.42E-04	4.27E-07	7.86E-03
1	3.62E-06	7.71E-03	1.49E-04	4.27E-07	7.86E-03
5	3.52E-06	7.68E-03	1.74E-04	4.26E-07	7.85E-03

10	3.40E-06	7.64E-03	1.94E-04	4.24E-07	7.84E-03
15	3.28E-06	7.60E-03	2.06E-04	4.23E-07	7.81E-03
20	3.17E-06	7.56E-03	2.12E-04	4.21E-07	7.78E-03
25	3.06E-06	7.53E-03	2.16E-04	4.20E-07	7.74E-03
50	2.57E-06	7.34E-03	2.20E-04	4.12E-07	7.56E-03
75	2.16E-06	7.16E-03	2.20E-04	4.04E-07	7.38E-03
100	1.81E-06	6.98E-03	2.20E-04	3.96E-07	7.20E-03
125	1.52E-06	6.81E-03	2.20E-04	3.89E-07	7.03E-03
150	1.27E-06	6.64E-03	2.20E-04	3.81E-07	6.86E-03
175	1.08E-06	6.48E-03	2.20E-04	3.74E-07	6.70E-03
200	1.17E-06	6.32E-03	2.20E-04	3.67E-07	6.54E-03